

0193V

JOURNAL OF

ELECTROANALYTICAL CHEMISTRY

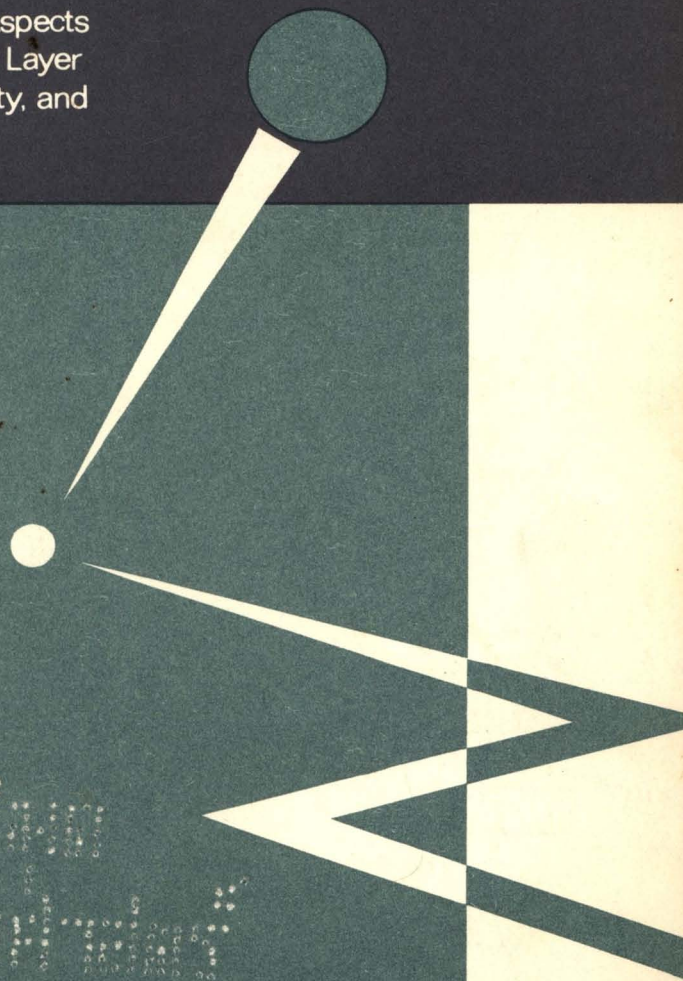
AND INTERFACIAL ELECTROCHEMISTRY

International Journal devoted to all Aspects
of Electroanalytical Chemistry, Double Layer
Studies, Electrokinetics, Colloid Stability, and
Electrode Kinetics.

EDITORIAL BOARD:

- F. BOCKRIS (Philadelphia, Pa.)
- J. CLARLOT (Paris)
- L. CONWAY (Ottawa)
- J. LAHAY (New York)
- S. FRUMKIN (Moscow)
- J. HERST (Brussels)
- H. HIBASHI (Kyoto)
- J. JEMULA (Warsaw)
- J. KIES (Delft)
- J. LANGANE (Cambridge, Mass.)
- J. KLEMA (Wageningen)
- C. MILNER (Harwell)
- J. OTTEWILL (Bristol)
- J. PAGE (London)
- J. RYMONS (Bristol)
- J. REILLEY (Chapel Hill, N.C.)
- J. MERANO (Padua)
- J. VON STACKELBERG (Bonn)
- J. CHI (Kyoto)
- J. MAN (Prague)

ELSEVIER



GENERAL INFORMATION

Types of contributions

- (a) Original research work not previously published in other periodicals.
- (b) Reviews on recent developments in various fields.
- (c) Short communications.
- (d) Bibliographical notes and book reviews.

Languages

Papers will be published in English, French or German.

Submission of papers

Papers should be sent to one of the following Editors:

Professor J. O'M. BOCKRIS, John Harrison Laboratory of Chemistry,
University of Pennsylvania, Philadelphia 4, Pa. 19104, U.S.A.

Dr. R. H. OTTEWILL, Department of Chemistry, The University, Bristol 8, England.

Dr. R. PARSONS, Department of Chemistry, The University, Bristol 8, England.

Professor C. N. REILLEY, Department of Chemistry,
University of North Carolina, Chapel Hill, N.C. 27515, U.S.A.

Authors should preferably submit two copies in double-spaced typing on pages of uniform size. Legends for figures should be typed on a separate page. The figures should be in a form suitable for reproduction, drawn in Indian ink on drawing paper or tracing paper, with lettering etc. in thin pencil. The sheets of drawing or tracing paper should preferably be of the same dimensions as those on which the article is typed. Photographs should be submitted as clear black and white prints on glossy paper. Standard symbols should be used in line drawings, the following are available to the printers:

▼ ▽ ■ □ ● ◎ ■ ◻ ◆ ◻ ■ + ×

All references should be given at the end of the paper. They should be numbered and the numbers should appear in the text at the appropriate places.
A summary of 50 to 200 words should be included.

Reprints

Fifty reprints will be supplied free of charge. Additional reprints (minimum 100) can be ordered at quoted prices. They must be ordered on order forms which are sent together with the proofs.

Publication

The *Journal of Electroanalytical Chemistry and Interfacial Electrochemistry* appears monthly and has four issues per volume and three volumes per year.

Subscription price: \$ 70.00 or Sfr. 304.00 per year; \$ 17.50 or Sfr. 76.00 per volume; plus postage. Additional cost for copies by air mail available on request. For advertising rates apply to the publishers.

Subscriptions

Subscriptions should be sent to:

ELSEVIER SEQUOIA S.A., P.O. Box 851, 1001 Lausanne 1, Switzerland

*In continuation of a
well-known book series:*

ORGANOMETALLIC CHEMISTRY REVIEWS

SECTION B ANNUAL SURVEYS

A new Elsevier Sequoia Journal

The "Annual Surveys of Organometallic Chemistry" (Seyferth-King) published so far in book form have been the standard reference work for, and unanimously appraised by, any scientist or researcher, teacher or student wanting to keep abreast with the progress made in all fields of organometallic chemistry.

In order to channel through these annual surveys to the reader faster than a book appearing only once a year would permit, their continuation is now published in the form of a journal entitled **Organometallic Chemistry Reviews — Section B — Annual Surveys** (three to four issues to the volume, one volume per year). The first volume is Vol. 4, the three volumes of the book series now being back volumes to the Journal.

The Journal "Organometallic Chemistry Reviews" published since 1966 will continue as **Organometallic Chemistry Reviews — Section A — Subject Reviews**.

Publishers:



Elsevier Sequoia S.A.

4 Avenue Ruchonnet
1001 LAUSANNE 1

P.O. Box 851
Switzerland

From A to Z

Keep updated on all developments in Organometallic Chemistry

Actinides
Aluminium
Antimony
Arsenic

Beryllium
Bismuth
Boron

Cadmium
Calcium
Chromium
Cobalt
Copper

Ferrocene

Gallium
Germanium
Gold

Hafnium

Indium
Iridium
Iron

Lanthanides
Lead
Lithium

Magnesium
Manganese

Mercury
Molybdenum

Nickel
Niobium

Osmium
Osmocene

Palladium
Platinum
Potassium

Rhenium
Rhodium
Ruthenium
Ruthenocene

Sodium
Silicon
Silver

Tantalum
Technetium
Thallium
Tin
Titanium
Tungsten

Vanadium

Zinc
Zirconium

The Authors:

D. Seyferth
R.B. King

E.C. Ashby
R.W. Bott
E.J. Bulten
F. Calderazzo
G.O. Doak
J.J. Eisch
L.D. Freedman
W.H. Glaze
J.G. Luyten
D.S. Matteson
J.G. Noltes
L.C. Willemsens



Order Form

Please detach and complete this form, and return it to your usual subscription agent or to: Elsevier Sequoia S.A., P.O. Box 851, 1001 Lausanne 1, Switzerland.

Please enter my/our order for the items marked "X" below

Subscriptions to be entered: until cancelled for current year only.

Opinions on Organometallic Chemistry Reviews - Annual Surveys

"...worth having on the bookshelf."

(Nature)

"...invaluable to anyone working in the field..."

(Analytica Chimica Acta)

«Die übersichtliche, klare Darstellung und die kritische, sachkundige Auswahl werden dieser Reihe einen festen Platz überall dort sichern, wo Interesse an der Organometall-Chemie besteht.»

(Österr. Chemiker-Zeitung)

"The value of this ready reference work to those working on organometallic chemistry can hardly be overestimated."

(Chemistry and Industry)

Subscription to **Organometallic Chemistry Reviews, Section B, Annual Surveys** (Sfrs 83.50 = approx. US\$ 19.80 or £ 8.7.0 incl. postage) starting with Vol. 4, No. 1, 1968.

Seyferth/King: "Annual Surveys of Organometallic Chemistry", Vol. 1 (covering the year 1964).

id., Vol. 2 (covering the year 1965).

id., Vol. 3 (covering the year 1966).

Please note: The preceding three items are the back volumes of Organometallic Chemistry Reviews, Section B, Annual Surveys. Prices will be quoted on request.

Subscription to Organometallic Chemistry Reviews, Section A, Subject Reviews (Sfrs 70.50 = approx. US\$ 16.30 or £ 7.1.0. incl. postage).

Organometallic Chemistry Reviews, Section A, Vol. 1, 1966 (Back Volume) Sfrs 76.25 = approx. US\$ 17.50 or £ 7.12.6. incl. postage.

Organometallic Chemistry Reviews, Section A, Vol. 2, 1967 (Back Volume) Sfrs 76.25 = approx. US\$ 17.50 or £ 7.12.6. incl. postage.

Payment: check enclosed please send invoice

Please send me/us a free sample copy of: Organometallic Chemistry Reviews — Section A — Subject Reviews Organometallic Chemistry Reviews — Section B — Annual Surveys.

Date: _____ Signature: _____


Name: _____

Company or Institution: _____

Street or P. O. Box: _____

City: _____ Zip Code/Postal Number: _____

Country: _____

 Please note: All invoices will be made out in Swiss Francs. Foreign currency equivalents given for guidance only and subject to change. Payments in currency other than Swiss Francs are welcome at official Swiss exchange rate, on day of payment.

Order Form (see overleaf)

Please send me/us also further information on following Elsevier Sequoia Journals:

- Journal of Organometallic Chemistry
- Journal of Electroanalytical Chemistry and Interfacial Electrochemistry
- Journal of the Less-Common Metals
- Materials Science and Engineering
- Powder Technology
- Thin Solid Films
- Wear / Usure / Verschleiss

Your name and address on the back of this form, please!

Please complete this form and return it to your usual subscription agent or to:
Elsevier Sequoia S.A., P.O. Box 851, 1001 Lausanne 1, Switzerland.

P. O. Box 851
CH-1001 LAUSANNE 1
Switzerland

Elsevier Sequoia S.A.

SUBSCRIPTION INFORMATION

Organometallic Chemistry Reviews Section B — Annual Surveys

(1 volume per year; 3-4 issues
to the volume; 1968 = Vol. 4)

Subscription rates:

Sales price	Sfrs 78.—
Postage	<u>Sfrs 5.50</u>
Total	<u>Sfrs 83.50</u>

Organometallic Chemistry Reviews Section A — Subject Reviews

(1 volume per year, 4 issues to
the volume; 1968 = Vol. 3)

Subscription rates:

Sales price	Sfrs 65.—
Postage	<u>Sfrs 5.50</u>
Total	<u>Sfrs 70.50</u>

Back Volumes:

Sales prices	Sfrs 72.00,
Postage & handling	<u>Sfrs 4.25</u>
Total	Sfrs 76.25 per volume

For further information
please contact:

Elsevier Sequoia S.A.

4 Av. Ruchonnet, P.O. Box 851
1001 Lausanne 1, Switzerland

Telephone: (021) 23 72 13
Cables: ELSEVIER Lausanne



JOURNAL OF ELECTROANALYTICAL CHEMISTRY
AND
INTERFACIAL ELECTROCHEMISTRY

VOL. 19 (1968)

JOURNAL
of
ELECTROANALYTICAL CHEMISTRY
and
INTERFACIAL ELECTROCHEMISTRY

AN INTERNATIONAL JOURNAL DEVOTED TO ALL
ASPECTS OF ELECTROANALYTICAL CHEMISTRY,
DOUBLE LAYER STUDIES, ELECTROKINETICS,
COLLOID STABILITY AND ELECTRODE KINETICS

EDITORIAL BOARD

- | | |
|--|--|
| J. O'M. BOCKRIS (<i>Philadelphia, Pa.</i>) | J. LYKLEMA (<i>Wageningen</i>) |
| G. CHARLOT (<i>Paris</i>) | G. W. C. MILNER (<i>Harwell</i>) |
| B. E. CONWAY (<i>Ottawa</i>) | R. H. OTTEWILL (<i>Bristol</i>) |
| P. DELAHAY (<i>New York</i>) | J. E. PAGE (<i>London</i>) |
| A. N. FRUMKIN (<i>Moscow</i>) | R. PARSONS (<i>Bristol</i>) |
| L. GIERST (<i>Brussels</i>) | C. N. REILLEY (<i>Chapel Hill, N.C.</i>) |
| M. ISHIBASHI (<i>Kyoto</i>) | G. SEMERANO (<i>Padua</i>) |
| W. KEMULA (<i>Warsaw</i>) | M. VON STACKELBERG (<i>Bonn</i>) |
| H. L. KIES (<i>Delft</i>) | I. TACHI (<i>Kyoto</i>) |
| J. J. LINGANE (<i>Cambridge, Mass.</i>) | P. ZUMAN (<i>Prague</i>) |

VOL. 19

1968



ELSEVIER SEQUOIA S.A.
LAUSANNE

COPYRIGHT © 1968 BY ELSEVIER SEQUOIA S.A., LAUSANNE

PRINTED IN THE NETHERLANDS

APPLICATION OF THE METHOD OF TIME-DOMAIN REFLECTOMETRY TO THE STUDY OF ELECTRODE PROCESSES

RICHARD PAYNE

Air Force Cambridge Research Laboratories, L. G. Hanscom Field, Bedford, Mass. (U.S.A.)

(Received April 1st, 1968)

INTRODUCTION

Experimental observation of slow relaxation processes occurring in the metal-aqueous solution electrical double layer have been reported recently. BOCKRIS and coworkers¹⁻³ have been concerned with the frequency-dependence of the a.c. impedance, as measured by the bridge method at low audio frequencies, for mercury and other electrodes. The frequency dispersion has been attributed to a relaxation process characterised by a distribution of relaxation times centered about a time several orders of magnitude shorter than the time scale of the measurements. SCHULDINER and coworkers^{4,5}, on the other hand, have employed a conventional current-step method to evaluate the impedance at a platinum electrode, from which they conclude that equilibration of the double layer may take up to 30-100 nsec after perturbation. However, it is clear in both of these approaches that the experimental method is being extended up to, and possibly beyond, its limit. The development of improved techniques is, therefore, highly desirable for the extension of kinetic measurements of this kind. One such approach is the use of optical methods. Another is the improvement of the electrical pulse methods using the recently developed techniques of time-domain reflectometry (TDR)*. This is purely an instrumental advance which improves the time resolution of the measurements by the use of transmission line techniques and the sampling oscilloscope. In this paper, the application of the TDR method to the measurement of impedance at the electrode-solution interface is described. The results of measurements at platinum electrodes in aqueous solutions are discussed.

TIME-DOMAIN REFLECTOMETRY

The heart of the TDR method is the sampling oscilloscope which uses the stroboscopic principle to reconstruct a wave form from samples taken from successive cycles of a repeated waveform. In this way the limitation in bandwidth of conventional cathode ray tubes and amplifiers is overcome. Bandwidths extending from d.c. to several gigahertz are possible with currently available instruments ($1\text{GHz} = 10^9\text{ Hz}$). The principle of the sampling oscilloscope is illustrated in Fig. 1. The input waveform is sampled for a very short interval of time (less than 0.5 nsec) during which the waveform voltage is measured and recorded as a dot on the CRT with a Y-displacement

* Time-domain reflectometry is the name of a technique developed by the Hewlett-Packard Company for the pulse testing of transmission lines using the sampling oscilloscope.

corresponding to the voltage at that instant. The next sample is taken during a subsequent cycle at a slightly later time in the cycle, at which the X-displacement of the CRT spot has increased correspondingly. In this way the instrument reconstructs the waveform point by point using a large number of samples. The signal appears as a succession of closely spaced dots which trace out the original waveform.

The basic set-up for TDR is shown in Fig. 2. A square pulse generator with a fast rise time (1 nsec, or better) is connected to the system under test by a section of transmission line. The incident waveform and its reflection from the load is monitored on the transmission line by a probe and a pick-off tee inserted in the line. The pulse

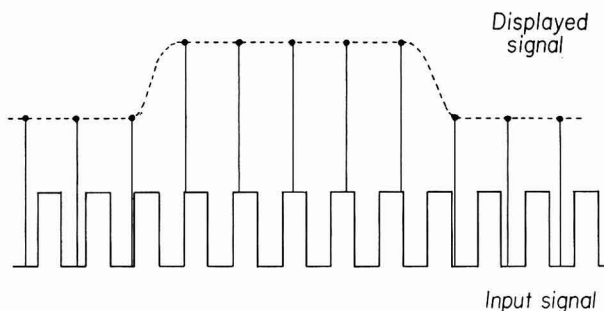


Fig. 1. Principle of the sampling oscilloscope.

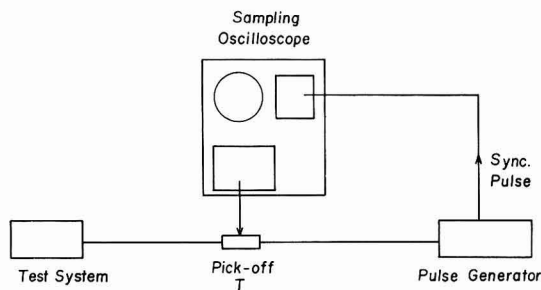


Fig. 2. Basic set-up for time-domain reflectometry.

generator repetition rate is synchronized with the oscilloscope by triggering pulses supplied either by the generator or the oscilloscope timing circuit. The oscilloscope "sees" the incident pulse and its reflection at the probing point separated in time by the interval required for the signal to travel from the probing point to the load, and return. For an air dielectric transmission line, the signal travels approximately at the speed of light in vacuo ($3 \cdot 10^8$ m/sec) so that the time delay between the arrival of the pulse and its reflection will be 3.3 nsec/m of line traversed in both directions, *i.e.*, from the probing point to the load and back again. Since the effective rise time of the sampling oscilloscope is only ~ 100 psec, it is possible to resolve reflections from impedance discontinuities on the line separated by no more than a centimeter or two. From the position (in time) of the reflection it is possible to determine the precise location of the discontinuity, while the nature of the impedance mismatch can be determined from an analysis of the shape of the reflected pulse. The application of this technique

to the study of electrochemical systems is obvious. By terminating the transmission line with a suitably designed electrochemical cell, the impedance of a working electrode can be measured at times of only a few nanoseconds or less after perturbation, simply by analysis of the reflection from the cell. It is not necessary to attach leads to the cell, which can, therefore, be completely isolated from the measuring instruments. The shape of the reflected pulse is characteristic of the terminating impedance producing the reflection. If the load is purely resistive, the reflected pulse has the same waveform but the amplitude and polarity depend on the value of the load resistance. This is illustrated in Fig. 3. When the load resistance (Z_L) is equal to the characteristic impedance (Z_0) of the transmission line (usually 50Ω) no reflection occurs, *i.e.*, all of the

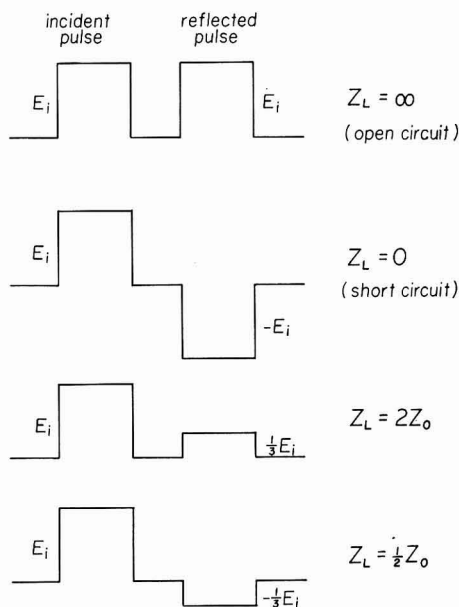


Fig. 3. Reflections from a purely resistive load (Z_L).

energy is absorbed. When Z_L is greater than Z_0 , the reflection is of the same polarity as the incident pulse, whereas for Z_L less than Z_0 the reflected pulse is inverted. The heights of the incident pulse (E_i) and the reflected pulse (E_r) are related through the equation⁶,

$$\rho = E_r/E_i = (Z_L - Z_0)/(Z_L + Z_0) \quad (1)$$

where ρ is the voltage reflection coefficient. The accurate measurement of ρ is the basis of a method of determining the characteristic impedance of the line using terminating resistors calibrated at d.c. Alternatively, the terminating resistance can be measured in terms of the known characteristic impedance with an accuracy of $\sim 0.1\%$. When the length of the incident pulse exceeds the time (t_a) required for it to travel from the probing point to the load and return (assuming a mismatched load impedance) the reflected pulse will appear partially superimposed on the incident pulse. When the pulse length exceeds $2t_a$, they will be wholly superimposed. By using various com-

binations of delay time and load resistance, complex multiple pulse trains and staircase waveforms can readily be generated. This may have useful applications in the study of complex electrode reactions.

When the terminating impedance is complex as it usually will be in an electrochemical system, the reflection no longer has the same waveform as the incident pulse. The situation for series and parallel LR and RC networks is illustrated in Fig. 4. The combination that is of most interest in electrochemical applications is the series RC network where R represents the resistance of the electrolyte solution in a cell containing a microelectrode of interfacial capacitance, C , and a counter electrode of large area.

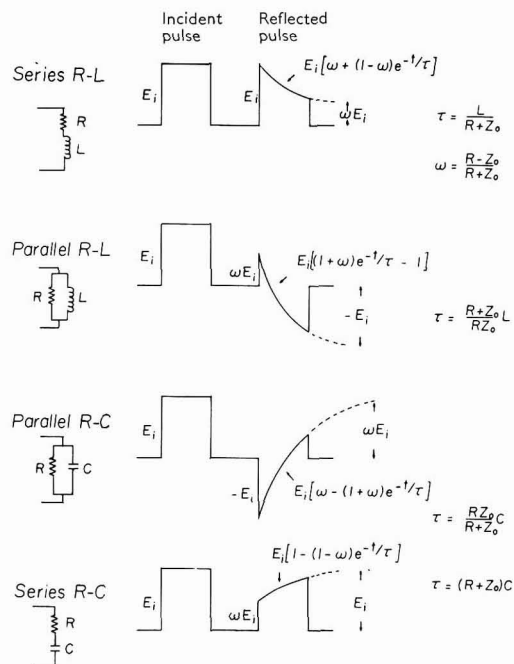


Fig. 4. Reflections from various complex impedance loads.

The response of this network to a voltage step function is as follows: at zero time (at the load) the capacitance appears as a zero impedance and the reflected wave steps to a value, $E_i(R-Z_0)/(R+Z_0)$ given by eqn. (1).

The capacitance subsequently charges through the load resistance and characteristic impedance of the line with a time constant (τ) equal to $(R+Z_0)C$. At infinite time, the capacitance is fully charged and appears as an open circuit so that the height of the reflected wave approaches E_i . The value of R can be determined from the reflected waveform by measuring the height of the initial step. The capacitance, C , then follows from the time constant obtained by measuring the time taken to complete a certain fraction of the exponential transition (e.g., $t_{0.5} = \tau \ln 2$). Alternatively, C can be obtained from the slope of the exponential charging curve at $t = 0$ which is easily shown to be⁷,

$$\left(\frac{dE_r}{dt}\right)_{t=0} = E_i \left[\frac{1}{\tau} \left(1 - \frac{R-Z_0}{R+Z_0} \right) \right] \quad (2)$$

A typical example of the response of a series RC network is shown in Fig. 5(c). The elements in this example were a 1/10 W carbon resistor of 23.5Ω and a 290-pF mica capacitor. Because R is smaller than the characteristic impedance of the line (50Ω) the initial step in the reflected wave is negative. The height of this step according to eqn. (1) should be 0.36 of the height of the incident pulse, or 1.5 cm, whereas, in fact, it is appreciably less. This is due to high frequency losses in the transmission line and the small loading effect of the probe, both of which must be taken into account in order to arrive at accurate values for the impedance. This is especially true in electrode impedance measurements where the capacity will usually be at least

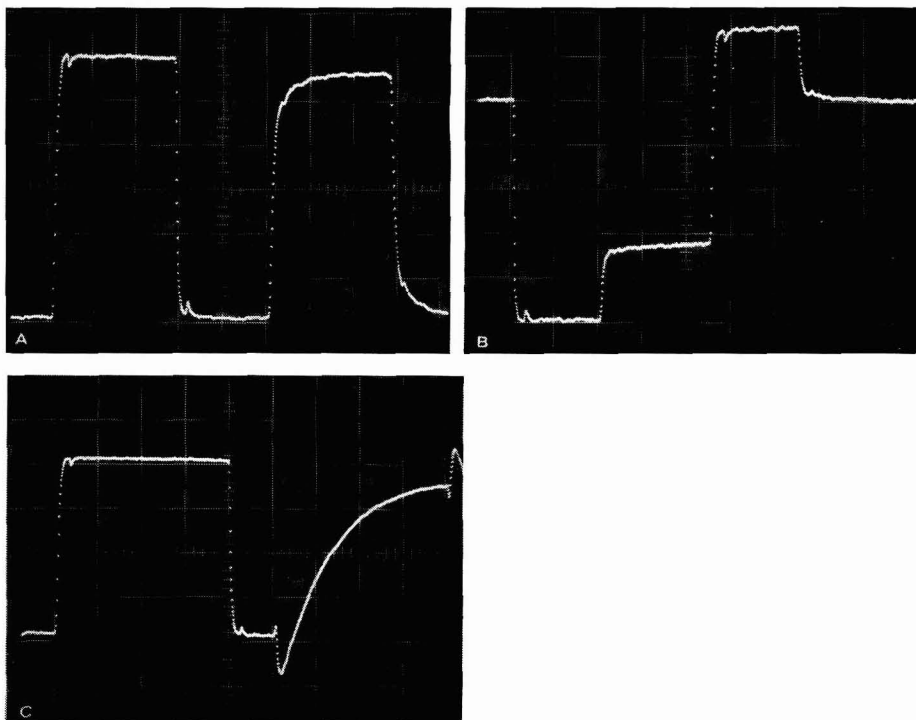


Fig. 5. (a), Reflection of a 60-nsec pulse from an open circuit load through a 50-nsec cable (RG 58C/U) showing rounding due to high frequency losses in the cable; (b), Complex waveform generated by superimposing reflection from a 200- Ω load on 90-nsec incident pulse. Load and probing point separated by 20 nsec cable. (c), Reflection of an 80-nsec pulse from series RC load (23.5Ω and 290 pF) through 50 nsec cable (RG-8A/U). Sweep rate, 20 nsec/cm.

a factor of ten larger so that only the initial stages of the exponential charging curve will be available for measurements. It is in this time region that the effects of high frequency line losses are significant. This problem can be circumvented by using a low loss transmission line, *i.e.*, an air dielectric line between the cell and the probing point. However, a 100-nsec time separation of incident and reflected waves would require an air transmission line of ~ 15 m length, which is inconveniently long. It is preferable, therefore, to eliminate this section of line completely. The reflected wave then appears superimposed on the incident wave. This has the disadvantage that the incident and

reflected waveforms cannot be viewed simultaneously. However, the shape of the incident pulse can be checked easily by replacing the cell by a standard $50\text{-}\Omega$ load. This procedure was followed in the measurements described below.

Cell design for electrode impedance measurements

The design of an electrochemical cell for TDR measurements raises a number of problems. The need to minimise the residual inductance of the electrode leads means that the dimensions of the cell must be as small as possible. The importance of this is illustrated by the fact that a 1 cm length of 26 S.W.G. wire has a self inductance of $\sim 0.01\ \mu\text{H}$ and an inductive impedance of $60\ \Omega$ at a frequency of 1GHz. This is sufficient to cause a significant reflection resulting in degradation of the electrode charging curve at short times. A further important problem is that of generating sufficient current density at the working electrode to produce a measurable potential change at short times. For example, in order to inject a charge density of $1\ \mu\text{C}/\text{cm}^2$ in a time of 1 nsec,

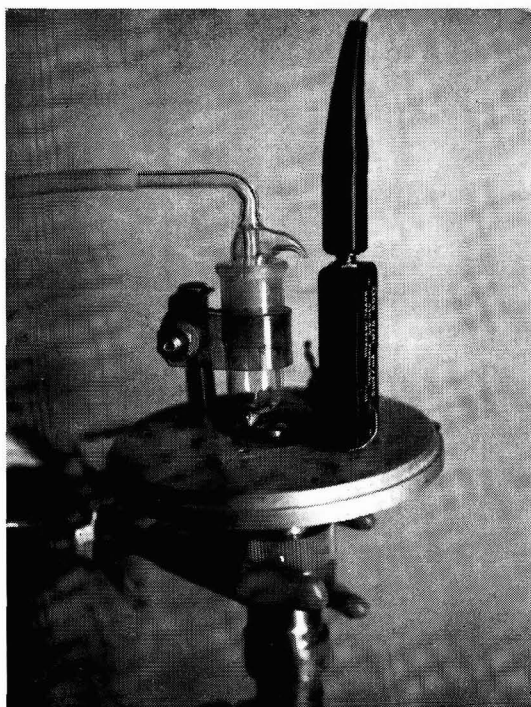


Fig. 6. Cell for electrode impedance measurements, mounted on General Radio type 874-ML component mount. The current transformer can be seen on the right.

a current density of $1000\ \text{A}/\text{cm}^2$ is required. Since the current capabilities of presently available pulse generators is usually no more than 200 mA, it is necessary to reduce the electrode area to $\sim 10^{-3}\ \text{cm}^2$ in order to achieve the required current density.

The cell used for the measurements described below is shown in Fig. 6. Its volume was approximately 1 ml. Platinum microelectrodes with geometric surface areas of $\sim 10^{-3}\ \text{cm}^2$ were prepared from 36 S.W.G. C.P. platinum wire sealed into a

Pyrex bead and clipped as close to the seal as possible. The remaining stub was then melted into a hemispherical electrode. The area of the electrode was calculated, assuming hemispherical shape, by measuring the diameter microscopically. Although cells were designed with a third (reference) electrode for galvanostatic measurements (described below) there is no advantage in the three-electrode arrangement since the iR drop in the cell cannot be isolated. This is because most of the iR drop occurs in the immediate vicinity of the microelectrode which is not accessible because of its minute size. In order to achieve accurate results it is advantageous to minimise the cell resistance. For this reason the preliminary measurements reported here were made with concentrated acid electrolytes. The series resistance was usually close to 20Ω .

In order to minimise the working electrode to reference electrode impedance, it was necessary to place the electrodes in the same compartment. Both counter and reference electrodes were platinised platinum wire hydrogen electrodes which could be checked against one another. The cell was held by a post and clip on a General Radio type 874-ML coaxial component mount. The counter electrode at the base of the cell was attached by a screw directly to the center conductor while the working electrode was usually grounded on the platform making the lead as short as possible. In experiments requiring current measurements, the working electrode lead was threaded through a Tektronix type CT1 current transformer before grounding. This enabled the current to be measured with minimum interference with the circuit.

Instrumentation

The sampling oscilloscope used in this work was the Tektronix, Model 661 with Type 4S2 sampling unit. The overall rise time of the system is 100 psec. The signal was picked off the transmission line through a coaxial tee (Tektronix Type VP1) using a passive probe (Tektronix, Types P6034 and P6035). The pulse generator normally used was a Hewlett-Packard, Type 215A (Pulse length 0–100 nsec, rise time 1 nsec). For certain experiments, a generator with a higher power capability (200 W) but longer rise time (15 nsec), a Hewlett-Packard, Type 214A was used. The transmission line consisted of a 5-nsec section of RG8A/U cable connected between the pulse generator and pick-off tee. In order to avoid high frequency cable losses the cell (mounted on a General Radio component mount, Type 874ML) was usually placed directly on the pick-off tee for TDR measurements. Under these conditions the reflection appears superimposed on the incident pulse with only a very small (~ 600 psec) displacement. For galvanostatic measurements the cell current was measured by means of a current transformer (Tektronix Type CT1 through which the grounded (microelectrode) lead of the cell was threaded. The lower frequency limit of the CT1 is 35 kHz: no noticeable droop in the square wave occurred for pulse lengths of up to 100 nsec. For longer pulses (214A generator) the current was measured by the voltage drop across a 0.1-Watt $10\text{-}\Omega$ resistor inserted in the ground lead. The voltage measuring probe in these experiments was placed directly either on the counter electrode or a third (reference) electrode with the probe case grounded through a clip attached to the cell mount. All connections on the line were made with General Radio, Type 874 connectors.

Control of the potential of the working electrode was achieved by external biasing applied to the transmission line at the generator output in the direct shunt feed mode using a second tee connector and a P6034 probe. Small distortions of the pulse waveform introduced by the biasing voltage could be compensated by adjust-

ment of the pulse shape controls. The applied potential could be measured at the cell using a Hewlett-Packard Type 3440A digital voltmeter under no-pulsing conditions.

RESULTS

The electrode capacitance at a platinum microelectrode in aqueous solutions of HClO_4 (1.3 M) and H_2SO_4 (5 M) was measured with current densities in the range 30–500 $\text{A}/\text{geometric cm}^2$ and pulse lengths of 10–100 nsec and 0.1–1 μsec . The time- and potential-dependence of the capacitance were investigated in the range 0–100 nsec and 0–1.5 V (*vs.* R.H.E.) respectively. In all measurements, the solution was saturated with hydrogen so that the measured potentials refer to a hydrogen reference electrode in the same solution. Solutions were purified before use by circulation over charcoal for a period of several days. As a check of the effectiveness of this procedure for the removal of organic impurities, the capacitance at a hanging mercury drop was measured in the solution as a function of potential and time. In the unpurified HClO_4 solutions the capacitance at the mercury drop was observed to fall rapidly to a low value, whereas in the purified solutions the capacitance was stable for long periods and was in excellent agreement with values obtained with a dropping electrode. Subsequent measurements with platinum electrodes gave values for the capacitance of $\sim 20 \mu\text{F}/\text{cm}^2$, or higher, which could not be significantly changed by anodic cleaning. It was concluded, therefore, that the charcoal extraction procedure was effective in purifying the solutions. As a further check, the electrode was subjected to a potentiostatically controlled cyclic linear potential sweep. No time variation or obvious signs of electrode contamination were found.

In order to reduce errors due to transmission line losses at high frequencies, the reflection from the impedance mismatch at the cell was normally viewed superimposed on the incident square pulse as mentioned earlier. A typical oscilloscope display is shown in Fig. 7. The initial transient peak is partly due to a reflection from the residual inductance of the cell leads and partly due to the fact that incident and reflected

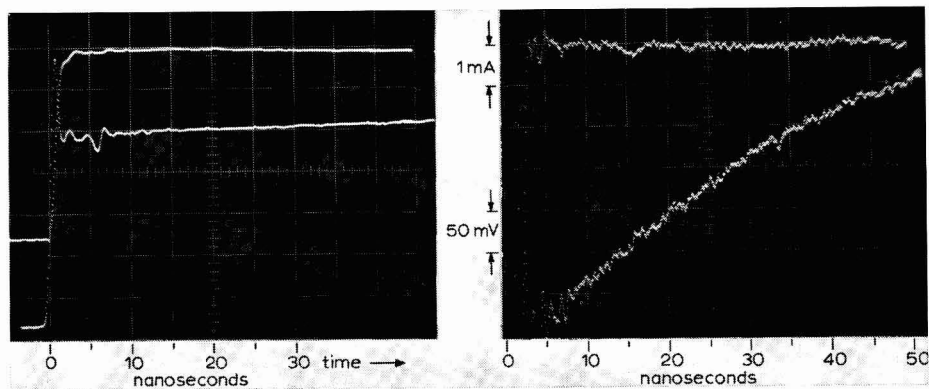


Fig. 7. Current step (upper trace, 20 mA/cm^2) and potential transient (0.5 V/cm) measured at the cell for a Pt electrode in 1.29 M HClO_4 . $E_H = 0.51$ V, $i = 77 \text{ A}/\text{cm}^2$.

Fig. 8. Current step (upper trace, 1 mA/cm^2) and potential transient (50 mV/cm) measured at the cell for a Pt electrode in 1.29 M HClO_4 . $E_H = 0$, $i = 61 \text{ A}/\text{cm}^2$.

pulses are not exactly superimposed because of the small but finite distance between the probing point and the load. The leading edge of the incident pulse is, therefore, not quite cancelled by the overlapping reflection. The inverted spike at 6 nsec occurs in all the measurements and is due to the reflection from a small capacitive mismatch at the oscilloscope connector which is subsequently re-reflected from the probe. This, unfortunately, limits the accuracy of measurements at times shorter than 10 nsec. The reflection can, however, be shifted to longer times by extending the probe cable with a suitable length of matched transmission line, although in practice the use of anything other than air line for this purpose can result in serious errors due to high frequency losses.

Since the object of this work was the investigation of dielectric relaxation processes in the double layer which, if they occur, should be evident as a time-dependence of the capacitance at short times, it was felt that a current step rather than a voltage step would provide a less ambiguous approach. Under galvanostatic conditions the potential transient for an ideal condenser (*i.e.*, no relaxation process) should be linear of slope i/C , where i is the current density and C the capacitance per unit area. Under such conditions, curvature of the potential-time transient would indicate a time-dependent capacitance and would be easy to verify. For a potential step, on the other hand, the charging is exponential and is, therefore, curved in the ideal case. Additional curvature due to time-dependence of the capacitance might, therefore, be difficult to detect. For this reason, most of the measurements reported were obtained by the current step method. Adequate constant current pulses could be obtained from the 215A generator by adjustment of the front panel pulse shape controls. A typical example of electrode polarisation with a current step and the resultant potential transient is shown in Fig. 8. The transient in this case is actually curved for reasons discussed below.

Application of d.c. bias to the line for the purpose of varying the electrode potential resulted in some deterioration of the pulse top flatness which could only be partially compensated by the pulse shape controls. In such cases, the pulse top variations were never more than 2% of the pulse height which would have no detectable effect on the condenser charging. Unfortunately, however, the potential transient is superimposed on a large iR pulse which is sensitive to small variation in the current pulse top and which, for reasons mentioned earlier, cannot be significantly reduced. The resultant distortion, however, was usually small and could be corrected for, although this remained a major source of inaccuracy. It should be mentioned that less than 10% of the current pulse is shown in Fig. 8 and that the potential transient is superimposed on an iR drop of no less than 2 V. Direct display of such large signals without overloading the amplifiers is a special advantage of the sampling oscilloscope. The bulk of this signal is backed off internally. The height of the pulse is measured with high accuracy by monitoring the backing-off voltage externally while using the full magnification of the system. This procedure was normally followed in order to measure the height of the current and iR pulses and also the applied potential using the 3440A voltmeter.

Anodic current and potential transients of the type shown in Fig. 8 were recorded over a potential range, 0–1.5 V. Corrections for variations in the current pulse top were made, where necessary, before measuring the slope. Within the experimental precision of the measurement (estimated at $\pm 10\%$) the measured capacitance was

time-independent in the range 1–100 nsec at all potentials, with the notable exception of the reversible hydrogen potential where the capacitance increased with time above ~ 30 nsec. The results were also substantially independent of the polarity of the pulse, again with the exception of an electrode held at the reversible hydrogen potential where a cathodic pulse resulted in a larger apparent capacitance at times greater than ~ 50 nsec. Finally, the results were normally independent of the repetition rate of the pulses. This is to be expected for a 100-nsec pulse repeated at a frequency of 1 kHz (the usual experimental rate) since the duty cycle (ratio of on to off time) is only 0.01%. Under these conditions, the electrode has ample time to return to equilibrium

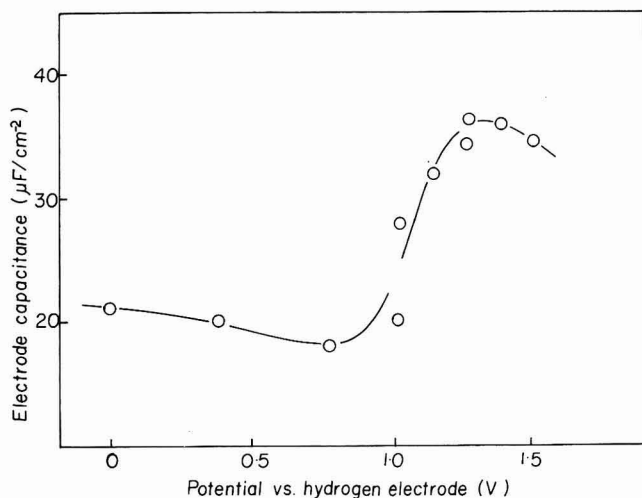


Fig. 9. Apparent capacitance at short times (< 50 nsec) for a Pt electrode in 5 M H₂SO₄ as a function of potential.

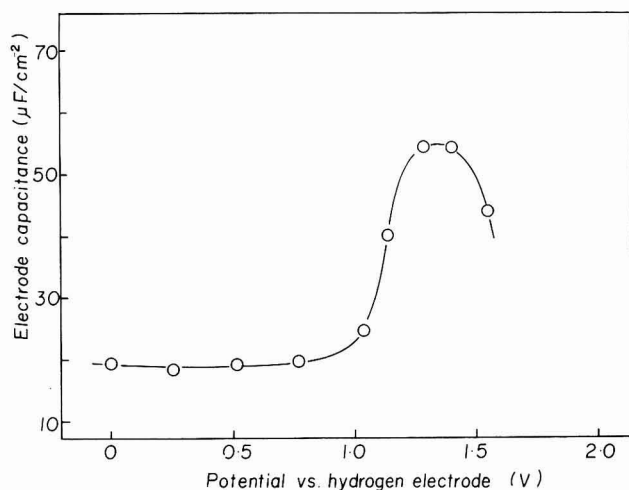


Fig. 10. Apparent capacitance at short times (< 50 nsec) for a Pt electrode in 1.29 M HClO₄ as a function of potential.

in between pulses. For an electrode at the hydrogen potential, however, repetition rate effects were readily noticeable for the longer pulses. These effects were traceable to the electrode reaction and are further discussed below.

The measured capacitance is plotted as a function of the applied potential in Fig. 9 ($5 M H_2SO_4$) and Fig. 10 ($1.3 M HClO_4$). The variation in both systems is similar. In the potential range $0 < E < 1.0 V$ the capacitance is $\sim 20 \mu F/cm^2$ and is approximately independent of the potential. At more positive potentials, the capacitance rises sharply to a maximum value of $40\text{--}50 \mu F/cm^2$. This behavior is in qualitative agreement with high frequency a.c. measurements reported by BECKER AND BREITER⁸ and BRINTSEVA AND KABANOV⁹ for H_2SO_4 solutions. Various interpretations of the capacitance rise have been proposed. The present results show that it is almost certainly a true ionic double-layer effect rather than a Warburg type of pseudocapacitance which could only arise at such short times from a process having an extraordinarily high exchange current.

The increase of the capacitance of the reversible hydrogen potential at times > 30 nsec is undoubtedly the effect of the hydrogen electrode reaction. This is suggested by the difference between anodic and cathodic pulsing and confirmed by the effect of hydrogen gas flow on the capacitance. Figure 11 shows a series of consecutive potential transients for constant current pulses of $1\text{-}\mu$ sec duration and $81\text{-}A/cm^2$ current density. The uppermost trace was obtained after very rapid anodic pulsing with the gas flow cut off, resulting in depletion of hydrogen on and in the vicinity of the electrode. The slope of this trace is equivalent to a capacitance of $\sim 200 \mu F/cm^2$.

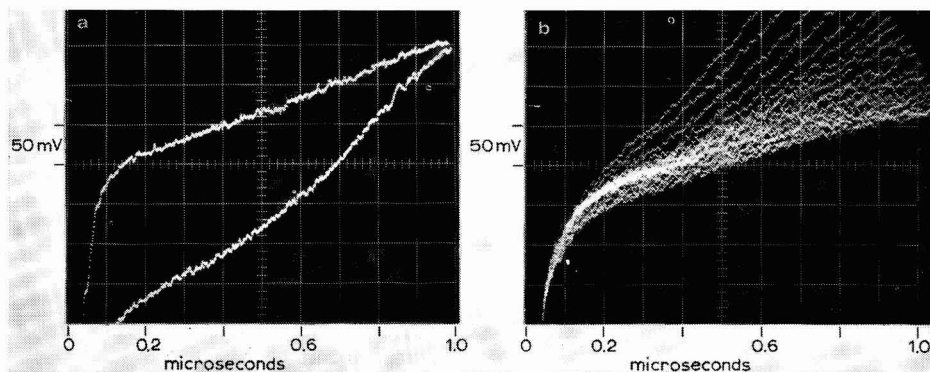


Fig. 11. Effect of hydrogen electrode reaction on Pt electrode capacitance in $5 M H_2SO_4$, potential transients for galvanostatic pulse ($i = 81 A/cm^2$). (a), Effect of pulse polarity; upper trace cathodic, lower trace anodic. (b), Slow equilibration of the electrode with hydrogen bubbling after rapid repeated anodic pulsing with hydrogen flow off.

Subsequent traces obtained at roughly one second intervals after restoring the gas flow, decreased in slope reaching a limiting value corresponding to a capacitance of $\sim 500 \mu F/cm^2$. The effect of hydrogen gas on the slope clearly extends down to times of ~ 50 nsec according to Fig. 11. By extrapolation of the linear slope at times below 50 nsec to longer times in traces like that in Fig. 8, it was estimated that roughly 30% of the charge goes into the electrode reaction at a current density of $\sim 70 A/cm^2$. From this, a first-order rate constant for the oxidation of adsorbed hydrogen of 10^5

cm sec⁻¹ was estimated assuming an initially saturated monolayer of 200 μC/cm². This is equivalent to an initial rate of 20 A/cm² compared with an exchange current of 0.54 A/cm² reported by PARSONS¹⁰ for the discharge step of the hydrogen evolution reaction on platinum (0.5 M HCl at 25°) and 2.3 A/cm² obtained by DOLIN AND ERSHLER¹¹ (1.0 M HCl). MUNSON¹² estimates a first-order rate constant in the range 30 – 3 · 10⁷ cm sec⁻¹ for the electrochemical desorption of adsorbed hydrogen or platinum. It seems reasonable to assume, therefore, that the observed increase of capacitance is due to oxidation of hydrogen adsorbed on the electrode.

DISCUSSION

The behavior of dielectrics in a rapidly changing electric field is well known from extensive studies of liquids and solid dielectrics¹³. The response of a typical dielectric with loss to a step field is illustrated in Fig. 12¹⁴. The polarisation increases

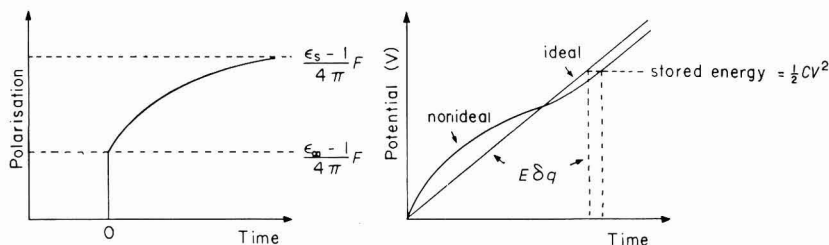


Fig. 12. Polarisation of a dielectric with loss by a step field.

Fig. 13. Constant current charging of a capacitor containing a dielectric with loss.

almost instantaneously at zero time to a value $(\epsilon_{\infty} - 1) F / 4\pi$ where ϵ_{∞} is the high frequency dielectric constant and F the applied field. This process which corresponds to electronic and atomic polarisation of the dielectric, is followed by the much slower polarisation of the molecular dipoles, which is substantially complete after a time, τ , the dipole relaxation time ($\sim 10^{-11}$ sec for water)¹³. Since the relaxation time is at least two orders of magnitude shorter than the time scale of the experiments described here, it is to be expected that no relaxation of the dielectric in the double layer would be observable in the accessible time range. There is, however, some reason to believe that the relaxation time in the double layer would be increased because of the constraints imposed by adsorption forces and the presence of other adsorbed species, although whether such effects could bring the dipole relaxation process within the accessible time range is a matter for experimental verification. BOCKRIS and coworkers¹⁻³ have concluded that the mean relaxation time for water dipoles in the double layer is $\sim 1 \mu\text{sec}$ (Hg electrode) or $0.1 \mu\text{sec}$ (Cu electrode) based on the frequency-dependence of the electrode impedance measured at audio frequencies. However, these conclusions are questionable in view of the long extrapolation of the time scale involved. Furthermore, it has been pointed out¹⁵ that the measurements can also be explained in terms of electrolyte penetration effects. It seems certain from the present measurements that no dielectric relaxation process occurs on a platinum electrode at such long times under the prevailing experimental conditions.

The response of a condenser containing a relaxing dielectric to a current step is

illustrated in Fig. 13. The ideal condenser is supposed to contain a structureless dielectric of dielectric constant equal to ϵ_s , the static dielectric constant of the real dielectric. The response of the ideal condenser will be a linear increase of the potential difference with time of slope i/C where i is the current density and C the capacity per unit area. The behavior of the real condenser is complex. The potential difference, E , at time, t , is given by:

$$E = \frac{4\pi x}{\epsilon} q \quad (3)$$

where x , ϵ and q are the instantaneous values of the thickness, dielectric constant and charge, respectively. The time-dependence of E follows by differentiation of eqn. (3),

$$\frac{dE}{dt} = \frac{4\pi x}{\epsilon} \left[i - q \left(\frac{\partial \ln \epsilon}{\partial t} + \frac{\partial \ln x}{\partial t} \right) \right] \quad (4)$$

Two limiting conditions can be noted:

(1) $t \ll \tau$; the dipoles are "frozen" and the last two terms in (4) vanish so that

$$\left(\frac{dE}{dt} \right)_{t \ll \tau} = \frac{4\pi x}{\epsilon_\infty} \quad (5)$$

The initial slope of the potential transient is, therefore, greater than the slope for the ideal condenser by a factor, $\epsilon_s/\epsilon_\infty$.

(2) $t \gg \tau$; the system is now in equilibrium so that ϵ is independent of time. Neglecting the variation of x with time, the slope of the potential transient is now given by

$$\left(\frac{dE}{dt} \right)_{t \gg \tau} = \frac{4\pi x}{\epsilon_s} \quad (6)$$

At a given time ($\gg \tau$) the real condenser will have absorbed a greater charge than the ideal condenser in charging to a given potential (see Fig. 13). The difference in the energy supplied ($E \delta q$) is evidently the energy dissipated as heat in the relaxation process. The general shape of the potential transient for constant current charging of a condenser containing a relaxing dielectric is expected to be sigmoid as shown in Fig. 13. It should be emphasised that at times shorter than τ the slope will be greater, corresponding to a lower apparent capacitance.

The recent galvanostatic pulse measurements of SCHULDINER and coworkers^{4,5} for platinum electrodes in various aqueous solutions do not seem consistent with this predicted behavior. In all systems studied, the slope of the potential transient was zero at short times, *i.e.*, the trace was *convex* rather than *concave* to the time axis. This is equivalent to an infinite differential capacitance at short times, which is difficult to reconcile with current theories of the double layer. The interpretation placed on these results also seems questionable. The "perturbation time", during which the electrode potential is observed to remain constant while charge flows into the electrode, obviously cannot be attributed to slow ionic relaxation since the ions themselves carry the charge. Furthermore, slow relaxation of the ionic atmosphere results in an increase in the conductance¹⁶. Such effects would in any case be unnoticeable at the concentrations and times involved in these measurements^{16,17}. If the ions were effectively "frozen" or if the dielectric were completely nonpolarisable at times within the accessible range, this would be manifest by the inability of the system to accept charge. The

first condition is possible at sufficiently short times and/or low concentrations. However, the second condition is hypothetical since the permittivity can never be less than unity. In view of the theoretical objections and the disagreement with the TDR measurements, which show normal behavior, these results should be viewed with caution.

Future work

The most obvious application of the TDR method in electrochemical studies is the measurement of rates of very fast reactions. First-order rate constants in excess of 1000 cm sec^{-1} are within the range of the method. However, the application to problems in the area of double layer is of greater theoretical importance. This will require extension of the measurements to mercury electrodes for which the structure of the double layer is much better understood. Of special theoretical interest is the possibility of detecting dipole reorientation, which is generally thought to be responsible for the capacity humps occurring in both aqueous and nonaqueous solvent systems. A start has been made in this direction. The results of TDR impedance measurements at a mercury electrode will be given in a future publication.

SUMMARY

1. A technique has been developed for the application of the methods of time-domain reflectometry to measurements of electrode impedance in electrochemical systems.

2. The impedance has been measured at a platinum electrode in aqueous HClO_4 and H_2SO_4 solutions. The capacitance is normally independent of time in the range 1–100 nsec except at the reversible hydrogen potential where the effect of the electrode reaction results in a time-dependent decrease of the electrode impedance at times > 30 nsec. No detectable relaxation of the double layer occurs within the time range of the experiments.

REFERENCES

- 1 J. O'M. BOCKRIS, W. MEHL, B. E. CONWAY AND L. YOUNG, *J. Chem. Phys.*, 25 (1956) 776.
- 2 J. O'M. BOCKRIS AND B. E. CONWAY, *J. Chem. Phys.*, 28 (1958) 707.
- 3 J. O'M. BOCKRIS, E. GILEADI AND K. MÜLLER, *J. Chem. Phys.*, 44 (1966) 1445.
- 4 S. SCHULDINER AND C. H. PRESBREY JR., *J. Electrochem. Soc.*, 111 (1964) 457.
- 5 B. J. PIERSMA, S. SCHULDINER AND T. B. WARNER, *J. Electrochem. Soc.*, 113 (1966) 1319.
- 6 H. H. SKILLING, *Electric Transmission Lines*, McGraw-Hill, New York, 1951.
- 7 *Time-Domain Reflectometry*. Hewlett Packard Company Application Note 62.
- 8 M. BECKER AND M. BREITER, *Z. Elektrochem.*, 60 (1956) 1080.
- 9 T. P. BRINTSEVA AND B. N. KABANOV, *Dokl. Akad. Nauk. SSSR*, 132 (1960) 868.
- 10 R. PARSONS, *Trans. Faraday Soc.*, 56 (1960) 1340.
- 11 P. DOLIN AND B. V. ERSHLER, *Acta Physicochim. USSR*, 13 (1940) 747.
- 12 R. A. MUNSON, *J. Phys. Chem.*, 66 (1962) 727.
- 13 C. P. SMYTH, *Dielectric Behavior and Structure*, McGraw Hill Book Company, New York, 1955.
- 14 H. FROHLICH, *Theory of Dielectrics*, Oxford University Press, Oxford, 1949.
- 15 R. DELEVIE, *J. Chem. Phys.*, 47 (1967) 2509.
- 16 O. M. ARNOLD AND J. W. WILLIAMS, *J. Am. Chem. Soc.*, 58 (1936) 2613.
- 17 G. C. BARKER, *J. Electroanal. Chem.*, 12 (1966) 495.

A.C. POLAROGRAPHIC BASE-CURRENT DEPRESSIONS NOT DUE TO ADSORPTION

D. BRITZ

Department of Chemistry, State University of New York at Buffalo, Buffalo, N.Y. (U.S.A.)

H. H. BAUER

Department of Chemistry, University of Kentucky, Lexington, Ky. (U.S.A.)

(Received January 19th, 1968)

INTRODUCTION

In a.c. polarography, one often observes that the base-current (*i.e.*, the current in the presence of only the supporting electrolyte) is lowered in some potential regions in the presence of the electroactive species; this is usually ascribed to adsorption of the electroactive species, with consequent lowering of the double-layer capacity. At the potential of the a.c. wave, the current exceeds the base-current. Figure 1 shows, schematically, the type of polarogram obtained with *m*-nitrophenol at pH 12 (discussed in detail elsewhere¹); the *m*-nitrophenol is adsorbed at potentials more positive than the a.c. wave and lowers the base-current in this region.

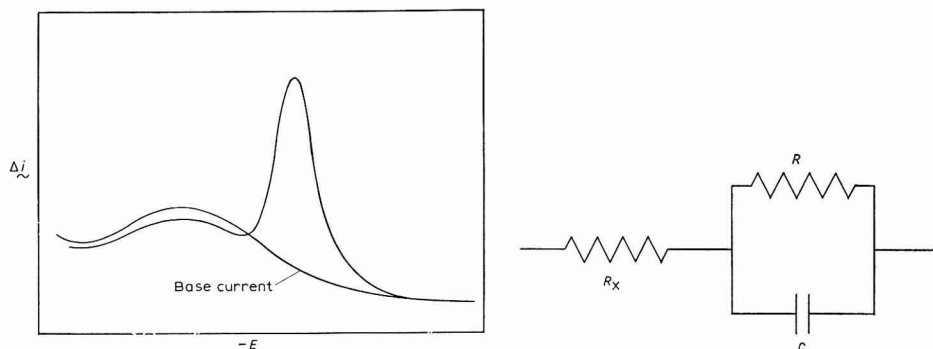


Fig. 1. Schematic a.c. polarogram of an adsorbable electroactive species.

Fig. 2. Equivalent high-frequency network of a polarographic cell.

While making accurate impedance measurements on this system, however, we observed a different kind of base-current depression: this occurred at high frequencies (2000 Hz and higher) and was a depression at a potential where the system showed a wave at low frequencies. This depression was greater than that caused by adsorption at other potentials, and investigation showed that it was not an adsorption effect, but a consequence of the vectorial addition of the series-resistance, the

double-layer reactance and faradaic-impedance vectors. REHBACH AND SLUYTERS² have discussed this type of effect briefly in general terms; it is the purpose of this paper to enquire into the phenomenon in more detail and to present some quantitative conclusions to aid in the interpretation of base-current lowering in practice.

THEORY

At this stage, the faradaic admittance will be regarded as purely resistive; this is not essential to the argument, but simplifies it. Comments on the general case are given at the end of this section.

The electrical network that is equivalent to the polarographic cell can then be represented as in Fig. 2. R_x is the series resistance, comprising the capillary and solution resistances, C the double-layer capacity and R the faradaic impedance, now a pure resistance. The faradaic admittance, or conductance, is R^{-1} ; in the absence of a reducible substance, $R^{-1}=0$, and in its presence, $R^{-1}>0$.

Consider the total impedance of the network, \vec{Z}_t , at a fixed angular frequency ω , as a function of the value of R^{-1} , for $0 \leq R^{-1} \leq \infty$. If \vec{Z}_{el} is the impedance of the parallel network formed by R and C , then \vec{Z}_t is given by:

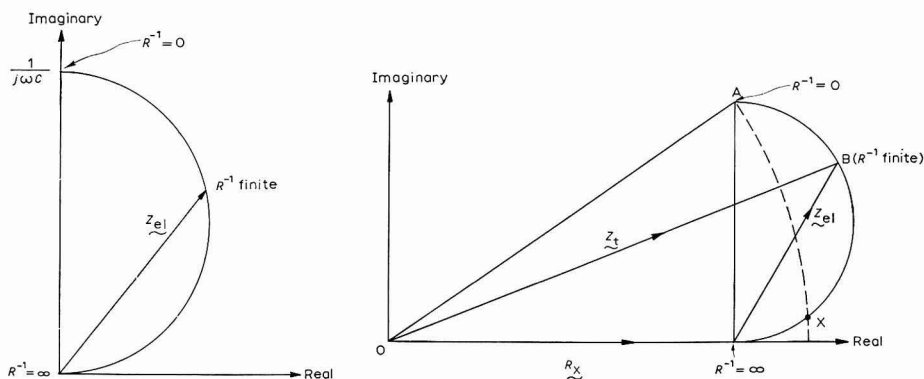
$$\vec{Z}_t = \vec{Z}_{el} + \vec{R}_x \quad (1)$$

where \vec{Z}_{el} is given by:

$$\vec{Z}_{el} = (R^{-1} - j\omega C)^{-1} \quad (2)$$

We note that for $R^{-1}=0$, $Z_{el} = (-j\omega C)^{-1}$ and for $R^{-1} \rightarrow \infty$, $Z_{el} \rightarrow 0$. In terms of a graphical vector representation, it is easy to show (see Appendix A) that, as we vary R^{-1} from zero to infinity, the vector \vec{Z}_{el} describes a semicircle (see Fig. 3).

Now, by eqn. (1) we add \vec{Z}_{el} to \vec{R}_x to obtain the total impedance, \vec{Z}_t ; this is shown in Fig. 4. The line OA is the impedance in the absence of a faradaic admittance



Figs. 3-4: Locus of (3) the electrode impedance, (4) the total cell impedance, as a function of R^{-1} .

or

$$\vec{Z}_t = R_x - (j\omega C)^{-1} \quad \text{for } R^{-1} = 0$$

and OB is the vector of \vec{Z}_t for a finite value of R^{-1} . We have drawn a dashed circular arc with radius OA and centre O; it is clear that for all values of \vec{Z}_t lying between point A and the point marked X, where the arc and the semicircle intersect, $OA < OB$. This means that for all corresponding values of R^{-1} , *the total impedance is greater than for $R^{-1} = 0$* . If we imagine, in Fig. 2, the value of R slowly decreasing from infinity, there will be an initial *increase* in the impedance of the total network.

It is of some interest to estimate the greatest possible increase, proportional to the impedance at $R^{-1} = 0$, that could be observed. It can be shown by simple algebra (see Appendix B) that the maximum magnitude of the vector \vec{Z}_t in Fig. 4 will be of that passing through the centre of the semicircle. Then,

$$|\vec{Z}_t| = \{R_x^2 + (2\omega C)^{-2}\}^{\frac{1}{2}} + (2\omega C)^{-1} \quad (3)$$

This expression is clearly a function (at a fixed frequency, ω) of R_x , or of the relative magnitudes of R_x and $(\omega C)^{-1}$. The proportional increase, r , is given by the maximum value of \vec{Z}_t as in eqn. (3) divided by the magnitude of line OA in Fig. 4, or

$$r = [\{R_x^2 + (2\omega C)^{-2}\}^{\frac{1}{2}} + (2\omega C)^{-1}] / \{R_x^2 + (\omega C)^{-2}\}^{\frac{1}{2}} \quad (4)$$

The maximum of r , r_{\max} , can now be calculated from the solution for R_x of the equation:

$$\left(\frac{\partial r}{\partial R_x}\right)_{\omega, C} = 0 \quad (5)$$

Differentiating eqn. (4) with respect to R_x , equating with zero and discarding trivial solutions, we obtain

$$R_x = \sqrt{2} \cdot (\omega C)^{-1} \quad (6)$$

Substitution for R_x in eqn. (4) gives:

$$r_{\max} = 2/\sqrt{3} = 1.154$$

Thus, the greatest possible increase in the impedance is 15.4%, or the greatest possible decrease in base-current is 13.4%.

Referring again to Fig. 3, it is seen that if the faradaic admittance is not purely resistive but has a phase-angle between zero and $\pi/2$, \vec{Z}_{e1} will not describe a semicircle but some other curve within the semicircle area. Many of these will still produce an increase in $|\vec{Z}_t|$, though not as great.

EXPERIMENTAL

The foregoing has been purely theoretical and appeared to be contrary to intuitive expectations. We performed the following experiment: a dummy cell was constructed from resistors and a capacitor; R_x was set at 150 Ω , C at 1 μF and R

was made variable. At the frequency 1600 Hz, R_x was thus equal approximately to $\sqrt{2} \cdot (\omega C)^{-1}$ and we should observe the greatest possible increase in impedance at some value of R at this frequency. The impedance of the network was measured by the technique used by us to measure the polarographic cell impedance³, as a function of the value of R , and the results are plotted in Fig. 5. The figure clearly shows that the impedance varies from 180 Ω , for $R = \infty$, first increases to a maximum of 202.5 Ω at $R = 100 \Omega$, and then decreases towards 150 Ω , the limiting value for $R = 0$. The proportional increase shows a maximum of approximately 15.4%, verifying the theory.

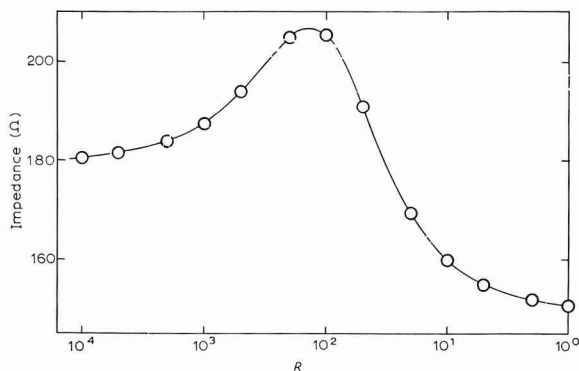


Fig. 5. Measured values of the total impedance of the dummy cell, against values of R .

COMPLEX-SHAPED POLAROGRAMS

REHBACH AND SLUYTERS² suggested that this phenomenon may produce a.c. polarograms of rather complex shape, showing, for example, depressions on either side of the wave peak; these authors did not, however, go further than to suggest schematically some possible shapes. We have performed some computations of a.c. polarographic waves, in order to find out what sort of polarograms one might observe under fairly "normal" conditions. To calculate these, we have assumed the equivalent electrical network as shown in Fig. 2, but with R now generalised to a faradaic admittance, \vec{Y}_f . The equations for the magnitude $|\vec{Y}_f|$ and the phase quantity, $\cot \phi$, are those given by BREYER AND BAUER⁴. The following quantities were assumed:

$n = 2$ (the number of electrons transferred)

$A = 5 \cdot 10^{-2} \text{ cm}^2$ (DME area)

$d = 1$ (the ratio of the diffusion coefficients of the oxidised and reduced species)

$D = 10^{-5} \text{ cm}^2 \text{ sec}^{-1}$ (diffusion coefficient)

$\alpha = 0.5$ (transfer coefficient)

$T = 300^\circ \text{ K}$

$C_{\text{ox}} = 10^{-3} \text{ M}$ (bulk concentration of the oxidised species)

$R_x = 100 \Omega$ (series resistance)

$C = 0.5 \mu\text{F}$ (double-layer capacity)

k , the heterogeneous rate constant, was given a range of values. The computations

were programmed in Fortran and carried out on an IBM 7044 electronic computer. A family of a.c. polarograms so computed is shown in Fig. 6, for a range of frequencies and for $k=0.03 \text{ cm sec}^{-1}$. The figure shows that the transition from a positive wave to a pure depression gives rise to polarograms with adjacent base-current depressions. If a polarogram such as that at 2000 Hz were observed experimentally, the observer might well have concluded that the depressions were caused by adsorption.

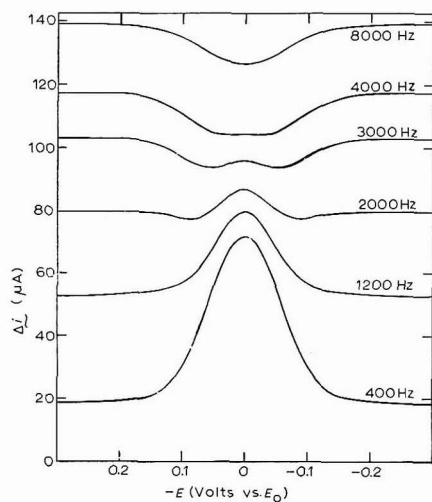


Fig. 6. Computed a.c. polarograms at some (marked) frequencies for $k=0.03 \text{ cm sec}^{-1}$, $R_x=100 \Omega$, $C=0.5 \mu\text{F}$.

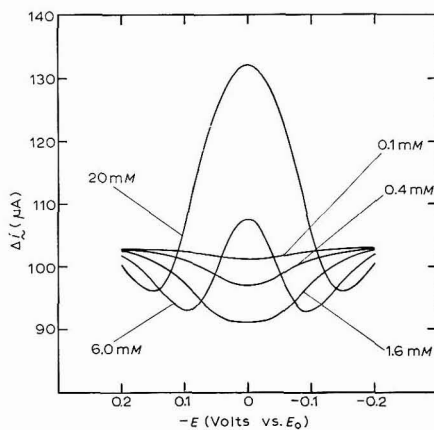


Fig. 7. Computed a.c. polarograms at 3000 Hz, and $k=0.01 \text{ cm sec}^{-1}$, for some concns. (marked, in mM)

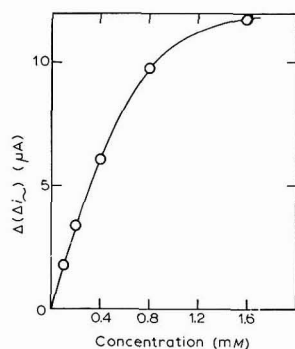


Fig. 8. Base-current depression at E_0 for the system in Fig. 7, against concn.

EFFECT OF CONCENTRATION

Figure 7 shows some computed polarograms at 3000 Hz, for $k=0.01 \text{ cm sec}^{-1}$, for a range of concentrations of the electroactive species. It is seen that at low concentrations only a depression appears; as the concentration increases, the depression at first deepens, and then develops a central positive wave. A plot of base-

current depression against concentration up to 1.6 mM is shown in Fig. 8—the curve is not unlike an adsorption isotherm and could, in practice, be mistaken for one, unless still higher concentrations were used, showing a subsequent decrease of the depression.

We conclude, then, that depressions in the base-current at or near an a.c. polarographic wave may be caused by the above-described phenomenon and need not be due to adsorption. In such cases, although the measured currents or impedances appear anomalous, calculation of the faradaic admittance will of course still yield significant results, within the experimental limits.

APPENDIX A

From eqn. (2),

$$\vec{Z}_{e1} = \mathbf{1}/(R^{-1} - j\omega C) = (R^{-1} + j\omega C)/(R^{-2} + \omega^2 C^2)$$

The real and imaginary parts of \vec{Z}_{e1} are therefore respectively

$$\text{Real}(\vec{Z}_{e1}) = R^{-1}/(R^{-2} + \omega^2 C^2) \quad (\text{A1})$$

$$\text{Imag.}(\vec{Z}_{e1}) = \omega C/(R^{-2} + \omega^2 C^2) \quad (\text{A2})$$

The magnitude of \vec{Z}_{e1} , consequently, is

$$\begin{aligned} |\vec{Z}_{e1}| &= [\{\text{Real}(\vec{Z}_{e1})\}^2 + \{\text{Imag.}(\vec{Z}_{e1})\}^2]^{\frac{1}{2}} \\ &= (R^{-2} + \omega^2 C^2)^{-\frac{1}{2}} \end{aligned} \quad (\text{A3})$$

and the phase angle θ of the impedance, \vec{Z}_{e1} , with respect to the real axis is given by:

$$\tan \theta = \omega CR \quad (\text{A4})$$

Now, \vec{Z}_{e1} describes a semicircle as in Fig. 3 if

$$(\mathbf{1}/\omega C)\cos(\pi/2 - \theta) = |\vec{Z}_{e1}|$$

i.e., if

$$(\mathbf{1}/\omega C)\sin \theta = |\vec{Z}_{e1}| \quad (\text{A5})$$

From (A4),

$$\sin \theta = \omega CR / (\mathbf{1} + \omega^2 C^2 R^2)^{\frac{1}{2}}$$

and (A5) becomes

$$|\vec{Z}_{e1}| = R / (\mathbf{1} + \omega^2 C^2 R^2)^{\frac{1}{2}}$$

which is identical with (A3). Therefore, \vec{Z}_{e1} does describe a semicircle as shown.

APPENDIX B

From eqns. (A1) and (A2) we have, using eqn. (1)

$$\text{Real}(\vec{Z}_t) = R_x + R^{-1}/(R^{-2} + \omega^2 C^2) \quad (\text{B1})$$

$$\text{Imag}(\vec{Z}_t) = \omega C/(R^{-2} + \omega^2 C^2) \quad (\text{B2})$$

$$\begin{aligned} |\vec{Z}_t|^2 \cdot (R^{-2} + \omega^2 C^2)^2 &= \omega^2 C^2 + R^{-2} + 2R_x R^{-1}(R^{-2} + \omega^2 C^2) + R_x^2(R^{-2} + \omega^2 C^2)^2 \\ &= (R^{-2} + \omega^2 C^2)(1 + 2R_x R^{-1}) + R_x^2(R^{-2} + \omega^2 C^2)^2 \end{aligned}$$

For variation of R , $|\vec{Z}_t|$ reaches a maximum when

$$\frac{d}{dR} \{ (1 + 2R_x R^{-1}) / (R^{-2} + \omega^2 C^2) + R_x^2 \} = 0$$

i.e., when

$$-2R_x(R^{-2} + \omega^2 C^2)R^{-2} = -2(1 + 2R_x R^{-1})R^{-3}$$

i.e., when

$$R + R_x = R_x \omega^2 R^2 C^2 \quad (\text{B3})$$

Now from Fig. 4,

$$\text{Imag}(\vec{Z}_t)/\text{Real}(\vec{Z}_t) = (2\omega C)^{-1}/R_x \quad (\text{B4})$$

if \vec{Z}_t passes through the centre of the semicircle.

Combining (B1), (B2) and (B4) yields:

$$\omega C / \{ R_x(R^{-2} + \omega^2 C^2) + R^{-1} \} = 1/2R_x \omega C$$

which reduces to eqn. (B3). Thus, when \vec{Z}_t passes through the centre of the semicircle, $|\vec{Z}_t|$ is a maximum.

ACKNOWLEDGEMENT

We wish to thank the Computing Center of the State University of New York at Buffalo for generous donations of computer time.

SUMMARY

The phenomenon of base-current depression due to the vector addition of series resistance, double-layer capacity and faradaic admittance is examined quantitatively. The maximum possible decrease in base-current is found to be 13.4%. The effect was verified experimentally by measurements on a "dummy" cell network. Some complex-shaped a.c. polarograms have been computed, the effects of frequency and concentration of the electroactive species being examined.

REFERENCES

- 1 D. BRITZ AND H. H. BAUER, *Electrochim. Acta*, in press.
- 2 M. REHBACH AND J. H. SLUYTERS, *Rec. Trav. Chim.*, 80 (1961) 469.
- 3 D. BRITZ AND H. H. BAUER, *J. Sci. Instr.*, 44 (1967) 843.
- 4 B. BREYER AND H. H. BAUER, *Alternating Current Polarography and Tensammetry*, Interscience Publishers Inc., New York, 1963, p. 43.

J. Electroanal. Chem., 19 (1968) 15-22

STOFFTRANSPORT AN EINER DOPPELELEKTRODE IN DER WAND EINES STRÖMUNGSKANALS

RAINER BRAUN

Institut für Physikalische Chemie und Elektrochemie, Technische Hochschule, München (Germany)
(Eingegangen am 28 November, 1967; reversioniert am 28 Februar, 1968)

I. EINLEITUNG

Bei der Untersuchung von Elektrodenreaktionen stören häufig unkontrollierte Transportvorgänge. Die Herstellung definierter Strömungen des Elektrolyten bringt oft eine wesentliche Erleichterung, da hier der Transport quantitativ erfasst werden kann¹⁻³. Vielfach treten bei Elektrodenreaktionen instabile Reaktionsprodukte auf, deren Erfassung durch geeignete Anordnungen wesentlich vereinfacht wird. Ein Beispiel hierfür ist die von FRUMKIN *et al.*⁴ behandelte Ringscheibenelektrode. Ein anderes Verfahren wurde von GERISCHER *et al.*⁵ entwickelt. Der Elektrolyt strömt in einem Kanal mit rechteckigem Querschnitt. Die beiden Arbeitselektroden, E₁ und E₂, sind in eine Kanalwand eingebettet. Als Elektroden dienen zwei ebene Goldbleche der Dicke 10 μ , 100 μ oder 200 μ , die durch eine isolierende Folie von 5–15 μ Stärke voneinander getrennt sind. Dieses Elektroden-Paket wird senkrecht in einen PVC-Zylinder eingepasst und mit Araldit verklebt. Die Stirnfläche des so hergestellten Elektrodenblockes EB überschneidet man plan mit einem Mikrotom; so kann man die Elektrodenflächen auch rasch erneuern. Die übrigen Teile der Messzelle befinden sich in einem Führungsstück, in das der Elektrodenblock EB genau passt (Abb. 1). Die Zu- und Ableitungskanäle treffen schräg auf die Stirnfläche des Elektrodenblocks auf. Der eigentliche Strömungskanal entsteht dadurch, dass zwischen Elektrodenblock und Führungsstück eine Kunststoff-Folie bekannter Dicke gepresst wird, in die eine rechteckige Öffnung mit den Abmessungen des Kanals eingeschnitten ist (Abb. 2–3). Die Gegenelektroden, G₁ und G₂, liegen in Nebenkanälen des Führungsstücks. Von den Bezugslektroden, B₁ und B₂, führen elektrolytische Sonden in die Nähe der Messelektroden. Der stromaufwärts gelegene Stromkreis 1 wird über einen gewöhnlichen Potentiostaten betrieben. Das hier erzeugte Elektrolyseprodukt wird von der Strömung zur Elektrode E₂ transportiert und hier analysiert. Zur Vermeidung elektrischer Kopplungen betreibt man den Stromkreis 2 mit einem transistorisierten Potentiostaten ohne Erdschluss.

Die Anwendungsmöglichkeiten dieser Methode zu kinetischen Untersuchungen werden durch theoretische Abschätzungen beträchtlich erweitert. Das in der vorausgegangenen Arbeit⁵ dargestellte einfache Modell soll an dieser Stelle vertieft und durch weiterführende Betrachtungen ergänzt werden.

II. KONVEKTIVE DIFFUSION IM STRÖMUNGSKANAL

Auf Kanäle mit rechteckigem Querschnitt, deren Höhe $2b$ klein im Vergleich zur Kanalbreite a ist, lassen sich die Gesetze für den beiderseits unendlich ausgedehnten Kanal anwenden. Für Reynoldszahlen $Re = 2bv_0/\nu \leq 2300$ (v_0 = mittlere Durchflussgeschwindigkeit) bleibt die Strömung laminar⁶. Der Kanaleinlauf soll aus einem konvergenten Rohrstück bestehen, da hier Grenzschichtablösung und Wirbelbildung unterdrückt werden⁷. Die Einlaufstörung ist nach einer Einlauflänge von $l_E = 0.08 \cdot Re b$ abgeklungen⁸. Hier lautet die Geschwindigkeitsverteilung:

$$v_x = \frac{3}{2}v_0(y/b)(2-y/b) \quad \text{für } 0 \leq y \leq 2b \quad v_y = v_z = 0 \quad (\text{II.1})$$

(x-Achse in Strömungsrichtung, y-Achse senkrecht zur Kanalwand). An der Kanalwand gilt in guter Näherung

$$v_x \approx \left(\frac{\partial v_x}{\partial y} \right)_{y=0} \cdot y = 3v_0 y/b \quad \text{für } y \ll b \quad (\text{II.2})$$

Enthält die strömende Flüssigkeit eine gelöste Substanz, die einen Aktivitätsgradienten besitzt, so findet der Stofftransport über molekulare Diffusion und makro-

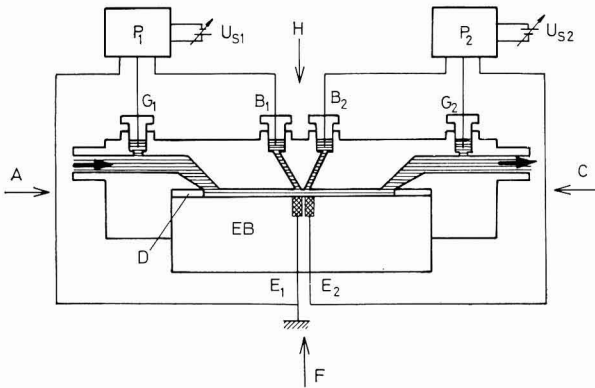


Abb. 1. Schematische Messanordnung. Index 1: Kreis 1; Index 2: Kreis 2. (P_1), Potentiostat; (P_2), erdfreier Potentiostat; (EB), Elektrodenblock; (D), Folie (Abstandshalter); (E), Messelektrode; (B), Bezugs elektrode; (G), Gegenelektrode; (U_s), Sollspannung.

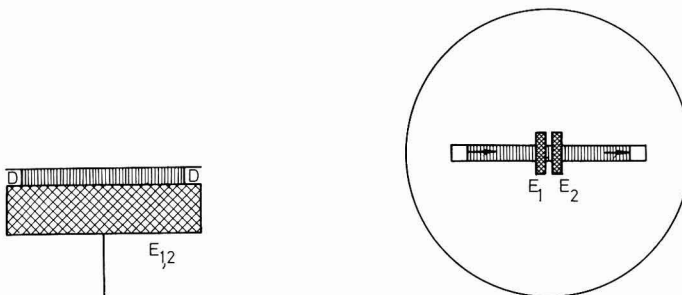


Abb. 2. Schnitt A-C in Aufsicht auf den Elektrodenblock mit Abstandshalter.

Abb. 3. Schnitt H-F durch den Strömungskanal.

skopische Flüssigkeitsbewegung statt. Dieser Vorgang heisst konvektive Diffusion. Ionen kann man bei hohem Leitsalzzusatz wie neutrale Partikel behandeln⁹. Da hier ausserdem Aktivitäts- und Diffusionskoeffizienten Konstanten sind, lautet die Gleichung der konvektiven Diffusion im stationären Fall für eine inkompressible Flüssigkeit

$$(\vec{v} \cdot \text{grad})c = D\Delta c \quad (\text{II.3})$$

Nachdem in wässrigen Lösungen die Prandtlsche Zahl, $\text{Pr} \approx 10^3$ und die Pecletzahl, $\text{Pe} = \text{RePr} \geq 10^4$ sind, beschränkt sich bei Elektrodenprozessen die Diffusion auf eine schmale wandnahe Zone¹⁰. Im Kanal überwiegt der konvektive Transport in Strömungsrichtung die Diffusion um Grössenordnungen, sodass Gl. (II.3) mit Gl. (II.2) folgenden Ausdruck ergibt:

$$\frac{3v_0 y}{b} \cdot \frac{\partial c}{\partial x} = D \cdot \frac{\partial^2 c}{\partial y^2} \quad (\text{II.4})$$

bzw.

$$\eta \frac{\partial c}{\partial \xi} = \frac{\partial^2 c}{\partial \eta^2} \quad \text{mit} \quad \xi = \frac{x}{l} \quad \text{und} \quad \eta = y \left(\frac{3v_0}{Dbl} \right)^{\frac{1}{3}} \quad (\text{II.5})$$

wobei l die Länge der Erzeugerelektrode ist.

III. DIFFUSIONSSTRÖME AN DER DOPPELELEKTRODE IM STRÖMUNGSKANAL

Für die mathematische Behandlung von Gl. (II.5) sei auf die Arbeiten von SUTTON¹¹ und ALBERY¹² hingewiesen.

Alle Konzentration beziehen sich auf die Ausgangskonzentration, c_0 . Läuft an der Erzeugerelektrode die Reaktion, $A \pm ne \rightarrow B$, im Bereich des Diffusionsgrenzstromes ab, so lauten die Randwerte für Gl. (II.5)

$$\xi = 0: c_A = 1; \quad \eta = 0: c_A = 0; \quad \lim_{\eta \rightarrow \infty} c_A = 1$$

Für $c_{A,1}$ erhält man als Funktion der Koordinaten $\xi = x/l$ und $\eta = y (D_A b l / 3v_0)^{\frac{1}{3}}$ die Beziehung:

$$c_{A,1}(\xi, \eta) = \frac{1}{\Gamma(\frac{2}{3})} \int_0^{\eta(9\xi)^{-\frac{1}{3}}} \exp(-u^3) du = E_{3\eta(9\xi)^{-\frac{1}{3}}} \quad (\text{III.1})$$

$E_{3(x)}$ ist die Fehlerfunktion dritten Grades nach der Definition der verallgemeinerten Fehlerfunktion

$$E_{n(x)} = \frac{1}{\Gamma(\frac{1+n}{n})} \int_0^x \exp(-\lambda^n) d\lambda \quad 13.$$

Die komplementäre Funktion soll als $Ec_{n(x)} = 1 - E_{n(x)}$ definiert werden. Gleichung (II.5) lautet in den hier verwendeten Koordinaten, ξ, η , für das Reaktionsprodukt B

$$\eta \frac{\partial c_B}{\partial \xi} = \frac{D_B}{D_A} \frac{\partial^2 c_B}{\partial \eta^2} \quad \text{mit der Lösung} \quad (\text{III.2})$$

$$c_{B,1}(\xi, \eta) = (D_A/D_B)^{\frac{2}{3}} E_{3\eta(D_A/9D_B\xi)^{-\frac{1}{3}}} \quad (\text{III.3})$$

Der Diffusionsgrenzstrom an der Erzeugerelektrode lautet in guter Übereinstimmung mit eigenen experimentellen Befunden:

$$I_{1,gr} = 1.16 n F c_0 (v_0/b)^{1/2} (D_A l)^{3/4} a = I_1 \quad (\text{III.4})$$

Für eine unendlich dünne Isolation kann man mit Hilfe der Methode von SUTTON¹¹ bei einer Elektrodenreaktion, $B \mp ne \rightarrow A$, an der Indikatorelektrode die Konzentrationsverteilung von B vor dieser Elektrode berechnen:

$$c_{B,2}(\xi, \eta) = (D_A/D_B)^{3/4} [E_{3\eta(D_A/9D_B)(\xi-1)^{-3/4}} - E_{3\eta(D_A/9D_B)\xi^{-3/4}}] \quad (\text{III.5})$$

Hat die Indikatorelektrode die Länge l_2 und ist $l_2/l = \lambda$, so ist die Stromausbeute Q für diesen Fall:

$$Q = -I_2/I_1 = 1 + \lambda^{3/2} - (1 + \lambda)^{3/2} \quad (\text{III.6})$$

Q hängt nicht von den Diffusionskoeffizienten der Stoffe A und B ab. Besitzt die Isolation eine endliche Dicke d bzw. $\vartheta = d/l$, so verläuft die Rechnung komplizierter. Dieser Fall wurde von MATSUDA behandelt¹⁴. Unabhängig von dieser Arbeit erhielten wir nach der Methode von ALBERY¹² das gleiche Resultat:

$$Q = 1 + \lambda^{3/2} [1 - F(\vartheta)] - (1 + \vartheta + \lambda)^{3/2} [1 - F(\vartheta/\lambda)(1 + \vartheta + \lambda)] - F(\vartheta/\lambda) \quad (\text{III.7})$$

wobei $F(\vartheta) = \frac{3^{1/2}}{2\pi} \int_0^\vartheta \frac{d\varrho}{\varrho^{3/2}(1+\varrho)} = \frac{3^{1/2}}{2\pi} \ln \frac{(1+\vartheta^{1/2})^3}{1+\vartheta} + \frac{3}{2\pi} \arctan \frac{2\vartheta^{1/2}-1}{3^{1/2}} + \frac{1}{4}$

von ALBERY UND BRUCKENSTEIN¹⁵ tabelliert wurde. Gleichung (III.7) gilt auch für eine Anordnung von zwei konzentrischen Ringelektroden an einer rotierenden Scheibe, wenn man λ durch $(r_4^3 - r_3^3)/(r_2^3 - r_1^3)$ und ϑ durch $(r_3^3 - r_2^3)/(r_2^3 - r_1^3)$ ersetzt, wobei r_1 der Innenradius, r_2 der Aussenradius der inneren Ringelektrode ist und entsprechend r_3 und r_4 die Dimensionen des äusseren Rings.

IV. ABSCHÄTZUNG DER ÜBERTRAGUNGSZEITEN UND DER WIRKUNG NACHGELAGERTER CHEMISCHER REAKTIONEN ERSTER ORDNUNG

An der Erzeugerelektrode läuft die Reaktion, $A \pm ne \rightarrow B$, ab. In der Lösung reagiert B homogen weiter in einer Reaktion erster Ordnung mit der Geschwindigkeitskonstanten, k . An der Indikatorelektrode wird das noch vorhandene B elektrochemisch nachgewiesen. Die Abklingzeit τ_R der Reaktion sei $\tau_R = 1/k$.

Zur Vereinfachung der weiteren Schreibweise definieren wir die Grösse K über

$$K^2 = (k/D^2)(bl/3v_0)^{3/2} = (1/D^2)(bl/3v_0)^{3/2} \cdot (1/\tau_R) \quad (\text{IV.1})$$

Dann gilt für B folgende Differentialgleichung

$$\eta \frac{\partial c}{\partial \xi} = \frac{\partial^2 c}{\partial \eta^2} - K^2 c \quad (\text{IV.2})$$

Die chemische Reaktion wird dann einen merklichen Einfluss auf die Übertragungsausbeute Q ausüben, wenn die durchschnittliche Übertragungszeit τ von der Erzeuger- zur Indikatorelektrode im Bereich der Grössenordnung der Abklingzeit τ_R der Reaktion liegt oder grösser als τ_R wird.

Um zu einer Abschätzung der mittleren Übertragungszeit τ zu kommen, gehen wir vom Konzentrationsprofil des stabilen Produkts aus und fassen dieses als eine Wahrscheinlichkeitsdichte für den Aufenthaltsort der Substanz B auf, was dadurch gerechtfertigt ist, dass die Diffusion ein statistischer Prozess ist. Dann können wir für jeden Ort x vor der ersten Elektrode einen Erwartungswert $\langle v_{x(x)} \rangle$ der mittleren konvektiven Transportgeschwindigkeit von B bilden¹⁶.

$$\langle v_{x(x)} \rangle = E_{(v_x)} = \int_0^\infty c v_x dy / \int_0^\infty c dy = (3Dx)^{\frac{1}{3}} \left(\frac{v_0}{b} \right)^{\frac{2}{3}} \frac{1}{\Gamma(5/3)} \quad (\text{IV.3})$$

Die mittlere Transportzeit $\tau_{(x)}$ ergibt sich dann zu

$$\tau_{(x)} = \int_0^x \frac{dx}{\langle v_{x(x)} \rangle} = \frac{3^{\frac{2}{3}}}{2} \Gamma(5/3) \frac{1}{D^{\frac{1}{3}}} \left(\frac{bx}{v_0} \right)^{\frac{2}{3}} \approx 2 K^2 \left(\frac{x}{l} \right)^{\frac{2}{3}} \tau_R \quad (\text{IV.4})$$

Verwendet man eine Doppelelektrode mit dünner Isolation und dünner Indikatorelektrode, so spielen sich die entscheidenden Vorgänge in der Hauptsache vor der Erzeugerelektrode ab. Die gesamte Übertragungszeit bis zum Ende der Indikatorelektrode ist dann

$$\tau \approx 2 K^2 (1 + \vartheta + \lambda)^{\frac{2}{3}} \tau_R \quad \text{für } \vartheta \ll 1; \lambda \ll 1$$

Hieraus folgt die Bedeutung der Grösse K^2 : Sie gibt das Verhältnis der konvektiven Übertragungszeit zur Abklingzeit der Reaktion an.

Die allgemeine Behandlung von Gl. (IV.2) für beliebiges K ist sehr kompliziert. Näherungslösungen lassen sich für die Bereiche $\tau < \tau_R$ und $\tau > \tau_R$ angeben. Im Falle $\tau < \tau_R$ kann man einen Zusammenhang mit der Übertragungsausbeute Q des stabilen Produkts herstellen.

$$Q^* = \exp(-k\tau) \cdot Q = \exp(-\tau/\tau_R) Q = \exp\{-2K^2(1 + \vartheta + \lambda)^{\frac{2}{3}}\} \cdot Q \quad (\text{IV.5})$$

In diesem Ansatz werden zwar auch Teilchen miterfasst, die nicht zur Abscheidung kommen, weil sie zu weit von der Elektrode entfernt sind; dadurch ist $\langle v_x \rangle$ zu gross und τ zu klein. Andererseits werden die am Ende der Erzeugerelektrode entstandenen Teilchen mit grösserer Wahrscheinlichkeit von der Indikatorelektrode erfasst; damit ist der durchschnittliche Transportweg zu gross angesetzt und τ zu gross. Beide Fehler wirken einander entgegen, und man kann erwarten, dass sich die angegebenen Ausdrücke bis auf einen Zahlenfaktor in der Grössenordnung von 1 experimentell verifizieren lassen.

Für den Fall $\tau > \tau_R$ empfiehlt sich die Behandlung von Gl. (IV.2) anstelle der Rechnung mit Übertragungszeiten. Hier wird die Konzentrationsverteilung des Reaktionsprodukts B hauptsächlich von Reaktion und Konvektion bestimmt. Führt man folgende Substitution durch

$$\zeta = K^{\frac{2}{3}} \xi = (bk^{\frac{2}{3}}/3v_0D^{\frac{1}{3}}) \cdot x \quad \text{und} \quad w = K\eta = (k/D)^{\frac{1}{3}} \cdot y$$

so erhält man die Differentialgleichung

$$w \frac{\partial c_B}{\partial \zeta} = \frac{\partial^2 c_B}{\partial w^2} - c_B \quad (\text{IV.6})$$

I. Zone der Erzeugerelektrode

In den Koordinaten, ξ, η , beträgt der Erzeugerstrom

$$i_1 = \int_0^1 \left(\frac{\partial c}{\partial \eta} \right)_{\eta=0} d\xi = 3^{3/2} \Gamma_{(3)}^2$$

Um die Konzentrationsverteilung vor der ersten Elektrode zu ermitteln, führen wir eine Laplacetransformation bezüglich ζ_1 , mit der transformierten Variablen s_1 durch

$$w s_1 \bar{c}_B - w c_{B^0} = \frac{\partial^2 \bar{c}_B}{\partial w^2} - \bar{c}_B \quad (\text{IV.7})$$

mit den Randbedingungen: $\zeta_1 = 0: c_{B^0} = 0; \lim_{w \rightarrow \infty} c_B = 0;$

$$\left(\frac{\partial c_B}{\partial w} \right)_{w=0} = - \left(\frac{\partial c_A}{\partial \eta} \right)_{\eta=0} \cdot \frac{d\eta}{dw} = - \frac{1}{3} \Gamma_{(3)}^2 \zeta_1^{-1/2}$$

$$\left(\frac{\partial \bar{c}_B}{\partial w} \right)_{w=0} = - \Gamma_{(3)}^2 / 3^{3/2} \Gamma_{(3)}^2 s_1^{-3/2}$$

Wir schreiben $3^{3/2} \Gamma_{(3)}^2 c_{B^0} / \Gamma_{(3)}^2 = u$ und $\sigma_1 = (w s_1 + 1) / s_1^{3/2}$ und erhalten an Stelle von Gl. (IV.7)

$$\sigma_1 \bar{u} = \frac{\partial^2 \bar{u}}{\partial \sigma_1^2} \quad \text{mit} \quad \lim_{w \rightarrow \infty} \bar{u} = 0; \quad \left(\frac{\partial \bar{u}}{\partial \sigma_1} \right)_{\sigma_1 = s_1^{-3/2}} = - \frac{1}{s_1} \quad (\text{IV.8})$$

$$\begin{aligned} \bar{u} &= - \frac{A i_{(\sigma_1)}}{s_1 A i'_{(s_1^{-3/2})}} = - A i_{(w s_1^{3/2} + s_1^{-3/2})} / s_1 A i'_{(s_1^{-3/2})} = \\ &= - A i_{(z_1^{3/2} + K^2 / z_1^{3/2})} / z_1 A i'_{(K^2 / z_1^{3/2})} \quad \text{mit} \quad f(z_1) = \circ F(\xi) \end{aligned} \quad (\text{IV.9})$$

Eine allgemeine Rücktransformation von Gl. (IV.9) erscheint als nahezu undurchführbar. Nachdem aber K gross sein soll, kann man die Ausdrücke der Airyfunktionen für grosse Argumente¹⁷ verwenden, um die Verteilung von B am Ende der ersten Elektrode näherungsweise zu erhalten.

$$A i_{(z)} \approx \frac{1}{\sqrt{4\pi}} \cdot z^{-1/2} \cdot \exp(-2z^{3/2}/3) \sum_{n=0}^{\infty} \frac{\Gamma(3n+1/2)}{(-36z^{3/2})^n \cdot n! \Gamma(n+1/2)} \quad (\text{IV.10a})$$

$$A i'_{(z)} \approx \frac{1}{\sqrt{4\pi}} \cdot z^{1/2} \cdot \exp(-2z^{3/2}/3) \sum_{n=0}^{\infty} \frac{\Gamma(3n+3/2)}{(-36z^{3/2})^n \cdot n! \Gamma(n+3/2)} \cdot \frac{1+6n}{1-6n} \quad (\text{IV.10b})$$

$$-z^{3/2} \frac{A i'_{(z^{-3/2})}}{A i_{(z^{-3/2})}} \approx 1 + z/4 - 5z^2/32 + \dots \quad (\text{IV.11a})$$

$$-z^{-3/2} A i_{(z^{-3/2})} / A i'_{(z^{-3/2})} \approx 1 - z/4 + 7z^2/32 - + \dots \quad (\text{IV.11b})$$

Die beiden letzten Ausdrücke haben für $z = 0.8$ einen Maximalfehler von 5%, für $z = 0.4$ einen Maximalfehler von 1%.

Am Ende der Erzeugerelektrode ist sicher $K^2/z_1^{\frac{2}{3}} > 1$. Wenn man sich auf den eigentlich interessanten Bereich in Wandnähe beschränkt gilt ferner $K^2/z_1^{\frac{2}{3}} \gg \eta z_1^{\frac{1}{3}}$. Für $\xi \approx 1$ gilt wegen $K > 1$:

$$(K^3/z_1 + \frac{2}{3}K\eta)^2 \gg (\frac{2}{3}K^2\eta^2 + \eta^3z_1)$$

Vernachlässigt man nun die kleinen Terme, so erhält man schliesslich

$$\bar{u} \approx \frac{\exp(-K\eta)}{Kz_1^{\frac{2}{3}}} \text{ bzw. } \frac{\exp(-K\eta)}{K\Gamma(\frac{2}{3})\xi^{\frac{2}{3}}} \text{ bzw. } c_B \approx \frac{\exp(-K\eta)}{3^{\frac{2}{3}}K\Gamma(\frac{2}{3})\xi^{\frac{2}{3}}} \quad (\text{IV.12})$$

Einen ähnlichen Ausdruck haben ALBERY UND BRUCKENSTEIN für die rotierende Scheibe gefunden, wobei sie den Diffusionsterm und den konvektiven Radialterm zur Behandlung des Problems gestrichen hatten¹⁸.

Die Lösung von Gl. (IV.12) erfüllt zwei Randbedingungen exakt, den Fluss an der Wand und das Verhalten im Unendlichen. Nur der dritten Randbedingung für $\xi=0$ kann nicht genügt werden. Setzt man die Näherung von c_B in die Differentialgleichung (IV.2) ein, so ergibt sich der Ausdruck $K^2 - \eta/3\xi^{\frac{1}{3}} \approx K^2$, d.h. für $K^2 \gg \eta/3\xi^{\frac{1}{3}}$ ist auch die Differentialgleichung näherungsweise erfüllt. Das trifft aber wieder auf die wandnahe Zone am Ende der Erzeugerelektrode zu, für die die Näherung abgeleitet wurde. Die Diskrepanzen für kleine ξ stören nicht, da hier unsere Näherung ohnehin nicht gilt. Da bei $\eta = \frac{1}{3}^{\frac{2}{3}}\Gamma(\frac{2}{3}) \approx 0.54$ bereits das Ende der Diffusionsschicht erreicht wird, und für $K^3 > 1$ die Reaktionsschicht kleiner als die Diffusionsschicht ist, kann man auf Grund der obigen Überlegungen für K die untere Grenze $K > 1.5$ angeben. Für den Geltungsbereich der in der Folge gemachten Näherungen dürfte es jedoch besser sein $K > 2$ zu benutzen.

Die Verwendung der Näherungsformeln für die Airyfunktionen bei der Rücktransformation ist möglich, weil diese Formeln auch für komplexe Argumente gelten.

2. Berechnung der Übertragungsausbeute Q_K für verschwindende Isolation ($d=0$)

In diesem Fall benötigt man die Rücktransformation vor der Erzeugerelektrode nicht, sondern kann mit einer zweifachen Laplacetransformation rechnen. Vor der Indikatorelektrode gilt dann

$$w \frac{\partial \bar{u}}{\partial \zeta_2} = \frac{\partial^2 \bar{u}}{\partial w^2} - \bar{u} \quad (\text{IV.13})$$

Führt man die zweite Laplacetransformation bezüglich ζ_2 mit s_2 als transformierter Variable durch, so erhält man

$$ws_2\bar{u} - s_2\bar{u}^0 = \frac{\partial^2 \bar{u}}{\partial w^2} - \bar{u} \text{ bzw. mit } \sigma_2 = (ws_2 + 1)/s_2^{\frac{2}{3}} \quad (\text{IV.14a})$$

$$\sigma_2\bar{u} = \frac{\partial^2 \bar{u}}{\partial \sigma_2^2} - wAi(\sigma_1)/s_1s_2^{\frac{2}{3}}Ai'_{(s_1^{-\frac{2}{3}})} \text{ mit } \lim_{w \rightarrow \infty} \bar{u} = 0; \lim_{w \rightarrow \infty} \bar{u}' = 0; \quad (\text{IV.14b})$$

Für den Fluss zur Indikatorelektrode gilt¹²

$$-\int_{s_2^{-\frac{2}{3}}}^{\infty} wAi(\sigma_1)Ai(\sigma_2)d\sigma_2/s_1s_2^{\frac{2}{3}}Ai'_{(s_1^{-\frac{2}{3}})} = s_2^{-\frac{1}{3}}Ai_{(s_2^{-\frac{2}{3}})} \cdot \left(\frac{\partial \bar{u}}{\partial w} \right)_{w=0} \quad (\text{IV.15})$$

$$\begin{aligned} \text{Mit } -\int_{s_2^{-\frac{2}{3}}}^{\infty} \sigma_1 Ai(\sigma_2) Ai(\sigma_1) d\sigma_2 = \\ = \left[\left(\frac{s_2}{s_1} \right)^{\frac{2}{3}} Ai'_{(s_1^{-\frac{2}{3}})} Ai_{(s_2^{-\frac{2}{3}})} - \left(\frac{s_2}{s_1} \right)^{\frac{2}{3}} Ai_{(s_1^{-\frac{2}{3}})} Ai'_{(s_2^{-\frac{2}{3}})} \right] / \left(1 - \frac{s_2}{s_1} \right) \end{aligned}$$

erhält man

$$\left(\frac{\partial \bar{u}}{\partial w} \right)_{w=0} = \frac{1}{s_1(s_1 - s_2)} \left[s_1^{\frac{1}{3}} - s_2^{\frac{1}{3}} \frac{Ai'_{(s_2^{-\frac{2}{3}})} Ai_{(s_1^{-\frac{2}{3}})}}{Ai_{(s_2^{-\frac{2}{3}})} Ai'_{(s_1^{-\frac{2}{3}})}} \right] \quad (\text{IV.16})$$

Die exakte Rücktransformation dieser Gleichung würde den Indikatorstrom für alle Werte von K ergeben. Die rechnerische Durchführung ist aber wohl kaum möglich. Nachdem s_1 und s_2 die transformierten Variablen von ζ_1 und ζ_2 sind, bei gleicher Dimensionierung der Elektroden an deren Ende aber $\zeta_1 = K^3$ und $\zeta_2 = K^3$ sind, gilt für $K > 1$: $\zeta_1, \zeta_2 \gg 1$. Daher kann man über s aussagen, dass $s < 1$ und $s^{-\frac{2}{3}} > 1$ sind. Dann darf man die Beziehungen von Gl. (IV.10) und (IV.11) zur näherungsweisen Rücktransformation heranziehen. Verwendet man die erste Näherung von Gl. (IV.11), so erhält man:

$$\int_0^{\zeta_2'} \left(\frac{\partial u}{\partial w} \right)_{w=0} d\zeta_2 = \frac{\Gamma(\frac{2}{3})}{4K} \quad \text{bzw.} \quad i_2 = \frac{1}{3^{\frac{2}{3}} \Gamma(\frac{2}{3}) \cdot 4K^3} \quad (\text{IV.17})$$

Schliesslich wird die Übertragungsausbeute

$$Q_K = -i_2/i_1 = 1/6K^3 \quad \text{für} \quad d=0 \quad (\text{IV.18})$$

Beachtlich ist die fehlende Abhängigkeit von ζ_2 . Das bedeutet, dass bei schnellen Reaktionen nahezu alles noch erfassbar B am vorderen Teil der Indikatorelektrode abreagiert, die Dimensionierung der Indikatorelektrode eine untergeordnete Rolle spielt, also in weiten Grenzen frei ist, ohne dass sich Q dadurch ändert. Der fehlende Zusammenhang mit dem Fall des stabilen Reaktionsprodukts ist nicht erstaunlich, da sich die Konzentrationsprofile in beiden Fällen erheblich unterscheiden. Für kleine K nähert sich der Ausdruck für \bar{u} dem stabilen Fall und man muss die gänzlich verschiedene Abschätzung von Anfang dieses Kapitels verwenden.

Die in diesem Abschnitt verwendete Näherung beschränkte sich auf die Verwendung der asymptotischen Ausdrücke für die Airyfunktionen und den Abbruch der darin enthaltenen Reihen.

3. Berechnung der Übertragungsausbeute Q_K für endliche Isolation

In den Koordinaten ζ, w hat die Isolationsdicke den Wert $K^3\vartheta$. ϑ müsste also den Betrag 0.01 annehmen, damit man $K^3\vartheta$ noch vernachlässigen kann. Die Dimensionierung von ϑ hat bei der Anfertigung einer Doppelektrode die untere Grenze von ca. 5μ . Dann sollte l wenigstens 0.5 mm sein. Nachdem die benützten Elektroden diese Bedingung oft nicht erfüllen, soll jetzt eine Abschätzung der Übertragungsausbeute für endliche Isolationsdicken vorgenommen werden. Eine dreifache Laplace-Transformation stösst schon im Laplaceraum auf erhebliche Schwierigkeiten. Deshalb verwenden wir für die Konzentrationsverteilung am Ende der ersten Elektrode die Näherungslösung Gl. (IV.12).

Am Ende der Erzeugerelektrode ist $c_B = e^{-w}/K\Gamma_{(\frac{4}{3})}3^{\frac{3}{2}}$

Schreibt man $u = e^{-w} - c_B \cdot 3^{\frac{3}{2}} K \Gamma_{(\frac{4}{3})}$, so gilt $w \frac{\partial u}{\partial \zeta} = \frac{\partial^2 u}{\partial w^2} - u$, weil e^{-w} Gl. (IV.6) erfüllt.

An der Isolation herrschen folgende Randbedingungen:

$$\zeta_1 = 0: u = 0; \lim_{w \rightarrow \infty} u = 0;$$

$$\left(\frac{\partial u}{\partial w} \right)_{w=0} = -1 \quad \text{wegen} \quad \left(\frac{\partial c_B}{\partial w} \right)_{w=0} = 0 \quad \text{und} \quad \left(\frac{\partial e^{-w}}{\partial w} \right)_{w=0} = -1$$

Eine Laplacetransformation bezüglich ζ_1 mit der transformierten Variable s_1 führt auf

$$w s_1 \bar{u} = \frac{\partial^2 \bar{u}}{\partial w^2} - \bar{u} \quad \text{bzw. mit} \quad \sigma_1 = \frac{w s_1 + 1}{s_1^{\frac{3}{2}}} \quad \text{auf} \quad \sigma_1 \bar{u} = \frac{\partial^2 \bar{u}}{\partial \sigma_1^2}$$

Die Lösung ist

$$\bar{u} = -A i_{(\sigma_1)} / s_1^{\frac{4}{3}} A i'_{(s_1^{-\frac{2}{3}})} \quad (\text{IV.19})$$

Gleichung (IV.19) ist die Randbedingung für $\zeta_2 = 0$. An der Indikatorelektrode ist für $w = 0$: $c_B = 0$; $u = 1$; $\bar{u} = 1/s_1$.

Die zweite Laplacetransformation bezüglich ζ_2 mit der transformierten Variable s_2 und der Substitution $\sigma_2 = (w s_2 + 1)/s_2^{\frac{3}{2}}$ führt auf

$$\frac{\partial^2 \bar{u}}{\partial \sigma_2^2} = \sigma_2 \bar{u} - \frac{w \bar{u}^0}{s_2^{\frac{3}{2}}} = \sigma_2 \bar{u} + w A i_{(\sigma_1)} / s_1^{\frac{4}{3}} s_2^{\frac{3}{2}} A i'_{(s_1^{-\frac{2}{3}})} \quad (\text{IV.20})$$

Mit der Methode von ALBERY¹² erhält man:

$$\frac{1}{s_2} \left(\frac{\partial \bar{u}}{\partial w} \right)_{w=0} = \frac{s_2^{\frac{1}{2}} A i'_{(s_2^{-\frac{2}{3}})}}{s_1 s_2^2 A i_{(s_2^{-\frac{2}{3}})}} + \frac{1}{s_1 s_2 (s_1 - s_2)} \left[1 - \frac{A i_{(s_1^{-\frac{2}{3}})} s_2^{\frac{1}{2}} A i'_{(s_2^{-\frac{2}{3}})}}{s_1^{\frac{4}{3}} A i'_{(s_1^{-\frac{2}{3}})} A i_{(s_2^{-\frac{2}{3}})}} \right] \quad (\text{IV.21})$$

Zur Rücktransformation benutzen wir wieder Gl. (IV.10) und (IV.11). Die erste Näherung ergibt:

$$\frac{1}{s_2} \left(\frac{\partial \bar{u}}{\partial w} \right)_{w=0} \approx -1/s_1 s_2^2 - 1/4 s_1 s_2 + 1/s_1 s_2 (1 + s_1/4) \cdot 0 - \zeta_2' - \frac{\exp(-4\zeta_1')}{4}$$

Mit der zweiten Näherung erhält man

$$\frac{1}{s_2} \left(\frac{\partial \bar{u}}{\partial w} \right)_{w=0} = -\frac{1}{s_1 s_2^2} - \frac{1}{4 s_1 s_2} + \frac{1}{(s_1 + 4) s_1} - \frac{5}{8} \cdot \frac{1}{s_1 + 4} \cdot 0 - \zeta_2' - \frac{7}{8} \exp(-4\zeta_1')$$

Damit werden i_2 und Q_K nach der ersten Näherung

$$i_2 = \frac{1}{3^{\frac{3}{2}} \Gamma_{(\frac{4}{3})} 4 K^3} \cdot \exp(-4K^3 \vartheta); \quad Q_K = \frac{1}{6 K^3} \cdot \exp(-4K^3 \vartheta);$$

und nach der zweiten Näherung

$$i_2 = \frac{7}{3^{\frac{3}{2}} \Gamma_{(\frac{4}{3})} \cdot 8 K^3} \cdot \exp(-4K^3 \vartheta); \quad Q_K = \frac{7}{12 K^3} \cdot \exp(-4K^3 \vartheta);$$

Die zweite Näherung liefert bis auf einen konstanten Zahlenfaktor das gleiche Ergebnis wie die erste. Dieser Faktor kann aber nur über das Experiment bestimmt werden, da die Zuverlässigkeit der zweiten Näherung insofern etwas problematisch ist, als man ein nicht rücktransformierbares Glied streichen muss, das durchaus einen Beitrag zu i_2 liefern kann.

Man kann noch die Übertragungsausbeute für den Fall $d=0$ nach derselben Näherung Gl. (IV.12) wie für $d \neq 0$ berechnen; hierzu benötigt man nur eine Laplace-transformation. Das Ergebnis ist jedoch mit Gl. (IV.18) identisch. Daraus ergeben sich zwei Folgerungen: Einmal ist der Näherungsansatz für das Konzentrationsprofil am Ende der ersten Elektrode brauchbar, zum anderen kann man die Beschränkung der Isolationsdicke auf die Fälle $K^3 \vartheta \gg 1$ aufgeben. Nachdem Q_K von der Länge der Indikatorelektrode unabhängig ist, gilt für beliebige Dimensionierung der Doppelektrode

$$Q_K = (1/6K^3) \cdot \exp(-4K^3\vartheta) = (D^{1/2}v_0/2k^2bl) \cdot \exp(-4k^2bd/3D^{1/2}v_0) \quad (\text{IV.22})$$

wobei der Faktor $1/6$ noch eine gewisse Unsicherheit trägt.

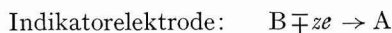
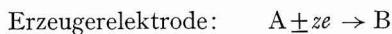
Bei unserer Anordnung hat die Erzeugerelektrode eine Länge von $l=100 \mu$ und $l=200 \mu$. Die Indikatorelektrode kann man auf $l_2=10 \mu$ dimensionieren, um den Reststrom klein zu halten, nachdem nur ihr vorderer Teil einen Beitrag zu Q_K liefert. Die Isolationsdicke d liegt im allgemeinen bei $d \approx 10 \mu$. Die untere Grenze erfassbarer Übertragungsausbeuten beträgt 1%. Variiert man b zwischen 0.1 mm und 0.3 mm, dann ist v_0 durch den Umschlag laminar—turbulent nach oben hin auf 11 m/sec beschränkt.

Im Bereich $\tau < \tau_R$ gilt Gl. (IV.5) für kleine K^2 am besten. Verwendet man als obere Grenze $K^2=0.1$, so ergibt sich mit den obigen Zahlenangaben für die obere Grenze erfassbarer Geschwindigkeitskonstanten ein Wert von $k \approx 4 \cdot 10^2 \text{ sec}^{-1}$. Die Übertragungsausbeute, Q^* , beträgt hier etwa $Q^* \approx 0.8 Q$.

Beim Fall $\tau > \tau_R$ verlangt die Gültigkeit der Näherung, dass $K^2 \geq 2$ ist. Damit erhält man ein Intervall von $10 \text{ sec}^{-1} \leq k \leq 10^4 \text{ sec}^{-1}$. Die Übertragungsausbeute Q_K hat hier nach Gl. (IV.22) Werte von $1\% < Q_K < 5\%$. Ergänzend zur Rechnung kann man die Abhängigkeit der Übertragungsausbeute von K auch mit einer Testreaktion bestimmen.

V. BERECHNUNG DER ÜBERTRAGUNGS-AUSBEUTE BEI EINER EINGELAGERTEN REAKTION ERSTER ORDNUNG

Häufig tritt der Fall ein, dass das Produkt der Elektrodenreaktion in einer chemischen Reaktion zum Ausgangsstoff zurückreagiert. Man hat dann folgendes Reaktionsschema:



Definieren wir K wie in den beiden vorhergehenden Kapiteln, so muss man folgendes System von Differentialgleichungen lösen:

$$\eta \frac{\partial c_A}{\partial \xi} = \frac{\partial^2 c_A}{\partial \eta^2} + K^2 c_B \quad \text{und} \quad \eta \frac{\partial c_B}{\partial \xi} = \frac{\partial^2 c_B}{\partial \eta^2} - K^2 c_B \quad (\text{V.1})$$

mit den Randwerten: $\eta=0: c_A=0; \left(\frac{\partial c_A}{\partial \eta}\right)_{\eta=0} + \left(\frac{\partial c_B}{\partial \eta}\right)_{\eta=0} = 0; \lim_{\eta \rightarrow \infty} c_A = 1; \lim_{\eta \rightarrow \infty} c_B = 0.$

Durch Addition beider Gleichungen erhält man:

$$\eta \frac{\partial (c_A + c_B)}{\partial \xi} = \frac{\partial^2 (c_A + c_B)}{\partial \eta^2} \quad \text{mit der Lösung } c_A + c_B = 1$$

Deshalb ist $\lim_{\eta \rightarrow 0} c_B = 1$

Führt man nun eine Laplacetransformation von Gl. (V.1) bezüglich ξ mit der transformierten Variable s durch, so erhält man:

$$\eta s \bar{c}_B = \frac{\partial^2 \bar{c}_B}{\partial \eta^2} - K^2 \bar{c}_B \quad \text{mit} \quad \lim_{\eta \rightarrow 0} \bar{c}_B = 1/s; \quad \lim_{\eta \rightarrow \infty} \bar{c}_B = 0;$$

Mit $\sigma = s^{\frac{1}{2}} + K^2/s^{\frac{3}{2}}$ wird die Lösung: $\bar{c}_B = A i_{(\sigma)} / s A i_{(K^2/s^{\frac{3}{2}})}$

Verwendet man Gl. (IV.10) in analoger Weise wie bei Gl. (IV.12), so ist am Ende der Erzeugerelektrode

$$\bar{c}_B \approx e^{-K\eta/s} - \circ e^{-K\eta} \quad (\text{V.2})$$

Dieses Ergebnis unterscheidet sich nur um den Faktor $3^{\frac{3}{2}} \Gamma(\frac{3}{2}) K$ von Gl. (IV.12). Deshalb kann man den Indikatorstrom auf dieselbe Weise wie in Kap. IV berechnen und erhält:

$$i_2 = (1/4K^2) \exp(-4K^3\vartheta) \quad (\text{V.3})$$

Für i_1 stellen wir ähnliche Überlegungen wie bei i_2 an und erhalten

$$i_1 = -L^{-1} \frac{1}{s_1} \left(\frac{\partial \bar{c}}{\partial \eta} \right)_{\eta=0, \xi=1} = K + 1/4K^2 \quad (\text{V.4})$$

Dieser Ausdruck gilt ebenso wie der für i_2 nur für grosse K . Schliesslich ist die Übertragungsausbeute

$$Q_{K'} = \frac{\exp(-4K^3\vartheta)}{4K^3(1+1/4K^3)} = \frac{\exp(-4K^3\vartheta)}{4K^3+1} \approx \left(\frac{3}{2}\right) Q_K \quad (\text{V.5})$$

Der Fall der eingelagerten Reaktion unterscheidet sich von der nachgelagerten hauptsächlich in der Grösse des Erzeugerstroms.

VI. DISKUSSION

Die Ergebnisse für die Doppelektrode in der Kanalströmung lassen sich mit gewissen Einschränkungen auch auf eine Doppelringelektrode an einer rotierenden Scheibe übertragen. Die Gleichung der konvektiven Diffusion mit homogener Lösungsreaktion erster Ordnung lautet an der rotierenden Scheibe

$$rw \frac{\partial c}{\partial r} - w^2 \frac{\partial c}{\partial w} = \frac{\partial^2 c}{\partial w^2} - K^2 c \quad \text{mit} \quad w = 0.799 \frac{\omega^{\frac{1}{2}}}{\nu^{\frac{1}{4}}} z; \quad K^2 = 1.57 \frac{h^{\frac{1}{2}}}{D^{\frac{3}{4}}} \quad (\text{VI.1})$$

(z = Normalkoordinate, ω = Kreisfrequenz)

Verwendet man die Vereinfachungen von ALBERY¹⁸ zur Behandlung von Gl. (VI.1) für die Ringscheibenelektrode, d.h. vernachlässigt man den konvektiven Normalterm $w^2(\partial c/\partial w)$ und wählt alle Radien in der Grössenordnung eines mittleren Radius $r_0 \approx r_{1,2,3,4}$, so geht Gl. (VI.1) in die analoge Beziehung für den Strömungskanal über

$$w \frac{\partial c}{\partial(r/r_0)} = \frac{\partial^2 c}{\partial w^2} - K^2 c \quad (\text{VI.2})$$

Für den Ausgangsstoff ist $K^2 = 0$; die Auswertung der unverkürzten Gl. (VI.1) ergibt:

$$c_A = E_{3[rw/(3r^3 - 3r_1^3)]^{\frac{1}{3}}} \\ i_1 = 2\pi \int_{r_1}^{r_2} \left(\frac{\partial c}{\partial w} \right)_{w=0} r dr \approx 3^{\frac{1}{3}} \pi r_0^{\frac{4}{3}} (r_2 - r_1)^{\frac{2}{3}} / \Gamma(\frac{4}{3}) \quad (\text{VI.3})$$

Die Konzentrationsverteilung von B am Ende der ersten Elektrode ist näherungsweise

$$c_B \approx \frac{\exp(-Kw)}{K \cdot 3^{\frac{1}{3}} \Gamma(\frac{4}{3})} \cdot \left(\frac{r_0}{r_2 - r_1} \right)^{\frac{1}{3}} \quad (\text{VI.4})$$

Schliesslich erhält man wie in Gl. (VI.22)

$$Q_K \approx \{r_0/6K^3(r_2 - r_1)\} \exp\{-4K^3(r_3 - r_2)/r_2\} \quad (\text{VI.5})$$

Die Gültigkeit dieser Beziehungen ist allerdings begrenzt. Einmal darf der vernachlässigte Konvektionsterm noch keine wesentliche Rolle spielen, zum anderen muss K so gross gewählt werden, dass $K^3(r_2 - r_1) \gg r_0$, da sonst die Näherung in Gl. (VI.4) ihren Sinn verliert. Letzteres bedeutet aber, dass Q_K eine sehr kleine Grösse wird. Bei der Messung sollte der Strom i_2 jedoch noch deutlich über dem Reststrom liegen. An einer Ringscheibenelektrode liegen günstigere Verhältnisse vor¹⁸; die dort geltenden Beziehungen haben eine sehr ähnliche Form:

$$Q_K = (7/4K^3) \exp\{-4K^3 \cdot (r_2 - r_1)/r_1\} \quad (\text{VI.6})$$

Bei der in der vorliegenden Arbeit behandelten Doppелеlektrode in der Kanalströmung liegen die einzigen Näherungen in der Rücktransformation, da hier die unveränderten Ausgangsgleichungen einer mathematischen Behandlung zugänglich sind. Die Kanalströmung besitzt noch zwei weitere Vorteile gegenüber der rotierenden Scheibe. Einmal ist das Strömungsprofil von der Viskosität völlig unabhängig, zum anderen kann man durch Verkleinerung der Kanalhöhe $2b$ die laminare Strömung bis zu sehr hohen Geschwindigkeiten aufrechterhalten (z.B. für $b = 0.1$ mm bis zu $v_0 = 11$ m/sec). Bei der rotierenden Scheibe erzielt man das nur durch möglichst kleine Dimensionierung von Scheibenelektrode und Ringelektrode; die Grenzen liegen jedoch hier in der Anwendbarkeit der Gesetze für eine unendlich ausgedehnte Scheibe. Bei einer Doppelringelektrode dürfte man hier auch auf mechanische und messtechnische Schwierigkeiten stossen.

Herrn Professor GERISCHER gilt für die Einführung in die Problemstellung mein besonderer Dank. Seine Anregungen trugen wesentlich zur Durchführung dieser Arbeit bei.

ZUSAMMENFASSUNG

Doppelelektrode in der Kanalströmung heisst eine Anordnung, in der zwei eng benachbarte Elektroden in die Wand eines Strömungskanals eingebettet sind. Die Reaktionsprodukte der ersten Elektrode können an der zweiten analysiert werden. Die Übertragungsausbeute Q für ein stabiles Produkt kann mit Hilfe von Laplace-Transformationen exakt berechnet werden, wenn das Produkt jedoch im Elektrolyten weiterreagiert, muss man Näherungen anwenden. Die Berechnungen wurden für Reaktionen erster Ordnung durchgeführt. Diese Überlegungen sind unter gewissen Bedingungen auf ein System von zwei konzentrischen Ringelektroden auf einer rotierenden Scheibe anwendbar.

SUMMARY

"Double-electrode in a channel flow" describes an arrangement in which two closely spaced electrodes are embedded in the wall of a channel. The reaction products of the first electrode can be analyzed at the second. The transfer efficiency, Q , of a stable product can be calculated exactly by using Laplace transformation but if there is any further reaction of the product in the electrolyte, one is forced to apply approximations. Calculations were made for first-order kinetics. These considerations are applicable, under certain conditions, to a system of two concentric ring-electrodes on a rotating disc.

REFERENCES

- 1 V. G. LEVICH, *Physicochemical Hydrodynamics*, Prentice Hall, Inc., Englewood Cliffs, 1959, chap. II.
- 2 S. L. MARCHIANO AND A. J. ARVIA, *Electrochim. Acta*, 12 (1967) 801.
- 3 H. MATSUDA, *J. Electroanal. Chem.*, 15 (1967) 109, 325.
- 4 A. FRUMKIN, L. NEKRASSOW, V. G. LEVICH UND JU. IVANOW, *J. Electroanal. Chem.*, 1 (1959) 84.
- 5 H. GERISCHER, I. MATTES UND R. BRAUN, *J. Electroanal. Chem.*, 10 (1965) 553.
- 6 H. SCHLICHTING, *Grenzschichttheorie*, Verlag G. Braun, Karlsruhe, 3. Auflage, 1958, S. 346.
- 7 H. SCHLICHTING, *Grenzschichttheorie*, Verlag G. Braun, Karlsruhe, 3. Auflage, 1958, S. 87 und S. 247.
- 8 H. SCHLICHTING, *Grenzschichttheorie*, Verlag G. Braun, Karlsruhe, 3. Auflage, 1958, S. 159.
- 9 V. G. LEVICH, *Physicochemical Hydrodynamics*, Prentice Hall, Inc., Englewood Cliffs, 1959, S. 293.
- 10 V. G. LEVICH, *Physicochemical Hydrodynamics*, Prentice Hall, Inc., Englewood Cliffs, 1959, S. 57.
- 11 W. G. L. SUTTON, *Proc. Roy. Soc., London*, 182 (1943) 48.
- 12 W. J. ALBERY, *Trans. Faraday Soc.*, 62 (1966) 191.
- 13 JAHNKE-EMDE-LÖSCH, *Tafeln höherer Funktionen*, Teubner Verlag, Stuttgart, 1960, S. 26.
- 14 H. MATSUDA, *J. Electroanal. Chem.*, 16 (1968) 153.
- 15 W. J. ALBERY UND S. BRUCKENSTEIN, *Trans. Faraday Soc.*, 62 (1966) 1924.
- 16 J. HEINHOLD UND K. GAEDE, *Ingenieur-Statistik*, Oldenbourg Verlag, München, Wien, 1964, S. 167.
- 17 *Handbook of Mathematical Functions*, Nat. Bur. Std. U.S., 1965, S. 446.
- 18 W. J. ALBERY UND S. BRUCKENSTEIN, *Trans. Faraday Soc.*, 62 (1966) 1946.

MOVING BOUNDARY ANALYSIS

OTTO HELLO

School of Chemistry, Hobart Technical College, Tasmania (Australia)

(Received December 20th, 1967; in revised form, March 15th, 1968)

INTRODUCTION

A method of ionic analysis is described in which a small sample is interposed between two long columns of solutions. For cationic analysis, one column is filled with a solution of only fast cations, *e.g.* H^+ , while the other column contains only slow cations, *e.g.* Li^+ . When a potential is applied between the ends of the columns, the cations within the sample will move towards the cathode between the H^+ ions of the leading electrolyte and the Li^+ ions of the trailing electrolyte. The unknown cations in the sample will be separated slowly into distinct layers in order of their mobilities. The boundaries formed between each layer are detected by two closely spaced platinum foil electrodes near the end of one or both of the columns. This system provides a method for the determination of ionic species and concentration.

EXPERIMENTAL

Figure 1 shows a diagram of the apparatus used. Perspex block B is connected with small-bore glass tubing to the junction blocks, C_1 and C_2 . Another piece of Perspex (shown shaded) is free to slide through the centre of block B. In this sliding valve is located a hole, No. 2, having the same diameter as the bore of the tubing, as well as two grooves cut as shown in Fig. 1. Small-bore tubing, fitted with ball valves, E_1 , E_2 and E_3 as shown, connect the apparatus with the electrolyte containers on top, and the drain beakers below. Electrolyte flow from the Ag/AgCl electrode compartments, A_1 and A_2 , is prevented by asbestos plugs, F_1 and F_2 . Two sets of electrodes, D_1 and D_2 , are provided to allow the detection of boundaries of both cation and anion simultaneously, if desired. In the present experiment, only the properties of cations were investigated.

There are several methods of preparing the electrodes:

(1) Each set of electrodes consists of two strips of platinum foil¹ which are placed, slightly staggered, on opposite sides of the column, as shown by D_1 in Fig. 1. The signal can be recorded by a pH-meter.

(2) The foil strips are placed level, opposite each other, in which case a conductivity measurement² can be used for boundary detection.

(3) A third method is that in which the platinum foils are glued on a 0.3-mm thick celluloid strip; this is then attached through a hole in the side of the glass tubing as shown by D_2 in Fig. 1. The signal may then be recorded with a current-sensitive system¹.

In each method, the electrodes were filed flush with the bore, and lightly platinised.

A test is prepared by first pulling the sliding valve in B to the right so that the centre hole in the valve lines up with holes No. 3 in the block, while the grooves form two channels between holes No. 1 and the glass tubes. When the valves, E_1 and E_3 , are pressed, carrier electrolytes are introduced from the reservoirs through holes No. 1 and the grooves, flushing through the two halves of the column, and out to the respective drain beakers. With the sliding valve in the same position, a sample is introduced to hole No. 3, after several rinses through ball valve, E_2 . When the sliding valve is moved so that its centre hole (chamber volume 0.01 ml) is aligned with hole No. 2 in block B, as shown in the diagram, ions in the sample are allowed to migrate with the carrier ions in the electric field produced by a potential of several hundred volts applied to the column electrodes, A_1 and A_2 .

In the experiment now described, the upper column contained the leading electrolyte, $10^{-3} N$ HCl, and the lower column the trailing electrolyte, $10^{-2} N$ LiCl, so that the unknown cations of the sample will now move upwards behind the H^+ ions, followed by the Li^+ ions. The anions of the sample are replaced by those of the leading electrolyte, thus providing a constant anion concentration, resulting in a constant migrating cation concentration.

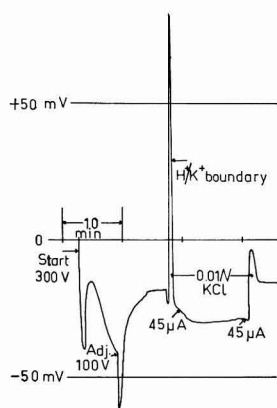
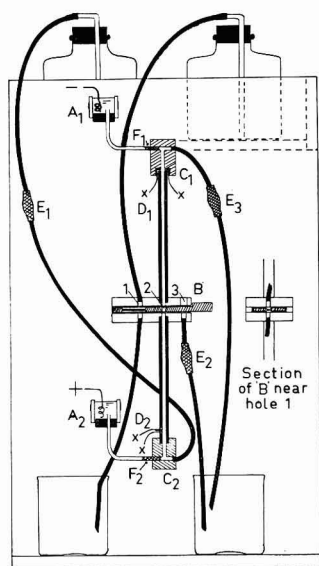


Fig. 1. Diagram of moving boundary apparatus. Length of tubes, 22 and 12 cm, i.d. 2.3 mm. Dimensions of block B, approx. $50 \times 25 \times 25$ mm; thickness of sliding valve 2.3 mm.

Fig. 2. Recorder-graph of 0.01 N KCl, as sample, between $10^{-3} N$ HCl and $10^{-2} N$ LiCl electrolytes. Voltage and current, as shown. Column length, 12 cm. Detector circuit is potentiometric.

RESULTS

Preliminary experiments were carried out on various concentrations of KCl, $ZnSO_4$, NH_4^+ ion and some cationic mixtures. A typical result is shown in Fig. 2 in

which the recorder-graph shows the sharp H^+/K^+ boundary followed by the less distinct K^+/Li^+ boundary, as a function of time. With constant current, the distance between the peaks is dependent on the concentration of the K^+ ion in the sample. Figure 3 shows the dependence of layer thickness (as measured by the electrical charge between peaks) on sample concentration. This relationship does not appear to depend on the concentration of the carrier electrolytes. The dashed line shows the theoretical expectation for the migration of pure KCl, as calculated coulometrically for a sample volume of 0.01 ml. A lower range of carrier electrolyte concentrations (*e.g.*, 10^{-4} N HCl and 10^{-3} N LiCl) gives better separation between peaks, as the current will be lower.

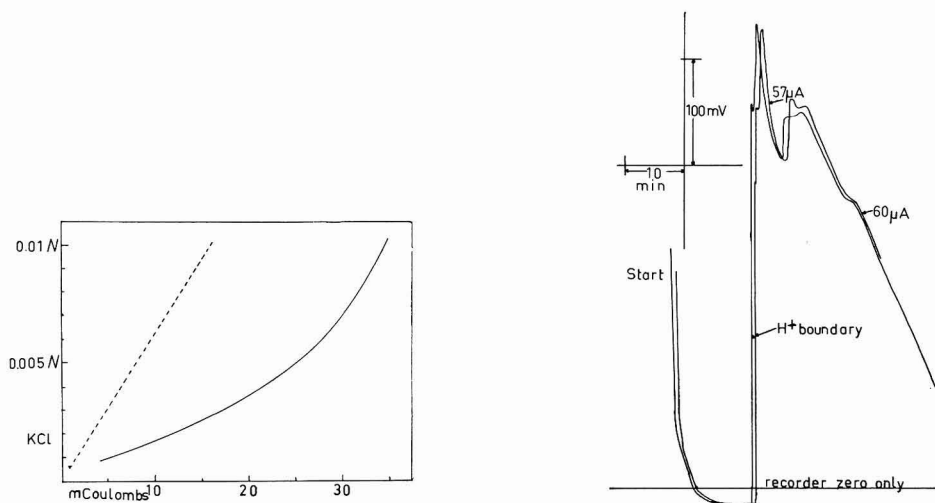


Fig. 3. Graph of K^+ ion concn. in the sample as function of electric charge between peaks; dashed line shows theoretical expectation.

Fig. 4. Duplicate recorder-graph of 0.1 N $ZnSO_4$ between 10^{-3} N HCl and 10^{-2} N LiCl electrolytes, 300 V, current as shown. Detector circuit is potentiometric.

This is especially useful when testing samples of low concentration, *e.g.*, below 0.002 N. On the other hand, $ZnSO_4$ did not show such a clear relationship as given for the K^+ ion in Fig. 3, particularly at higher concentrations, which showed formation of multiple peaks as indicated in Fig. 4. As the concentration decreased, the boundary became sharper and 10^{-4} N $ZnSO_4$ could still be detected easily. It was possible to obtain multiple peaks also from a 0.01 N KCl sample by putting it between 0.01 N HCl and 0.01 N LiCl carrier electrolytes at 100 V and with a 12-cm column. The resulting graph showed a very sharp initial peak followed by two less distinct peaks (not shown here).

An interesting test was made with NH_4^+ ions. First, they were introduced as 0.002 N NH_4OH between 10^{-4} N HCl and 10^{-3} N LiCl carrier electrolytes in a 22-cm column. With 350 V applied, the resulting H^+/NH_4^+ boundary peak was only a few seconds wide and appeared within 25 min, following which the NH_4^+/Li^+ peak appeared after 20 mins; the current was approximately $5 \mu A$. On the other hand, the times for the same solution acidified with HCl were 43 mins and 34 mins at $5 \mu A$,

respectively. This shows the different dissociation states of the NH_4 radical in the two solutions. The excess H^+ ions in the second sample also contributed to the slower movement of the H^+/NH_4^+ boundary. Some mixtures, such as Ca^{2+} or Ag^+ with the K^+ ion, showed clearly as separate peaks, while other mixtures did not always resolve well.

DISCUSSION

The apparatus described could have specific applications for ionic analysis, and offers a different approach to ionic research. In addition to the ion-migration experiments described, it is possible that the apparatus could be used for conventional electrophoresis since, in principle, it resembles a Tiselius electrophoresis cell³ but requires only one-thousandth of the size of sample. The sharp boundary peaks indicate that temperature control is not essential.

In contrast with the Tiselius method, which uses only one electrolyte, the present method allows boundaries to be formed without boundary anomalies. In this manner the electrical stability of the boundaries may overcome all other causes of physical instability, such as convection, diffusion, etc., within the solution.

No satisfactory explanation for the multiple peak formation on a single ionic species can be given. A possible cause could be isotopic separation, perhaps shown as incompleting boundaries. Other suggestions include complex ion formation and migration of the salt complex under the influence of the H^+ boundary.

The potentiometric detection system was the least susceptible to electrical disturbances, resulting in very smooth graphs. The circuit (see ref. 1) can also develop a H^+/K^+ boundary peak within $5 \mu\text{C}$. A conductometric circuit was abandoned because of interference from the oscillator. A sensitive conductometric system could, however, make possible identification of ions in the layers between the boundaries. It is suggested that some closely spaced (very thin) Pt wires could be used as detector electrodes to eliminate possible tube-wall interference. Duplicate pairs of detector electrodes (a short distance apart) separately linked to a detection system, would greatly improve correlation of results. Two or more columns could also be constructed between the same blocks, B and C, so that sample and standard could be run under identical conditions of potential and geometry. A screw fixture to move the sliding valve is recommended as a tight-fit is required to prevent leakage.

ACKNOWLEDGEMENT

The author would like to thank Mr. FRED PRESTON of the Electrical Engineering Department for assistance with the electrical circuits.

REFERENCES

- 1 E. PASSERON AND E. GONZALEZ, *J. Electroanal. Chem.*, 14 (1967) 393–398.
- 2 G. A. LONERGAN AND D. C. PEPPER, *J. Chem. Educ.*, 42 (1965) 82–85.
- 3 A. TISELIUS, *Proc. Faraday Soc.*, 33 (1937) 524.

J. Electroanal. Chem., 19 (1968) 37–40

DOUBLE-LAYER CHARGING IN CONSTANT-CURRENT CHRONOPOTENTIOMETRY AT A MERCURY-FILM ELECTRODE

W. T. DE VRIES*

Department of Chemistry, The Israel Institute of Technology, Haifa (Israel)

(Received February 6th, 1968)

INTRODUCTION

The distorting effect of double-layer charging on constant-current chronopotentiograms has recently been receiving considerable attention¹⁻³. The problem has been treated theoretically along different lines. RODGERS AND MEITES¹ used a numerical approach for solving the Fick diffusion equations, with the appropriate initial and boundary conditions. Our approach² was based on a formulation of the problem as a non-linear integral equation in terms of the surface concentrations of electroactive species, and OLMSTEAD AND NICHOLSON³ formulated an integral equation with the capacitive current as the function to be solved. The latter approach seems to be the most promising, as numerical evaluation of the integral equation of OLMSTEAD AND NICHOLSON proceeds *via* simple expressions. For a comparison of both approaches, reference should be made to the Appendix.

A treatment of the problem of double-layer charging in chronopotentiometry at a mercury-film electrode is of interest for two reasons. First, whereas for semi-infinite diffusion the sum of the dimensionless surface concentrations (at the electrode-solution interface) of electroactive species is a constant², this is not the case when diffusion of one electroactive species is restricted to a solution layer of finite thickness. In this case, the sum of surface concentrations depends on the course of the current function. This complicates theoretical analysis and is a test of the feasibility of the mathematical technique employed. Secondly, chronopotentiometric stripping is sometimes advocated as a technique in trace analysis⁴, and a theoretical evaluation of the potentialities of this method seems worthwhile from a practical viewpoint. A general treatment of reversible constant-current chronopotentiograms obtained at a mercury-film electrode has appeared recently⁵.

In this paper an attempt is made, therefore, to calculate theoretical constant-current chronopotentiograms of an amalgam-forming metal at a mercury-film electrode. Reduction, as well as oxidation is considered, and it is assumed that the electron transfer reaction proceeds reversibly. Linear diffusion is the sole means of mass transport; diffusion of Ox is considered to be semi-infinite, but that of Red is restricted to a mercury-film of thickness, l . A conventional formulation of this diffusion problem leads to the following integral equations for the surface concentrations of Ox and Red, respectively:

* Present address: Department of Chemistry, The Free University, Amsterdam (The Netherlands).

$$C_{O(0,t)} = C_{O^0} \mp \frac{I}{(\pi D_O)^{\frac{1}{2}}} \int_0^t \frac{q_F(\xi)}{(t-\xi)^{\frac{1}{2}}} d\xi; \quad (1)$$

$$C_{R(0,t)} = C_{R^0} \pm \frac{I}{(\pi D_R)^{\frac{1}{2}}} \int_0^t \frac{q_F(\xi)}{(t-\xi)^{\frac{1}{2}}} d\xi \pm \frac{2}{(\pi D_R)^{\frac{1}{2}}} \sum_{i=1}^{\infty} \int_0^t \frac{q_F(\xi)}{(t-\xi)^{\frac{1}{2}}} \exp\left[\frac{-i^2 l^2}{D_R(t-\xi)}\right] d\xi, \quad (2)$$

with C_{O^0} and C_{R^0} the initial concentrations of Ox and Red, homogeneously distributed throughout the aqueous solution and the mercury-film, respectively, and $q_F = i_F/nFA$ (A is the electrode area) the flux of electroactive species at the electrode surface. The subscript F is used to differentiate between this flux and the capacitive part of the current that is consumed in double-layer charging. When q_F is defined to be positive, the upper signs of eqns. (1) and (2) refer to a reduction process, while the lower signs apply to an oxidation process. Electrode potential is given by:

$$n(E - E_{\frac{1}{2}}) = (RT/F) \ln \{(D_O/D_R)^{\frac{1}{2}} C_{O(0,t)} / C_{R(0,t)}\}. \quad (3)$$

When the chronopotentiometric experiment is started at an initial potential, $n(E_i - E_{\frac{1}{2}})$,

$$C_{O^0} / C_{R^0} = \psi (D_R/D_O)^{\frac{1}{2}} = (D_R/D_O)^{\frac{1}{2}} \exp[(nF/RT)(E_i - E_{\frac{1}{2}})]. \quad (4)$$

REDUCTION CHRONOPOTENTIOTHERMOGRAMS

(a) Derivation of integral equation

It is assumed that reduction with a constant total flux, q , is started at an initial potential, E_i . When the initial concentration of Ox is denoted by C_{O^0} , that of Red is

$$C_{R^0} = (D_R/D_O)^{\frac{1}{2}} C_{O^0} / \psi. \quad (5)$$

The following dimensionless quantities are defined:

$$\gamma_O(\lambda) = C_{O(0,t)} / C_{O^0}; \quad (6)$$

$$\gamma_R(\lambda) = (D_R/D_O)^{\frac{1}{2}} C_{R(0,t)} / C_{O^0}; \quad (7)$$

$$\lambda = t/\tau; \quad (8)$$

$$\tau^{\frac{1}{2}} = C_{O^0} (\pi D_O)^{\frac{1}{2}} / 2q; \quad (9)$$

$$h = l^2 / D_R \tau; \quad (10)$$

$$\varphi_F(\lambda) = q_F(t) / q. \quad (11)$$

In the absence of double-layer charging, the surface concentration of Ox, and thus γ_O , becomes zero at the transition time, τ , and the electrode potential attains the value $-\infty$. Substitution of the appropriate dimensionless parameters into eqns. (1) and (2), and using eqn. (5) for the initial concentration of Red, results in the dimensionless forms of the Duhamel integrals:

$$\gamma_O(\lambda) = 1 - \frac{1}{2} \int_0^\lambda \frac{\varphi_F(\xi)}{(\lambda - \xi)^{\frac{1}{2}}} d\xi; \quad (12)$$

$$\gamma_R(\lambda) = \frac{I}{\psi} + \frac{1}{2} \int_0^\lambda \frac{\varphi_F(\xi)}{(\lambda - \xi)^{\frac{1}{2}}} d\xi + I(\lambda), \quad \text{with} \quad (13)$$

$$I(\lambda) = \sum_{i=1}^{\infty} \int_0^\lambda \frac{\varphi_F(\xi)}{(\lambda - \xi)^{\frac{1}{2}}} \exp\left[\frac{-i^2 h}{\lambda - \xi}\right] d\xi. \quad (14)$$

It is easily verified that the dimensionless faradaic flux is given by

$$\varphi_F(\lambda) = I + (C_d/nFq)(dE/dt), \quad (15)$$

with C_d the assumedly constant differential electrode double-layer capacity per unit area. From Nernst's law, the derivative of electrode potential can be found:

$$dE/dt = (RT/nF) \{C_O'(0,t)/C_O(0,t) - C_R'(0,t)/C_R(0,t)\}, \quad (16)$$

where primes denote differentiation with respect to time. Because of the relationship

$$\gamma_O(\lambda) + \gamma_R(\lambda) = I + I/\psi + I(\lambda), \quad (17)$$

one has in terms of dimensionless variables:

$$\frac{dE}{dt} = \frac{RT}{nF\tau} \left\{ \frac{\gamma_O'(\lambda)}{\gamma_O(\lambda)} + \frac{\gamma_O'(\lambda) - I'(\lambda)}{I + I/\psi - \gamma_O(\lambda) + I(\lambda)} \right\} \quad (18)$$

(primes now denote differentiation with respect to λ). Thus, the problem is described by the integral equation:

$$\gamma_O(\lambda) = I - \lambda^{\frac{1}{2}} - K \left\{ \int_0^\lambda \frac{\gamma_O'(\xi)}{\gamma_O(\xi)} \frac{d\xi}{(\lambda - \xi)^{\frac{1}{2}}} + \int_0^\lambda \frac{I'(\xi)}{I + I/\psi - \Gamma(\xi)} \frac{d\xi}{(\lambda - \xi)^{\frac{1}{2}}} \right\}, \quad (19)$$

with

$$K = (RT/nF) \cdot (C_d/nF) \cdot \{C_O^0(\pi D_O \tau)^{\frac{1}{2}}\}^{-1}; \quad (20)$$

$$I(\lambda) = \gamma_O(\lambda) - I(\lambda). \quad (21)$$

(b) Discussion of results

The numerical evaluation of eqn. (19) by HUBER's method is described in the Appendix. Theoretical potential-time curves were calculated for several values of K and h , and some pertinent results are summarized in Fig. 1 and Table 1. It appears that reversible reduction chronopotentiograms at a mercury-film electrode

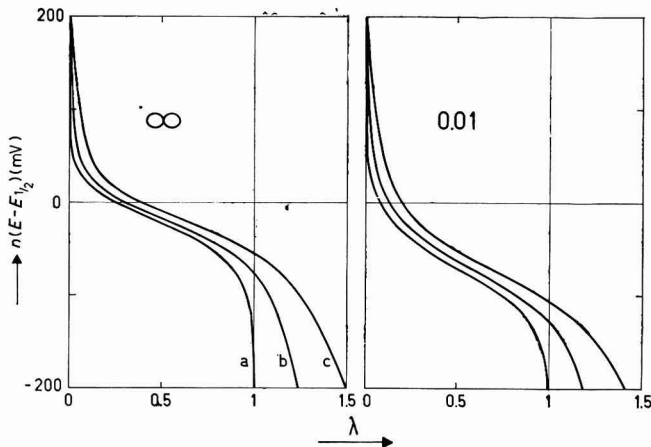


Fig. 1. Distorted reduction chronopotentiograms of an amalgam-forming metal at a mercury-film electrode, for semi-infinite diffusion ($h = \infty$) and $h = 0.01$, and for two values of the distortion parameter K : (b), 0.003; (c), 0.0075. Parameters h and K are defined by eqns. (10) and (20), respectively. The lowest curves would be obtained without double-layer charging: (a), $K = 0$.

TABLE I

PARAMETERS OF CORRECTED REDUCTION CHRONOPOTENTIOTRAGRAMS AT A MERCURY-FILM ELECTRODE

Initial potential $200/n$ mV in all cases. $nE_{\frac{1}{2}}$ is the quarter-wave potential found by the construction of DELAHAY AND MATTAX⁶; λ_{corr}^* is the dimensionless transition time found by REINMUTH'S modified construction (b)⁶, and λ_{corr}^{**} is obtained by application of eqn. (4), ref. 6. REINMUTH'S graphical construction (b) was slightly superior to other procedures. Parameters h and K are defined by eqns. (10) and (20), respectively.

h	$nE_{\frac{1}{2}} \text{ (mV)}$			% Error in λ_{corr}^*		% Error in λ_{corr}^{**}	
	K			K		K	
	0	0.003	0.0075	0.003	0.0075	0.003	0.0075
∞	0	1.7	2.6	-1.7	1.9	0.0	-0.05
3	0.0	2.0	2.6	-0.8	1.8	-0.4	-0.6
1	-0.1	2.1	2.8	-0.9	0.9	-4.4	-4.2
0.3	-3.2	-1.8	0.6	-1.8	0.1	8.3	8.7

can be treated by graphical methods in the same way as those for semi-infinite diffusion when $h \geq 0.3$. However, when this condition must be fulfilled, the time scale on which the experiment is carried out is rather severely restricted. Even with a mercury-film thickness as high as 50μ (possibly an upper limit because of sagging of the film), transition times should not be shorter than 8 sec. Applicability of derivative chronopotentiometry is possible with good accuracy only down to $h \geq 3$.

From the work of BOS AND VAN DALEN⁵ it is apparent that in the h -interval, $0.01 \leq h \leq 1$, a transition takes place from semi-infinite diffusion behaviour to the situation where diffusion in the mercury-film can be considered to be infinitely fast, with a homogeneous distribution of Red throughout the film at any instant. A detailed study of distorted chronopotentiograms in this region seems rather unpromising, as it is unlikely that a single correction method will give a reasonably accurate value of the transition time for all values of h . On the other hand, the limiting case of $h \rightarrow 0$ seems to be of sufficient practical interest to warrant a detailed investigation and this is described in the following section.

(c) Case of $h \rightarrow 0$

In the absence of double-layer charging, the expression for $\gamma_R(\lambda)$ reduces to the following expression when h approaches zero⁵:

$$\gamma_R(\lambda) = 1/\psi + (\pi/4h)^{\frac{1}{2}}\lambda, \quad (22)$$

and electrode potential is given by

$$n(E - E_{\frac{1}{2}}) = (RT/F) \ln \{ (1 - \lambda^{\frac{1}{2}}) / (1/\psi + (\pi/4h)^{\frac{1}{2}}\lambda) \}. \quad (23)$$

It can be shown that the influence of h on the E , λ -curves consists of a shift along the potential axis by defining a new potential scale:

$$nE^* = n(E - E_{\frac{1}{2}}) - (RT/F) \ln (4h/\pi)^{\frac{1}{2}}. \quad (24)$$

Equation (23) then assumes the form:

$$nE^* = (RT/F) \ln \{ (1 - \lambda^{\frac{1}{2}}) / (1/\psi^* + \lambda) \}, \quad \text{with} \quad (25)$$

$$\psi^* = \exp [(nF/RT)E_i^*], \quad (26)$$

with the latter equation analogous to eqn. (4), but written in terms of an initial potential, nE_i^* (eqn. (24)).

When Γ/ψ^* is negligibly small (which is the case for $nE_1^* \geq 200$ mV), $nE^* = 0$ for $\lambda = 0.38197$, and the maximal value of $dE/d\lambda$ occurs at $\lambda = 0.51728$.

The integral equation representation of E, λ -curves distorted by capacity current can be reformulated to demonstrate that a change in h only shifts the E, λ -curve along the potential axis. In order to do this, one defines:

$$\gamma_R^*(\lambda) = (4h/\pi)^{1/2} \gamma_R(\lambda) = \Gamma/\psi^* + \int_0^\lambda \varphi_F(\xi) d\xi, \quad (27)$$

where the integral arises from the approximation^{7,8} of $I(\lambda)$ for $h \rightarrow 0$. Combination of eqns. (23), (24) and (27) gives:

$$nE^* = (RT/F) \ln \gamma_O(\lambda)/\gamma_R^*(\lambda), \quad (28)$$

and it is evident that eqn. (28) can now be used to derive an integral equation analogous to eqn. (19), but in which h does not occur:

$$\gamma_O(\lambda) = \Gamma - \lambda^{1/2} - K \left\{ \int_0^\lambda \frac{\gamma_O'(\xi)}{\gamma_O(\xi)} \frac{d\xi}{(\lambda - \xi)^{1/2}} + \int_0^\lambda \frac{\gamma_R^{*'}(\xi)}{\gamma_R^*(\xi)} \frac{d\xi}{(\lambda - \xi)^{1/2}} \right\}, \quad (29)$$

with K defined by eqn. (20).

This analysis was substantiated by appropriate numerical calculations, and analysis of theoretical E, λ -curves led to the following conclusions:

(i) The formulas for $h \rightarrow 0$ are valid with good accuracy up to $h = 0.1$.

(ii) Graphical correction of distorted chronopotentiograms, between $nE^* = 200$ mV and $nE^* = -200$ mV (at 25°) is best carried out by a Delahay-Mattax procedure⁶, with l_3 dividing the horizontal distance between l_1 and l_2 in the ratio $0.382:0.618$, and measuring the transition time at the intersection of l_3 and the chronopotentiogram. Transition times thus obtained are accurate within $\pm 4\%$ for $K \leq 0.01$ and $h \leq 0.1$. Also, the potential at the intersection of l_3 and the chronopotentiogram is very close to zero (error $\leq 2.6/n$ mV).

(iii) For an initial potential, $nE_1^* = 200$ mV, the equations

$$\lambda_{\max}'/\lambda_{\max} = 1 + 43.7 K, \quad (30)$$

or

$$\tau = 1.9332 t_{\max}' - 0.56138 C_a/nv_0 \quad (30a)$$

can be applied in derivative chronopotentiometry^{2,6}, and the transition time thus obtained has an error for $K = 0.01$, of -0.1% for $h = 0.01$, -1.2% for $h = 0.03$, and -2.9% for $h = 0.1$.

It can thus be concluded that one can measure transition times as short as 1 sec with a mercury-film thickness of 10μ , and analyze the chronopotentiograms by one of the methods described in this section.

OXIDATION CHRONOPOTENTIGRAMS

(a) Integral equation

Derivation of the integral equation describing oxidation chronopotentiograms obtained at a mercury-film electrode and distorted by capacity current proceeds along the same lines as in the previous case. The initial concentration of Red is

denoted by C_R^0 , and that of Ox is given by

$$C_O^0 = (D_R/D_O)^{\frac{1}{2}} \psi C_R^0. \quad (31)$$

The definitions of dimensionless parameters are slightly different from those for a reduction process:

$$\gamma_O(\lambda) = (D_O/D_R)^{\frac{1}{2}} C_O(0,t)/C_R^0; \quad (32)$$

$$\gamma_R(\lambda) = C_R(0,t)/C_R^0; \quad (33)$$

$$\lambda = t/\tau_\infty; \quad (34)$$

$$\tau_\infty^{\frac{1}{2}} = C_R^0(\pi D_R)^{\frac{1}{2}}/2q, \quad (35)$$

with τ_∞ the transition time that would be obtained in the absence of double-layer charging and with infinite mercury-film thickness. Essentially the same steps as in the case previously considered lead to the integral equation:

$$\gamma_O(\lambda) = \psi + \lambda^{\frac{1}{2}} - K \left\{ \int_0^\lambda \frac{\gamma_O'(\xi)}{\gamma_O(\xi)} \frac{d\xi}{(\lambda-\xi)^{\frac{1}{2}}} + \int_0^\lambda \frac{I'(\xi)}{I + \psi - I(\xi)} \frac{d\xi}{(\lambda-\xi)^{\frac{1}{2}}} \right\}, \quad (36)$$

with K and $I(\lambda)$ now defined by

$$K = (RT/nF) \cdot (C_d/nF) \cdot \{C_R^0(\pi D_R \tau_\infty)^{\frac{1}{2}}\}^{-1}; \quad (37)$$

$$I(\lambda) = \gamma_O(\lambda) + I(\lambda), \quad (38)$$

where $I(\lambda)$ is defined by eqn. (14). The quantities, h and $\varphi_F(\lambda)$, are defined by eqns. (10) and (11), respectively.

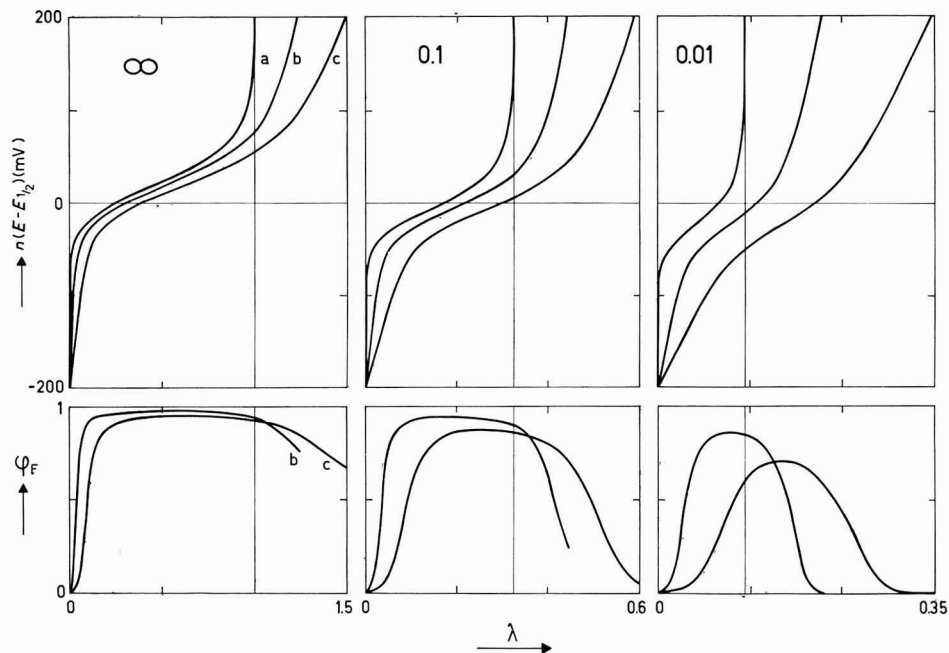


Fig. 2. Distorted oxidation chronopotentiograms of an amalgam-forming metal at a mercury-film electrode, for semi-infinite diffusion ($h = \infty$), $h = 0.1$, and $h = 0.01$. Values of K are 0.003 and 0.0075. Parameter K is now defined by eqn. (37). The uppermost curves would be obtained without double-layer charging ($K = 0$). The lowest figures show the course of the dimensionless faradaic flux.

TABLE 2

PARAMETERS OF CORRECTED OXIDATION CHRONOPOTENTIOTRAGRAMS AT A MERCURY-FILM ELECTRODE
 The remarks pertaining to Table 1 also apply here, except that K is now defined by eqn. (37)

h	$nE_{\frac{1}{2}} (mV)$			% Error in λ_{corr}^*		% Error in λ_{corr}^{**}	
	K	K	K	K	K	K	K
	0	0.003	0.0075	0.003	0.0075	0.003	0.0075
∞	0	-1.7	-2.6	-1.7	1.9	0.0	-0.05
3	-0.6	-2.4	-3.0	0.0	2.4	1.0	0.4
1	-5.6	-7.3	-7.9	0.5	3.5	-3.4	-7.7
0.3	-14.4	-15.8	-16.3	1.5	5.6	-12.1	-19.9

(b) Numerical calculations and results

The description of the numerical evaluation of eqn. (36) is given in the Appendix. Results of the calculations are presented in Fig. 2 and Table 2. From Table 2 it can be inferred that distorted mercury-film oxidation chronopotentiograms can be treated graphically as those for semi-infinite diffusion, for $h > ca. 0.3$, although the corresponding formulae for derivative chronopotentiometry^{2,6} are valid with good accuracy only until $h \geq 3$.

Figure 2 shows that with K remaining the same, distortion becomes more pronounced with decreasing h . For the same reasons as in the case of reduction chronopotentiograms, a detailed study of distorted chronopotentiograms for intermediate h -values was not carried out. The case of $h \rightarrow 0$, however, was investigated in detail (see next section).

From Fig. 2 it is apparent that for small values of h the approximately straight initial and final segments of the E, λ -curve have equal slopes. This is caused by the rapid removal of Red from the thin layer. Initially, the surface concentration of Red decreases and that of Ox increases during electrolysis. When removal of Red is nearly complete, the current efficiency, and thus the supply of Ox, drops almost to zero, and the surface concentration of Ox decreases by diffusion into the aqueous solution. The almost zero current efficiency for the faradaic process after the removal of Red from the mercury-film causes the electrode potential to change as that of a pure capacitance charged by a constant current:

$$\alpha = ndE/d\lambda = (RT/nF)/2K, \quad (39)$$

where α is the slope of both the initial and final straight segments of the E, λ -curve. While the tangent to the initial segment has the equation:

$$nE(\lambda) = nE_i + \alpha\lambda, \quad (40)$$

that of the tangent to the final segment is:

$$nE(\lambda) = nE_i - \alpha \int_0^\lambda \varphi_F(\xi) d\xi + \alpha\lambda, \quad (41)$$

where the integral denotes the amount of charge used for oxidation of Red and which was thus ineffective in double-layer charging. This integral is equal to $\alpha nC_R^0/q\tau_\infty$ because of the practically complete removal of Red near the end of the chronopotentiogram. From eqns. (40) and (41) it follows that the horizontal distance

between the two parallel tangents is equal to:

$$\Delta\lambda = lC_R^0/q\tau_\infty, \quad (42)$$

or

$$\Delta t = lC_R^0/q, \quad (42a)$$

that is, equal to the theoretical transition time for an oxidation chronopotentiogram at a mercury-film electrode, for $h \rightarrow 0$ (see eqn. (42) of ref. 5)*.

(c) Case of $h \rightarrow 0$

Also, for an oxidation process it is advantageous to reformulate eqn. (36) in terms of other parameters for small values of h . Besides a new potential scale a new dimensionless time-axis is also defined:

$$nE^* = n(E - E_{\frac{1}{2}}) - (RT/F) \ln (4h/\pi)^{\frac{1}{2}}; \quad (43)$$

$$\mu = (\pi/4h)^{\frac{1}{2}}\lambda. \quad (44)$$

This definition of the dimensionless time-axis means a normalization of time *versus* the transition time of an oxidation chronopotentiogram in the absence of double-layer charging, for $h \rightarrow 0$ (see eqn. (42) of ref. 5). Without double-layer charging, the equations for the surface concentration functions are:

$$\gamma_O(\mu) = \psi + (4h/\pi)^{\frac{1}{2}}\mu^{\frac{1}{2}}; \quad (45)$$

$$\gamma_R(\mu) = 1 - \mu, \quad (46)$$

leading to the E, μ -curve equation

$$nE^* = (RT/F) \ln \{(\mu^{\frac{1}{2}} + \psi^*)/(1 - \mu)\}, \quad (47)$$

with ψ^* defined by eqn. (26), and $nE_{\frac{1}{2}}^*$ defined in terms of the new potential scale (eqn. (43)). It is easily established that for negligibly small ψ^* ($nE_{\frac{1}{2}}^* \leq -200$ mV), $nE^* = 0$ for $\mu = 0.38197$, and the minimal value of $dE/d\mu$ occurs at $\mu = 0.41421$.

Derivation of the non-linear integral equation describing E, μ -curves distorted by double-layer charging can now be accomplished by defining a new surface concentration, $\gamma_O^*(\mu)$:

$$\gamma_O^*(\mu) = (\pi/4h)^{\frac{1}{2}}\gamma_O(\mu), \quad (48)$$

so that electrode potential is given by

$$nE^* = (RT/F) \ln \gamma_O^*(\mu)/\gamma_R(\mu). \quad (49)$$

The integral equation sought then assumes the form

$$\gamma_O^*(\mu) = \psi^* + \mu^{\frac{1}{2}} - K^* \left\{ \int_0^\mu \frac{\gamma_O^{*'}(\xi)}{\gamma_O^*(\xi)} \frac{d\xi}{(\mu - \xi)^{\frac{1}{2}}} + \int_0^\mu \frac{\gamma_R'(\xi)}{\gamma_R(\xi)} \frac{d\xi}{(\mu - \xi)^{\frac{1}{2}}} \right\}, \quad (50)$$

with

$$K^* = (RT/nF) \cdot (C_a/nF) \cdot (lC_R^0)^{-1}; \quad (51)$$

$$\gamma_R(\mu) = 1 - \int_0^\mu \varphi_F(\xi) d\xi. \quad (52)$$

It should be noted that the distortion parameter, K^* , is determined by the ratio of

* This also applies to chronopotentiometry with restricted diffusion of both Ox and Red⁰, and is thus of special interest to this technique.

double-layer capacity and *total* amount of Red originally present in the mercury-film, while h does not occur in the equations.

Results of appropriate numerical calculations analyzed according to these ideas verified this analysis, and conclusions can be summarized as follows:

(i) Graphical correction of distorted chronopotentiograms, between $nE^* = -200$ mV and $nE^* = 200$ mV (at 25°) is best carried out by the same Delahay-Mattax procedure⁶ as in the case of distorted *reduction* chronopotentiograms for $h \rightarrow 0$. When the transition time is taken as $\mu_1 = 1$ (or $\lambda_1 = (4h/\pi)^{1/2}$), this correction method gives good accuracy (error $\leq 4\%$) for $K^* \leq 0.01$ and $h \leq 0.001$. However, when the transition time is calculated according to

$$\lambda_1 = (4h/\pi)^{1/2} - h/3, \quad (53)$$

or

$$\mu_1 = 1 - (\pi h)^{1/2}/6 \quad (53a)$$

(which can be derived by combination of eqns. (23) and (40) of ref. 5), applicability of this graphical correction method extends up to $h = 0.1$, also with an error of less than 4%. The potential at the intersection of l_3 and the chronopotentiogram is very close to the null point of the new potential scale (error $\leq 4.7/n$ mV for $K^* \leq 0.01$ and $h \leq 0.1$). Because the tangents to the approximately straight initial and final segments of the chronopotentiogram are almost parallel, measuring the transition time at a potential other than the intersection of l_3 and the chronopotentiogram gives nearly the same result. Shifts of ± 40 mV change the measured transition time by only *ca.* 1%.

(ii) Derivative chronopotentiometry is of little use; although the calculated values of μ_{\min}'/μ_{\min} vary in a regular fashion with h and K^* , simple correlations between μ_{\min}'/μ_{\min} and K^* have a very narrow range of validity, and their accuracy is less than that of the graphical correction method.

ACKNOWLEDGEMENTS

This work was supported by the U.S. National Bureau of Standards, Washington. Reproduction of this article, with the customary credit to the source, is permitted. The active interest in this work of Professor M. ARIEL is gratefully acknowledged.

APPENDIX

(a) Numerical evaluation of eqn. (19) by Huber's method

The principle of HUBER's method was explained earlier². Thus, $\gamma_0(\lambda)$ and $\Gamma(\lambda)$ are approximated by linear functions; dropping the subscript, O, one has in the interval $(j-1)\delta \leq \lambda \leq j\delta$:

$$\gamma(\lambda) = (\alpha_j/\delta)\lambda - j\alpha_j + \gamma_j; \quad (54)$$

$$\alpha_j = \gamma_j - \gamma_{j-1}; \quad (55)$$

$$\Gamma(\lambda) = (A_j/\delta)\lambda - jA_j + \Gamma_j; \quad (56)$$

$$A_j = \Gamma_j - \Gamma_{j-1}. \quad (57)$$

It is easily ascertained that both $\gamma(\lambda)$ and $\Gamma(\lambda)$ are monotonously decreasing functions.

In view of this, and the similarity in form between eqn. (19) and eqn. (21) of ref. 2, one can write immediately:

$$\gamma_j = 1 - (j\delta)^{\frac{1}{2}} - KJ, \quad (58)$$

with

$$\begin{aligned} J = & -\delta^{-\frac{1}{2}} \left\{ \sum_{k=k_-}^{j-1} s_k^{-1} \ln \frac{s_k^{-1} \{(j-k+1)(j-k)\}^{\frac{1}{2}} + \{(j-k+1)^{\frac{1}{2}} - (j-k)^{\frac{1}{2}}\} - s_k}{s_k^{-1} \{(j-k+1)(j-k)\}^{\frac{1}{2}} - \{(j-k+1)^{\frac{1}{2}} - (j-k)^{\frac{1}{2}}\} - s_k} \right. \\ & + 2 \sum_{k=1(k \neq k_-)}^{j-1} t_k^{-1} \arctan \frac{(j-k+1)^{\frac{1}{2}} - (j-k)^{\frac{1}{2}}}{t_k + t_k^{-1} \{(j-k+1)(j-k)\}^{\frac{1}{2}}} \\ & + \sum_{k=1}^{j-1} R_k^{-1} \ln \frac{R_k^{-1} \{(j-k+1)(j-k)\}^{\frac{1}{2}} - \{(j-k+1)^{\frac{1}{2}} - (j-k)^{\frac{1}{2}}\} - R_k}{R_k^{-1} \{(j-k+1)(j-k)\}^{\frac{1}{2}} + \{(j-k+1)^{\frac{1}{2}} - (j-k)^{\frac{1}{2}}\} - R_k} \\ & \left. - \delta^{-\frac{1}{2}} \{2v \arctan v + W \ln (1+W)/(1-W)\} \right\}; \quad (59) \end{aligned}$$

$$p_k = (j-k)\alpha_k + \gamma_k; \quad (60)$$

$$p_k < 0 \text{ for } k = k_-; \quad p_k > 0 \text{ for } k \neq k_-; \quad (61)$$

$$P_k = (j-k)A_k + \Gamma_k; \quad (62)$$

$$R_k = \{(1+1/\psi - P_k)/-A_k\}^{\frac{1}{2}}; \quad (63)$$

$$s_k = (p_k/\alpha_k)^{\frac{1}{2}}; \quad (64)$$

$$t_k = (p_k - \alpha_k)^{\frac{1}{2}}; \quad (65)$$

$$v = \{-(\gamma_j - \gamma_{j-1})/\gamma_j\}^{\frac{1}{2}}; \quad (66)$$

$$W = \{-(\Gamma_j - \Gamma_{j-1})/(1+1/\psi - \Gamma_j)\}^{\frac{1}{2}}. \quad (67)$$

Because of eqn. (21) one can write:

$$\Gamma_j = \gamma_j - I(j\delta) \quad (68)$$

and $I(j\delta) = I_j$ is given by^{7,8}:

$$I_j = \delta^{\frac{1}{2}} S_3 + \delta^{\frac{1}{2}} (Z_1 - B_1) \varphi_{F,j}; \quad (69)$$

$$\varphi_{F,j} = \varphi_F(j\delta); \quad (70)$$

$$S_3 = B_1 \varphi_{F,j-1} + \sum_{k=1}^{j-1} [\{(\varphi_{F,k} - \varphi_{F,k-1})(j-k) + \varphi_{F,k}\} Z_{j-k+1} - (\varphi_{F,k} - \varphi_{F,k-1}) B_{j-k+1}]; \quad (71)$$

$$Z_U = z_U - z_{U-1}; \quad (72)$$

$$B_U = b_U - b_{U-1}; \quad (73)$$

$$z_U = \sum_{i=1}^{\infty} z_{U,i} = \sum_{i=1}^{\infty} (2U^{\frac{1}{2}} \exp[-i^2 h/\delta U] - 2(\pi i^2 h/\delta)^{\frac{1}{2}} \operatorname{erfc}(i^2 h/\delta U)^{\frac{1}{2}}); \quad (74)$$

$$b_U = \frac{2}{3} \sum_{i=1}^{\infty} (U^{\frac{1}{2}} \exp[-i^2 h/\delta U] - (i^2 h/\delta) z_{U,i}). \quad (75)$$

For small values of h one may use the approximation^{7,8}:

$$S_3 = -\frac{2}{3} S_2 + \pi^{\frac{1}{2}} \left\{ \frac{1}{2} (h/\delta)^{-\frac{1}{2}} S_1 + \frac{1}{90} (h/\delta)^{\frac{3}{2}} \varphi_{F,j-1} - \frac{1}{945} (h/\delta)^{\frac{5}{2}} (2\varphi_{F,j-1} - \varphi_{F,j-2}) \right\}; \quad (76)$$

$$Z_1 - B_1 = -\frac{2}{3} + \pi^{\frac{1}{2}} \left\{ \frac{1}{4} (h/\delta)^{-\frac{1}{2}} + \frac{1}{6} (h/\delta)^{\frac{1}{2}} - \frac{1}{90} (h/\delta)^{\frac{3}{2}} + \frac{1}{945} (h/\delta)^{\frac{5}{2}} \right\}; \quad (77)$$

$$S_1 = \frac{1}{2} \varphi_{F,0} + \sum_{k=1}^{j-1} \varphi_{F,k}; \quad (78)$$

$$S_2 = -\varphi_{F,j-1} + \sum_{k=1}^{j-1} (\varphi_{F,k} - \varphi_{F,k-1}) \{ (j-k+1)^{\frac{3}{2}} - (j-k)^{\frac{3}{2}} \} + \frac{3}{2} j^{\frac{1}{2}} \varphi_{F,0}. \quad (79)$$

Finally, the faradaic flux, φ_F , is calculated by:

$$\varphi_{F,j} = (Q_{F,j} - Q_{F,j-1}) / \delta; \quad (80)$$

$$Q_{F,j} = -\frac{8\delta^{\frac{1}{2}}}{3\pi} \gamma_j - \frac{8\delta^{\frac{1}{2}}}{3\pi} \left[-\gamma_{j-1} + \sum_{k=1}^j \alpha_k \{ (j-k+1)^{\frac{3}{2}} - (j-k)^{\frac{3}{2}} \} \right] \quad (81)$$

(See eqn. (41) of ref. 2; the parabolic differentiation used there to find $\varphi_{F,j}$ is replaced by first-order differentiation in conformity with the first-order differentiation implicit in the approximate equations (76) and (77)).

The course of the numerical calculations is now fairly obvious. Starting with an estimate for γ_j , one obtains the corresponding estimate for I_j by successively calculating $Q_{F,j}$, $\varphi_{F,j}$, I_j , and finally I_j with eqn. (68). Thus, eqn. (58) can be solved for γ_j by means of a zero-seeking computer procedure *via* repeated bisection and interpolation. Estimates of γ_j should not be greater than a maximum value which is determined by the condition $I_j - I_{j-1} < 0$; this maximum can be expressed in terms of known expressions not containing γ_j . Repeated evaluation of I_j with each new estimate of γ_j is not such a formidable task as might seem at first sight; the involved summations in the various intermediate equations have to be evaluated only once for each value of j .

Inspection of the pertinent formulae reveals that a prior knowledge of $\varphi_{F,0}$ is necessary in order to calculate γ_1 . It was found that varying $\varphi_{F,0}$ between the values 0 and 0.25 had no effect and a value of 10^{-12} was used throughout. It was also found that the approximate solution could be used for $h \leq 0.01$.

A value of $\delta = 0.01$ was used for all calculations; temperature was assumed to be 25° . Electrode potential was calculated by:

$$n(E - E_{\frac{1}{2}}) = (RT/F) \ln \{ \gamma_j / (1 + 1/\psi - I_j) \}. \quad (82)$$

Derivative E, λ -curves were calculated by the procedure described earlier². The calculations were programmed in Algol-60 and carried out with an Elliott 503 digital computer of the Israel Institute of Technology computer centre.

(b) *Evaluation of eqn. (36)*

The numerical evaluation of $\gamma_0(\lambda)$ and $I(\lambda)$ from eqn. (36) follows the same course as that of eqn. (19). The results of the integrations, however, differ, because now $I(\lambda)$ is a monotonously increasing function. Moreover, although $\gamma_0(\lambda)$ initially also increases, this function decreases when stripping is nearly complete. Thus, eqn. (36) leads to the expression:

$$\gamma_j = \psi + (j\delta)^{\frac{1}{2}} - KJ, \quad (83)$$

where the subscript, O, has been dropped again, and with J given by:

$$\begin{aligned}
 J = & \delta^{-\frac{1}{2}} \left\{ \sum_{k=1}^{m; k=k_-} s_k^{-1} \ln \frac{s_k^{-1} \{(j-k+1)(j-k)\}^{\frac{1}{2}} - \{(j-k+1)^{\frac{1}{2}} - (j-k)^{\frac{1}{2}}\} - s_k}{s_k^{-1} \{(j-k+1)(j-k)\}^{\frac{1}{2}} + \{(j-k+1)^{\frac{1}{2}} - (j-k)^{\frac{1}{2}}\} - s_k} \right. \\
 & + 2 \sum_{k=m+1(k \neq k_-)}^{j-1} t_k^{-1} \arctan \frac{(j-k+1)^{\frac{1}{2}} - (j-k)^{\frac{1}{2}}}{t_k + t_k^{-1} \{(j-k+1)(j-k)\}^{\frac{1}{2}}} \\
 & + 2 \sum_{k=1(k \neq K_-)}^{j-1} (R_k'')^{-1} \arctan \frac{(j-k+1)^{\frac{1}{2}} - (j-k)^{\frac{1}{2}}}{(R_k'') + (R_k'')^{-1} \{(j-k+1)(j-k)\}^{\frac{1}{2}}} \\
 & + \sum_{k=K_-} (R_k')^{-1} \ln \frac{(R_k')^{-1} \{(j-k+1)(j-k)\}^{\frac{1}{2}} + \{(j-k+1)^{\frac{1}{2}} - (j-k)^{\frac{1}{2}}\} - R_k'}{(R_k')^{-1} \{(j-k+1)(j-k)\}^{\frac{1}{2}} - \{(j-k+1)^{\frac{1}{2}} - (j-k)^{\frac{1}{2}}\} - R_k'} \\
 & \left. + \delta^{-\frac{1}{2}} (f_{(m)} + 2W' \arctan W') \right\}; \tag{84}
 \end{aligned}$$

$$\gamma_k - \gamma_{k-1} > 0 \quad \text{for } k \leq m; \quad \gamma_k - \gamma_{k-1} < 0 \quad \text{for } k > m; \tag{85}$$

$$\mathbf{1} + \psi - P_k < 0 \quad \text{for } k = K_-; \quad \mathbf{1} + \psi - P_k > 0 \quad \text{for } k \neq K_-; \tag{86}$$

$$R_k' = \{(\mathbf{1} + \psi - P_k) / -A_k\}^{\frac{1}{2}}; \tag{87}$$

$$R_k'' = \{(\mathbf{1} + \psi - P_k) / A_k\}^{\frac{1}{2}}; \tag{88}$$

$$f_{(m)} = v' \ln (\mathbf{1} + v') / (\mathbf{1} - v') \quad \text{for } k \leq m; \tag{89}$$

$$f_{(m)} = 2v \arctan v \quad \text{for } k > m; \tag{89a}$$

$$v' = \{(\gamma_j - \gamma_{j-1}) / \gamma_j\}^{\frac{1}{2}}; \tag{90}$$

$$W' = \{(\Gamma_j - \Gamma_{j-1}) / (\mathbf{1} + \psi - \Gamma_j)\}^{\frac{1}{2}}. \tag{91}$$

The quantities p_k , k_- , P_k , s_k , t_k , and v are defined by eqns. (60)–(62) and (64)–(66). Γ_j is now given by:

$$\Gamma_j = \gamma_j + I_j, \tag{92}$$

and evaluation of I_j follows exactly the procedure outlined in the previous section, except that the right-hand side of eqn. (81) must be multiplied by $-\mathbf{1}$ in order to get the correct expression for $Q_{F,j}$.

Whereas the condition, $\mathbf{1} + \psi - \Gamma_j = \gamma_R(j\delta) \geq 0$, leads to a maximal value of the estimate of γ_j , the condition, $\Gamma_j - \Gamma_{j-1} \geq 0$, leads to a minimum value. When an estimate of γ_j lies outside the interval thus defined, this leads to a breakdown of the calculations because of an attempted root extraction of a negative number (see eqn. (91)).

The numerical calculations were done in the manner described above, except that δ was chosen to be *ca.* 1/100 of the theoretical transition time obtained in the absence of double-layer charging⁵.

(c) *Integral equation formulation according to Olmstead and Nicholson*

The approach used by OLMSTEAD AND NICHOLSON³ is much to be preferred to that used presently. These workers formulated a non-linear integral equation in

terms of the capacity current, *i.e.*, the quantity, $\Gamma - \varphi_F(\lambda)$. Following this approach, for an oxidation process:

$$\gamma_o(\lambda)/\gamma_R(\lambda) = \psi \exp \left[\left(\frac{\Gamma}{2K} \right) \int_0^\lambda \{ \Gamma - \varphi_F(\xi) \} d\xi \right], \quad (93)$$

and substituting the appropriate Duhamel integrals into this equation, gives:

$$\psi + \frac{1}{2} \int_0^\lambda \frac{\varphi_F(\xi)}{(\lambda - \xi)^{\frac{1}{2}}} d\xi = \psi \exp \left[\frac{\lambda}{2K} - \frac{\Gamma}{2K} \int_0^\lambda \varphi_F(\xi) d\xi \right] \times \left\{ \Gamma - \frac{1}{2} \int_0^\lambda \frac{\varphi_F(\xi)}{(\lambda - \xi)^{\frac{1}{2}}} d\xi - I(\lambda) \right\}, \quad (94)$$

with $I(\lambda)$ defined by eqn. (14). It is apparent that application of HUBER'S method to eqn. (94) yields an equation for $\varphi_{F,j}$ which can be solved in the usual way (*cf.* section (a); many formulae presented there can be applied with this approach). Electrode potential is given by:

$$n(E - E_{\frac{1}{2}}) = n(E_i - E_{\frac{1}{2}}) + \frac{RT}{F} \left(\frac{\lambda}{2K} - \frac{\Gamma}{2K} \int_0^\lambda \varphi_F(\xi) d\xi \right). \quad (95)$$

SUMMARY

Constant-current chronopotentiograms of an amalgam-forming metal at a mercury-film electrode, distorted by double-layer charging, are calculated. The problem is formulated as a non-linear integral equation which can be evaluated numerically. The differential electrode double-layer capacity is assumed to be constant. Reduction and oxidation chronopotentiograms are considered and evaluation of results follows two main approaches: (i) a range of mercury-film thickness and transition time (combined into one parameter, h) is established in which the resulting E, t -curves can be treated in the same manner as those for semi-infinite diffusion ($h = \infty$); (ii) methods are outlined by which distorted chronopotentiograms, for $h \rightarrow 0$, can be corrected, and the applicability of these methods for higher values of h is investigated.

REFERENCES

- 1 R. S. RODGERS AND L. MEITES, *J. Electroanal. Chem.*, 16 (1968) 1.
- 2 W. T. DE VRIES, *J. Electroanal. Chem.*, 17 (1968) 31.
- 3 M. L. OLMSTEAD AND R. S. NICHOLSON, *J. Phys. Chem.*, submitted for publication.
- 4 E. BARENDRECHT, *Stripping Voltammetry*, in *Electroanalytical Chemistry*, Vol. 2, edited by A. J. BARD, Marcel Dekker, New York, 1967.
- 5 P. BOS AND E. VAN DALEN, *J. Electroanal. Chem.*, 17 (1968) 21.
- 6 W. T. DE VRIES, *J. Electroanal. Chem.*, 17 (1968) 469.
- 7 W. T. DE VRIES AND E. VAN DALEN, *J. Electroanal. Chem.*, 14 (1967) 315.
- 8 W. T. DE VRIES, Dissertation, Free University, Amsterdam, 1967.
- 9 C. R. CHRISTENSEN AND F. C. ANSON, *Anal. Chem.*, 35 (1963) 205.

EFFECT OF DOUBLE-LAYER CHARGING IN PROGRAMMED-CURRENT CHRONOPOTENTIOMETRY

W. T. DE VRIES*

Department of Chemistry, Israel Institute of Technology, Haifa (Israel)

(Received March 8th, 1968)

INTRODUCTION

In programmed-current chronopotentiometry, the applied cell current varies according to some power of time¹:

$$i_0 = i/A = \beta t^r, \quad (1)$$

with i , the cell current and A , the electrode area. This technique has received renewed attention² in connection with a proposal of PETERS AND BURDEN³ to measure the $dE/dt, t$ -curve during a chronopotentiometric experiment, instead of the E, t -curve. This offers a convenient means of measuring the transition time objectively and of eliminating that part of the electrode double-layer charging that occurs near the end of the chronopotentiogram. It has been demonstrated abundantly⁴⁻⁶ that double-layer charging, which causes the current efficiency of the faradaic process of interest to be less than 100%, is a troublesome phenomenon: an accurate value of the transition time can only be found from a distorted constant-current chronopotentiogram by more or less laborious correction methods⁴⁻⁷. A technique has been proposed⁸ which seeks to eliminate this error by holding the faradaic current at its desired value.

Programmed-current chronopotentiometry has some advantages over the conventional technique employing a constant cell current^{1,2}. The technique employing $r = \frac{1}{2}$ (current varying with the square root of time) is especially advantageous in analytical applications because there is then a linear relationship between concentration of electroactive species and transition time⁹. This, and the fact that reversible programmed-current chronopotentiograms distorted by capacity current are easily calculated by a method developed earlier⁵, led us to investigate the effect of double-layer charging also in this case.

THEORY

Derivation of pertinent equations will not be given here, as this has no new features and follows exactly the course outlined earlier^{1,2,5}. The assumptions are that the electron transfer reaction proceeds reversibly, and a reduction process which starts at an initial potential, E_i , is considered. The initial concentration of

* Present address: Department of Chemistry, The Free University, De Lairesestraat 174, Amsterdam (The Netherlands).

Ox, C_0^0 , is constant throughout the solution, and this applies also to Red, the concentration of which is determined by E_1 . Mass transport is effected only by semi-infinite diffusion. When the cell current varies according to eqn. (1), the equations describing the potential-time curve in the absence of double-layer charging are:

$$n(E - E_1) = (RT/F) \ln \{ \gamma(\lambda) / [\tau + \tau/\psi - \gamma(\lambda)] \}; \quad (2)$$

$$\gamma(\lambda) = C_0(0, t) / C_0^0 = 1 - \lambda^{r+1/2}; \quad (3)$$

$$\lambda = t/\tau; \quad (4)$$

$$\tau^{r+1/2} = C_0^0 D_0^{1/2} \Gamma(r + 3/2) / q_0 \Gamma(r + 1); \quad (5)$$

$$q_0 = \beta/nF; \quad (6)$$

$$\psi = \exp [(nF/RT)(E_1 - E_1)], \quad (7)$$

with $\gamma(\lambda)$ the dimensionless surface concentration (at the electrode/solution interface) of Ox, τ the transition time and $\Gamma(x)$ the gamma function with argument, x .

When double-layer charging is taken into account, the faradaic flux, q_F , is given by:

$$q_F = q_0 t^r + (C_d/nF) \cdot dE/dt, \quad (8)$$

with C_d the differential electrode double-layer capacity per unit area. The dimensionless integral equation describing programmed-current chronopotentiograms distorted by double-layer charging is:

$$\gamma(\lambda) = 1 - \lambda^{r+1/2} - K \int_0^\lambda \frac{d\gamma(\xi)}{d\xi} \left\{ \frac{1}{\gamma(\xi)} + \frac{1}{1 + 1/\psi - \gamma(\xi)} \right\} \frac{d\xi}{(\lambda - \xi)^{1/2}}; \quad (9)$$

$$K = \frac{RT}{nF} \frac{C_d}{nF} \frac{1}{C_0^0 (\pi D_0 \tau)^{1/2}} = \frac{RT}{nF} \frac{C_d}{\beta \tau^{r+1}} \frac{\Gamma(r + 3/2)}{\Gamma(r + 1)}. \quad (10)$$

Equation (9) can be evaluated numerically by Huber's method⁵; the resulting equation can be written as:

$$\gamma(j\delta) = \gamma_j = 1 - (j\delta)^{r+1/2} - KJ, \quad (11)$$

where δ is the width of the intervals into which the λ -axis is divided, and J is given by eqn. (29) of ref. 5.

The integral of the dimensionless faradaic flux, $\varphi_F(\lambda)$, is calculated in a slightly different way:

$$\int_0^\lambda \varphi_F(\xi) d\xi = - \frac{4\delta^{1/2}}{3\pi^{1/2}} \frac{\Gamma(r+1)}{\Gamma(r+3/2)} \sum_{k=1}^j \alpha_k \{ (j-k+1)^{3/2} - (j-k)^{3/2} \}; \quad (12)$$

$$\varphi_F(\lambda) = q_F(t) / (q_0 \tau^r); \quad (13)$$

$$\alpha_j = \gamma_j - \gamma_{j-1} \quad (14)$$

(see eqns. (40) and (41) of ref. 5).

RESULTS AND DISCUSSION

The numerical calculations were carried out as described earlier⁵. Some dis-

torted E, λ -curves are shown in Fig. 1, together with the variations of current efficiency during electrolysis. In the absence of double-layer charging, the dimensionless faradaic flux would be given by $\varphi_F = \lambda^r$ (see eqns. (1), (6), and (13)), and thus the quantity φ_F/λ^r , plotted in Fig. 1, represents the fraction of applied cell current consumed by the faradaic process. The course of the E, λ -curves near the origin arises from the fact that initially the electrode potential varies as the time integral of the current, and only with $r=0$ (constant current) does this result in an approximately straight initial segment.

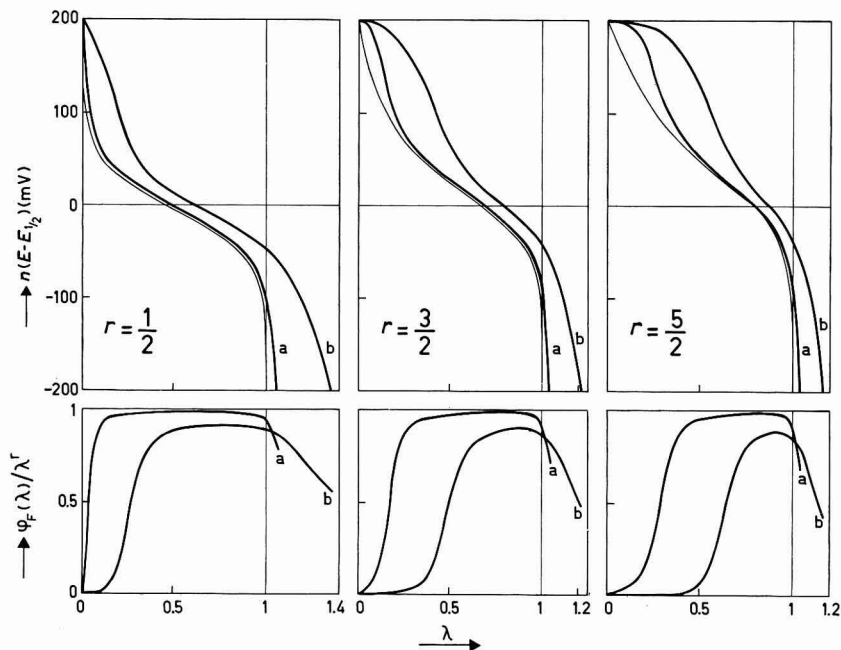


Fig. 1. E, λ -curves distorted by double-layer charging, for $r = \frac{1}{2}$, $\frac{3}{2}$, and $\frac{5}{2}$, and for $K = 10^{-3}$ (a) and 10^{-2} (b). The lowest curves are obtained in the absence of double-layer charging. The lower set of figures depicts the variations in current efficiency during electrolysis.

The region of minimal potential change becomes narrower with increasing r and K . Apparently, when r and/or K increases, the faradaic process occurs at a greater average current density than in the absence of double-layer charging, or with $r \leq 0$. This is also reflected in the variations of current efficiency: the increased average current density causes an increase also in the rate of potential change and thus a decrease in current efficiency.

Notwithstanding the profound influence of double-layer charging, distorted programmed-current chronopotentiograms can yield fairly accurate estimates of the transition time, at least theoretically. A detailed investigation was carried out only for the r -values, $\frac{1}{2}$, 1, and $\frac{3}{2}$, for the range $10^{-4} \leq K \leq 10^{-2}$.

One approach is offered by derivative chronopotentiometry^{2,3}. As in the case of a constant current⁵, linear relationships exist between $\lambda_{\max}'/\lambda_{\max}$ and K ; the following equations hold for an initial potential of $200/n$ mV at 25° :

$$r = \frac{1}{2}: \lambda_{\max}'/\lambda_{\max} = 1 + 37.3 K, \text{ or} \quad (15)$$

$$\tau = 2 t_{\max}' - 1.0814 C_d/n\beta\tau^{\frac{1}{2}} \text{ (maximal error 0.3\%);} \quad (15a)$$

$$r = 1: \lambda_{\max}'/\lambda_{\max} = 1 + 35.4 K, \text{ or} \quad (16)$$

$$\tau = 1.824 t_{\max}' - 1.2091 C_d/n\beta\tau \text{ (maximal error 0.6\%);} \quad (16a)$$

$$r = \frac{3}{2}: \lambda_{\max}'/\lambda_{\max} = 1 + 35.0 K, \text{ or} \quad (17)$$

$$\tau = 1.732 t_{\max}' - 1.3494 C_d/n\beta\tau^{\frac{3}{2}} \text{ (maximal error 1.3\%).} \quad (17a)$$

With increasing r , the proportionality factors in eqns. (15)–(17) became less constant in the range, $10^{-4} \leq K \leq 10^{-2}$.

In order to apply these equations, it is necessary to adjust the initial potential at the value, $200/n$ mV. In the case of a constant current^{5,6}, $E_{\frac{1}{2}}$ could be found by a Delahay–Mattax construction⁷, and therefore programmed-current E, λ -curves were analyzed analogously. The lines, l_1 and l_2 , were drawn in the chronopotentiogram (between $+200/n$ and $-200/n$ mV), tangent to the steep initial segment and to the final segment, respectively. The line, l_3 , was drawn dividing the horizontal distance between l_1 and l_2 in the ratio $\lambda_0: (1 - \lambda_0)$ (for λ_0 , see Table 1). The intersection potential, E_s (at the intersection of l_3 with the E, λ -curve), was not equal to zero but varied with both r and K . The quantity, E_s/r , however, while varying with K , was found to be nearly independent of r . Values of E_s/r for several values of K are given in Table 2; a plot constructed with the aid of this table and used in conjunction with

TABLE 1

PARAMETERS OF PROGRAMMED-CURRENT CHRONOPOTENTIOTRAGRAMS IN THE ABSENCE OF DOUBLE-LAYER CHARGING

λ_0 is the dimensionless time at which $E = E_{\frac{1}{2}}$; at λ_{\max} , the derivative of the reduction chronopotentiogram attains its maximal value. Equations for these quantities are given in refs. 1 and 2, respectively.

r	λ_0	λ_{\max}	r	λ_0	λ_{\max}
0	0.25000	0.44444	$\frac{3}{2}$	0.70711	0.57735
$\frac{1}{2}$	0.50000	0.50000	2	0.75787	0.60586
1	0.62996	0.54288	$\frac{5}{2}$	0.79370	0.62996

TABLE 2

VARIATION OF $E_s/2r$ WITH K

Values of E_s found by the Delahay–Mattax construction⁷ do not deviate more than $1.3/n$ mV from those given in the Table, for $r = \frac{1}{2}$ and $10^{-4} \leq K \leq 10^{-2}$. For $r = 1$, maximum error is $0.5/n$ mV; for $r = \frac{3}{2}$, $3.2/n$ mV. For an oxidation chronopotentiogram, signs should be reversed.

K	$E_s/2r$ (mV)	K	$E_s/2r$ (mV)
0.0001	-1.6	0.001	-3.9
0.0002	-1.9	0.002	-5.3
0.0004	-2.7	0.004	-7.7
0.0006	-3.2	0.006	-9.1
0.0008	-3.5	0.008	-10.5
0.0010	-3.9	0.010	-11.7

the graphical Delahay–Mattax construction, should enable one to find $E_{\frac{1}{2}}$ and adjust the starting potential at the desired value.

The various graphical correction methods studied earlier⁷ were also applied. It was found that Reinmuth's procedure (c), when suitably modified gave good results for $r = \frac{1}{2}$, 1, and $\frac{3}{2}$ (Table 3).

Although this theoretical investigation indicates that it should be possible to obtain accurate transition times from distorted E, λ -curves, programmed-current chronopotentiometry seems to hold little promise. Even in the absence of double-layer charging, this technique has only slight advantages over that employing a constant current, and the effects of double-layer charging seem to nullify these advantages altogether.

TABLE 3

GRAPHICAL CORRECTION OF DISTORTED PROGRAMMED-CURRENT CHRONOPOTENTIOTRAGRAMS

The construction method is that of REINMUTH (c)⁷, where l_4 is shifted towards more positive potentials by an amount, $n\Delta E$. The measured transition time should be multiplied by the factor given in the Table; the greatest error is given in the last column. For an oxidation chronopotentiogram, the shift of l_4 should be towards more negative potentials.

r	$n\Delta E$ (mV)	Factor	Maximal error (%)
$\frac{1}{2}$	190	1.038	2.0
1	190	1.013	1.5
$\frac{3}{2}$	220	0.960	2.0

One advantage cited by SHULTS AND MUELLER² in favour of programmed-current chronopotentiometry is the possibility of minimizing solution composition changes by increasing r . Certainly this can also be done, when employing a constant current, by increasing the current: the charge consumed by the faradaic process (without double-layer charging) is equal to $i\tau$, and this quantity varies inversely proportional to i .

ACKNOWLEDGEMENTS

This work was supported by the U.S. National Bureau of Standards, Washington. Reproduction of this article, with the customary credit to the source, is permitted. The active interest in this work of Professor M. ARIEL is gratefully acknowledged.

SUMMARY

The effect of double-layer charging on programmed-current chronopotentiograms (with current density varying according to the equation, $i_0 = \beta t^r$) is investigated theoretically. Calculated E, t -curves distorted by double-layer charging are analyzed, and methods for obtaining an accurate estimate of the transition time are presented. It is concluded that programmed-current chronopotentiometry offers no advantages over the simpler technique employing a constant current.

REFERENCES

- 1 R. W. MURRAY AND CH. N. REILLEY, *J. Electroanal. Chem.*, 3 (1962) 64.
- 2 W. D. SHULTS AND T. R. MUELLER, *J. Electroanal. Chem.*, 12 (1966) 354.
- 3 D. G. PETERS AND S. L. BURDEN, *Anal. Chem.*, 38 (1966) 530.
- 4 R. S. RODGERS AND L. MEITES, *J. Electroanal. Chem.*, 16 (1968) 1.
- 5 W. T. DE VRIES, *J. Electroanal. Chem.*, 17 (1968) 31.
- 6 M. L. OLMSTEAD AND R. S. NICHOLSON, *J. Phys. Chem.*, submitted for publication.
- 7 W. T. DE VRIES, *J. Electroanal. Chem.*, 18 (1968) 469.
- 8 W. D. SHULTS, F. E. HAGA, T. R. MUELLER AND H. C. JONES, *Anal. Chem.*, 37 (1965) 1415.
- 9 H. HURWITZ AND L. GIERST, *J. Electroanal. Chem.*, 2 (1961) 128.

J. Electroanal. Chem., 19 (1968) 55-60

THE ADMITTANCE OF THE IDEAL REVERSIBLE ELECTRODE WITH
ADSORPTION OF REACTANTS.
ANALYSIS OF THEORETICAL ASPECTS

PAUL DELAHAY

Department of Chemistry, New York University, New York, N.Y. 10003 (U.S.A.)

(Received January 20th, 1968)

A theory of the admittance of the ideal reversible electrode was recently reported from this laboratory¹. This theory embodies the idea of coupling of charging and faradaic processes, originally advanced by the writer², and makes use of the explicit forms of the time-derivatives of the surface excesses, as corrected^{3,4} from previously used forms⁵. The theory¹ corresponds to a particular case, *i.e.*, for an infinite exchange current, of the previously reported⁶ more general theory. Some aspects of theory and some problems raised by its application, which were not treated before, will be considered here, and correlation with SLUYTERS' recent work⁷ will be made*.

ADMITTANCE OF THE IDEAL REVERSIBLE ELECTRODE

We consider a simple electrode reaction, $O + ze = R (z > 0)$, for the usual conditions prevailing in electrode impedance measurements. Species R is in solution either in the electrolyte or in the electrode (amalgam). The exchange current for charge transfer is supposed to be so high that the kinetics of charge transfer can be ignored for the frequency range considered here.

The electrode admittance was derived¹ by solving** the diffusion problem on the basis of the three previously proposed equations². The surface excesses, Γ_O and Γ_R , were expressed as $\Gamma_O(c_O, E)$ and $\Gamma_R(c_R, E)$, respectively, it being understood that there are only 2 independent variables (Nernst equation). These results were re-derived by the writer by using $\Gamma_O(c_O, E)$ and $\Gamma_R(c_O, E)$. The new results, used in this paper, are equivalent to the previous results¹ but differ somewhat from them, particularly in the explicit forms of the parameters. Several errors were made in the transcription of the final results (not in the derivation¹⁸) in ref. 1***. The fact that some error must have been made was pointed out by SLUYTERS⁷.

* Comments about ref. 7 would also apply to TIMMER's thesis⁸, now in preparation, in so far as it contains the same or equivalent statements as ref. 7. SLUYTERS⁷ notes that his paper is abstracted from this thesis. The manuscript of ref. 7 was kindly communicated to the writer by Dr. SLUYTERS.

** SLUYTERS states⁷, with reference to eqn. (4) of ref. 1, that one of our boundary conditions is incorrect. There are in fact two eqns. (4) in ref. 1. The first eqn. (4) reduces exactly to the boundary condition used by SLUYTERS after introduction of the explicit forms of the partial derivatives correctly given by eqns. (5) and (6) in ref. 1. The second eqn. (4) in ref. 1 contains c_O^s as the first term on the right-hand side whereas this term should be c_R^s as it is in the first eqn. (4). This was a mistake of transcription and not an error in the derivation¹⁸.

*** See erratum, *J. Electroanal. Chem.*, 18 (1968) 336.

The resistance, R , and capacity, C , of the parallel equivalent circuit for the electrode admittance are:

$$R = (c_{\text{R}}^{\text{s}}/\lambda B)(\xi_{\text{r}}^2 + \xi_{\text{i}}^2)/(K\xi_{\text{r}} + H\xi_{\text{i}}) \quad (1)$$

$$C = (\lambda B/c_{\text{R}}^{\text{s}}\omega) \{[(H\xi_{\text{r}} - K\xi_{\text{i}})/(\xi_{\text{r}}^2 + \xi_{\text{i}}^2)] + w\} \quad (2)$$

Notations are given in Table 1. The resistance, R , has the compact form of the product of the following quantity (expressed in ohms cm²)

$$c_{\text{R}}^{\text{s}}/\lambda B = -[RT/(zF)^2](2/\omega)^{\frac{1}{2}}(1/c_{\text{O}}^{\text{s}}D_{\text{O}})^{\frac{1}{2}} \quad (3)$$

which is inversely proportional to $\omega^{\frac{1}{2}}$, by a *dimensionless* function of powers of $\omega^{\frac{1}{2}}$.

TABLE 1

NOTATIONS IN EQNS. (1) AND (2)*

$B = -(zF/RT)c_{\text{R}}^{\text{s}}$	<i>Dimensionless parameters</i>
$H = H_0 + H_1\omega^{\frac{1}{2}}$	$g = F_{\text{O}}^{(\text{O})}(2\omega/D_{\text{R}})^{\frac{1}{2}}$
$K = K_1\omega^{\frac{1}{2}} + K_2\omega$	$m = F_{\text{R}}^{(\text{O})}(2\omega/D_{\text{R}})^{\frac{1}{2}}$
$\lambda = zFc_{\text{O}}^{\text{s}}(\omega D_{\text{O}}/2)^{\frac{1}{2}}$	$n = (F_{\text{O}} + F_{\text{R}})^{(\text{E})}(1/B)(2\omega/D_{\text{R}})^{\frac{1}{2}}$
$\xi_{\text{r}} = \varrho_0$	$Q = (c_{\text{O}}^{\text{s}}/c_{\text{R}}^{\text{s}})(D_{\text{O}}/D_{\text{R}})^{\frac{1}{2}}$
$\xi_{\text{i}} = \varrho_0 + \varrho_1\omega^{\frac{1}{2}}$	$S = c_{\text{O}}^{\text{s}}/c_{\text{R}}^{\text{s}}$
<i>Frequency-independent parameters</i>	$u = (1/zF)(2\omega/D_{\text{O}})^{\frac{1}{2}}q^{(\text{O})}$
$\varrho_0 = Q(1 + Q)$	$w = (1/BS)(2\omega/D_{\text{O}})^{\frac{1}{2}}[(q/zF) + F_{\text{O}}]^{(\text{E})}$
$\varrho_1 = (g + m)SQ\omega^{-\frac{1}{2}}$	
$H_0 = -2Q$	
$H_1 = -K_1 = -[Qn + (Qu + gS)]\omega^{-\frac{1}{2}}$	
$K_2 = n(Qu + gS)\omega^{-1}$	

* *Notations:* c_{O}^{s} and c_{R}^{s} , bulk concentrations of O and R, respectively; q , charge density on the electrode; F_{O} and F_{R} , relative surface excesses of O and R; D , F , R , T as usual; the superscripts (O) and (E) represent the independent variables, c_{O}^{s} and E , with respect to which the quantities with one of these superscripts are differentiated.

The quantity, Q , is related to the potential, E , by the polarographic theory of reversible waves if generation *in situ* is adopted. Thus

$$E = E_{\frac{1}{2}} + (RT/zF) \ln Q$$

where $E_{\frac{1}{2}}$ is the half-wave potential. Q can also be calculated directly if the D 's are known or it can be determined from electrode admittance data as shown in the section on analysis of data.

The coefficients of this function are indexed to indicate the power α of the factor $(\omega^{\frac{1}{2}})^{\alpha}$ by which each parameter is multiplied, e.g., K_1 is multiplied by $\omega^{\frac{1}{2}}$, K_2 by $(\omega^{\frac{1}{2}})^2$, etc. The indexed parameters are expressed in terms of dimensionless quantities and zero or negative powers of $\omega^{\frac{1}{2}}$. Some elegance is claimed for this formalism, but from a purely pragmatic point of view any formula can be regarded as satisfactory as long as it is correct. A similar comment applies to the capacity, C .

The explicit dependence of frequency is shown in the following expanded equations in which all coefficients are frequency-independent except λ and w (both proportional to $\omega^{\frac{1}{2}}$)

$$R = \frac{c_{\text{R}}^{\text{s}}}{\lambda B} \frac{\varrho_0^2 + (\varrho_0 + \varrho_1\omega^{\frac{1}{2}})^2}{(K_1\omega^{\frac{1}{2}} + K_2\omega)\varrho_0 + (H_0 + H_1\omega^{\frac{1}{2}})(\varrho_0 + \varrho_1\omega^{\frac{1}{2}})} \quad (4)$$

$$C = \frac{\lambda B}{c_{\text{R}}^{\text{s}}\omega} \left[\frac{(H_0 + H_1\omega^{\frac{1}{2}})\varrho_0 - (K_1\omega^{\frac{1}{2}} + K_2\omega)(\varrho_0 + \varrho_1\omega^{\frac{1}{2}})}{\varrho_0^2 + (\varrho_0 + \varrho_1\omega^{\frac{1}{2}})^2} + w \right] \quad (5)$$

DOUBLE-LAYER PARAMETERS

Four double-layer parameters

If we leave out from eqns. (4) and (5) the quantities that do not pertain to the double layer, we are left with q_1 , $K_1 (= -H_1)$, K_2 , $H_1 q_1$, $K_2 q_1$ and $w\omega^{-\frac{1}{2}}$. This set reduces to q_1 , K_1 , K_2 and $w\omega^{-\frac{1}{2}}$ and corresponds to the following dimensionless quantities:

$$g + m = (\Gamma_O + \Gamma_R)^{(O)} (2\omega/D_R)^{\frac{1}{2}} \quad (6)$$

$$n = -(\Gamma_O + \Gamma_R)^{(E)} (RT/zF) (1/c_R^s) (2\omega/D_R)^{\frac{1}{2}} \quad (7)$$

$$Qu + gS = (q/zF + \Gamma_O)^{(O)} (c_O^s/c_R^s) (D_O/D_R)^{\frac{1}{2}} (2\omega/D_O)^{\frac{1}{2}} \quad (8)$$

$$w = -(q/zF + \Gamma_O)^{(E)} (RT/zF) (1/c_O^s) (2\omega/D_O)^{\frac{1}{2}} \quad (9)$$

The corresponding double-layer parameters, $(\Gamma_O + \Gamma_R)^{(O)}$, $(\Gamma_O + \Gamma_R)^{(E)}$, $[(q/zF) + \Gamma_O]^{(O)}$ and $[(q/zF) + \Gamma_O]^{(E)}$, are the first derivatives, with respect to c_O^s and E , of the thermodynamic quantities, $\Gamma_O + \Gamma_R$ and $(q/zF) + \Gamma_O$, which appear in the equation of the electrocapillary curve for the ideal reversible electrode considered here. We write this equation*

$$d\gamma = -(q - zF\Gamma_R)dE - (\Gamma_O + \Gamma_R)RT \, d \ln c_O^s \quad (10a)$$

$$= -[(q + zF\Gamma_O) - zF(\Gamma_O + \Gamma_R)]dE - (\Gamma_O + \Gamma_R)RT \, d \ln c_O^s \quad (10b)$$

where γ is the interfacial tension. This equation is approximate because it is written in terms of the concentration, c_O^s , rather than the chemical potential of the salt-producing species, O, in solution. This simplification is justified here because of the large excess of supporting electrolyte in solution**. Note also that q is not a thermodynamic quantity for the ideal reversible electrode because $q + zF\Gamma_O$ cannot be split by thermodynamic argument alone.

It should be noted that the time-derivatives of $\Gamma_O + \Gamma_R$ and $q + zF\Gamma_O$ already appear in the starting three general equations² used in solving the diffusion problem. Formulation in terms of 4 double-layer parameters is thus contained in the theory from its very start.

Correlation with electrocapillary curve data

In the present theory, the electrode admittance is interpreted purely in terms of (a) thermodynamic parameters characterizing the perturbation of the double layer of an ideal reversible electrode, (b) the thermodynamics of the electrode reaction (Nernst equation) and (c) the transport process, assumed to be purely diffusion in presence of a large excess of supporting electrolyte. This is the only information that one would expect to introduce into the theory, and also to obtain from experiment, because kinetics of the electrode reaction is not considered.

More detailed information is necessary in the general theory⁶ when the kinetics of charge transfer is introduced. *Six* double-layer parameters are then needed, namely the first derivatives of $\Gamma_O + \Gamma_R$ and $q + zF\Gamma_O$ with respect to the *three*

* See MOHILNER⁹ for a very thorough treatment.

** The diffusion problem could have been expressed in terms of activities rather than concentrations, and correlation with the rigorous double-layer quantities would then have been made.

independent variables, c_0^s , c_R^s and E . The exchange current (or some other kinetic parameters) is also introduced.

The foregoing considerations show that nothing new is learned about the double layer of the ideal reversible electrode that cannot be obtained by the time-honored determination of electrocapillary curves for ideal reversible electrodes*. The electrode impedance yields the first partial derivatives of $\Gamma_O + \Gamma_R$ and $q + zF\Gamma_O$ with respect to the two independent variables characterizing the system, whereas electrocapillary curve determinations give** the quantities, $\Gamma_O + \Gamma_R$ and $q + zF\Gamma_O$. Integration of the derivatives, obtained from impedance measurements, requires one integration constant for each quantity. These constants can be determined by electrocapillary curve measurements or by introduction of non-thermodynamic arguments. *Accurate* determination of electrocapillary curves with amalgam-electrodes is a fairly arduous task (in contrast with simple but not very accurate drop-time measurements), whereas impedance measurements are somewhat easier, especially if one is not too demanding about cell and electrode geometry. Finally, it is noted that the thermodynamic approach has the obvious and distinct advantage of not requiring a model, whereas this is not the case in the interpretation of admittance measurements. The theoretical path in the latter method is less direct and certainly much longer than in the thermodynamic approach, as is clearly shown by the fact that the problem was unravelled only 20 years after the first electrode admittance measurements for fast processes*** (RANDLES and, independently, ERSHLER, 1947) and several unsuccessful attempts in which the coupling between the faradaic and charging processes was not recognized.

The foregoing comments also apply to other electrochemical relaxation methods, and the current–overvoltage–time relationships recently derived^{11,12} could be rewritten, accordingly in the particular case of the ideal reversible electrode. Four double-layer parameters would appear in the resulting equations, and the additional thermodynamic relationship, about to be discussed, would also apply.

Reduction to three independent double-layer parameters

The four parameters, $(\Gamma_O + \Gamma_R)^{(O)}$, $(\Gamma_O + \Gamma_R)^{(E)}$, $[(q/zF) + \Gamma_O]^{(O)}$ and $[(q/zF) + \Gamma_O]^{(E)}$, reduce to *three independent* parameters as is realized if the cross-derivatives****, $\partial^2\gamma/\partial \ln c_0^s \partial E$ and $\partial^2\gamma/\partial E \partial \ln c_0^s$ of eqn. (10b), are taken. Thus

$$(\Gamma_O + \Gamma_R)^{(E)} = (zF/RT)c_0^s \{ [(q/zF) + \Gamma_O]^{(O)} - (\Gamma_O + \Gamma_R)^{(O)} \} \quad (11)$$

The three independent parameters are, *e.g.*, $[(q/zF) + \Gamma_O]^{(O)}$, $[(q/zF) + \Gamma_O]^{(E)}$ and $(\Gamma_O + \Gamma_R)^{(O)}$, the parameter, $(\Gamma_O + \Gamma_R)^{(E)}$, being then given by eqn. (11). One can of course select any one of the three derivatives in eqn. (11) as the dependent parameter.

SLUYTERS⁷, referring to unpublished work by REINMUTH, expresses the electrode admittance in terms of three double-layer quantities, one of these quantities being a combination of two double-layer parameters. He did not state that the reduc-

* FRUMKIN¹⁰ in one of his first papers had already made such electrocapillary curve studies with amalgam-electrodes in 1920!

** SLUYTERS states⁷ that the quantities, $\Gamma_O + \Gamma_R$ and $q + zF\Gamma_O$, are obtained from electrode admittance measurements but he probably means the first derivatives of these quantities with respect to the two independent variables.

*** FRUMKIN had already made such measurements in 1940 in hydrogen overvoltage studies.

**** The same procedure was applied to the ideal polarized electrode¹³.

tion from four to three parameters follows directly from the thermodynamics of the electrocapillary curve. The choice of three parameters is not unique as is shown in the discussion of eqn. (11), and neither is this point made by SLUYTERS⁷.

Equation (11) is now written in terms of our dimensionless parameters, namely

$$n = S(g + m) - (Qu + gS) \quad (12)$$

One of the parameters, q_1 , K_1 or K_2 , appearing in eqns. (4) and (5) for R and C can now be eliminated. We eliminate K_2 which is easily derived as

$$K_2 = (q_1 - QK_1)(K_1 - q_1)/Q(1 - Q)^2 \quad (13)$$

We are left in eqns. (4) and (5) with the three independent parameters, q_1 , K_1 and $w\omega^{-\frac{1}{2}}$.

In retrospect, one could re-derive R and C by using three independent double-layer parameters from the start by means of eqn. (11). This would lead, of course, to the same result as reported here. However, we did not follow this more direct approach, and neither did SLUYTERS⁷.

The thermodynamic restriction of eqn. (11) on the four double-layer parameters also provides the explanation for the seemingly abnormal positive slope of the $R\omega^{\frac{1}{2}}$ vs. $\omega^{\frac{1}{2}}$ plot in Fig. 1 of ref. 1. SLUYTERS⁷ considers this slope as abnormal and infers from this and other arguments that our treatment¹ was in error. Actually, the values plotted in this diagram are correct, as the writer ascertained by recalculating the coordinates of several points. The abnormal slope simply results from the choice of double-layer parameters which are not self-consistent. Thus, the diagram has no physical significance but is correct for the parameters that were used.

It should be noted that $dR\omega^{\frac{1}{2}}/d\omega^{\frac{1}{2}} \rightarrow 0$ for $\omega^{\frac{1}{2}} \rightarrow 0$, and consequently the curve in Fig. 1 should have a horizontal tangent at $\omega^{\frac{1}{2}} = 0$. The same comment applies to SLUYTERS' Fig. 1⁴ which shows a linear extrapolation for $0 \leq \omega^{\frac{1}{2}} \leq 50$ with a negative slope down to $\omega^{\frac{1}{2}} = 0$.

Selection of independent variables

Instead of using c_{O^s} and E as independent variables, one can just as well select c_{R^s} and E or c_{O^s} and c_{R^s} . One can equally use the linear combination $\psi = c_{O^s}D_{O^{\frac{1}{2}}} + c_{R^s}D_{R^{\frac{1}{2}}}$ and E , as was done by SLUYTERS⁷. The use of ψ has the practical advantage that this quantity is invariant when E varies in polarographic generation *in situ*. The use of ψ has the disadvantages (a) of mixing purely thermodynamic quantities with transport quantities (D_{O^s} and D_{R^s}), and (b) of complicating the expressions for the double-layer parameters. If generation *in situ* is not adopted, there is no advantage in using ψ .

CONDITION FOR APPLICABILITY OF THE CLASSICAL THEORY (WARBURG ADMITTANCE)

In the limiting case, for which the Warburg theory holds, the elements R and C of eqns. (1) and (2) are:

$$R = \frac{c_{R^s}}{\lambda B} \frac{zq_0}{H_0} = \frac{RT}{(zF)^2} \left(\frac{2}{\omega}\right)^{\frac{1}{2}} \left(\frac{1}{c_{O^s}D_{O^{\frac{1}{2}}}} + \frac{1}{c_{R^s}D_{R^{\frac{1}{2}}}}\right) \quad (14)$$

$$C = \frac{\lambda B}{c_R s \omega} \frac{H_0}{2q_0} + q^{(E)} = \frac{(zF)^2}{RT} \frac{1}{(2\omega)^{\frac{1}{2}}} \frac{1}{1/c_0 s D_0^{\frac{1}{2}} + 1/c_R s D_R^{\frac{1}{2}}} + q^{(E)} \quad (15)$$

Equations (14) and (15) are immediately obtained by setting $(g+m) = n = Qu + gS = 0$, and by introducing $\Gamma_0^{(E)} = 0$ in w . Note that $q^{(E)}$ appears in eqn. (15) since C is the capacity corresponding to the total electrode admittance and not the capacity for the faradaic part only.

The conditions under which the classical theory can be applied for all practical purposes can be established immediately by comparing eqns. (14) and (15) with eqns. (4) and (5). Comparison of eqns. (4) and (14) yields the following two simultaneous conditions:

$$|q_1| \omega^{\frac{1}{2}} \ll q_0 \quad (16)$$

$$|K_2| \omega \ll |H_0| \quad (17)$$

Note: (a) q_0 is always positive and the equality, $H_1 = -K_1$ (Table 1), was used in arriving at eqn. (17); (b) K_2 is given by eqn. (13) in terms of q_1 and K_1 . Comparison of eqn. (5) with eqn. (15) yields the additional condition:

$$|2H_1 \omega^{\frac{1}{2}} + 2q_0 w| \ll |H_0| \quad (18)$$

Conditions (16)–(18) must be satisfied simultaneously for the classical theory to be applicable. Explicit forms of these conditions are:

$$|(\Gamma_0 + \Gamma_R)^{(O)}| (2\omega/D_R)^{\frac{1}{2}} \ll (1+Q)/S \quad (19)$$

$$|(\Gamma_0 + \Gamma_R)^{(E)}| (q/zF + \Gamma_0)^{(O)} | (RT/zF) (1/c_R s) (\omega/(D_0 D_R)^{\frac{1}{2}}) \ll 1 \quad (20)$$

$$\left| \begin{aligned} & (\Gamma_0 + \Gamma_R)^{(E)} \frac{RT}{zF} \frac{1}{c_R s} \left(\frac{2\omega}{D_R} \right)^{\frac{1}{2}} - \left(\frac{q}{zF} + \Gamma_0 \right)^{(O)} \left(\frac{2\omega}{D_0} \right)^{\frac{1}{2}} \\ & - \left(\frac{q}{zF} + \Gamma_0 \right)^{(E)} (1+Q) \frac{RT}{zF} \frac{1}{c_0 s} \left(\frac{2\omega}{D_0} \right)^{\frac{1}{2}} \end{aligned} \right| \ll 1 \quad (21)$$

The quantity, $(\Gamma_0 + \Gamma_R)^{(E)}$, in conditions (20) and (21) can be eliminated by means of eqn. (11). These conditions, to be satisfied simultaneously, become more stringent with increasing frequency. They are always satisfied for $\omega \rightarrow 0$. Note also that these conditions may not be fulfilled, *in principle*, for sufficiently high *positive* or *negative* values of double-layer parameters.

A particularly simple situation, in which the classical theory holds although there is strong adsorption, could be observed when eqns. (1) and (2) reduce to eqns. (14) and (15) but with $(q+zF\Gamma_0)^{(E)}$ instead of $q^{(E)}$ in eqn. (15). In this case, the double-layer capacity observed in presence of O can be significantly different from that for the supporting electrolyte alone, but there is no other complication. The analysis of data is then straightforward (*e.g.*, by SLUYTERS' complex plane analysis).

ANALYSIS OF EXPERIMENTAL DATA

The problem is to determine the three independent double-layer parameters. This can be done in two ways: (a) determine q_1 , K_1 and $\omega\omega^{-\frac{1}{2}}$ by making use of eqn. (13) to obtain K_2 ; (b) determine the four parameters, q_1 , K_1 , K_2 and $\omega\omega^{-\frac{1}{2}}$,

from experimental data. The second procedure has the disadvantage, in comparison with the first, of involving the determination of one more parameter, but has the advantage of providing an independent check of the computation by means of eqn. (13). This relationship is automatically verified in the first procedure and thus cannot be used for further verification.

The analysis can best be carried out by using data obtained over the full frequency range in which measurements are made. This is certainly more advantageous than to use only the limits for $\omega \rightarrow 0$ and $\omega \rightarrow \infty$ because the computation of these limits by extrapolation may be somewhat uncertain, particularly for $\omega \rightarrow \infty$. Recent improvements¹⁵ in bridge design (use of transformer-ratio bridges) and a better understanding of the requirements for cell and electrode design, which have made it possible to push the upper limit of double-layer capacity measurements* well above 100 KHz, may reduce the uncertainty on the limits for $\omega \rightarrow \infty$. It remains to be seen whether accuracy would be sufficiently high, at the highest frequencies that can now be used, especially in view of the serious limitation imposed by ohmic drop in the cell.

It is suggested that analysis of data over the whole frequency range can be accomplished by a *variational method*. Such methods have not been applied by electrochemists, to the writer's knowledge, primarily because there was no real need for them**. The power of these methods, coupled with the high speed of present-day digital computers, is such that the determination of the 4 or 3 parameters, discussed here, from experimental data is an easy task. Of course, *unambiguous* assignment of parameters is only feasible provided sufficiently accurate experimental data are available. The last restriction is the only real one, and the complexity of the equations is a relatively minor aspect of the problem***.

Variational computations can be started with any educated guess of the values of the parameters to be determined, barring complications resulting from oscillation or non-convergence of the solution. It is, however, profitable to start with approximate values of the parameters to be determined. It will be shown how these approximate values can be computed from the limits for $\omega \rightarrow 0$ and $\omega \rightarrow \infty$ prior to any variational computation. It is even possible, but by no means certain that such a simple analysis suffices in some instances despite its disadvantage of using only data in the lower and upper frequency ranges.

The points being made here can be summarized as follows: (a) it suffices to have even very approximate values of the parameters to be determined as a starting point; (b) these starting values can be computed by the method described below or by any other suitable method; (c) the application of a variational method will then improve the accuracy on the parameters to any degree that is justified by the accuracy

* LORENZ¹⁶ had already published in 1960 results of such measurements with frequencies reaching above 1 MHz.

** Electrochemists learned to use the Laplace transformation, introduced by BRDIČKA AND KOUTECKÝ (1947) in electrochemical problems, when they attacked problems which could be solved conveniently, but not uniquely, by this method.

*** This comment also applies to the possibility of application of our general theory⁶. SLUYTERS considers⁷ that "the resulting equations are so complicated that it seems impossible to use them for analysing data". This comment would have been almost valid before the advent of high-speed digital computers. The real difficulty is the need for sufficiently accurate data and not the complexity of the equations. No opinion is ventured here whether the accuracy requirements can be met with present techniques of measurements.

of experimental data; (d) the need for "manual" methods for the most accurately feasible analysis of data, whether they be elegant or tortuous, is no longer so pressing once it is realized that the accuracy can be improved by rather powerful computational techniques as much as is warranted by the accuracy of experimental data. These comments apply also to the analysis of data obtained by any of the relaxation methods in electrode kinetics whenever there is a difficult computational problem. The use of computers just for the sake of it is not advocated.

TABLE 2

SOME LIMITS

$R_{\omega \rightarrow 0} \rightarrow \infty$
$R_{\omega \rightarrow \infty} \rightarrow 0$
$C_{\omega \rightarrow 0} \rightarrow \infty$
$C_{\omega \rightarrow \infty} \rightarrow (B/c_{R^s})(\lambda/\omega^{\frac{1}{2}})[-K_2/q_1 + w/\omega^{\frac{1}{2}}]$
$(\omega^{\frac{1}{2}}R)_{\omega \rightarrow 0} \rightarrow (c_{R^s}/B)(\omega^{\frac{1}{2}}/\lambda)(2q_0/H_0)(= -c_{R^s}/B)(\omega^{\frac{1}{2}}/\lambda)(I + Q)$
$(\omega^{\frac{1}{2}}R)_{\omega \rightarrow \infty} \rightarrow (c_{R^s}/B)(\omega^{\frac{1}{2}}/\lambda) q_1^2/(q_0K_2 + q_1H_1)$
$(\omega^{\frac{1}{2}}C)_{\omega \rightarrow 0} \rightarrow (B/c_{R^s})(\lambda/\omega^{\frac{1}{2}})(H_0/2q_0)(= - (B/c_{R^s})(\lambda/\omega^{\frac{1}{2}}) I/(I + Q))$
$(\omega^{\frac{1}{2}}C)_{\omega \rightarrow \infty} \rightarrow \infty$
$(\omega^{\frac{1}{2}}RC)_{\omega \rightarrow 0} \rightarrow \infty$
$(\omega^{\frac{1}{2}}RC)_{\omega \rightarrow \infty} \rightarrow (w/\omega^{\frac{1}{2}}) q_1^2/(K_2q_0 + H_1q_1)$
$(\omega RC)_{\omega \rightarrow 0} \rightarrow I$
$(\omega RC)_{\omega \rightarrow \infty} \rightarrow \infty$
$\left(\frac{d\omega^{\frac{1}{2}}R}{d\omega^{\frac{1}{2}}}\right)_{\omega \rightarrow 0} \rightarrow 0$
$\left(\frac{d\omega^{\frac{1}{2}}R}{d\omega^{\frac{1}{2}}}\right)_{\omega \rightarrow \infty} \rightarrow 0$
$\left(\frac{d\omega^{\frac{1}{2}}C}{d\omega^{\frac{1}{2}}}\right)_{\omega \rightarrow 0} \rightarrow \frac{B}{c_{R^s}} \frac{\lambda}{\omega^{\frac{1}{2}}} \left[\frac{2H_1q_0 - H_0q_1}{2q_0^2} + \frac{w}{\omega^{\frac{1}{2}}} \right]$
$\left(\frac{d\omega^{\frac{1}{2}}C}{d\omega^{\frac{1}{2}}}\right)_{\omega \rightarrow \infty} \rightarrow \frac{B}{c_{R^s}} \frac{\lambda}{\omega^{\frac{1}{2}}} \left[-\frac{K_2}{q_1} + \frac{w}{\omega^{\frac{1}{2}}} \right]$

Some of the limits used in the analysis are listed in Table 2. The procedure is as follows:

(a) H_0 , and consequently Q (Table 1), is obtained from $(\omega^{\frac{1}{2}}R)_{\omega \rightarrow 0}$ and/or $(\omega^{\frac{1}{2}}C)_{\omega \rightarrow 0}$.

(b) $w\omega^{-\frac{1}{2}}$ is computed from:

$$w\omega^{-\frac{1}{2}} = (c_{R^s}/B)(\omega^{\frac{1}{2}}/\lambda)[(\omega^{\frac{1}{2}}RC)_{\omega \rightarrow \infty}/(\omega^{\frac{1}{2}}R)_{\omega \rightarrow \infty}] \quad (22)$$

and from the independently determined value of D_0 (appearing in λ), e.g., from polarographic diffusion current constant. The parameter, $(q + zF\Gamma_0)^{(E)}$, is thus obtained.

(c) Compute K_2/q_1 from $C_{\omega \rightarrow \infty}$ using the value of $w\omega^{-\frac{1}{2}}$ calculated in (b).

(d) Note that

$$\varrho_1 = (\omega^{\frac{1}{2}} RC)_{\omega \rightarrow \infty} (\omega \omega^{-\frac{1}{2}})^{-1} [(K_2/\varrho_1)\varrho_0 + H_1] \quad (23)$$

where $\omega \omega^{-\frac{1}{2}}$ and K_2/ϱ_1 are now known. Introduction of ϱ_1 from eqn. (23) in $(d\omega^{\frac{1}{2}}C/d\omega^{\frac{1}{2}})_{\omega \rightarrow 0}$ then yields a linear equation in H_1 which is solved. Compute then ϱ_1 from eqn. (23); ϱ_1 thus yields $(\Gamma_0 + \Gamma_R)^{(D)}$.

(e) Compute K_2 from the values K_2/ϱ_1 and ϱ_1 obtained in (c) and (d), respectively.

(f) Determine $n\omega^{-\frac{1}{2}}$ from the values of $H_1 = -K_1$ and K_2 in Table I, the combination of which yields

$$Qn\omega^{-\frac{1}{2}} + (K_2/n\omega^{-\frac{1}{2}}) + H_1 = 0 \quad (24)$$

This yields $(\Gamma_0 + \Gamma_R)^{(E)}$.

(g) From K_2 and $n\omega^{-\frac{1}{2}}$ determine $(Qu + gS)\omega^{-\frac{1}{2}}$, *i.e.*, $(q + zF\Gamma_0)^{(G)}$.

No use was made of the thermodynamic relationship (II) in this procedure, and this equation can thus be used for the purpose of verification. One could use eqn. (I3), after division on the left-hand side and right-hand side by ϱ_1 , and introduce ϱ_1 from eqn. (23). The only unknown is then K_1 which can thus be determined. Once $K_1 (= -H_1)$ is known, ϱ_1 is obtained from eqn. (23) and K_2 from eqn. (I3). Steps (f) and (g) then follow. This modified procedure avoids the use of $(d\omega^{\frac{1}{2}}C/d\omega^{\frac{1}{2}})_{\omega \rightarrow 0}$.

The foregoing method of analysis has the advantage of not requiring iteration and the disadvantages of using only the limits. No claim is made here about the accuracy that can be achieved, especially since there may be a propagation of errors as the parameters are successively computed. Anyway, accuracy can be increased as much as desired, and allowed by the accuracy of experiment, by further variational computation, as already noted.

CORRELATION BETWEEN REINMUTH'S EQUATIONS, AS RE-DERIVED BY SLUYTERS, WITH EQUATIONS (1) AND (2)

SLUYTERS states^{4,7} that equations for the electrode impedance for the ideal reversible electrode were derived by REINMUTH on the basis of the writer's three general equations². Use was also made of the correct time-derivatives of the surface excesses given independently by SLUYTERS⁴ and by us³. SLUYTERS re-derived REINMUTH's results, as yet unpublished, by following the procedure which we had used before^{1,5,6} and which is inspired from GERISCHER's derivation¹⁵ of the classical theory of the faradaic impedance. The identity of SLUYTERS' eqns. (AI4) and (AI5) in ref. 7 with the foregoing eqns. (1) and (2) [that is with eqns. (I0) and (II) of ref. 1 with the correct parameters] is shown in Appendix.

ACKNOWLEDGEMENT

This work was supported by the Office of Naval Research. Dr. D. J. KOIJMAN raised the question of the number of double-layer parameters required in the theory, and Mr. B. BARON pointed out the corresponding thermodynamic restriction. Both of them verified the algebra leading to eqns. (1) and (2). Dr. D. M. MOHILNER, Colorado State University, made valuable comments on the thermodynamics of the ideal reversible electrode and the approximations in eqn. (I0) (not fully discussed here).

APPENDIX

SLUYTERS's eqns. (A14) and (A15), which are listed below under eqns. (25) and (26), give the real and imaginary parts of the electrode admittance and contain the partial derivatives of $q + zF\Gamma_0$ and $\Gamma_0 + \Gamma_R$ with respect to the two independent variables selected by REINMUTH, namely E and the linear combination, $c_0^s D_0^{\frac{1}{2}} + c_R^s D_R^{\frac{1}{2}}$ (our notations). Equations (A14) and (A15) are then transformed by SLUYTERS to reduce the number of double-layer parameters from 4 to 3. Equations (A14) and (A15) were selected for comparison to avoid the inverse transformation.

SLUYTERS reports⁷:

$$Y_{el}' = \frac{1}{2\sigma\omega^{-\frac{1}{2}}} - zF \frac{\sigma_R}{\sigma} \omega\gamma_E \frac{U}{2+2U+U^2} + \frac{q_\psi(2\omega)^{\frac{1}{2}}\omega\gamma_E}{2+2U+U^2} \quad (25)$$

$$Y_{el}'' = \frac{1}{2\sigma\omega^{-\frac{1}{2}}} - zF \frac{\sigma_R}{\sigma} \omega\gamma_E \frac{2+U}{2+2U+U^2} - \frac{q_\psi(2\omega)^{\frac{1}{2}}\omega\gamma_E(1+U)}{2+2U+U^2} + \omega q_E \quad (26)$$

with the following parameters transposed into our notations

$$\sigma = \{RT/2^{\frac{1}{2}}(zF)^2\} \{1/c_0^s D_0^{\frac{1}{2}} + 1/c_R^s D_R^{\frac{1}{2}}\} \quad (27)$$

$$\sigma_R/\sigma = \{1 + \exp[-(zF/RT)(E - E_{\frac{1}{2}})]\}^{-1} \quad (28)$$

$$U = (2\omega)^{\frac{1}{2}} [\partial(\Gamma_0 + \Gamma_R)/\partial\psi_e]_{Ee} \quad (29)$$

$$\psi = (c_0)_{x=0} D_0^{\frac{1}{2}} + (c_R)_{x=0} D_R^{\frac{1}{2}} \quad (30)$$

$$\gamma_E = [\partial(\Gamma_0 + \Gamma_R)/\partial E_e]_{\psi_e} \quad (31)$$

$$q_\psi = [\partial(q + zF\Gamma_0)/\partial\psi_e]_{Ee} \quad (32)$$

$$q_E = [\partial(q + zF\Gamma_0)/\partial E_e]_{\psi_e} \quad (33)$$

The various coefficients listed by SLUYTERS were calculated in terms of our parameters, and the results are listed in Table 3. This conversion is quite straightforward and is as follows:

TABLE 3

CORRELATION BETWEEN SLUYTERS' PARAMETERS AND THOSE IN THE PRESENT PAPER

$$\begin{aligned} \sigma &= -\omega^{\frac{1}{2}}(c_R^s/2\lambda B)(1+Q) = -\omega^{\frac{1}{2}}(c_R^s/2\lambda BQ)\xi_r \\ \sigma_R/\sigma &= Q/(1+Q) = Q^2/\xi_r \\ U &= S(g+m)/(1+Q) = \xi_i/\xi_r - 1 \\ \gamma_\psi &= \{S(g+m)/(1+Q)\} 1/(2\omega)^{\frac{1}{2}} = (\xi_i/\xi_r - 1) 1/(2\omega)^{\frac{1}{2}} \\ \gamma_E &= B \left[n - \frac{S(g+m)}{1+Q} \right] \left(\frac{D_R}{2\omega} \right)^{\frac{1}{2}} = B \left(1 + n - \frac{\xi_i}{\xi_r} \right) \left(\frac{D_R}{2\omega} \right)^{\frac{1}{2}} \\ q_\psi &= zF[Qu + Sg] \frac{1}{1+Q} \frac{1}{(2\omega)^{\frac{1}{2}}} = zF[Qu + Sg] \frac{Q}{\xi_r} \frac{1}{(2\omega)^{\frac{1}{2}}} \\ q_E &= zFBS \left[w - \frac{uQ + Sg}{Q(1+Q)} \right] \left(\frac{D_0}{2\omega} \right)^{\frac{1}{2}} = zFBS \left[w - \frac{1}{\xi_r} (uQ + Sg) \right] \left(\frac{D_0}{2\omega} \right)^{\frac{1}{2}} \end{aligned}$$

One has

$$d(\Gamma_O + \Gamma_R) = [\partial(\Gamma_O + \Gamma_R)/\partial c_O^s]_{E_e} d(c_O)_{x=0} + [\partial(\Gamma_O + \Gamma_R)/\partial E_e]_{c_O^s} dE \quad (34)$$

$$\begin{aligned} d(\Gamma_O + \Gamma_R) &= [\partial(\Gamma_O + \Gamma_R)/\partial \psi_e]_{E_e} d\psi_{x=0} + [\partial(\Gamma_O + \Gamma_R)/\partial E_e]_{\psi_e} dE \\ &= \gamma_\psi d\psi_{x=0} + \gamma_E dE \end{aligned} \quad (35)$$

where $\psi = \psi_e$ for $E = E_e$. γ_ψ in SLUYTERS' notation is γ_{ψ_e} .

One has

$$d\psi = D_O \frac{1}{2} d(c_O)_{x=0} + D_R \frac{1}{2} d(c_R)_{x=0} \quad (36)$$

The differential, $(dc_R)_{x=0}$, is obtained by differentiating $(c_R)_{x=0}$ expressed by a Taylor series of the two variables $(c_O)_{x=0}$ and E (truncation after the first derivatives). The partial derivatives in the Taylor series are evaluated by the Nernst equation. Thus

$$d(c_R)_{x=0} = (c_R^s/c_O^s) [d(c_O)_{x=0} - (zF/RT)c_O^s dE] \quad (37)$$

Hence

$$d\psi_{x=0} = D_O \frac{1}{2} [1 + (1/Q)] d(c_O)_{x=0} + D_R \frac{1}{2} B dE \quad (38)$$

Comparison of eqns. (34) and (35) after introduction of $d\psi_{x=0}$ in terms of $d(c_O)_{x=0}$ and $d(c_R)_{x=0}$ yields after conversion to our notations, the values of γ_ψ and γ_E listed in Table 3. A similar procedure is followed for q_ψ and q_E .

Substitution of the parameters of Table 3 into eqns. (25) and (26) yields after some algebra:

$$\frac{1}{Y_{ei}'} = R = \frac{c_R^s}{\lambda B} \frac{\xi_r^2 + \xi_i^2}{[nQ + (1+n)(Qu + gS)]\xi_r + [-Q(2+n) - (Qu + gS)]\xi_i} \quad (39)$$

$$Y_{ei}'' = \omega C = \frac{\lambda B}{c_R^s} \left\{ \frac{[-Q(2+n) - (Qu + gS)]\xi_r - [nQ + (1+n)(Qu + gS)]\xi_i}{\xi_r^2 + \xi_i^2} + w \right\} \quad (40)$$

It is easily shown that eqns. (39) and (40) are identical with partially explicit forms of eqns. (1) and (2).

SUMMARY

The following theoretical aspects of the admittance of the ideal reversible electrode are examined: (a) description in terms of four double-layer parameters related to the thermodynamics of the electrocapillary curve for an ideal reversible electrode; (b) reduction to three independent double-layer parameters as a direct consequence of the electrocapillary curve equation; (c) selection of independent variables; (d) condition for applicability of the classical Warburg theory; (e) introduction of variational methods in the assignment of parameters from experimental data and the attending requirements for accurate experimental data; (f) analysis of data from the limits for $\omega \rightarrow 0$ and $\omega \rightarrow \infty$ as a starting point for any variational computation; (g) correlation with the general theory for any exchange current; (h) correlation with SLUYTERS' work.

REFERENCES

- 1 P. DELAHAY AND K. HOLUB, *J. Electroanal. Chem.*, 16 (1968) 131.
- 2 P. DELAHAY, *J. Phys. Chem.*, 70 (1966) 2373.
- 3 P. DELAHAY, K. HOLUB, G. G. SUSBIELLES AND G. TESSARI, *J. Phys. Chem.*, 71 (1967) 779.
- 4 B. TIMMER, M. SLUYTERS-REHBACH AND J. H. SLUYTERS, *J. Electroanal. Chem.*, 15 (1967) 343.
- 5 P. DELAHAY AND G. G. SUSBIELLES, *J. Phys. Chem.*, 70 (1966) 3150.
- 6 K. HOLUB, G. TESSARI AND P. DELAHAY, *J. Phys. Chem.*, 71 (1967) 2612.
- 7 B. TIMMER, M. SLUYTERS-REHBACH AND J. H. SLUYTERS, *J. Electroanal. Chem.*, 18 (1968) 93.
- 8 B. TIMMER, Thesis, State University of Utrecht, 1968.
- 9 D. M. MOHLNER, *Electroanalytical Chemistry*, Vol. 1, edited by A. J. BARD, Marcel Dekker, New York, 1966, pp. 242-409.
- 10 A. N. FRUMKIN, *Phil. Mag.*, 40 (1920) 363.
- 11 K. HOLUB, *J. Electroanal. Chem.*, 17 (1968) 277.
- 12 G. G. SUSBIELLES AND P. DELAHAY, *J. Electroanal. Chem.*, 17 (1968) 289.
- 13 P. DELAHAY, *Double Layer and Electrode Kinetics*, Interscience Publishers, New York, 1965, p. 28.
- 14 M. SLUYTERS-REHBACH, B. TIMMER AND J. H. SLUYTERS, *J. Electroanal. Chem.*, 15 (1967) 151.
- 15 R. D. ARMSTRONG, W. P. RACE AND H. R. THIRSK, *Electrochim. Acta*, 13 (1968) 215.
- 16 W. LORENZ, *Z. Physik Chem. (Frankfurt)*, 26 (1960) 424.
- 17 H. GERISCHER, *Z. Physik. Chem. (Leipzig)*, 198 (1951) 286.
- 18 K. HOLUB, private communication.

J. Electroanal. Chem., 19 (1968) 61-72

ON THE IMPEDANCE OF GALVANIC CELLS

XXIV. THE IMPEDANCE OF THE $\text{In}^{3+}/\text{In}(\text{Hg})$ ELECTRODE REACTION IN KSCN AND KCl SOLUTION*

B. TIMMER, M. SLUYTERS-REHBACH AND J. H. SLUYTERS

Laboratory of Analytical Chemistry, State University, Utrecht (The Netherlands)

(Received February 9th, 1968)

INTRODUCTION

A recent paper¹ has presented a critical discussion of some important theories for the electrode impedance in the case that the electroactive species are specifically adsorbed at the electrode-solution interface. It was argued that the equations given by REINMUTH^{1,2} are the most satisfactory yet available for reversible systems. Experimental results were described for the $\text{Pb}^{2+}/\text{Pb}(\text{Hg})$ system in M KNO_3 -KCl mixtures. It was shown that impedances for 0.5 mM Pb^{2+} could be analysed according to the equations given by REINMUTH.

The concentration-dependence of the reactant adsorption has not so far been studied. It was shown in Part XXII of this series² that indium is strongly adsorbed from KSCN solutions at the electrode-solution interface. In this paper, the concentration-dependence of this indium adsorption is investigated.

Cell impedances have also been measured in the limiting current region of In^{3+} , because interesting phenomena appear at these potentials. It is known that in both KSCN and halides as supporting electrolyte, a minimum appears in the limiting current region³⁻⁷. These minima have been investigated provisionally with a.c. currents⁴⁻⁶. At the potentials at which the minimum appears in the d.c. current, *negative* cell impedances were reported. Recently⁸, we have presented theoretical equations for the faradaic impedance valid for systems with a potential-dependent charge transfer rate constant, k_{sh} . Under certain conditions a negative faradaic impedance can be expected from these expressions. The negative impedances are analysed here according to the complex plane method. An attempt has been made to explain the resulting parameters of the faradaic impedance according to the expressions based on a potential-dependent k_{sh} ⁸.

A minimum appears in the limiting current in KSCN as well as KCl solutions^{3,4}. Moreover, in both solutions the reduction of In^{3+} is catalyzed by SCN' and Cl' , respectively. These facts are possibly related to the adsorption of the electroactive species as indium is known to be adsorbed from KSCN solutions². The possible adsorption of indium from KCl solutions has therefore been investigated.

* Abstracted from B. TIMMER, Ph.D. thesis, State University of Utrecht, 1968.

EXPERIMENTAL

All impedance measurements were performed in the usual way with a DME^{2,9} (knock-off time, 3.6 sec). Solutions were prepared from reagent-grade chemicals and acidified to pH 3 with 0.1 *N* HNO₃. All potentials are referred to the SCE. Experiments were performed at 25°.

For most electrode systems d.c. polarograms were also recorded, with a Metrohm Polarecord type E 261 R. The currents at the end of drop-life were measured with as little damping of the polarograph as possible. In this way instantaneous currents could be measured. Diffusion coefficients were calculated from the limiting currents using the Ilkovic equation in its classical form.

Impedance data are analysed according to the procedures given in Part XXIII¹. We have shown⁸ that the usual complex plane method^{9,10} may also be used in the case of negative impedances.

RESULTS

Concentration-dependence of the specific adsorption of indium from KSCN solutions

Experiments have been carried out with a solution of 0.2 mM In³⁺ in 1 *M* KSCN, in order to compare the results with those for 0.4 mM In³⁺, obtained previously². The frequency-dependence of Y_{el}' (real part of the electrode admittance) is found to be *not* in accordance with the classical equations^{9,10} between 320 Hz and 1500 Hz, because of the strong specific adsorption of indium, as was the case for the 0.4 mM In³⁺ solution². If the adsorption of indium is proportional to concentration, for every potential and frequency (*cf.* eqns. (1), (3) and (7) of ref. 1)

$$2(Y_{el}')_{0.2mM} = (Y_{el}')_{0.4mM}$$

and

$$2(Y_{el}'' - \omega C_{HF})_{0.2mM} = (Y_{el}'' - \omega C_{HF})_{0.4mM}$$

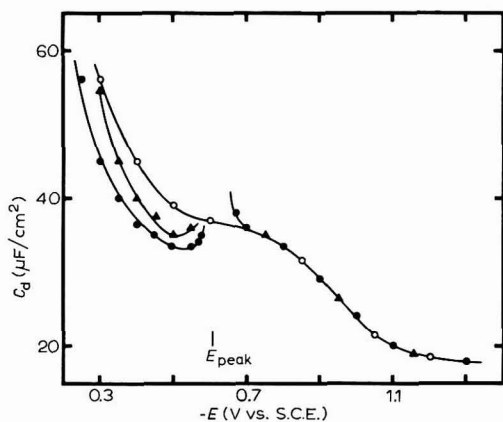


Fig. 1. Double-layer capacitance curves for In³⁺ in 1 *M* KSCN outside the peak region. $C_{In^{3+}}$: (○), 0; (▲), 0.2; (●), 0.4 mM.

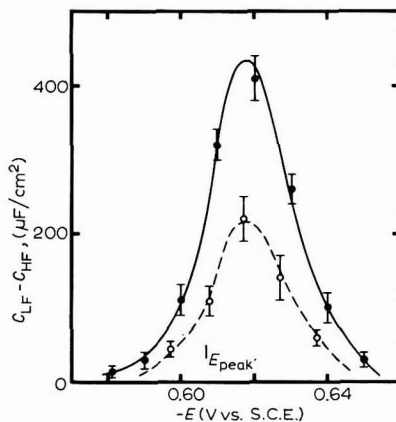


Fig. 2. $(C_{LF} - C_{HF})$ -values for 0.4 mM In³⁺: (●), ref. 2 and 0.2 mM In³⁺: (○), 1 *M* KSCN. (---), $\frac{1}{2}(C_{LF} - C_{HF})$ -values for 0.4 mM In³⁺.

where Y_{el}'' is the imaginary component of the electrode admittance, ω the angular a.c. frequency and C_{HF} the high frequency double-layer capacitance. If $C_{HF}=40 \mu\text{F}/\text{cm}^2$ is taken in conjunction with the data of 0.4 mM In^{3+} of ref. 2, these relations are obeyed.

For a quantitative comparison, C_{LF} , C_{HF} and u' should be evaluated from the experimental data according to the procedures proposed in ref. 1 (C_{LF} is the low frequency capacitance and u' a parameter describing the adsorption isotherm). It appeared that the data could be interpreted very well with the equations given by REINMUTH^{1,2}, as was the case² for 0.4 mM In^{3+} . The results obtained according to the procedures (P3) of ref. 1, are presented in Figs. 1 and 2 and Table 1. As can be seen from Fig. 2, $C_{LF}-C_{HF}$ appears to be proportional to the In^{3+} concentration.

TABLE 1
DATA FOR 0.2 mM In^{3+} IN 1 M KSCN

$-E$ (mV)	$\sigma_{theor.}$ ($\Omega \text{ cm}^2 \text{ sec}^{-\frac{1}{2}}$)	σ_{exp} ($\Omega \text{ cm}^2 \text{ sec}^{-\frac{1}{2}}$)	C_{LF} ($\mu\text{F cm}^{-2}$)	$C_{LF} - C_{HF}$ ($\mu\text{F cm}^{-2}$)	C_{HF} ($\mu\text{F cm}^{-2}$)	u' ($\text{sec}^{\frac{1}{2}}$)
570	4500	3500 ± 400	35.0 ± 0.4			
580	1470	1350 ± 100	37.5 ± 1			
590	515	490 ± 20	45 ± 2	~ 12		~ 0.02
600	228	200 ± 30		45 ± 10	35 ± 5	0.03
610	165			160 ± 20	35 ± 10	0.04
620	228			220 ± 30	25 ± 15	0.02-0.03
630	515			140 ± 30	20 ± 30	0.01
640	1470	1000 ± 300	86 ± 6	60 ± 10	25 ± 15	≤ 0.01
650	4500	4100 ± 500	53 ± 2	20 ± 10	35 ± 5	< 0.01
660			41.5 ± 0.3			

$\sigma_{theor.}$ has been calcd. according to eqn. (4) with $\sigma_m = 165 \Omega \text{ cm}^2 \text{ sec}^{-\frac{1}{2}}$ and $E_{\frac{1}{2}} = -610 \text{ mV}$. σ_{exp} are the exptl. Warburg coefficient values, obtained from plots¹ of Y_{el}''/ω vs. ω ; $u' = \sqrt{2} [\partial(\Gamma_0 + \Gamma_R)/\partial\psi]_{E^0}$.

In Part XXIII, the increased capacitance values, caused by the adsorption of lead from KCl solutions, could be interpreted with a simple model¹, *i.e.*, a linear adsorption isotherm for the oxidized species and no adsorption of the reduced form, $\Gamma_0 = kC_0$ and $\Gamma_R = 0$ (Γ is the surface excess and C_0 the surface concentration of Ox). We have shown earlier² that the same model holds for the capacitances evaluated for 0.4 mM In^{3+} . It can be derived that¹

$$C_{LF} - \left(\frac{\partial q}{\partial E}\right)_\psi = \frac{n^2 F^2}{RT} \frac{\exp \varphi_{m,\sigma}}{(1 + \exp \varphi_{m,\sigma})^3} \Gamma_0^* \quad (1)$$

where $\psi = C_0/D_0 + C_R/D_R$; $\varphi_{m,\sigma} = nF(E - E_{\frac{1}{2}})/RT$ and $\Gamma_0^* = kC_0^*$ with C_0^* the bulk concentration; the other symbols have their usual meaning. Because $(\partial q/\partial E)_\psi$ is not known, it is assumed that¹ $(\partial q/\partial E)_\psi \approx C_{HF}$. A plot of $C_{LF} - C_{HF}$ against $\exp \varphi_{m,\sigma}/(1 + \exp \varphi_{m,\sigma})^3$ for the data of Table 1 shows that eqn. (1) is obeyed (*cf.* Fig. 6 of ref. 2). It is found from such a plot that $\Gamma_0^* = (0.45 \pm 0.15) \cdot 10^{-10} \text{ mole/cm}^2$ for 0.2 mM In^{3+} . When this value is compared with that for 0.4 mM In^{3+} , $(0.85 \pm 0.25) \cdot 10^{-10} \text{ mole/cm}^2$ (ref. 2), it can be concluded from the concentration-dependence of Γ_0^* as well as from the potential-dependence of the enhancement of the capacitance, $C_{LF} - C_{HF}$, that a linear adsorption isotherm holds for indium adsorption for $C_{\text{In}^{3+}} \leq 0.4$

mM. Unfortunately, this cannot be checked for much higher indium concentrations because measurements are not feasible under these conditions (the faradaic impedance becomes very small compared to the ohmic resistance of the cell).

The values of u' of Table 1 may be explained with the same model as was used for eqn. (1). It is easily verified that

$$u' = \sqrt{2} [\partial(I_{\text{O}} + I_{\text{R}}) / \partial \psi]_E = k \sqrt{2/D_{\text{O}}} [1 + \exp(\varphi_{\text{m},\sigma})] \quad (2)$$

Hence, u' should be potential-dependent; at anodic potentials, $u' \approx k \sqrt{2/D_{\text{O}}}$, decreasing continuously to zero at cathodic potentials. The u' -values of Table 1 show this behaviour reasonably well. At the half-wave potential, $\varphi_{\text{m},\sigma} = 0$, $u' = k / \sqrt{2D_{\text{O}}}$, holds. If the values, $k = (2.1 \pm 0.6) \cdot 10^{-4}$ cm and $D_{\text{O}} = 6.0 \cdot 10^{-6}$ cm²/sec are introduced, $u' = (6 \pm 2) \cdot 10^{-2}$ sec^{1/2} is calculated, in agreement with the experimental value of u' at -610 mV (Table 1).

Indium adsorption from KCl solutions

The possible adsorption of indium from KCl solutions has been investigated by measuring impedances of 0.4 mM In³⁺ in 1 M KCl as a function of frequency (320 Hz–1500 Hz) and potential. Surprisingly, the analysis of Y_{el}' shows *no* indication of adsorption of indium from chloride solutions. The frequency-dependence of Y_{el}' for potentials near $E_{\frac{1}{2}}$ cannot be accounted for with REINMUTH's expressions^{1,2}, since experimentally, Y_{el}' / ω decreases with frequency. The decrease of Y_{el}' / ω indicates some irreversibility of the electrode reaction^{9,10}. The analysis according to the classical equations, cf. procedure (PI) of ref. 1, with

$$1/Y_{\text{el}}' = \theta + \sigma \omega^{-1/2} + \sigma^2 \omega^{-1} / (\theta + \sigma \omega^{-1/2}) \quad (3)$$

where θ is the charge transfer resistance and σ the Warburg coefficient, yields consistent results (Table 2). The experimental σ -values are in agreement with theory⁹

$$\sigma = \sigma_{\text{m}} \cosh^2 \frac{1}{2} \varphi_{\text{m},\sigma} \quad (4a)$$

$$\sigma_{\text{m}} = 4 RT / n^2 F^2 \sqrt{2} (C_{\text{O}}^* \sqrt{D_{\text{O}}} + C_{\text{R}}^* \sqrt{D_{\text{R}}}) \quad (4b)$$

with $\sigma_{\text{m}} = 85 \pm 5 \Omega \text{ cm}^2 \text{ sec}^{1/2}$ and $E_{\frac{1}{2}} = -593$ mV.

TABLE 2

EXPERIMENTAL DATA FOR 0.4 mM In³⁺ IN 1 M KCl

$-E$ (mV)	σ ($\Omega \text{ cm}^2 \text{ sec}^{-1/2}$)	θ ($\Omega \text{ cm}^2$)	C_d ($\mu\text{F cm}^{-2}$)	k_{ch} for $\alpha = 0.5$ (cm sec^{-1})	k_{sh} for $\alpha = 0.2$ (cm sec^{-1})	$-q_{\text{Cl}}^{-1}$ ($\mu\text{C cm}^{-2}$)
550	2900 ± 150	< 6	36.2 ± 0.4	> 0.15	> 0.7	7.6
560	1000 ± 30	< 2	34.7 ± 0.5	> 0.25	> 0.7	7.1
570	350 ± 10	1.7 ± 0.7	34.5 ± 0.5	0.2 ± 0.1	0.4 ± 0.1	6.7
580	152 ± 10	1.5 ± 0.3	33 ± 1	(12 ± 2) · 10 ⁻²	(20 ± 3) · 10 ⁻²	6.3
590	85 ± 5	2.2 ± 0.2	34 ± 1	(7 ± 1) · 10 ⁻²	(6.2 ± 0.5) · 10 ⁻²	5.9
600	100 ± 10	3.5 ± 0.4	32 ± 1.5	(4.7 ± 0.6) · 10 ⁻²	(3.5 ± 0.4) · 10 ⁻²	5.6
610	180 ± 15	7.3 ± 0.5	30.9 ± 0.6	(3.1 ± 0.4) · 10 ⁻²	(1.7 ± 0.2) · 10 ⁻²	5.3
620	490 ± 50	21 ± 2	29.7 ± 0.3	(1.8 ± 0.3) · 10 ⁻²	(0.7 ± 0.1) · 10 ⁻²	5.0
630	1950 ± 150	59 ± 6	28.4 ± 0.3	(1.2 ± 0.3) · 10 ⁻²	(0.3 ± 0.1) · 10 ⁻²	4.7

The q_{Cl}^{-1} values have been given by GRAHAME AND PARSONS¹⁸.

The θ -values of Table 2 may be used for obtaining the charge transfer coefficient, α , and the rate constant, k_{sh} . For $C_R^* = 0$ and $D_O = D_R$ with $\beta = 1 - \alpha$ (eqn. (13a) of ref. 11)

$$\theta = (RT/n^2 F^2 k_{sh} C_O^*) \{ \exp \beta \varphi_{m,\sigma} + \exp(-\alpha \varphi_{m,\sigma}) \} \quad (5)$$

Thus, for the faradaic region, $\theta / \{ \exp \beta \varphi_{m,\sigma} + \exp(-\alpha \varphi_{m,\sigma}) \}$ should be constant. For $\alpha = 0.9 \pm 0.1$ this appeared to be the case. Furthermore, one obtains $k_{sh} = 0.06 \pm 0.02$ cm/sec. Note that the "d.c. reversible" equations for θ and σ hold for this k_{sh} -value and the general equations (eqns. (12) of ref. 11) need not be used.

From the experimental Y_{el}'' values, the double-layer capacitance, C_d , was calculated with^{9,10}

$$\omega C_d = Y_{el}'' - Y_{el}' / (p + 1) \quad (6)$$

where $p = \theta / \sigma \omega^{-1/2}$. The resulting capacitances were found to be frequency-independent and equal to the C_d -values for the supporting electrolyte alone over the whole potential range. Consequently, the classical Randles' circuit holds for the $In^{3+}/In(Hg)$ system in 1 M KCl and it appears from both the potential- and frequency-dependence of Y_{el}' , and the C_d -values, that indium is not specifically adsorbed from KCl solutions.

Minima in the In^{3+} limiting current

D.c. polarograms have been recorded for some solutions of indium (Fig. 3). Only the curves for 2 mM In^{3+} in 1 M KCl and 1 M KSCN have been presented in Fig. 3, as for other (lower) concentrations almost identical polarograms were obtained. As can be seen from Fig. 3, a minimum appears in the limiting current in 1 M KCl and 1 M KSCN solutions, in agreement with the literature³⁻⁵. In 1 M $KNO_3 + 12$ mM KCl, the limiting current is not reached at all (*cf.* ref. 7).

Cell impedances have also been measured for the solutions of Fig. 3. In 1 M KCl and 1 M KSCN, *negative* faradaic impedances were found at potentials of the

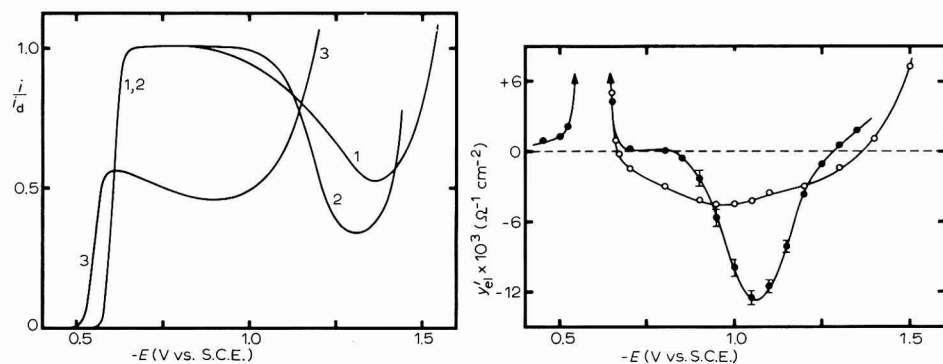


Fig. 3. Direct current polarograms for: (1), 2 mM In^{3+} in 1 M KCl; (2), 2 mM In^{3+} in 1 M KSCN; (3), 0.43 mM In^{3+} in 1 M $KNO_3 + 12$ mM KCl. The current is given as a fraction of the limiting current, i_d .

Fig. 4. The real component of the electrode admittance as a function of potential (in-phase a.c. polarogram) for 2 mM In^{3+} in: (○), 1 M KCl; (●), 1 M KSCN.

minimum in the d.c. current when the experimental data were analysed with the complex plane method^{1,8,9}. The frequency-dependence of Y_{ei}' (eqn. (3)) shows no effect of diffusion polarization ($Y_{ei}' \approx 1/\theta$, constant with frequency) at these potentials, although it should be remembered that for small Y_{ei}' -values, e.g. $< 3 \cdot 10^{-3} \Omega^{-1} \text{ cm}^{-2}$, it is difficult to draw this conclusion. The C_a -values were evaluated from Y_{ei}'' (eqn. (6) with $p = \infty$) and found equal to the C_a -values for the supporting electrolyte alone, indicating that no adsorption of reactants is present at these potentials. In Fig. 4 are shown the experimental Y_{ei}' -values for 2 mM In^{3+} in 1 M KCl and 1 M KSCN. No accurate measurements could be made in the peak potential region because of the high In^{3+} concentration.

Finally, the measured cell impedances for the third solution of Fig. 3, i.e., 0.43 mM In^{3+} in 1 M $\text{KNO}_3 + 12$ mM KCl, were investigated. From the frequency-dependence of Y_{ei}' for 480 mV $\leq -E \leq 570$ mV, the values of θ and σ were evaluated with eqn. (3). The results are summarized in Table 3. The C_a -values calculated with eqn. (6) were found to be equal to those for the supporting electrolyte, indicating that no specific adsorption of indium is present. $Y_{ei}' \approx 0$ was found for 600 mV $< -E < 1000$ mV; for $-E > 1000$ mV, increasing positive Y_{ei}' were computed (cf. Fig. 4).

TABLE 3

EXPERIMENTAL DATA FOR 0.43 mM In^{3+} IN 1 M $\text{KNO}_3 + 12$ mM KCl

$-E$ (mV)	σ ($\Omega \text{ cm}^2 \text{ sec}^{-\frac{1}{2}}$)	θ ($\Omega \text{ cm}^2$)	C_a ($\mu\text{F cm}^{-2}$)	$-E$ (mV)	σ ($\Omega \text{ cm}^2 \text{ sec}^{-\frac{1}{2}}$)	θ ($\Omega \text{ cm}^2$)	C_a ($\mu\text{F cm}^{-2}$)
480	15000		31.2 ± 0.1	530	< 120	36 ± 2	31.8 ± 0.2
490	4700 ± 300	< 50	31.7 ± 0.2	540	< 200	58 ± 2	31.5 ± 0.2
500	1400 ± 200	38 ± 6	31.7 ± 0.2	550		113 ± 5	31.4 ± 0.2
510	500 ± 80	30 ± 3	31.7 ± 0.3	560		270 ± 20	31.2 ± 0.1
520	230 ± 70	29 ± 1	31.8 ± 0.3	570		730	30.8 ± 0.1

It is not possible to determine σ_m and $E_{\frac{1}{2}}$ accurately from the experimental σ -values with eqn. (4), as σ is known only at the anodic side of $E_{\frac{1}{2}}$. If σ_m is taken as equal to $79 \Omega \text{ cm}^2 \text{ sec}^{-\frac{1}{2}}$ (cf. $\sigma_m = 85 \Omega \text{ cm}^2 \text{ sec}^{-\frac{1}{2}}$ for 0.40 mM In^{3+} in 1 M KCl, so that for 0.43 mM In^{3+} , $\sigma = 4.0 \cdot 85 / 4.3 = 79$) it follows from the experimental σ -values that $E_{\frac{1}{2}} = -537 \pm 1$ mV. An attempt can then be made to analyse the θ -data using this $E_{\frac{1}{2}}$ -value. The evaluation of k_{sh} and α cannot be made with eqn. (5) because the system is too irreversible, so that the "d.c. reversible" equation no longer holds over the whole peak potential range¹¹. Note that the "d.c. reversible" eqn. (4) is still valid at potentials anodic of $E_{\frac{1}{2}}$. One has for θ (eqn. (12a) of ref. 11) with $D_O = D_R = D$ and $C_R^* = 0$

$$\theta = (RT/n^2 F^2 k_{sh} C_O^*) \{a + \exp \alpha \varphi_{m,\sigma} + \exp(-\beta \varphi_{m,\sigma})\} / \exp(-\beta \varphi_{m,\sigma}) [a\beta + \exp \alpha \varphi_{m,\sigma}] \quad (7)$$

where $a = D/\delta k_{sh}$ with δ the diffusion layer thickness; $\delta = \sqrt{3\pi Dt}/7$ for a DME. If the θ -data of Table 3 are analysed according to eqn. (7) as described for the data of Table 2, it follows that $k_{sh} = (3.1 \pm 0.4) \cdot 10^{-3} \text{ cm/sec}$ and $\alpha = 0.90 \pm 0.05$.

DISCUSSION

(i) The σ -values necessary for the analysis of the experimental data for 0.4 mM In^{3+} (ref. 2) and 0.2 mM In^{3+} (this paper) in 1 M KSCN were calculated from eqn. (4) with the diffusion coefficient obtained from d.c. polarograms ($D_0 = 6.0 \cdot 10^{-6}$ cm²/sec). For potentials not too close to $E_{\frac{1}{2}}$ it is also possible to obtain accurate experimental σ -values by extrapolation of $Y_{ei'}/\sqrt{\omega}$ to $\omega \rightarrow 0$ (eqn. (4) of ref. 1). In general, these values agree with theoretical σ -values (cf. Table 1). For potentials near $E_{\frac{1}{2}}$, the extrapolation of $Y_{ei'}/\sqrt{\omega}$ is barely feasible. As shown in a preceding section, there is no adsorption of indium in 1 M KCl and experimental σ -values can be obtained over the whole peak potential region in 1 M KCl (Table 2). It was found that $\sigma_m = 85 \pm 5 \Omega \text{ cm}^2 \text{ sec}^{-\frac{1}{2}}$, which is exactly equal to the value for σ_m calculated with $D_0 = 6.0 \cdot 10^{-6}$ cm²/sec from eqn. (4b). As the limiting currents in 1 M KCl and 1 M KSCN are equal for the same In^{3+} concentration it can be concluded that the correct theoretical σ -values have been used for the analysis of the data for 1 M KSCN.

(ii) There is no explanation yet for the fact that indium is specifically adsorbed from KSCN solutions and not from KCl solutions. More is needed to be known about the specific species (*i.e.*, indium complexes) that are adsorbed and about their concentrations in certain solutions. The first is not known, the latter only rather inaccurately in most solutions^{12,20}. The fact that the indium couple in KCl is not completely reversible and that indium is not adsorbed simultaneously at the interface from KCl solutions, whereas in KSCN the electrode reaction is reversible together with adsorption of indium, supports the hypothesis that adsorption of reactants renders an electrode reaction reversible².

The minimum in the limiting current (found in 1 M KCl as well as in 1 M KSCN) cannot be related to the specific adsorption of indium as adsorption is present only for the latter solution. Moreover, the surface concentration of In^{3+} and thus the In^{3+} adsorption, will be very low at these negative potentials.

(iii) The experimental θ -values for the indium electrode reaction in 1 M KCl and in 1 M $\text{KNO}_3 + 12$ mM KCl (Tables 2 and 3) can be interpreted with a potential-independent k_{sh} and α -value. However, the evaluated α -value ($\alpha = 0.9$) is rather extreme. Earlier investigations on the charge transfer reaction of indium have yielded less extreme α -values¹³⁻¹⁶, although most of the reported α -values should be considered carefully, *e.g.* because of the potential-dependency of k_{sh} which complicates the analysis of d.c. current-voltage curves. The irreversibility in the d.c. current reported for 1 M KSCN¹³ cannot be true because in that case we would have found a completely different behaviour of $Y_{ei'}$ for indium in 1 M KSCN. It should be noted that in refs. 4 and 5 it is stated that the d.c. polarogram is reversible, in contradiction with ref. 13.

The analysis of the θ -values of Tables 2 and 3 yields for $\alpha \leq 0.8$, a potential-dependent k_{sh} . A potential-dependency of k_{sh} is not unlikely in view of the shape of the polarograms in Fig. 3. The minimum in the curves for 1 M KCl and 1 M KSCN indicates that some peculiarity in the electrode reaction is present. The curve for 1 M $\text{KNO}_3 + 12$ mM KCl is even stranger. If $k_{sh} = 3.1 \cdot 10^{-3}$ cm/sec and $\alpha = 0.9$ were correct, as was evaluated from the θ -data of Table 3, a normal d.c. wave should have been found (*e.g.*, $i/i_d = 0.90$ and 0.95 for $E = -650$ and -700 mV, respectively)

in contrast with the experimental curve (Fig. 3). Consequently, it is reasonable to suppose that k_{sh} is potential-dependent.

Recently, we have presented equations for the faradaic impedance valid for systems with a potential-dependent k_{sh} ⁸. The θ -values of Table 2 have been analysed according to these equations (eqn. (8a) of ref. 8) for $\alpha = 0.5$ and 0.2 . The resulting k_{sh} -values were found to be dependent of electrode potential (Table 2). Also similar results may be obtained for other α -values. It appears, therefore, that k_{sh} for the indium electrode reaction in $1 M$ KCl is potential-dependent. The lower the α chosen, the larger is this potential-dependency. Because an accurate value for α is not yet known, no definite set of potential-dependent k_{sh} -values can be given.

Recently¹⁷, we have presented a study on the zinc electrode reaction in mixed potassium halide solutions. For these systems, the variation of k_{sh} at the standard potential with iodide concentration could be interpreted by assuming that k_{sh} depends on the specifically adsorbed charge, q^1 , of the anions of the supporting electrolyte, as follows:

$$k_{sh} = k_{sh}^* \exp(bq^1) \quad (8)$$

where k_{sh}^* and b are independent of q^1 . Equation (8) infers that the activation energy for the charge transfer step depends linearly on q^1 . This relation was found by varying q^1 by changing the supporting electrolyte. Of course, q^1 may also be changed by varying the electrode potential as in our experiments. If the potential-dependent k_{sh} -values of Table 2 for the indium couple in $1 M$ KCl are plotted against q_{Cl}^1 , as given by GRAHAME AND PARSONS¹⁸, it appears that eqn. (8) indeed may be used also when q^1 , and consequently k_{sh} , varies with potential (Fig. 5). No Frumkin correction¹⁹

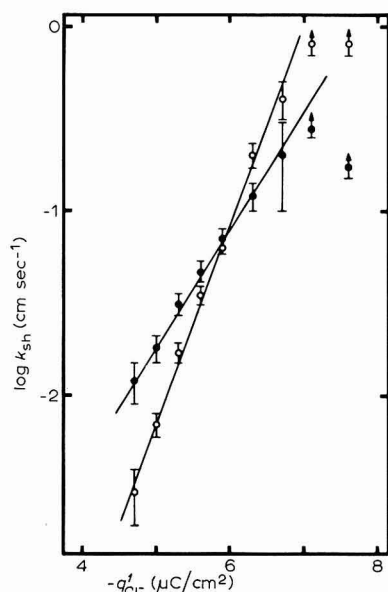


Fig. 5. Plots of the potential-dependent k_{sh} -values of Table 2 according to eqn. (8); α -values: (●), 0.5; (○), 0.2.

has been applied in Table 2 as this correction will not change much in the small potential range covered. It is possible that the electrode reaction is completely reversible in 1 M KSCN, and quasi-irreversible in 1 M KCl, not because indium is adsorbed from the former solution, as argued in section (ii), but because SCN' ions are more strongly adsorbed than Cl' ions, *cf.* eqn. (8).

The charge transfer data of Table 3 could also be analysed in the same way as presented above for the data of Table 2, but as there is no available q^1 -data for 1 M KNO₃ + 12 mM KCl, this has not been done here.

(iii) Finally, the phenomena at the minimum of the d.c. wave (Figs. 3 and 4) can be interpreted, at least qualitatively, with the equations given in Part XX of this series⁸ for systems with a potential-dependent k_{sh} . Equations⁹⁻¹¹ based on a k_{sh} constant with potential, are useless in this respect because they can never explain a minimum in the d.c. wave, nor negative Y_{ei}' -values. With $D_O = D_R = D$ and $\exp \varphi_{m,\sigma} \ll 1$, valid for the negative potentials at the minimum⁸,

$$i/i_d = 1/(1 + a \exp \beta \varphi_{m,\sigma}) \quad (9)$$

$$\frac{di}{dE} = \frac{a}{a + \exp(-\beta \varphi_{m,\sigma})} \cdot \frac{1}{\theta} = \left(1 - \frac{i}{i_d}\right) \frac{1}{\theta} \quad (10)$$

$$\theta = \{RT/n^2 F^2 k_{sh}(E)\} (1 + a \exp \beta \varphi_{m,\sigma}) / [a(\beta - g) + \exp \alpha \varphi_{m,\sigma}] C_O^* \quad (11)$$

where $a = D/\delta k_{sh}(E)$ as in eqn. (7), i and i_d are the currents at the end of drop-life and

$$g = \{RT/nF k_{sh}(E)\} (dk_{sh}/dE) \quad (12)$$

In order to explain the phenomena described with these equations, we assume that k_{sh} depends on q^1 , *e.g.* according to eqn. (8), (*cf.* refs. 17 and 20). It is known that the anions of the supporting electrolyte are desorbed at sufficiently negative potentials¹⁹, just at the potentials of the minimum. Thus, for these potentials, q^1 , and thus k_{sh} , decreases, $a \sim k_{sh}^{-1}$ increases sharply and i/i_d becomes smaller than unity, although $\exp \beta \varphi_{m,\sigma}$ still decreases (eqn. (9)). Also, a Frumkin correction¹⁹, for which α and the charge, z , of the reactant should be known, causes k_{sh} to be potential-dependent. However, this effect is much too small to explain the phenomena.

Equation (10) shows that the slope of the d.c. polarogram has a sign equal to that of θ ($=1/Y_{ei}'$). It can be seen by comparing Figs. 3 and 4, that Y_{ei}' is indeed negative for potentials at which i decreases. At the minimum of the d.c. polarogram ($di/dE = 0$), Y_{ei}' is also zero, as it should be according to eqn. (10). The "peak potential" of the negative Y_{ei}' -wave does not correspond to the inflection point in the negative branch of the d.c. polarogram (di/dE minimal), because of the term $a/[a + \exp(-\beta \varphi_{m,\sigma})] = 1 - i/i_d$ in eqn. (10) that is smaller at less negative potentials.

SCN' ions are more strongly adsorbed than Cl' ions and desorbed at more negative potentials. Consequently, the collapse of the d.c. current begins earlier for 1 M KCl than for 1 M KSCN (Fig. 3). At the same time, the minimum is deeper for 1 M KSCN. The corresponding Y_{ei}' -curves show a similar behaviour: after the normal first positive peak, Y_{ei}' -curves show a similar behaviour: after the normal first positive peak, $Y_{ei}' \approx 0$ is found for above 100 mV, and larger negative Y_{ei}' -values are calculated for 1 M KSCN.

From eqn. (12) it follows that g may be large when k_{sh} changes rapidly with

potential. As soon as g is larger than β , θ (and Y_{el}') becomes negative, *cf.* eqn. (11) with $\exp \alpha \varphi_{m,\sigma}$ small.

It is not possible to interpret the results of Figs. 3 and 4 quantitatively according to eqns. (9)–(12) because too many parameters, especially α , are unknown. Only eqn. (10) can be used directly for comparing a.c. and d.c. curves. It is easily checked that the curves of Figs. 3 and 4 obey eqn. (10). Consequently, the experimental data are in agreement with the theoretical relation between a.c. and d.c. curves, as given by eqn. (10).

In general, $\exp \alpha \varphi_{m,\sigma}$ may be omitted in eqn. (11). In that case eqn. (11) becomes, by introducing eqn. (9)

$$\theta = (RT\delta/n^2 F^2 DC_o^*) \cdot (i_d/i) \cdot 1/(\beta - g) = (RT/nF) 1/i(\beta - g) \quad (13)$$

Thus, the Y_{el}' -values ($=1/\theta$) of Fig. 4 together with i_d/i from Fig. 3, yield $\beta - g$ as a function of potential. In this way, at the potentials of the minimum of Y_{el}' , we obtain for 1 M KSCN, $\beta - g \approx -0.15$ and for 1 M KCl, $\beta - g \approx -0.06$. From the d.c. curves of Fig. 3, k_{sh} may be calculated from eqn. (9) by choosing a value for β . The k_{sh} -values obtained are potential-dependent and if g is evaluated from this potential-dependency with eqn. (12), the same $\beta - g$ values are found as evaluated from Y_{el}' with eqn. (13). Therefore, $\beta - g$ can be evaluated from the experimental data but because β itself is not known, no k_{sh} -values as a function of potential can be obtained and eqn. (8) cannot be checked. It should be noted that eqn. (8) may not be valid for very low q^1 -values because the reaction mechanism changes for these cases, *e.g.*, the electrode reaction becomes controlled by a preceding chemical reaction in the double layer⁷, *cf.* ref. 20. Also, the nature of the wave after the minimum should be known⁴ if the whole polarogram is to be interpreted.

The phenomena at the minimum (Figs. 3 and 4) can therefore be explained qualitatively with eqns. (9)–(12) based on a potential-dependent k_{sh} ; for a quantitative treatment, additional experiments are needed to provide the necessary data (*cf.* ref. 21).

SUMMARY

The $\text{In}^{3+}/\text{In}(\text{Hg})$ system in KSCN and KCl solutions has been investigated using both d.c. and a.c. measurements. The experimental data are analysed and interpreted according to theoretical equations presented recently.

It is shown that the specific adsorption of indium from 1 M KSCN follows a linear adsorption isotherm up to 0.4 mM. No specific adsorption of indium can be detected from KCl solutions. The electrode reaction in 1 M KCl is not completely reversible: $k_{sh} = (6 \pm 2) \cdot 10^{-2}$ cm/sec at the standard potential, supporting the hypothesis that adsorption of reactants renders an electrode reaction reversible.

Also, the minima in the In^{3+} limiting current have been studied. It appears that the faradaic impedance is negative at the potentials of the minimum. The phenomena are explained qualitatively with equations based on a potential-dependent k_{sh} . Some arguments are presented for this potential-dependency; it is proposed that k_{sh} depends exponentially on the specifically adsorbed charge, q^1 , of the anions of the supporting electrolyte. The exponential dependence of k_{sh} on q^1 was verified for 0.4 mM In^{3+} in 1 M KCl at potentials near the half-wave potential.

ACKNOWLEDGEMENT

This investigation was supported in part by the Netherlands Foundation for Chemical Research (SON) with financial aid from the Netherlands Organisation for the Advancement of Pure Research (ZWO).

REFERENCES

- 1 B. TIMMER, M. SLUYTERS-REHBACH AND J. H. SLUYTERS, *J. Electroanal. Chem.*, 18 (1968) 93.
- 2 B. TIMMER, M. SLUYTERS-REHBACH AND J. H. SLUYTERS, *J. Electroanal. Chem.*, 15 (1967) 343.
- 3 A. G. STROMBERG AND KH. Z. BRAINING, *Zh. Fiz. Khim.*, 35 (1961) 2016.
- 4 T. TAKAHASHI AND H. SHIRAI, *Rev. Polarog. (Kyoto)*, 11 (1963) 155.
- 5 N. TANAKA, T. TAKEUCHI AND R. TAMAMUSHI, *Bull. Chem. Soc. Japan*, 37 (1964) 1435.
- 6 R. TAMAMUSHI AND K. MATSUDA, *J. Electroanal. Chem.*, 12 (1966) 436.
- 7 A. J. ENGEL, J. LAWSON AND D. A. AIKENS, *Anal. Chem.*, 37 (1965) 203.
- 8 M. SLUYTERS-REHBACH, B. TIMMER AND J. H. SLUYTERS, *Z. Physik. Chem. N.F.*, 52 (1967) 89.
- 9 M. SLUYTERS-REHBACH AND J. H. SLUYTERS, *Rec. Trav. Chim.*, 82 (1963) 525, 535.
- 10 M. SLUYTERS-REHBACH, D. J. KOOYMAN AND J. H. SLUYTERS, *Polarography 1964*, edited by G. J. HILLS, Macmillan, London, p. 135.
- 11 B. TIMMER, M. SLUYTERS-REHBACH AND J. H. SLUYTERS, *J. Electroanal. Chem.*, 14 (1967) 169, 181.
- 12 L. G. SILLÉN AND A. E. MARTELL, *Stability Constants of Metal-ion Complexes*, The Chemical Society, London, Spec. Publ. 17, 1964.
- 13 Y. NARUSAWA, J. HASHIMOTO AND H. HAMAGUCHI, *Bull. Chem. Soc. Japan*, 38 (1965) 234.
- 14 J. N. GAUR AND D. S. JAIN, *Electrochim. Acta*, 11 (1966) 1661.
- 15 D. S. JAIN AND J. N. GAUR, *Electrochim. Acta*, 12 (1967) 413.
- 16 V. V. LOSEV, A. J. MOLODOV AND V. V. GORODETZKI, *Electrochim. Acta*, 12 (1967) 475.
- 17 P. TEPPEMA, M. SLUYTERS-REHBACH AND J. H. SLUYTERS, *J. Electroanal. Chem.*, 16 (1968) 165.
- 18 D. C. GRAHAME AND R. PARSONS, *J. Am. Chem. Soc.*, 83 (1961) 1291. Dr. R. PARSONS kindly supplied additional data not given in the paper.
- 19 P. DELAHAY, *Double Layer and Electrode Kinetics*, Interscience Publishers Inc., New York, 1965.
- 20 J. G. LAWSON AND D. A. AIKENS, *J. Electroanal. Chem.*, 15 (1967) 193.
- 21 M. SLUYTERS-REHBACH, J. S. M. C. BREUKEL AND J. H. SLUYTERS, *J. Electroanal. Chem.*, 19 (1968) 85.

J. Electroanal. Chem., 19 (1968) 73-83

ELECTRODE KINETICS AND DOUBLE-LAYER STRUCTURE

II. THE POTENTIAL-DEPENDENCE OF THE KINETIC PARAMETERS OF THE $Zn^{2+}/Zn(Hg)$ ELECTRODE REACTION

M. SLUYTERS-REHBACH, J. S. M. C. BREUKEL AND J. H. SLUYTERS

Laboratory of Analytical Chemistry, State University, Utrecht (The Netherlands)

(Received February 15th, 1968)

INTRODUCTION

Recently¹, we presented a study concerning the relation between the standard heterogeneous rate constant, k_{sh} , of the $Zn^{2+}/Zn(Hg)$ electrode reaction and the composition of the base solution, consisting of 1 *M* mixed halides.

In the case of [(1- x) *M* KCl + x *M* KI] base electrolyte the increase of k_{sh} with increasing x was especially marked; this could be plausibly interpreted by the hypothesis that the specific adsorption of iodide (or iodide + chloride) anions in the inner part of the double layer reduces the activation energy of the charge transfer reaction. In fact, a linear correlation was found between $\log k_{sh}$ (*i.e.*, activation energy) and the specifically adsorbed charge, q^1 . However, following a theory of BLACKLEDGE AND HUSH² in a more generalized form, another explanation was possible, based on the assumption that the electrode reaction proceeds *via* two or more zinc-iodide complexes at a much greater rate than *via* the zinc-chloride or zinc-aquo complexes (complex reactants model). Although we preferred the first explanation (specific anion adsorption model) no definite decision between the two could be made on the basis of the reported experiments, which were performed at constant potential, q^1 , the eventual concentration of ZnI_n complexes in the solution being varied simultaneously by changing the iodide concentration.

If, for any base electrolyte, the electrode potential is varied, the amount of specifically adsorbed anions changes independently and, consequently, a decision between the two models is possible in this way: if the specific anion adsorption model holds, the rate constant will depend on the electrode potential. We therefore investigated the kinetics of the $Zn^{2+}/Zn(Hg)$ electrode reaction as a function of the electrode potential by means of the faradaic impedance method. In our opinion this method is pre-eminently suitable for this purpose because of the easy introduction of a d.c. polarizing circuit³. Moreover, a theory of the potential-dependence of the faradaic impedance in the case of a potential-dependent k_{sh} is available⁴. In this paper, the results obtained in 1 *M* KI, KBr, KCl and $NaClO_4$ solutions are described and discussed.

EXPERIMENTAL

Cell impedances were measured in the usual way, using a cell with a dropping mercury electrode (drop time, 3 sec) and a mercury pool electrode connected to the leads of the a.c. bridge described earlier³. The potential of the DME was measured against a SCE by means of a vacuum tube voltmeter. The cell was kept at 25° and the solution was de-aerated with tank nitrogen, purified by passage through a vanadous sulfate solution. The cell solution was usually made up of 1 *M* base electrolyte, 10⁻³ *M* HCl or HClO₄, and ZnSO₄ in concentrations varying from 10⁻³ *M* for measurements in 1 *M* KI near to the half-wave potential, to 2 · 10⁻² *M* for measurements at far cathodic and far anodic potentials. In the other base electrolytes, the Zn²⁺ concentrations were 1 · 10⁻² and 2 · 10⁻² *M* throughout. For all systems, the double-layer capacitance of the DME in the supporting electrolyte was also measured.

In order to correct the d.c. potential scale in the a.c. measurements for the *iR* drop occurring in the cell at these high concentrations, d.c. polarograms were recorded with a Metrohm three-electrode polarograph. The *iR* drop never exceeded 10 mV.

RESULTS

As we intended to calculate the faradaic impedance by means of the complex plane analysis of Randles equivalent circuit^{3,5,6}, it was necessary to check whether the chosen electrode system is in accordance with this circuit. Therefore, the components, *Z'* and *Z''*, of the cell impedance were measured at fixed potentials (-0.92, -1.00 and -1.25 V vs. SCE) as a function of frequency, together with the value of the ohmic resistance, *R*_Ω, at a potential outside the faradaic region. From these data we calculated the components, *Y*_{el'} and *Y*_{el''}, of the electrode admittance as described earlier^{5,7}. The frequency-dependence of *Y*_{el'} and *Y*_{el''} appeared to be consistent with the expressions:

$$Y_{el'} = \frac{\theta + \sigma\omega^{-\frac{1}{2}}}{(\theta + \sigma\omega^{-\frac{1}{2}})^2 + \sigma^2\omega^{-1}} = \frac{1}{\sigma\omega^{-\frac{1}{2}}} \frac{p+1}{p^2+2p+2} \quad (1a)$$

$$Y_{el''} = \frac{\sigma\omega^{-\frac{1}{2}}}{(\theta + \sigma\omega^{-\frac{1}{2}})^2 + \sigma^2\omega^{-1}} + \omega C_d = \frac{1}{\sigma\omega^{-\frac{1}{2}}} \frac{1}{p^2+2p+2} + \omega C_d \quad (1b)$$

In other words, application of the so-called frequency variation method^{3,5,7} yielded frequency-independent and reasonable values for the charge transfer resistance, *θ*, the Warburg coefficient, *σ*, and the double-layer capacitance, *C*_d. Moreover, the latter was equal to the value obtained in the supporting electrolyte, and it is concluded therefore that the electrode system can be described by the Randles circuit with no significant adsorption of Zn²⁺ or Zn at the electrode-solution interface.

This result led us to conclude that the more sensitive concentration variation method could be used for the definite experiments. Therefore, *Z'* and *Z''* were measured as a function of potential for various Zn²⁺ concentrations at a fixed frequency. At each potential, *Y*_{el''} was plotted against *Y*_{el'} with the Zn²⁺ concentration as varying parameter, and from the slope, equal to 1/(*p*+1), the so-called "irreversibility quotient", *p* = *θ*/σ $\omega^{-\frac{1}{2}}$, was obtained. This was done for 0.42, 1, 2 and 4 KHz in the case of KI and KCl but only for 1 KHz in the cases of KBr and NaClO₄. The

values of $p/\omega^{\frac{1}{2}} = p' = \theta/\sigma$ calculated at the various frequencies were found to be consistent within experimental error. The mean values are plotted against the d.c. potential in Fig. 1. From p and Y_{el}' , the values of θ and σ were calculated according to eqn. (1a). The results for a Zn^{2+} concentration of $2 \cdot 10^{-2} M$ are given in Figs. 2 and 3. In the case of the $1 M$ KI base electrolyte, the values close to the half-wave potential are calculated from measurements at 10^{-3} or $5 \cdot 10^{-3} M$ Zn^{2+} concentrations but multiplied by $1/20$ or $5/20$, respectively.

For $NaClO_4$, the values of p' and σ near the peak potential are very inaccurate because of the high irreversibility and only the plots at far anodic and cathodic potentials are given. For the sake of clarity, accuracy limits are indicated only at some relevant points.

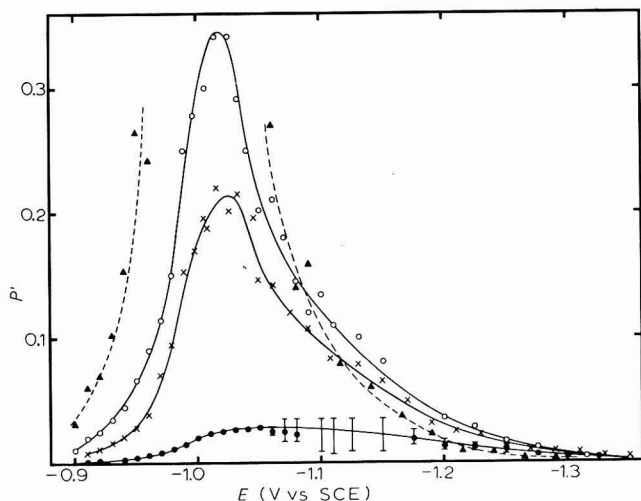


Fig. 1. Potential-dependence of $p' = \theta/\sigma$ for the $Zn^{2+}/Zn(Hg)$ reaction in different $1 M$ base electrolytes. (●) KI, (×) KBr, (○) KCl, (▲) $NaClO_4$.

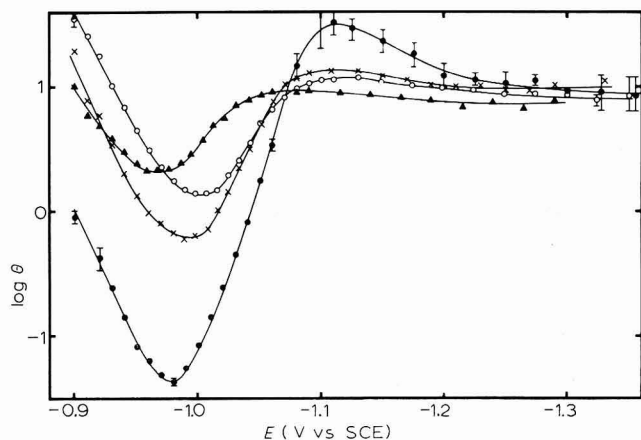


Fig. 2. The transfer resistance as a function of potential for $2 \cdot 10^{-2} M$ Zn^{2+} . (●) KI, (×) KBr, (○) KCl, (▲) $NaClO_4$.

In all cases the measurements were possible over a wide potential range, -0.9 to -1.35 V vs. SCE. This is not surprising for KCl and NaClO₄ solutions, because k_{sh} -values of approximately $3 \cdot 10^{-3}$ and $5 \cdot 10^{-3}$ cm sec⁻¹ (as usually reported for the Zn²⁺/Zn(Hg) reaction in these solutions^{1,2,8}) are sufficiently low to give rise to irreversible behaviour, *i.e.*, the values of σ at far negative potentials are relatively low so that the faradaic admittance is substantially different from zero⁹ (*cf.* eqn. (1)).

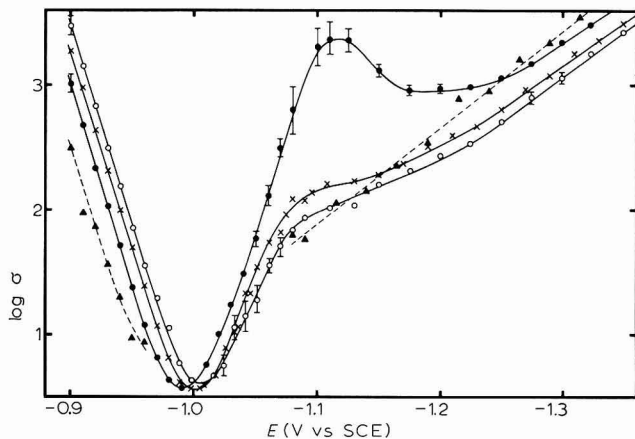


Fig. 3. The Warburg coefficient as a function of potential for $2 \cdot 10^{-2}$ M Zn²⁺. (●) KI, (×) KBr, (○) KCl, (▲) NaClO₄.

Irreversible behaviour is not to be expected if $k_{sh} = ca. 10^{-1}$ cm sec⁻¹, as is relevant to the Zn²⁺/Zn(Hg) reaction in 1 M KI^{1,8}. For example, at -1.25 V, $\log \sigma$ would be equal to about 5, whereas we measured $\log \sigma = 3$. The similarity of the values in the far cathodic region for all solutions is a first indication that, at these potentials, k_{sh} is of the same order of magnitude irrespective of the base electrolyte. As the values of θ and p at more positive potentials, near -1.0 V, are markedly dependent on the base electrolyte, this must mean that k_{sh} decreases significantly with decreasing potential in the case of 1 M KI and probably also for 1 M KBr.

ANALYSIS OF FARADAIC IMPEDANCE PARAMETERS

Theoretical expressions for θ , σ and p' in the present case of an irreversible electrode reaction at the DME with potential-dependent apparent rate constant and the Red-component initially absent, can be derived from the general equations, published earlier^{4,9}, by introduction of $a_O/a_R = (D_O/D_R)^{\frac{1}{2}}$ and $C_R^* = 0$:

$$\theta = \frac{RT}{n^2 F^2 C_O^* k_{sh}^{\alpha}} \frac{a_O (D_R/D_O)^{\frac{1}{2} \beta} \exp(\beta j) + \exp(j) + 1}{a_O (\beta - g) + (D_O/D_R)^{\frac{1}{2} \beta} \exp(\alpha j)} \quad (2)$$

$$\sigma = \frac{RT}{n^2 F^2 \sqrt{2} C_O^* D_O^{\frac{1}{2} \alpha} D_R^{\frac{1}{2} \beta}} \frac{a_O (D_R/D_O)^{\frac{1}{2} \beta} \exp(\beta j) + \exp(j) + 1}{a_O (\beta - g) + (D_O/D_R)^{\frac{1}{2} \beta} \exp(\alpha j)} \{ \exp(\alpha j) + \exp(-\beta j) \} \quad (3)$$

$$p' = \theta / \sigma = (D_O^{\frac{1}{2} \alpha} D_R^{\frac{1}{2} \beta} \sqrt{2} / k_{sh}^{\alpha})^{-1} \{ \exp(\alpha j) + \exp(-\beta j) \} \quad (4)$$

with

$$g = (RT/nFk_{sh}^a)(dk_{sh}^a/dE) = (RT/nF)(d \ln k_{sh}^a/dE) \quad (5)$$

$$j = (nF/RT)(E - E_{\frac{1}{2}}^r) = (nF/RT)(E - E_0) - \ln(D_R/D_O)^{\frac{1}{2}} \quad (6)$$

$$a_0 = D_0^{\frac{1}{2}}/(3/7\pi t)^{\frac{1}{2}}k_{sh}^a \quad (7)$$

The introduction of the reversible half-wave potential instead of the standard potential has been made for convenience.

The subject of interest, the apparent rate constant, k_{sh}^a , as a function of E , will most easily be calculated from p' if j and α (or β) are known. The values of the diffusion coefficients may be taken from d.c. polarographic experiments; we will accept the literature values⁹, $D_O = \frac{1}{2}D_R = 8 \cdot 10^{-6}$ cm²sec⁻¹. Evidently, an error in these values will cause only a systematic error in k_{sh}^a without influencing the relative potential-dependence.

i. Determination of $E_{\frac{1}{2}}^r$

If k_{sh}^a is sufficiently large, the terms in a_0 can be dropped in eqns. (2) and (3), so that the so-called "d.c. reversible equations" for θ and σ result^{3,9}:

$$\theta_{rev} = (RT/n^2F^2C_O^*k_{sh}^a)(D_R/D_O)^{\frac{1}{2}\beta} \{ \exp(\beta j) + \exp(-\alpha j) \} \quad (8)$$

$$\sigma_{rev} = (RT/n^2F^2/\sqrt{2}C_O^*D_O^{\frac{1}{2}}) \{ \exp(j) + 2 + \exp(-j) \} = \frac{1}{4}\sigma_m \{ \exp(j) + 2 + \exp(-j) \} \quad (9)$$

If, in addition $|j|$ is sufficiently large, *i.e.*, $E - E_{\frac{1}{2}}^r > (0.08/n)V$, the plot of $\log \sigma$ vs. E becomes a straight line with slope, $n/0.059$ V⁻¹.

According to Fig. 3, this case occurs for the KI system in the potential regions, $-0.9 < E < -0.95$ and, $-1.04 < E < -1.09$. The intersection ordinate of these two linear sections appears to be equal to $\log \sigma_m - \log 4$, as eqn. (9) prescribes. Therefore, the abscissa of the intersection point may be set equal to the reversible half-wave potential, yielding $E_{\frac{1}{2}}^r = -0.995$ V vs. SCE.

For the KCl system, the theoretical $1/0.03$ V⁻¹ slope in the $\log \sigma$ -plot is found only in the anodic region, but with the literature value $k_{sh}^a = ca. 5 \cdot 10^{-3}$ cm sec⁻¹ and $t = 3$ sec it can be calculated that the difference between eqns. (3) and (9) is negligible down to $E \approx E_{\frac{1}{2}}^r$. Consequently, $E_{\frac{1}{2}}^r$ will be equal to the potential where the extrapolated ordinate of the anodic straight section is equal to $\log \sigma_m - \log 4$. The resulting value is $E_{\frac{1}{2}}^r = -1.005$ V vs. SCE. The same procedure can be applied to the plot for the KBr system ($k_{sh} = ca. 10^{-3}$ cm sec⁻¹) giving $E_{\frac{1}{2}}^r = -1.00$ V.

In the case of NaClO₄ base electrolyte, no use could be made of σ_m because of its high inaccuracy and the non-validity of eqn. (9). Only between -0.90 and -0.94 V is a straight line in the $\log \sigma$ -plot (Fig. 3) found, parallel to the other plots, about 13 mV positive to the plot for KI. As there is no reason to suppose that the diffusion coefficients of Zn²⁺ in 1 M NaClO₄ and 1 M KI solution differ significantly, it can be deduced that the reversible half-wave potential in NaClO₄ is *ca.* 0.98 V vs. SCE.

ii. Determination of $(\alpha + g)$

A separate determination of the transfer coefficient, which necessarily involves the examination of θ or p' as a function of potential, is theoretically impossible when k_{sh} is expected to be potential-dependent. Only the "apparent" transfer coefficients, $\alpha^a = \alpha + g$ or $\beta^a = \beta - g$, can be obtained, in which g itself may also depend

on the potential. A careful estimation at as many potentials as possible is thus required.

A plot of $\log p'$ vs. E will be most generally applicable, for which can be derived from eqn. (4):

$$\text{at } E - E_{\frac{1}{2}}r > \frac{0.08}{n} V: \quad \frac{d \log p'}{dE} = - \frac{n}{0.059} (\alpha + g) \quad (10a)$$

$$\text{at } E - E_{\frac{1}{2}}r < - \frac{0.08}{n} V: \quad \frac{d \log p'}{dE} = \frac{n}{0.059} (\beta - g) \quad (10b)$$

$$\text{Otherwise} \quad \frac{d \log [p' \{ \exp(j) + 1 \}]}{dE} = \frac{n}{0.059} (\beta - g) \quad (10c)$$

In the case of d.c. reversible behaviour, as shown by a straight line with slope, $n/0.059 V^{-1}$ in the $\log \sigma$ vs. E plot (see above), the information may be obtained directly from θ , as

$$\text{at } E - E_{\frac{1}{2}}r > \frac{0.08}{n} V: \quad \frac{d \log \theta_{\text{rev}}}{dE} = \frac{n}{0.059} (\beta - g) \quad (11a)$$

$$\text{at } E - E_{\frac{1}{2}}r < - \frac{0.08}{n} V: \quad \frac{d \log \theta_{\text{rev}}}{dE} = - \frac{n}{0.059} (\alpha + g) \quad (11b)$$

$$\text{otherwise,} \quad \frac{d \log [\theta_{\text{rev}} \{ \exp(j) + 1 \}]}{dE} = - \frac{n}{0.059} (\alpha + g) \quad (11c)$$

This procedure is essentially identical with the first one, but it is to be preferred when k_{sh} is rather low (as for the KCl medium) because then the accuracy in θ is much better than in p' . Note that, although in the anodic region the d.c. dependence obeys reversible behaviour, the faradaic impedance itself is still almost completely charge transfer-controlled.

In the far cathodic potential region, eqn. (2) can be simplified, as in the case of constant k_{sh}^0 , to

$$\theta_- = \frac{RT}{n^2 F^2} \frac{(3/7\pi t)^{\frac{1}{2}}}{C_0^* D_0^{\frac{1}{2}}} \frac{i}{\beta - g} = \frac{RT}{n F i_d} \frac{i}{\beta - g} \quad (12)$$

where i_d is the limiting current density in the d.c. polarogram. Thus, θ is independent of k_{sh} and potential (see Fig. 2), and $(\beta - g)$ can be obtained directly from the combination of the a.c. and d.c. polarographic experiment. In the same potential region we have from eqn. (3)

$$\sigma_- = (RT/n^2 F^2 \sqrt{2} C_0^* D_0^{\frac{1}{2}} \alpha D_R^{\frac{1}{2}} \beta) \{ k_{\text{sh}}^0 (3/7\pi t)^{\frac{1}{2}} \exp(-\beta j) / D_0^{\frac{1}{2}} (\beta - g) \} \quad (13)$$

and if g is not strongly potential-dependent,

$$d \log \sigma_- / dE = - (n/0.059) (\beta - g) \quad (14)$$

The results of the application of these procedures to the experimental data, summarized in Table I, appear to be satisfactorily consistent in each of the reported potential regions. The inaccuracy is *ca.* 0.03, except at potentials more negative than $-1.2 V$, where it is *ca.* 0.01. The potential divisions in Table I have been chosen so that the change of the transfer coefficient with potential is clearly evident.

TABLE 1

APPARENT TRANSFER COEFFICIENTS AS A FUNCTION OF POTENTIAL

E	$NaClO_4$		KCl		KBr		KI		Obtained from
	$\alpha + g$	$\beta - g$	$\alpha + g$	$\beta - g$	$\alpha + g$	$\beta - g$	$\alpha + g$	$\beta - g$	
0.90-0.95	0.48		0.42		0.40		0.37		p'
				0.57		0.65		0.63	θ_{rev}
		0.42		0.45		0.38		0.43	$p'(\exp j + 1)$
0.95-0.98			0.57		0.66		0.60		$\theta_{rev}(\exp j + 1)^{-1}$
				0.45		0.28		0.12	$p'(\exp j + 1)$
0.99-1.01			0.57		0.66		0.90		$\theta_{rev}(\exp j + 1)^{-1}$
				0.21		0.22		0.02	$p'(\exp j + 1)$
1.02-1.04					0.82		0.95		$\theta_{rev}(\exp j + 1)^{-1}$
		0.23		0.23		0.11		0.05	p'
1.05-1.08							0.98		θ_{rev}
1.08-1.15		0.23		0.19		0.12			p'
1.2-1.3		0.23		0.20		0.21			p'
		0.22		0.22		0.22		0.13	$\theta - j_g$
		0.22		0.22		0.21		0.22	$\sigma -$
1.3-1.4		0.22		0.22		0.21		0.19	$\sigma -$

The marked potential-dependence of $\alpha + g$ and $\beta - g$ needs further consideration, which will be based on the specific anion adsorption model postulated in our previous paper¹. In principle, the origin of a substantial value for g may be twofold:

$$g = \frac{RT}{nF} \frac{d \ln k_{sh}^a}{dE} = \frac{RT}{nF} \frac{d \ln k_{sh}^f}{dE} - \alpha \frac{d\phi_2}{dE} \quad (15)$$

where k_{sh}^f is the true formal rate constant¹ and ϕ_2 is the potential of the outer Helmholtz plane. If $\ln k_{sh}^f$ is a linear function of the amount of specifically adsorbed anions, q^1 , the first term on the right-hand side of eqn. (15) will be proportional to dq^1/dE . Consequently, it will be positive and its value will in general decrease in the order $KI > KBr > KCl > NaClO_4$.

In the far cathodic region, the observed values of $\beta - g$ are the same in all base electrolytes. As the specific adsorption of even iodide ions at these potentials is extremely weak¹⁰, this result indicates that here, $g = -\alpha dq^1/dE$, which can be calculated to be -0.03 from double-layer data for $1 M$ KI ¹⁰, $1 M$ KBr ¹¹ and $1 M$ KCl ¹² and will most probably be the same for $1 M$ $NaClO_4$. The most probable value for β is therefore $0.22 - 0.03 = 0.19 \pm 0.01$. For $NaClO_4$ and KCl base electrolytes, $\beta - g = 0.22 \pm 0.02$ is maintained up to *ca.* -1.02 V, fully in accordance with the fact that specific adsorption from these solutions is only minor in that potential region. In the case of KI , and to a lesser extent for KBr , lower values for $\beta - g$ and higher values for $\alpha + g$ are found on going to more positive potentials; this can be interpreted as due to the contribution of $d(\ln k_{sh}^f)/dE$ to g , parallel to the increase of dq^1/dE ¹⁰.

Near the reversible half-wave potential, however, a sudden increase in $\beta - g$ (decrease in $\alpha + g$) is observed in all supporting electrolytes, which continues until a constant value, $\beta - g = 0.60 \pm 0.03$, is reached in the anodic region. Along the lines of our interpretation this would mean that g becomes largely negative, which is improbable and cannot, of course, be explained with our model. Since the same value for $\beta - g$ is found at -0.9 to -0.95 vs. SCE in all solutions, the effect of dq^1/dE seems to have vanished, though the differences in θ and p' still indicate a marked

dependence of the charge transfer rate on the nature of the base electrolyte. Our results are in agreement with those of HUSH AND BLACKLEDGE¹³ who interpreted the anomalous low value of α (their β) at anodic potentials as being indicative of a two-step electrode reaction mechanism with the Zn^{+} -ion as an intermediate.

iii. Rate constant as a function of potential

Concluding that in the cathodic potential region the experimental data seem to come up to our expectations, we calculated k_{sh}^{a} -values from p' for all base electrolytes at potentials between -1.0 and -1.35 V (see Fig. 1) using eqn. (4) with $\beta=0.19$, $\alpha=1-\beta$, and $E_{\frac{1}{2}r} = -0.98, -1.005, -1.002$ and -0.995 V vs. SCE, respectively for NaClO_4 , KCl, KBr and KI solutions. The results (see Fig. 4) show a marked

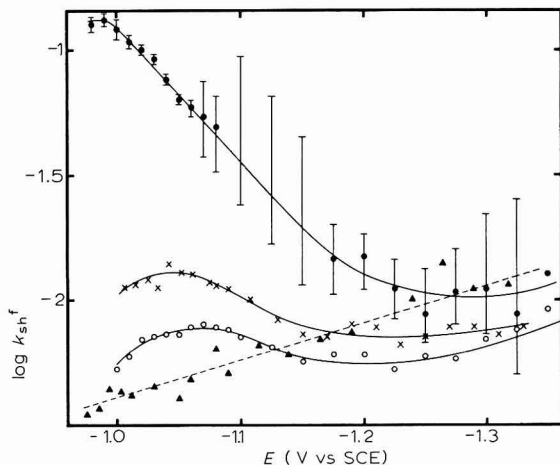


Fig. 4. Apparent standard heterogeneous rate constants as a function of potential, calcd. with $\beta = 0.19$. (●) KI, (×) KBr, (○) KCl, (▲) NaClO_4 .

TABLE 2

APPARENT RATE CONSTANTS AT THE REVERSIBLE HALF-WAVE POTENTIAL AND IN THE ANODIC AND CATHODIC REGIONS

Base electrolyte	$k_{\text{sh}}^{\text{a}} \cdot 10^3$		
	$E > -0.95$ (V vs. SCE)	$E = E_{\frac{1}{2}r}$	$E = -1.3$ (V vs. SCE)
1 M NaClO_4	5.3	3.6	11
1 M KCl	9.6	6.3	6.5
1 M KBr	34	11	7.5
1 M KI	350	125	10

potential-dependence of the apparent rate constant, and for KI and KBr, the expected significant increase of k_{sh}^{a} with E . The k_{sh}^{a} -values at the reversible half-wave potential, listed in Table 2, are in good agreement with literature data⁸. Table 2 also contains the k_{sh}^{a} -values calculated from θ or p' at the anodic potentials, taking $\beta=0.6$ (see discussion) and at the far cathodic side, taking $\beta=0.19$.

DISCUSSION

Adequacy of the theory

Our theory of the potential-dependence of the faradaic impedance is based on the diffusion layer theory, which is known not to be exactly representative for the mass transport at a DME. A more rigorous treatment based on the semi-infinite linear diffusion theory, but only for constant k_{sh} , has been given by DELMASTRO AND SMITH¹⁴, especially for the theory of a.c. polarography. The final expression in this work is given in terms of i/i_{rev} , which represents the deviation from reversible behaviour. It is easily derived that the potential-dependence of our σ and θ can be expressed with the aid of the function, $F(\lambda t^{\frac{1}{2}})$:

$$\frac{\sigma_{rev}}{\sigma} = \frac{\theta_{rev}}{\theta} = F(\lambda t^{\frac{1}{2}}) = 1 + \left(\frac{7}{3\pi}\right)^{\frac{1}{2}} \frac{(1.61 + \lambda t^{\frac{1}{2}})}{(1.13 + \lambda t^{\frac{1}{2}})^2} [\beta \exp(-j) - \alpha] \quad (16)$$

where θ_{rev} and σ_{rev} are given by eqns. (8) and (9) and

$$\lambda = (k_{sh}^a / D_O^{\frac{1}{2}} \alpha D_R^{\frac{1}{2}} \beta) [\exp(\alpha j) + \exp(-\beta j)] = \sqrt{2} p' \quad (17)$$

Note that the anodic transfer coefficient is represented by α in our notation, and by β in SMITH'S notation. Different expressions are given in ref. 14 for $F(\lambda t^{\frac{1}{2}})$, depending on the type of electrode model. The most rigorous theory leads to a very complicated expression but a good approximation for a DME seems to be the "expanding plane model" which leads to eqn. (16). This can be compared with our treatment after combination of eqn. (2) with (8), or (3) with (9), together with (7) and (17):

$$\sigma_{rev}/\sigma = \theta_{rev}/\theta = 1 + \{(\beta - g)\exp(-j) - (\alpha + g)\} / \{1 + \lambda(3/7\pi t)^{\frac{1}{2}}\} \quad (18)$$

This suggests that β and α appearing in eqn. (16) must be considered as apparent transfer coefficients, in which the potential-dependence of the rate constant is incorporated.

It can be calculated that the difference between eqns. (18) and (16) is always less than 15% and as a rule does not exceed a few percent if $\lambda t^{\frac{1}{2}} > 7$. In our case, with $t = 3$ sec, this means $\lambda > 4$, or $p' < 0.35$. Except for $NaClO_4$, this condition is met for the $Zn^{2+}/Zn(Hg)$ reaction (Fig. 1). Moreover, the potential-dependence of p' is independent of the nature of $F(\lambda t^{\frac{1}{2}})$, so there are no serious objections to the use of the diffusion-layer theory, which has the advantage that the idea of a potential-dependent rate constant is easily introduced into the equations. The only condition for this is negligibility of the effect of higher-order derivatives of k_{sh} to E by the use of low amplitudes⁴.

Significancy of the potential-dependency of k_{sh}^a

The error in $\log k_{sh}^a$, caused by the inaccuracy in p' , is indicated for the KI case in Fig. 4 by the vertical bars. For the other systems, similar limits are relevant in the far cathodic region but as a rule the error is less than in the KI case at the other potentials. For $NaClO_4$ and KCl , p' is very inaccurate at potentials near $E_{\frac{1}{2}}$ and more reliable values for k_{sh}^a were obtained from θ using eqn. (2) in which a_0 , being of only minor influence, is estimated according to eqn. (7). In principle, a successive approximation procedure is possible, but this appeared to be superfluous.

Other sources of uncertainty are the choices of $E_{\frac{1}{2}}$ and α . An error of 10 mV

in $E_{\frac{1}{2}}^r$ —which is certainly not exceeded in our study—would cause a negligible error if $E \approx E_{\frac{1}{2}}$, and a systematical error increasing to 0.06 in $\log k_{sh}^a$ for $E - E_{\frac{1}{2}}^r < -40$ mV with $\alpha \approx 0.8$. The inaccuracy of 0.02 in α (see Table 1) causes an error in $\log k_{sh}^a$, increasing from zero at $E - E_{\frac{1}{2}}^r = 0$ to 0.14 at $E - E_{\frac{1}{2}}^r = 350$ mV.

Thus, it can be concluded that the apparent rate constant of the $Zn^{2+}/Zn(Hg)$ reaction, calculated from our experiments as indicated above, is significantly potential-dependent in the cases of 1 M KI, 1 M KBr and 1 M $NaClO_4$ as supporting electrolytes. In the case of 1 M KCl it is just on the border of significance, probably as a result of the compensating effect of the attributions of specific adsorption (k_{sh}^f increases with E) and the Frumkin correction ($d\phi_2/dE$ is positive, see eqn. (15)).

Nevertheless, it may be noted that this conclusion is based on an unproved—and improvable—assumption, namely a constant, $\beta = 0.19 \pm 0.02$, in the whole cathodic region. The observations in the anodic region suggest that another interpretation of our experimental facts, namely a constant, k_{sh}^a , and a potential-dependent β , should not be excluded *a priori*. In other words, β could be calculated as a function of E with eqn. (4) in which the measured values of p' are introduced, together with the k_{sh}^a -value (determined at $E = E_{\frac{1}{2}}$) where α and β disappear from the exponentials. However, in the cases of KI and KBr this would lead to improbably low β -values of 0.1, and even 0.0, and it is difficult to explain why this does not occur in the other base electrolytes, where $\beta = 0.22$ would suffice. Moreover, in the very far cathodic region ($E < -1.3$ V vs. SCE) one would have $\beta = 0.17$ for KBr and $\beta = 0.10$ for KI, which is definitely inconsistent with the potential-dependence of θ and σ (see Figs. 2 and 3 and Table 1). Also, the maximum in the σ vs. E plot for KI can be explained only by a decrease of k_{sh}^a with decreasing E and so even if β is potential-dependent, a potential-dependent rate constant is very likely for KI and KBr.

Relation between k_{sh} and double-layer structure

The qualitative correlation between $\log k_{sh}^a$ and the amount of specific adsorption of halide ions is evident after inspection of Fig. 4 in connection with q^1 -data¹⁰⁻¹². For a quantitative comparison it seems most realistic first to apply the Frumkin correction using ϕ_2 -data from refs. 10-12 and $\alpha = 0.81$. The resulting "true formal" $\log k_{sh}^f$ -values (see ref. 1) appear to be nearly independent of potential for $NaClO_4$ solution: only a slight gradual increase in $\log k_{sh}^f$ is observed from -3.66 at $E = E_{\frac{1}{2}}$ to -3.55 at $E = -1.35$ V vs. SCE. This is easily ascribed to a small systematic error in the chosen value of β . Thus, in 1 M $NaClO_4$ solution anion adsorption is either absent, or has no influence on the rate constant of the zinc reaction. For the three other solutions, k_{sh}^f is found to be a function of potential. The values obtained, pertaining to various potentials, are plotted against the corresponding q^1 -values, in Fig. 5*. It should be noted that the plots for KCl and KBr may have to be shifted upwards somewhat if a correction for complex formation is required¹. The shift will not exceed 0.2 in $\log k_{sh}^f$.

The following conclusions may be drawn: (a) if $q^1 = 0$, the rate constant is the same for all base electrolytes within experimental error; (b) the accelerating

* In the original data, the q^1 -values for Br^- are positive at far cathodic potentials¹¹. On consultation with one of the authors, we shifted the q^1 vs. E curve upwards until it coincided with those of Cl^- and I^- at potentials between -1.3 and -1.4 V vs. SCE, in order to have a better comparison.

effect of specifically adsorbed chloride and bromide ions seems to be larger than that of iodide ions; (c) the accelerating effects of adsorbed iodide ions at negative potentials (up to *ca.* -1.1 V) is larger than at more positive potentials (-1.1 to -1.0 V *vs.* SCE). This may be interpreted as a decrease in effectiveness when q^1 is large (a kind of saturation effect) but, in our opinion, it is more probable that the anomalous behaviour at anodic potentials (*vide infra*) is already incipiently present at moderately cathodic potentials. In KCl, KBr and KI this seems to cause k_{sh}^a to attain a limiting value near $E = E_{\frac{1}{2}}$. Note that the decrease in k_{sh}^a at $E > E_{\frac{1}{2}}$, indicated in Fig. 4,

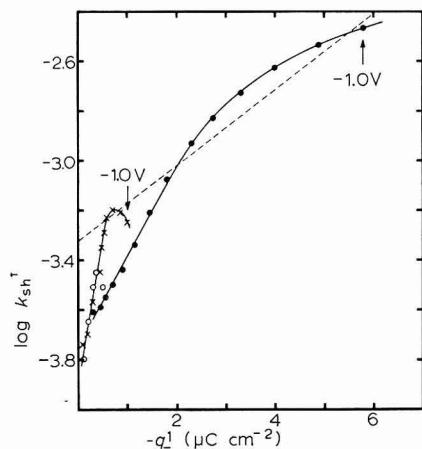


Fig. 5. „True” rate constants, plotted against the amount of specially adsorbed anions. (—) From the present work, with potential as varied parameter; (---), from ref. 1, at constant potential (-1.0 V *vs.* SCE) in $(1-x)$ M KCl + x M KI soln. (●) KI, (×) KBr, (○) KCl.

will be eliminated by choosing a higher value for β , which would be in accordance with the experimental facts. It is of interest in this connection that the smaller slope in the KI-curve in Fig. 5 closely resembles that of the straight line we obtained in our previous work¹ for $\log k_{sh}^T$ *vs.* q^1 measured at the standard potential (*ca.* -1.0 V *vs.* SCE) in mixtures of $(1-x)$ MKCl + x MKI (dashed line in Fig. 5).

The kinetic parameters of the $Zn^{2+}/Zn(Hg)$ reaction

The kinetic aspects of the zinc reaction although frequently considered as a classical subject have not to our knowledge been studied before in such a wide potential range as presented in this work. As in most relaxation methods, no d.c. polarisation is applied, the potential range covered by variation of the Ox/Red ratio is very small and close to E_0 . Also, analysis of the d.c. current-voltage curve yields, as a rule, kinetic parameters pertaining to the half-wave potential. It may be clear that the physical meaning of such results should be considered preferably within the scope of a larger potential range if there is reason to suspect complications in the reaction mechanism. For example, the frequently reported value, $\beta^a = 0.3$, pertains to a potential region where the gradual increase from 0.2 (for KI, even from 0.0) at the cathodic side, to 0.6 at the anodic side starts.

An apparent rate constant of 0.0 for the zinc reaction in 1 M KI at moderately cathodic potentials was also observed by BLACKLEDGE AND HUSH². They interpreted

this as being indicative of a chemical reaction in the double layer, preceding charge transfer. However, our interpretation based on the idea of a potential-dependent rate constant seems more reasonable, since there is little doubt that β is different from zero at more cathodic potentials. It was mentioned earlier¹ that more of these authors' results could be interpreted with the specific anion adsorption model.

Our experiments in the anodic range confirm the anomalous transfer coefficient found already though less convincingly, by HUSH AND BLACKLEDGE¹³. In principle an "apparent" transfer coefficient is also concerned here, but in view of the common value found in all base solutions, we believe that we determined a "true" transfer coefficient (only the Frumkin correction might introduce $g \approx -0.03$) and that the mechanism of the electrode reaction is indeed different at anodic and cathodic potentials. As HUSH AND BLACKLEDGE suggest, there may be a two-step reaction mechanism. Another possibility is the interference of a chemical reaction preceding the oxidation and following the reduction, *i.e.*, coupled to the Red component. This reaction could be the formation and dissociation of Zn_2 molecules in the amalgam, the occurrence of which has recently been reported¹⁵. In both cases, however, the question remains, why does the effect of the base electrolyte on the rate constant still exist (see Table 2), whereas the potential-dependence of this effect is absent ($g=0$), or at least equal in all base electrolytes. If $g=0$, the apparent rate constants in the anodic region can be calculated from θ with eqn. (8) or from β' with eqn. (4). The results, listed in Table 2, are substantially higher than the k_{sn}^a -values obtained at the half-wave potential.

In conclusion, the impedance of the $Zn^{2+}/Zn(Hg)$ reaction in different media is consistent with the assumption that specific adsorption of anions accelerates the electrode reaction. However, the experiments in the anodic potential region reveal a complication in the reaction mechanism which cannot be clarified at present. It will be of interest to investigate this further and also to study the effect of specific adsorption on a system that is not complicated by a potential-dependent transfer coefficient.

ACKNOWLEDGEMENT

The authors wish to express their gratitude to Dr. B. TIMMER for valuable discussions of the present work. Dr. R. PARSONS is thanked for kindly supplying the double-layer data quoted in refs. 10-12. The present investigations have been carried out in part under the auspices of the Netherlands Foundation of Chemical Research (S.O.N.) with financial aid from the Netherlands Organization for the Advancement of Pure Research (Z.W.O.).

SUMMARY

The impedance of the $Zn^{2+}/Zn(Hg)$ electrode in 1 M KI, KBr, KCl and $NaClO_4$ solutions has been measured as a function of potential, using an externally polarised dropping mercury electrode. The potential-dependence of the faradaic impedance has been carefully analysed. It is shown that, in general, both the apparent rate constant and the apparent transfer coefficient are potential-dependent. In the cathodic potential region (-1.05 to -1.35 V *vs.* SCE) the results are in accordance

with a constant value, $\beta = 0.19 \pm 0.02$ for the "true" cathodic transfer coefficient and a potential-dependent rate constant which increases if the amount of specifically adsorbed anions increases. In the anodic potential region (-0.90 to -0.95 V vs. SCE) a significantly different transfer coefficient is found, $\beta = 0.60 \pm 0.03$, which indicates that the mechanism of the electrode reaction depends on the d.c. potential. It is suggested that the interpretation of kinetic parameters and the testing of simple theories with such systems should be approached with caution.

REFERENCES

- 1 P. TEPPEMA, M. SLUYTERS-REHBACH AND J. H. SLUYTERS, *J. Electroanal. Chem.*, 16 (1968) 165.
- 2 J. BLACKLEDGE AND N. S. HUSH, *J. Electroanal. Chem.*, 5 (1963) 435.
- 3 M. SLUYTERS-REHBACH AND J. H. SLUYTERS, *Rec. Trav. Chim.*, 82 (1963) 525, 535.
- 4 M. SLUYTERS-REHBACH, B. TIMMER AND J. H. SLUYTERS, *Z. Physik. Chem. N.F.*, 52 (1967) 89.
- 5 B. TIMMER, M. SLUYTERS-REHBACH AND J. H. SLUYTERS, *J. Electroanal. Chem.*, 18 (1968) 93.
- 6 J. E. B. RANGLES, *Discussions Faraday Soc.*, 1 (1947) 11.
- 7 M. SLUYTERS-REHBACH, B. TIMMER AND J. H. SLUYTERS, *J. Electroanal. Chem.*, 15 (1967) 151.
- 8 N. TANAKA AND R. TAMAMUSHI, *Electrochim. Acta*, 9 (1964) 963.
- 9 B. TIMMER, M. SLUYTERS-REHBACH AND J. H. SLUYTERS, *J. Electroanal. Chem.*, 14 (1967) 169.
- 10 D. C. GRAHAME AND R. PARSONS, *J. Am. Chem. Soc.*, 83 (1961) 1291.
- 11 J. LAWRENCE, R. PARSONS AND R. PAYNE, *J. Electroanal. Chem.*, 16 (1968) 193.
- 12 D. C. GRAHAME, *J. Am. Chem. Soc.*, 80 (1958) 4201.
- 13 N. S. HUSH AND J. BLACKLEDGE, *J. Electroanal. Chem.*, 5 (1963) 420.
- 14 J. R. DELMASTRO AND D. E. SMITH, *J. Electroanal. Chem.*, 9 (1965) 192.
- 15 B. K. HOVSEPIAN AND I. SHAIN, *J. Electroanal. Chem.*, 14 (1967) 1.

J. Electroanal. Chem., 19 (1968) 85-97

CHRONOPOTENTIOMETRY OF THE Ag-AgCl SYSTEM AND ANALYSIS FOR THE CHLORIDE ION

ROBERT E. MEYER, FRANZ A. POSEY AND PAUL M. LANTZ

Chemistry Division, Oak Ridge National Laboratory, Oak Ridge, Tenn. (U.S.A.)

(Received January 8th, 1968; in revised form, March 6th, 1968)

Although the theoretical basis of chronopotentiometry is well established for many types of reactions, relatively few analytical applications have been described. Further, little attention has been paid to the case of quasi-reversibility, and there is a tendency to report results as either reversible or irreversible. We present here a discussion of quasi-reversibility of reactions of the type illustrated by the formation of AgCl upon silver, and in addition we show that this system can be used for a simple and accurate analysis for the chloride ion.

DELAHAY, MATTAX AND BERZINS¹ investigated theoretically the case of anodic oxidation of a metal with formation of an insoluble substance and gave the equation for the chronopotentiometric wave assuming that the Nernst equation applies to the reaction. In addition, they showed that reproducible transition times can be obtained for the Ag-AgCl system at a chloride concentration of 5 mM. They reported, however, that the slope which they obtained from the conventional plot of $\log [1 - (t/\tau)^{1/2}]$ vs. potential was 67 mV rather than the theoretical value of 59 mV, at 25°. Furthermore, the value of the solubility product which they calculated from their results is somewhat higher than the generally accepted value, a result which they attributed to the small diameter of the particles of AgCl. They also suggested that reactions of this type might be useful for analytical purposes.

THEORY

The shape of chronopotentiometric waves has been the subject of many treatments and excellent reviews are available²⁻⁴. However, little consideration has been given to the general case of quasi-reversible kinetics. Recently, ANDERSON AND MACERO⁵ have treated the quasi-reversible case for forward and reverse waves. Their treatment covers the case of the reaction, $\text{Ox} + e^- = \text{Red}$, where both species are under diffusion control. For the case considered here (*i.e.*, the case of a single diffusing reactant ion and an insoluble reaction product) the equations are somewhat different and a graphical method can be used to determine the kinetic constants of the reaction. These equations are given below because our results show that under the conditions investigated here, the formation of AgCl proceeds quasi-reversibly; *i.e.*, the exchange current and the polarizing current are of the same general order of magnitude.

We assume, as did DELAHAY *et al.*¹, that the presence of AgCl on the electrode

surface does not significantly affect the general rate expressions*. JAENICKE, TISCHER AND GERISCHER⁶ have shown that compact highly resistive films are not formed at the current densities used in our work, and therefore no significant resistance is to be expected.

The overall expression for the current density is given by the following equation:

$$[i = i_0(C_i/C_0) \exp [\alpha z(E - E_0)F/RT] - i_0 \exp [-(1-\alpha)z(E - E_0)F/RT]] \quad (1)$$

where

$$[i_0 = zFk_a C_0 \exp [+ \alpha z E_0 F/RT] = zFk_c \exp [-(1-\alpha)z E_0 F/RT]] \quad (2)$$

In these equations, k_a and k_c are heterogeneous rate constants for the anodic and cathodic reactions, respectively. C_i is the concentration of the diffusing ion at the interface, C_0 the initial concentration throughout the solution, α the transfer coefficient for the anodic reaction, and the rest of the terms have their usual significance. The equilibrium potential, E_0 , is the potential that a Ag-AgCl electrode system will attain at the concentration, C_0 ; at this potential $C_i = C_0$. Implicit in these equations is the assumption that the activity of AgCl remains constant during polarization.

The standard boundary conditions for chronopotentiometry are satisfied for this case and therefore²⁻⁴,

$$C_i/C_0 = [1 - (t/\tau)^{1/2}] \quad (3)$$

where

$$\tau^{1/2} = \pi^{1/2} z F \mathcal{D}^{1/2} C_0 / 2i \quad (4)$$

and where \mathcal{D} is the diffusion coefficient of the diffusing ion and τ , the transition time, is the time at which C_i theoretically decreases to zero.

Setting $\exp [z(E - E_0)F/RT] = \theta$, we have from eqns. (1) and (3),

$$i/i_0 = (C_i/C_0) \theta^\alpha - \theta^{-(1-\alpha)} \quad (5)$$

or

$$[1 - (t/\tau)^{1/2}] = (i/i_0) \theta^{-\alpha} + \theta^{-1} \quad (6)$$

If $(E - E_0)$ and τ are known, then the unknown parameters, αz and i_0 , may be obtained from the chronopotentiometric waves by plotting the data according to the following equation, which is derived from eqn. (6).

$$\log \{ [1 - (t/\tau)^{1/2}] - \theta^{-1} \} = \log (i/i_0) - (\alpha z/2.3) (E - E_0)F/RT \quad (7)$$

The quantity on the left is plotted *vs.* $(E - E_0)F/RT$, and the slope and intercept yield αz and i_0 , respectively.

From eqn. (6) we note that if $i \ll i_0$, then

$$E = E_0 - (2.3RT/zF) \log [1 - (t/\tau)^{1/2}] \quad (8)$$

and if $i \gg i_0$, we have

$$E = E_0 + (2.3RT/\alpha z F) \log (i/i_0) - (2.3RT/\alpha z F) \log [1 - (t/\tau)^{1/2}] \quad (9)$$

Equations (8) and (9) are, respectively, the equations for reversible and irreversible

* By making this assumption, we do not consider the complexities that could arise due to crystal growth and related phenomena. Our justification for this assumption is that the equations so derived adequately describe the chronopotentiometric waves. A study of the mechanism of formation of AgCl would be interesting but beyond the scope of this work.

waves. If the reaction is completely irreversible, then the term θ^{-1} in eqn. (7) is negligible, and a plot according to eqn. (7) is essentially identical with the standard treatment of irreversible waves. As the reaction approaches reversibility, this method of determining the kinetic constants becomes less accurate, for the expression $(1 - (t/\tau)^{\frac{1}{2}} - \theta^{-1})$ approaches zero (*cf.* eqn. (8)).

If $\alpha z = \frac{1}{2}$, then eqn. (6) may be solved explicitly for E . For positive values of i , we have after setting $s = \theta^{\frac{1}{2}}$

$$i/i_0 = (C_i/C_0)s - 1/s \quad (10)$$

This is a quadratic equation in s which can be solved to give:

$$s = [i/i_0 + \{(i/i_0)^2 + 4C_i/C_0\}^{\frac{1}{2}}] / (2C_i/C_0) \quad (11)$$

or

$$E = E_0 + 4.6(RT/F) \log \{ [i/i_0 + \sqrt{(i/i_0)^2 + 4[1 - (t/\tau)^{\frac{1}{2}}]}] / 2[1 - (t/\tau)^{\frac{1}{2}}] \} \quad (12)$$

Chronopotentiometric waves of the three types are plotted in Fig. 1. For the reversible case (*cf.* eqn. (8)) the potential begins to depart from the equilibrium poten-

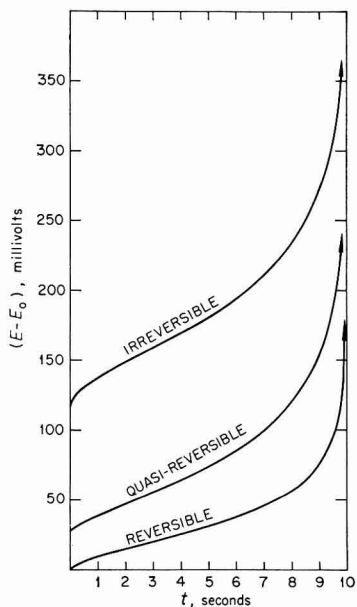


Fig. 1. Theoretical chronopotentiometric waves for the process, $M + X^- - e^- = MX$ (insoluble). $\tau = 10$ sec, $z = 1$, $\alpha = \frac{1}{2}$; quasi-reversible case, $i/i_0 = 1$; irreversible case, $i/i_0 = 10$.

tial smoothly and slowly, and the rise in potential at the transition time is quite distinct. For the other two cases (*cf.* eqns. (9) and (12)) there is a marked jump in potential initially and a less distinct rise in potential at the transition time. However, with the use of appropriate techniques, the transition time may be determined without difficulty in all cases.

In practice, the potential does not increase indefinitely to infinity as indicated in Fig. 1. Rather, the potential tends to level off at the next electrode reaction, and a

point of inflection is observed very near the transition time. For many cases, it is preferable to determine the transition time by observing this point of inflection through electronic differentiation. At the point of inflection, a peak in the derivative curve is observed, and the transition time can be determined with much more precision. This differentiation technique is especially useful if the reaction is irreversible or quasi-reversible, for in these cases the potential will shift much more than in the reversible case and the potential may then move into the region of the next half before a well-defined rise is observed.

The use of the derivative to determine the transition time by this method has been reported by IWAMOTO⁷. More recently^{8,9}, derivative chronopotentiometry has been used to determine the transition time by a different technique.

EXPERIMENTAL

Apparatus

The design of the cell was based on that of MORRIS AND LINGANE¹⁰ and is shown in Fig. 2. The electrode was cut from silver sheet and held firmly in place by the large stainless-steel bolt. The working area of the electrode was defined by the cut-out

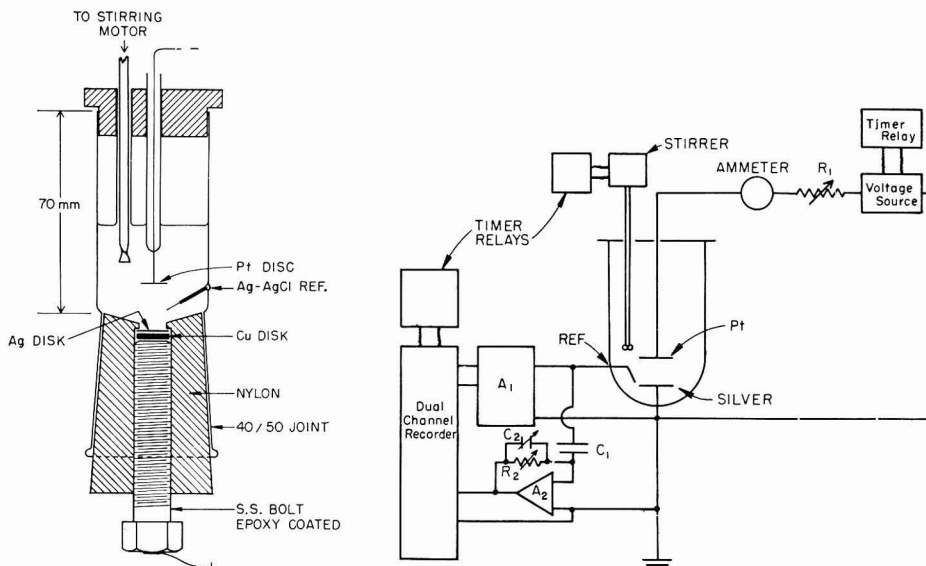


Fig. 2. Cell for chronopotentiometric waves and their derivatives. See text for details.

Fig. 3. Schematic diagram of apparatus for recording chronopotentiometric waves and their derivatives. See text for details.

in the nylon bottom of the cell, and had an area of 1.13 cm². The counter-electrode was a platinum disk placed symmetrically above the silver disk, and the reference electrode was a silver-silver chloride electrode placed directly into the solution. Care was taken to place the electrode near, but just to the side of, the silver disk. All but a few millimeters of the top of the silver reference electrode were insulated with epoxy resin. Measurements with a calomel reference electrode showed that during polarization the

potential of the Ag-AgCl reference electrode stayed constant to within one or two millivolts.

Care had to be taken to keep the electrode clean. Before use, the electrodes were inspected for visual imperfections, polished with a very fine abrasive (*e.g.*, silver polish) and thoroughly degreased and rinsed with alcohol and distilled water. Periodically, the electrode was removed and treatment was repeated. Poorly defined chronopotentiometric waves and irreproducible transition times were generally the signal for recleaning. Care was also taken to prevent gas formation due to excessive polarization. Finally, it was found necessary to reduce the AgCl on the surface after each oxidation cycle with the relay system described below.

The measurement circuit is shown in Fig. 3. Constant current was supplied by a John Fluke Model 407 regulated power supply (John Fluke Manufacturing Co., Seattle, Washington) feeding through an adjustable bank of resistors (R_1). The voltage and resistance were always great enough to insure constant current. The polarity of the current was reversed for the oxidation and reduction cycles by means of a switch operated by a timer relay. The potential of the silver electrode was monitored with a Keithley model 610 electrometer (A_1) (Keithley Instruments, Inc., Cleveland, Ohio) coupled to one channel of a Hewlett-Packard model 7100B dual-channel recorder (Hewlett Packard-Moseley Div., Pasadena, Calif.) The derivative of the $E-t$ curve was also monitored and recorded on the other channel of the recorder. The derivative was supplied by a derivative unit which made use of a Philbrick P65AU operational amplifier (A_2) (Philbrick Researches, Inc., Boston, Mass.) The differentiating capacitor had a value of $20 \mu\text{F}$ and the resistor (R_2) was varied to give gain sufficient to drive the recorder. The current was monitored either with ammeters or by measuring the voltage drop across precision resistors. When ammeters were used, they were always calibrated by the ORNL Standards Laboratory. The sequence of operations (explained below) was controlled by adjustable timer relays (Cycl-Flex HP5 series) (Eagle-Signal Co., Moline, Ill.).

Reagents

No special reagents are required for the analyses. One series of test solutions was made up from Long Island Sound sea water. Sulfuric acid, sodium nitrate, or sodium sulfate were used as inert electrolyte, generally at $0.5 M$.

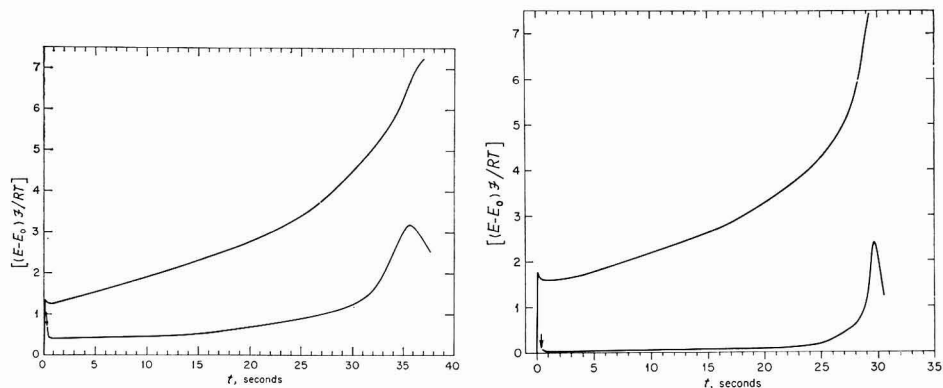
Analytical procedure

Solutions containing inert electrolyte and known amounts of sodium chloride were used to determine the chronopotentiometric constant, $K = \tau^{1/2}i/C_0$ (*cf.* eqn. (4)), over the concentration range of interest. The unknown solutions were made up to approximately ($\pm 25\%$) the same concentration of inert electrolyte, and the current was adjusted until the observed transition time was about equal (generally $\pm 10\%$) to that used for the standard solutions. The concentration was then calculated from the relation, $C_0 = \tau^{1/2}i/K$. For maximum accuracy, the electrode was calibrated immediately before use. Analyses with an accuracy of $\pm 3\%$ can be obtained with only occasional calibration (*e.g.*, daily) if care is taken not to damage the electrode surface by abrasion or allowing it to dry out. Electrodes were pre-aged as discussed below by running them through a cycle of at least ten formations and reductions of the AgCl film at the highest concentration of Cl^- in the concentration range of interest.

The transition time was determined by the following sequence of operations: initially, a reduction current was applied to reduce any AgCl formed on the surface. Stirring was also applied during and for a short time after the reduction cycle. A delay of usually about 30 sec was followed by the actual oxidation cycle. The recorder drive was turned on a few seconds before the initiation of the oxidation cycle, and, after the wave was recorded, the reduction cycle was begun again. Thus, the total cycle was repeated in about one minute for the shorter transition times. The reduction was always carried out with the same value of current as the oxidation cycle but extending over a slightly longer time to insure complete reduction of the AgCl. After a few complete cycles, the transition times in an individual series were generally reproducible to within 1%.

RESULTS AND DISCUSSION

Typical chronopotentiograms are shown in Figs. 4 and 5. The derivative of each $E-t$ curve is shown on the same time axis but with an arbitrary vertical axis. The transition time so measured corresponded closely to transition times measured by conventional techniques applied to the $E-t$ curves^{2,3}. However, for unfavorable conditions, the graphical techniques were quite arbitrary, and the use of the derivative was essential to the accurate determination of the transition time.



Figs. 4-5. Chronopotentiometric waves and their derivatives for formation of AgCl on Ag. (4) $C_0 = 4.86 \cdot 10^{-3} M$ NaCl, $i = 3.26 \cdot 10^{-4} A/cm^2$, $\tau = 35.6$ sec, $0.5 M Na_2SO_4$. (5) $C_0 = 4.95 \cdot 10^{-2} M$ NaCl, $i = 3.35 \cdot 10^{-3} A/cm^2$, $\tau = 29.7$ sec, $0.5 M Na_2SO_4$.

A small amount of overshoot is observed in Figs. 4 and 5 at the initial section of the $E-t$ curve. This overshoot was observed also when an oscilloscope was used to monitor the potential. However, if the AgCl was formed on a previously formed AgCl layer, the overshoot was not observed. We conclude that a slight amount of crystallization overvoltage may be involved. The overshoot did not interfere with the analysis.

Figure 6 is a plot of $\log(1 - (t/\tau)^{1/2})$ vs. E for the case shown in Fig. 4. Examination of eqns. (8) and (9) show that such a plot should be linear if this $E-t$ curve represents either the reversible or the irreversible case. Except for the initial section, the plot is linear and has a slope of 91 mV/decade. If the reaction were reversible, the slope would be about 59 mV/decade. The deviation from 59 mV/decade is too large

to be explained by a small perturbation from reversibility. Examination of the potential scale of Figs. 4 and 5 shows that the potential has not departed far enough from the equilibrium potential for the reverse reaction (cathodic) in this case to be neglected. Generally, the reverse reaction cannot be neglected unless there is at least a 120-mV difference from the equilibrium potential. For these reasons we have analyzed the reaction as a case of quasi-reversibility, and eqn. (7) may be used.

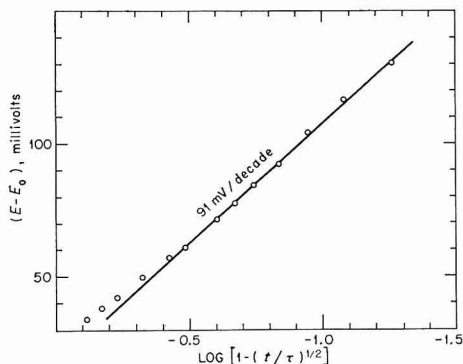
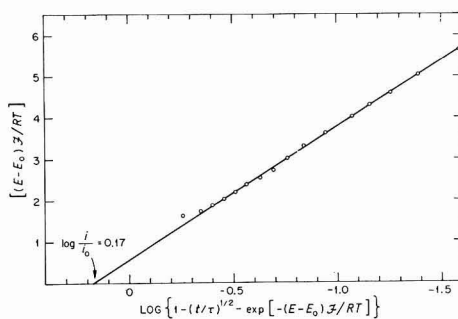
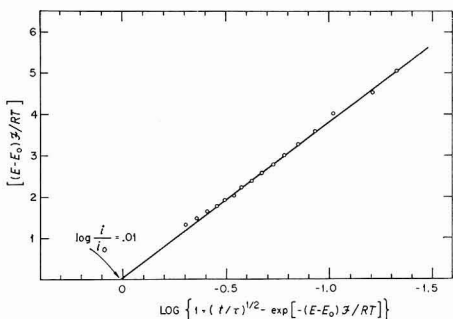


Fig. 6. Plot of $\log [1 - (t/\tau)^{1/2}]$ vs. E ; test for reversibility. $C_0 = 4.86 \cdot 10^{-3} M$ NaCl, $i = 3.26 \cdot 10^{-4} A/cm^2$, $\tau = 35.6$ sec, $0.5 M$ Na₂SO₄.



Figs. 7-8. Determination of i_0 and αz from chronopotentiometric waves. (7) $C_0 = 4.86 \cdot 10^{-3} M$ NaCl, $i = 3.26 \cdot 10^{-4} A/cm^2$, $\tau = 35.6$ sec, $0.5 M$ Na₂SO₄. (8) $C_0 = 4.95 \cdot 10^{-2} M$ NaCl, $i = 3.35 \cdot 10^{-3} A/cm^2$, $\tau = 29.7$ sec, $0.5 M$ Na₂SO₄.

Figures 7 and 8 show plots according to eqn. (7). The plots are linear except for the initial sections of the curve and the kinetic constants are reasonable. Values of α ranging from about 0.5 to 0.8 have been found and generally the exchange current is about the same order of magnitude as the polarizing current. Table 1 shows some of the results. Since the formation of the AgCl on a solid silver electrode is not a well-defined, reproducible process, variability in the kinetic constants is to be expected. It should be emphasized that these constants refer to the formation of thin, porous films of AgCl on silver. Deviation of the initial section of the curves of Figs. 7 and 8 results from the fact that overshoot is observed on the initial section of the $E-t$ curve.

Table 2 shows the variation of the chronopotentiometric constant with transition time at 0.01 M . Here it is shown that this constant varies only slightly from transition

tion times of about 60 sec to about 3 sec. Below 10 sec the constant rises, and below about 0.5 sec it is difficult to obtain a reproducible time. Analyses at transition times of 1–10 sec can be performed by carrying out calibration and determinations at approximately the same transition times. The amount of variation in transition time that can be tolerated depends on the precision required. According to Table 2, a variation of about -1 and $+5$ sec must not be exceeded at a transition time of 5 sec, in order to keep the permissible error within 1%. For the same precision, a much larger variation can be tolerated at transition times greater than 10 sec. At lower concentrations, the

TABLE 1

KINETIC CONSTANTS DERIVED FROM CHRONOPOTENTIOMETRIC WAVES

C_0, NaCl ($M \cdot 10^{-3}$)	i ($A/cm^2 \cdot 10^{-4}$)	τ (sec)	α	i_0 ($A/cm^2 \cdot 10^{-4}$)
4.9	2.56	56.7	0.63	3.32
4.9	4.42	20.6	0.52	4.07
4.9	6.63	9.7	0.56	6.19
4.9	8.85	5.8	0.56	5.92
4.86	3.26	35.6	0.61	3.17
9.93	8.40	19.75	0.79	6.10
49.5	33.5	29.7	0.71	22.8

TABLE 2

VARIATION OF CHRONOPOTENTIOMETRIC CONSTANT WITH TRANSITION TIME
0.01 M Cl⁻, 0.5 M Na₂SO₄

Current density (mA/cm^2)	Transition time (sec)	$K(= \tau^{1/2} i / C_0) \cdot 10^{-2}$
0.460	56.1	3.45
0.535	45.0	3.60
0.663	30.0	3.64
0.918	20.0	3.63
1.154	10.0	3.65
1.657	5.0	3.71
1.88	4.0	3.76
2.21	2.96	3.81
2.77	1.98	3.90
4.09	1.03	4.16
5.66	0.50	4.0

TABLE 3

COMPARISON OF CHRONOPOTENTIOMETRIC AND CHLORIDOMETRIC METHODS FOR
CHLORIDE ANALYSIS OF LONG ISLAND SOUND WATER

Chloridometric(M)	Chronopotentiometric (M)	% Difference
0.2171	0.2123	-2.2
0.1094	0.1098	0.4
0.05537	0.05570	0.6
0.02749	0.02769	0.7
0.01388	0.01398	0.7
0.006961	0.006933	-0.4
0.001865	0.001866	0.05

variation in the chronopotentiometric constant with transition time becomes somewhat greater. We therefore always reproduce the transition time to $\pm 10\%$ at concentrations below $0.005 M Cl^-$.

Table 3 shows a series of actual determinations which were done under conditions designed to obtain maximum precision. The electrode was calibrated with solutions of known concentration at transition times of close to 5 sec (these analyses have been carried out at transition times of 5 sec rather than the more usual 20–40 sec because of our interest in applying this method to flow cells, as described below). With the same electrode surface and interspersed between the calibration runs, the unknowns were run also at transition times of 5 sec. These unknowns were prepared by dilution with distilled water of a sample of the Long Island Sound sea water as shown in Table 3. Analyses of the unknowns were carried out by a Buchler-Cotlove Chloridometer (Buchler Instruments, Inc., Ft. Lee, N. J.) an instrument which makes use of coulometric titration and which we have found to be accurate to 1%. The agreement between the two methods of analyses is within the sum of the precisions expected for the two methods.

Table 4 shows a test of reproducibility and stability of an electrode that was prepared as described above and cycled through a series of oxidations and reductions

TABLE 4
TEST OF REPRODUCIBILITY OF ELECTRODE

Order of determination	Concn. Cl^- (M)	$K (= \tau^{1/2}/C_0) \cdot 10^{-2}$	Mean $K \cdot 10^{-2}$	Rel. Std. Dev. (%)
1	0.0005	3.74	3.98	3.8
7		3.91		
13		4.10		
19		4.08		
25		4.06		
2	0.00075	3.95	3.94	1.3
9		3.87		
15		3.92		
18		3.97		
23		4.01		
3	0.001	4.07	3.98	2.5
6		3.84		
16		4.08		
20		3.94		
22		3.96		
4	0.005	3.72	3.75	0.8
10		3.73		
11*		3.79		
14		3.75		
24		3.78		
5	0.01	3.72	3.74	1.5
8		3.70		
12		3.76		
17		3.83		
21		3.70		

* Run No. 11 begun after leaving cell standing overnight containing $0.005 M Cl^-$.

at a concentration of $0.01 M$ Cl^- before use. The entire series was run over a period of two days. Examination of this table shows that analyses in this range of concentrations should be accurate to within a few per cent without frequent calibration. We have not been able to obtain reproducible transition times at concentrations below $0.0003 M$ because the derivative peak broadens. In addition, we have found that extensive use of the electrode at concentrations above $0.1 M$ changes the electrode surface so that it is advisable to recalibrate the electrode if it is to be used again in the concentration range of Table 4. This is not a serious disadvantage, however, since calibration is a very simple procedure.

The substances used as inert electrolyte (Na_2SO_4 , H_2SO_4 , NaNO_3 , all at $0.5 M$) were interchanged without changing the value of the chronopotentiometric constant. In so doing, the pH was also changed significantly without effect. Other experiments using HCl as the unknown and Na_2SO_4 as the inert electrolyte also confirmed this result. Reducing the concentration of inert electrolyte from $0.5 M$ to $0.1 M$ increased the transition time by a few per cent. In general, we tried to maintain its concentration at $0.5 M \pm 25\%$, but satisfactory analyses could easily be accomplished at $0.1 M$. De-aeration was found to be unnecessary even at the lowest concentrations. Operation of a second cell with diffusion upward rather than downward also did not affect the results under the conditions of this work.

Aging of the electrode had a beneficial effect at the lower concentrations (below $0.002 M$). Silver which was freshly prepared generally showed high transition times at concentrations of $0.002 M$ or below. After an electrode had been aged and used for several determinations, only slight increases in transition times were noted. For this reason, we generally preaged electrodes by running through a series of at least ten oxidations and reductions at the highest concentration of Cl^- .

Finally, we have found that well-defined chronopotentiometric waves can be produced on silver already covered with a thin layer of AgCl . However, this type of surface was much more difficult to reproduce over a wide range of concentrations and currents than the surface formed by complete reduction of the silver chloride.

DISCUSSION

The transition time was easily and precisely determined by the derivative method described above. Whether the transition time so determined corresponds accurately to that defined by the condition, $C_1 = 0$, is not certain, however. For cases where the potential changes sharply enough so that the transition time can be determined directly from the $E-t$ curve, the two methods give closely corresponding results. For use in analysis, accurate determinations of τ are not necessary, however; only precision and reproducibility are required.

More serious is the validity of the assumption that the chloride ion is depleted uniformly across the electrode surface with 100% current efficiency. A small rise in transition time at low concentrations is frequently observed (*cf.* Table 4), and this may indicate that all of the silver ion does not form AgCl at the surface. Either another compound, perhaps the oxide, is formed, or the silver ion leaves the surface without forming insoluble AgCl in a distance short compared to the thickness of the diffusion layer. The fact that aging lowers the transition time at low concentrations suggests that freshly cleaned silver surfaces may not offer many nucleation sites for formation

of AgCl. Alternatively, at freshly prepared silver surfaces there may be an excess of active sites so that Ag^+ may diffuse from the electrode surface before it can form AgCl.

From the practical standpoint, it is only necessary to reproduce the current efficiency in each run in order to use this technique for analysis. The most important factors for doing this are first, to remove completely the AgCl formed before repeating a run; second, to run the calibration curves and the unknown curves with a carefully reproduced cycle of operations, and finally, to pre-age the electrode as described above.

Use of this techniques offers certain advantages compared to other methods of analysis for the chloride ion. It should be noted that a much simpler apparatus than that shown in Fig. 2 can be used and that, although a Ag-AgCl reference electrode is used, it is only necessary that the potential of this electrode remain approximately constant or drift uniformly during the measurement. Highly accurate measurement of potential therefore is not required as in potentiometric methods of analysis. In fact, it is not even necessary to measure the potential, for only the derivative of the $E-t$ curve is required for analysis.

The rapidity and simplicity of this method suggests its use in a flow cell; use of this method is projected in desalination research for routine monitoring of certain process streams. The useful concentration range of the method ($0.5 - 5 \cdot 10^{-4} M$) is ideal for this application, for this is just the concentration range of interest in desalination.

ACKNOWLEDGEMENT

The authors are indebted to J. KERLEY of the Chemical Technology Division, Oak Ridge National Laboratory, for skilful assistance in making the measurements, and to K. A. KRAUS, Director's Division, Oak Ridge National Laboratory, and G. MAMANTOV, Department of Chemistry, University of Tennessee, Knoxville, Tenn., for fruitful advice and discussions. This research was jointly sponsored by the Office of Saline Water, U.S. Department of the Interior, and U.S. Atomic Energy Commission under contract with the Union Carbide Corporation.

SUMMARY

Chronopotentiometry of the formation of AgCl upon silver electrodes is described. The kinetic constants for this reaction are derived from the chronopotentiometric waves, which are interpreted to be quasi-reversible. A method of analysis for the chloride ion based upon this system is described.

REFERENCES

- 1 P. DELAHAY, C. C. MATTAX, T. BERZINS, *J. Am. Chem. Soc.*, 76 (1954) 5319.
- 2 P. DELAHAY, *New Instrumental Methods in Electrochemistry*, Interscience, New York, 1954.
- 3 M. PAUNOVIC, *J. Electroanal. Chem.*, 14 (1967) 447.
- 4 D. G. DAVIS, *Applications of Chronopotentiometry to Problems in Analytical Chemistry*, in *Electroanalytical Chemistry, Vol. I*, edited by A. J. BARD, Marcel Dekker, New York, 1966, p. 157.
- 5 L. B. ANDERSON, D. J. MACERO, *Anal. Chem.*, 37 (1965) 321.
- 6 W. JAENICKE, R. P. TISCHER and H. GERISCHER, *Z. Elektrochem.*, 59 (1955) 448.
- 7 R. T. IWAMOTO, *Anal. Chem.*, 31 (1959) 1062.
- 8 D. G. PETERS and S. L. BURDEN, *Anal. Chem.*, 38 (1966) 530.
- 9 P. E. STURROCK, G. PRIVETT and A. R. TARPLEY, *J. Electroanal. Chem.*, 14 (1967) 303.
- 10 M. D. MORRIS and J. J. LINGANE, *J. Electroanal. Chem.*, 6 (1963) 300.

THE ELECTROREDUCTION OF NIOBIUM(V) IN HYDROCHLORIC ACID SOLUTIONS AT MERCURY ELECTRODES

II. CONTROLLED-POTENTIAL COULOMETRY AND STIRRED-POOL CHRONOAMPEROMETRY*

JOHN G. McCULLOUGH† AND LOUIS MEITES‡§

Department of Chemistry, Polytechnic Institute of Brooklyn, Brooklyn, New York (U.S.A.)

(Received March 11th, 1968)

The polarographic and chronopotentiometric behavior of niobium(V) in concentrated hydrochloric acid solutions was described in a previous article¹. This paper describes the results obtained in controlled-potential electrolyses under comparable conditions. The products of these electrolyses were identified by coulometry and polarography.

EXPERIMENTAL

The potentiostat and current integrator, originally obtained from Analytical Instruments, Inc. (Wolcott, Conn.) and previously modified as described elsewhere^{2,3}, were further modified during this work to simplify the adjustment of the gain of the potentiostat and to increase the accuracy of the integrator. Details may be obtained from the junior author's thesis.

Electrolyses were performed at $24 \pm 2^\circ$ in a three-compartment cell with a mercury-pool working electrode stirred by a propeller. A cell having a conical working-electrode compartment⁴ was used initially to maximize the ratio of electrode area to solution volume. However, experimentation showed that electrolysis rates were more nearly proportional to the area stirred by the propeller than to the total electrode area. This observation led to the design of the cell shown in Fig. 1. Its cylindrical working-electrode compartment, 5 cm in diameter, permits the use of a much larger propeller. When this is at rest, its four blades are almost covered by the mercury, as shown by the dashed line. When it is rotated fast enough, the mercury pool is deeply dished, as shown by the solid lines, but little or no splashing occurs. A mass-transfer constant (β) equal to 10^{-2} sec^{-1} could be obtained; a simple half-reaction characterized by such a value would be 99.9% complete in about 12 min. The working-electrode compartment was closed with a Neoprene stopper, drilled to admit the propeller shaft through a Teflon bushing, a fritted-glass gas-dispersion

* This paper is based on a thesis submitted by JOHN G. McCULLOUGH to the Faculty of the Polytechnic Institute of Brooklyn in partial fulfillment of the requirements for the Ph.D. degree in June, 1967.

† Present address: Union Carbide Chemicals Division, P.O. Box 65, Tarrytown, N.Y., U.S.A.

‡ To whom correspondence and requests for reprints should be addressed.

§ Present address: Department of Chemistry, Clarkson College of Technology, Potsdam, N.Y.

cylinder for de-aeration, a nitrogen exit tube, a dropping mercury electrode, and the reference electrode, whose tip dragged in the surface of the working electrode. The formation of calomel by reaction with dissolved oxygen was obviated by thorough de-aeration of the solution to be electrolyzed, followed by introduction of mercury through the stopcock at the bottom of the working-electrode compartment.

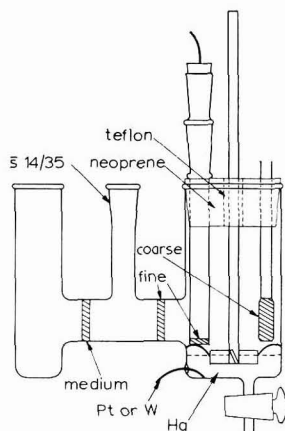


Fig. 1. Double-diaphragm controlled-potential electrolysis cell providing high values of the mass-transfer constant, β .

The volume of solution electrolyzed was always 75 ml and the concentration of hydrochloric acid was always 10.75 F . A silver-silver chloride-1 F potassium chloride reference electrode¹ was used, but all potentials given in this paper are corrected to refer to the SCE.

All other experimental techniques have been described previously¹.

RESULTS AND DISCUSSION

Current-time curves

Solutions containing between 0.9 and 9 mF niobium(V) were reduced at -0.65 , -0.70 and -0.75 V vs. SCE; these potentials lie between the foot and the half-wave potential of the second polarographic wave¹. The resulting plots of log current versus time were concave upward, and were dissected into several linear segments in the manner described previously⁵. The quantity of electricity represented by each segment was calculated from its slope and intercept, and was combined with the known amount of niobium in the sample to compute the corresponding value of n . The results are shown in Table 1. When the line segments were well-defined, the sum of these n -values agreed within 1% with the overall value, n_T , obtained coulometrically in the same electrolysis. Occasionally, the first segment was ill-defined, and its n -value was then found by difference, as indicated in Table 1. The precision of the graphical n -values was usually about ± 0.03 F/mole. In the reduction of 9 mF niobium at -0.656 V, however, the electrolytic rate constants, β_2 and β_3 , were so nearly equal that accurate dissection was difficult. In this case, the uncertainty in n_2 and n_3 is about 0.12, although the uncertainty in their sum is much

TABLE 1
 RESULTS OF CONTROLLED-POTENTIAL ELECTROLYSES

No. of samples	$C_{Nb}(mF)$	$E_{w.e.}$ (V vs. SCE)	Stage no.	n (F/mole)	β (ksec ⁻¹)
4	8.1-9.3	656±2	1	0.49±0.02	9.82±0.25
			2	0.60±0.13	1.66±0.11
			3	0.82±0.11	0.73±0.04
			4	0.18±0.04	0.20±0.02
			2 + 3	1.42±0.04	
			n_T	2.07±0.005	
1	8.1	709	1	0.54	8.90
			2	1.22	1.32
			3	0.25	0.51
			n_T	2.03	
6	8.1-9.5	757±2	1	0.41±0.02	12.0±0.9
			2	1.59±0.02	2.06±0.15
			n_T	2.00±0.01	
3	0.86-0.93	656±2	1	*0.83±0.03	7.7±1.4
			2	0.56±0.03	1.26±0.15
			3	0.72±0.02	0.38±0.06
			n_T	2.11±0.03	
7	0.86-1.08	754±2	1	*0.31±0.02	14.5±1.7
			2	1.38	3.54±0.34
			3	0.48	1.58
			2 + 3	1.86±0.06	
			n_T	2.17±0.03	

* By subtraction: $n_1 = n_T - (n_2 + n_3)$

less. The overall coulometric value, n_T , depended only on the niobium concentration and the potential of reduction, and not at all on the history of the solution: boiling, prior reduction and oxidation, and aging for up to 6 months had no effect. Within the experimental precision, the quantity of electricity consumed in reoxidizing any reduced solution at -0.30 V was exactly equal to that consumed in preparing it from niobium(V).

Disproportionation of niobium(IV)

The reduction of 9 mF niobium(V) at -0.65 V consumes about 2 electrons/atom and appears to involve four separate electron-transfer steps. It was thought that this unusually large number of steps might be illusory, and that the mechanism proposed by VIVARELLI⁶⁻⁸ might account for the current-time curves:



For this scheme it is shown in Appendix 1 that a plot of $i^{-1/2}$ vs. t should become linear for large values of t . Such a plot for the reduction of 8.1 mF niobium at -0.656 V did have a linear segment, but this occurred at intermediate values of t and its

slope corresponded to $k = 0.07 \text{ l mole}^{-1} \text{ sec}$. This is much smaller than the rate constant obtained by VIVARELLI ($0.56 \text{ l mole}^{-1} \text{ sec}^{-1}$) which was in turn much too small to account for the polarographic data reported earlier¹. In addition, as is shown below, electrolytically-produced niobium(IV) is quite stable under the conditions employed here. It was concluded that reaction (2) played a very minor role, if any, in the electrolytic reductions, and that the coulometric n -values in Table I were real.

Polarography of reduced niobium solutions

In order to identify the reduction products, polarograms of partly reduced solutions were obtained in the electrolytic cell at various stages of electrolyses under different conditions. Figure 2 shows the envelopes of polarograms obtained during the reduction of 5.5 mF niobium at -0.654 V . Curve a shows the two reduction waves of niobium(V). Curve b shows the composite cathodic-anodic wave of the niobium(IV)-(V) couple. Curves c and d show another anodic wave, which is

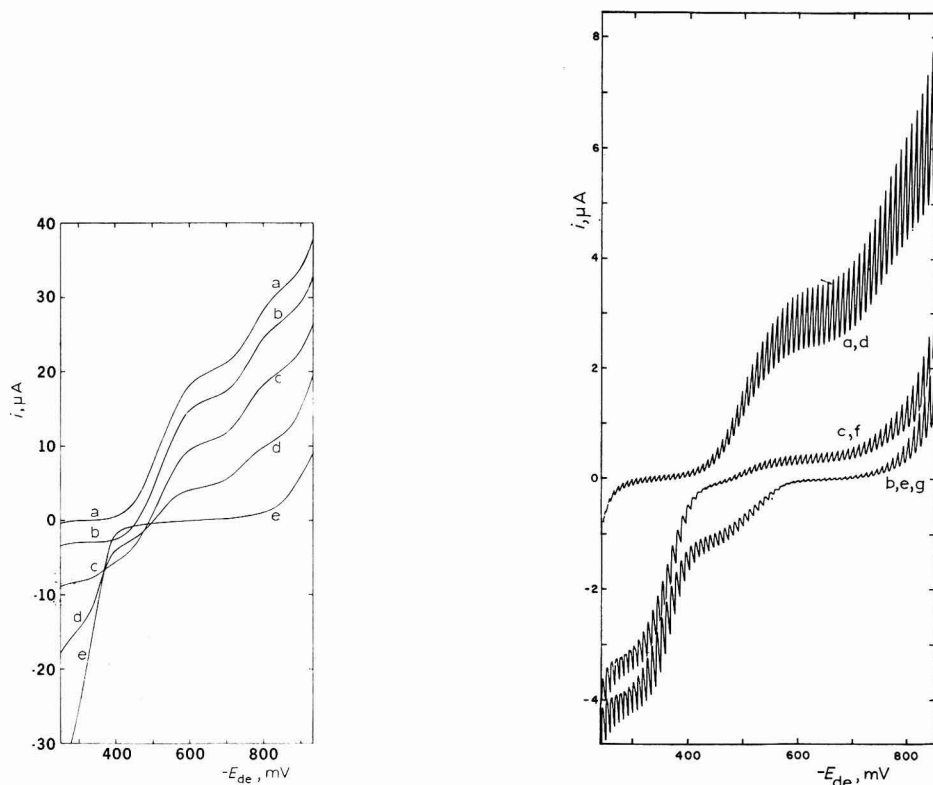


Fig. 2. Envelopes of polarograms of a soln. initially containing 5.5 mF Nb(V) after successive partial reductions at -0.654 V vs. SCE to average oxidation numbers of: (a), 5; (b), 4.78; (c), 4.36; (d), 3.71; (e), 3.0.

Fig. 3. Polarograms of a soln. containing 1.08 mF Nb(V) (a), before reduction, $\bar{n} = 5$; followed by (b), reduction at -0.75 V , $\bar{n} = 2.75$; (c), oxidation at -0.45 V , $\bar{n} = 3.20$; (d), further oxidation at -0.30 V ; (e), reduction at -0.75 V ; (f), oxidation at -0.45 V ; and (g), reduction at -0.75 V .

due to the oxidation of niobium(III). Curve e, obtained after all of the niobium had been reduced to niobium(III), shows the same anodic wave (which has a maximum at this concentration) but no other identifiable wave. Subsequent reoxidation at -0.30 V regenerated the first polarogram. Each of these polarograms remained unchanged on allowing the solution to stand for as long as an hour, showing that the reduced niobium species are stable in the absence of air.

A solution containing 1.08 mF niobium(V), whose polarogram is shown in Fig. 3a, was reduced at -0.75 V to an average oxidation number, \bar{n} , of $+2.75$ as indicated by coulometry, and its polarogram, Fig. 3b, was recorded. Oxidation at -0.45 V increased \bar{n} to $+3.20$, and the polarogram in Fig. 3c was obtained. Further oxidation at -0.30 V then regenerated niobium(V), and the polarogram of the resulting solution was identical with Fig. 3a. Further electrolyses gave similar coulometric and polarographic results, as shown in the figure. In addition to the anodic wave of niobium(III) at about -0.38 V, Fig. 3b shows another anodic wave at about the same potential as that due to niobium(IV). It cannot be due to niobium(IV), however, since the average oxidation state of the niobium in this solution was considerably below 3. A plot of $\log [i/(i_a - i)]$ for this wave had the non-linear form characteristic of two closely overlapping waves. It was found previously¹ that the cathodic current at -0.65 V was approximately proportional to the concentration, C_5 , of niobium(V), so that $i_5 = k_5 C_5$. A value of k_5 under the conditions of Fig. 3 was obtained from curve a and employed to calculate C_5 for the solution of curve c. Subtracting this from the total concentration of niobium gave C_3 , the concentration of niobium(III) responsible for the anodic wave at -0.38 V, and permitted the evaluation of k_3 in the equation, $i_3 = k_3 C_3$, for the limiting current of this wave. The values of k_3 and k_5 thus obtained in replicate measurements were in close agreement. The former was used to compute C_3 for the solution of Fig. 3b. Subtraction of the sum of these from the total concentration of niobium gives C_x , the concentration of niobium(x) responsible for the anodic wave at -0.52 V. Conservation of mass and charge require for Fig. 3b

$$C_{\text{Nb}} = C_3 + C_x \quad (3)$$

$$\bar{n}C_{\text{Nb}} = 3C_3 + xC_x \quad (4)$$

where C_{Nb} is the total concentration of niobium and \bar{n} is its average oxidation state as determined by coulometry. An average of all the results gave $x = 2.2 \pm 0.3$, showing that the extra anodic wave is due to niobium(II). Niobium(II) having been identified, the processes occurring during each of these electrolyses could be enumerated in Table 2, where the stoichiometric coefficients are fractions of the total amount of niobium.

Reduction at positive potentials

An 8.1 mF solution of niobium(V) was reduced at potentials on the rising part of the first polarographic wave. Successive reductions at -0.407 and -0.459 V gave linear plots of $\log i$ vs. t , for which $\beta = [-d \ln i/dt]$ was about 10 ksec⁻¹, and reduced the niobium to an average oxidation state, $\bar{n} = 4.75$. Polarograms obtained after each of these reductions resembled Fig. 2b, and showed the presence of niobium(IV) and (V). When, upon subsequent reduction at -0.509 V, the plot of $\log i$ vs. t began to become concave upward, the reduction was stopped, and a polaro-

gram like Fig. 2c was obtained, showing the presence of niobium(III), (IV), and (V). Similar results were obtained with a solution containing 0.93 mF niobium(V), except that \bar{n} could be decreased to +4.20 at -0.529 V before the plot of $\log i$ vs. t became concave upward and the anodic wave of niobium(III) appeared. Figure 4 shows the effects of \bar{n} on the heights of the cathodic and anodic portions of the composite wave of the niobium(V)-(IV) couple at a total niobium concentration of 0.93 mF.

TABLE 2

OVERALL REACTIONS OCCURRING IN ELECTROLYSES OF A 1.08 mF NIOBIUM SOLUTION

Process	$-E_{w.e.}(mV)$	Reaction
Reduction	748	$Nb(+5) \rightarrow 0.80 Nb(+3) + 0.20 Nb(+2)$
Oxidation	451	$0.20 Nb(+2) \rightarrow 0.11 Nb(+5) + 0.09 Nb(+3)$
Oxidation	300	$0.89 Nb(+3) \rightarrow 0.89 Nb(+5)$
Reduction	750	$Nb(+5) \rightarrow 0.78 Nb(+3) + 0.22 Nb(+2)$
Oxidation	452	$0.22 Nb(+2) \rightarrow 0.17 Nb(+5) + 0.05 Nb(+3)$
Reduction	749	$0.17 Nb(+5) \rightarrow 0.05 Nb(+3) + 0.12 Nb(+2)$

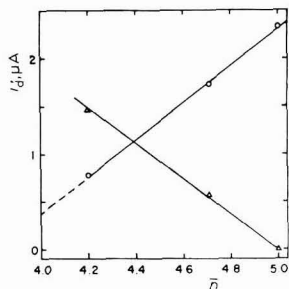


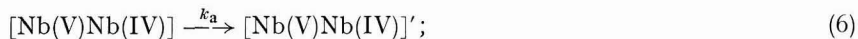
Fig. 4. The effects of the average oxidation number, \bar{n} , on the polarographic diffusion currents of (○), Nb(V); (△), Nb(IV) in mixtures in which the sum of the concns. of Nb(V) and Nb(IV) is 0.93 mF.

Mechanism of reduction

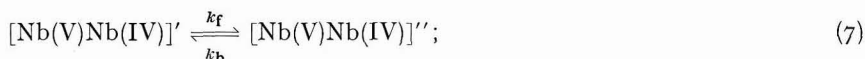
The products of reduction at various potentials having been identified, the data in Table 1 can be explained and reconciled with the polarographic results¹. Consider first the reduction of 8-9 mF niobium(V) at -0.65 V. Since $n_1=0.5$, the first step must be the one-electron mass-transfer-controlled reduction of a dimer:



The product is electrolytically inert and is converted successively to a reducible form and another inert form:



$$0.2 \ll k_a < 360 \text{ sec}^{-1}$$



$$0.01 \ll k_f < 0.2 \text{ sec}^{-1}$$

$$k_b \simeq \beta_2 = 1.7 \cdot 10^{-3} \text{ sec}^{-1}$$

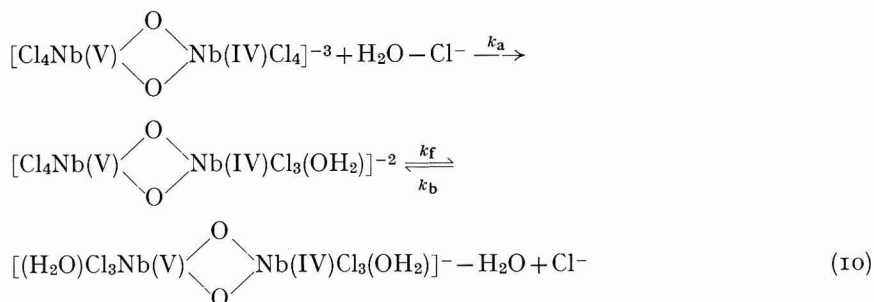
The rate constants are estimated as follows. According to the Nernst diffusion-layer hypothesis the mass-transfer constant, β , is given by

$$\beta = DA/V\delta \tag{8}$$

The mean time, τ , of diffusion across such a layer is approximately¹⁰

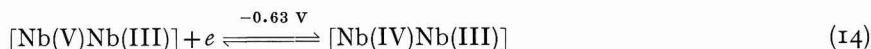
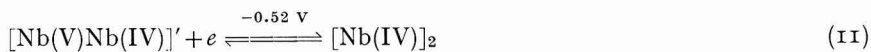
$$\tau = \delta^2/D \tag{9}$$

Polarographic results¹ and the Ilkovič equation, together with measured values of β_1 , A , and V and the above equations, give $D = 4.0 \cdot 10^{-6} \text{ cm}^2 \text{ sec}^{-1}$, $\delta = 1.1 \cdot 10^{-4} \text{ cm}$ and $\tau = 2.8 \cdot 10^{-3} \text{ sec}$. Reaction (6) is complete at the dropping electrode, where the drop life is about 5 sec, and $[\text{Nb(V)Nb(IV)}]'$ is further reduced before it can undergo reaction (7). These considerations establish the lower limit of k_a and the upper one of k_f . At the stirred pool, $[\text{Nb(V)Nb(IV)}]$ is swept into the bulk of the solution in 2.8 msec, so that k_a must be less than $(2.8 \text{ msec})^{-1}$; it undergoes reactions (6) and (7) in much less than the mean residence time, $1/\beta_1$, in the bulk of the solution, so that $k_f \gg \beta_1 = 0.01 \text{ sec}^{-1}$. If $[\text{Nb(V)}]_2$ is a doubly-charged anion as previously suggested¹, reactions (6) and (7) may be



where only the intermediate product can be further reduced.

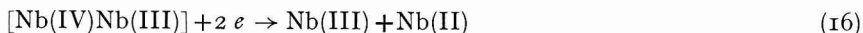
Because the rate constant, β_2 , for the second reduction step is independent of potential, it cannot correspond to an electron-transfer process; because it is much smaller than the mass-transfer constant, β_1 , it cannot correspond to a diffusion-controlled process. It must therefore represent the rate of a chemical reaction such as the reverse of (7) (thus $k_b = \beta_2 = 1.7 \cdot 10^{-3} \text{ sec}^{-1}$), followed by (11)–(14):



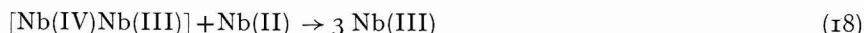
About 80% of the $[\text{Nb(IV)}]_2$ is swept into the bulk of the solution, where it dissociates; the remainder undergoes reactions (13)–(14), so n_2 is about 0.6. In a polarographic

measurement, most of the $[\text{Nb(IV)}]_2$ remains at the surface of the electrode, where its concentration is relatively high; the proportions are approximately reversed, and reactions (5), (6), (11), (13) and (14) produce a first wave for which n is approximately 1.4.

The third and fourth steps of the reduction of 9 mF niobium at -0.65 V are due to reactions (15) and (16), respectively:

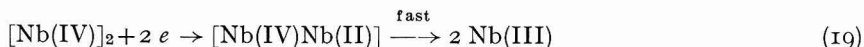


Some of the niobium(II) thus produced is consumed by reacting with niobium(IV):



but some of the niobium(II) escapes these reactions, with the result that the overall value of n is appreciably above 2.

At -0.71 V, reaction (15), whose rate is potential-dependent, becomes faster than the reverse of reaction (7), and the second and third reduction steps merge. At -0.76 V the fourth step, reaction (16), is so fast that it too merges with the second step. In addition, an appreciable fraction of the $[\text{Nb(IV)}]_2$ is reduced directly, bypassing reactions (12)–(18):



Because of reaction (19), very little monomeric Nb(II) is produced and n_T approaches 2.00. At the dropping electrode, reactions (5), (6), (11) and (19) yield an n -value of 2.0 for the combined waves.

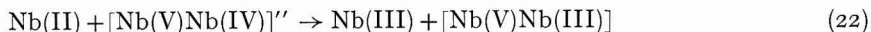
Both monomers and dimers are present in 0.9 mF solutions of niobium(V), and the first step in their controlled-potential reduction at -0.65 V is due to reactions (5) and (20):



The experimental value, $n_1 = 0.83$, indicates that about 66% of the niobium(V) atoms are monomeric. The second step is due to reactions (7) and (11)–(14) and the third step to reactions (15), (17) and (18). A fourth step, due to reactions (16)–(18), could not be detected by the graphical dissection procedure at this low concentration, but its presence lowered the apparent slope of the third segment of the log (current)–time plot sufficiently to make n_3 somewhat lower, and n_2 somewhat higher, than is predicted by the above scheme.

The reduction of 0.9 mF niobium(V) at -0.75 V proceeds in the first step according to reactions (5) and (20), as before. The rate of the third step indicates that it must be due to reactions (7), (11) and (19). At this low concentration and negative potential, unlike all the other cases, monomeric niobium(IV) can be reduced before $[\text{Nb(V)Nb(IV)}]$, and the second step is due to reactions (15), (17), (21) and (22).





It is shown in Appendix 2 that reactions (15) and (17) constitute a catalytic scheme for which a plot of $\log i$ vs. t will be concave downward, and that graphical dissection of such a plot will over-estimate the value of n . In the present case, the reactant is also regenerated by reactions (21) and (22). This increases the downward curvature of the $\log i$ - t plot and makes the over-estimate of n_2 worse, and consequently leads to erroneously low values for n_1 . A similar effect is probably responsible for the fact that n_1 is a little below 0.5 for the reduction of 9 mF niobium(V) at -0.75 V.

In the experiments described above, when niobium(V) solutions were reduced at increasingly negative potentials on the rising part of the first polarographic wave, only reactions (5)–(7) and (20) occurred at the more positive potentials. Linear plots of $\log i$ vs. t and polarograms like Fig. 2b resulted, and only niobium(IV) was produced. At more negative potentials, reactions (11)–(14) occurred, plots of $\log i$ vs. t were concave upward, and the presence of niobium(III) was indicated by its anodic wave in polarograms like Fig. 2c. More dilute niobium(V) solutions, in which monomers predominated, could be reduced further without producing niobium(III), owing to the occurrence of reaction (20) simultaneously with reaction (5). In Fig. 4 the height of the first wave of niobium(V) is extrapolated to $\bar{n}=4$. The intercept is positive, showing that $[\text{Nb(V)Nb(IV)}]$, which had not been reduced electrolytically at positive potentials, could be reduced at the dropping electrode at -0.65 V to an average oxidation number below 4 by reactions (6), (11), (13) and (14).

One solution containing 0.93 mF niobium(V) was carefully reduced at positive potentials until it contained about 80% niobium(IV) and about 10% each of niobium(V) and (III). It was then reduced completely at -0.75 V to 24% niobium(II)–76% niobium(III). The principal reactions were (15) and (17), and the initial conditions for the kinetic scheme discussed in Appendix 2 were approximately satisfied. In the notation used there, $[A]^0$ was $0.74 \cdot 10^{-3}$ F, R was 0.24, and β' was $2.8 \cdot 10^{-3}$ sec⁻¹. These values yield $\beta \cong 1.5 \cdot 10^{-3}$ sec⁻¹ at -0.750 V for reaction (15), and $k_2 \cong 7.6$ l mole⁻¹ sec⁻¹ for reaction (17).

In the succession of electrolyses described in Table 2 and Fig. 3, the mechanism of the first two reductions at -0.75 V was given above. The oxidations at -0.45 V involved reactions (23) and (20)



accompanied by reactions (17) and (21). The complexity of this mechanism undoubtedly accounts for the shape of the niobium(II) polarographic wave mentioned above. The oxidation at -0.30 V was due simply to



Since the last reduction in Table 2 was begun with only one-sixth of the niobium in the +5 state, the second-order reactions (17) and (21) were much slower, and relatively more niobium(II) and less niobium(III) were produced.

CONCLUSIONS

The electrochemical behavior of niobium in 10.75 F hydrochloric acid can

be explained by assuming the existence of several dimeric species, whose niobium atoms are joined by two oxygen bridges¹, and probably by an intermetallic bond such as has been inferred in solid NbI₄^{14,15}. Dimers containing niobium in the same oxidation state, [Nb(V)]₂ and [Nb(IV)]₂, can dissociate reversibly, and more or less rapidly, to give the respective monomers. Dimers whose niobium atoms differ in oxidation state by one, [Nb(V)Nb(IV)] and [Nb(IV)Nb(III)], dissociate much more slowly and the odd electron may be shared by the metal atoms. [Nb(V)Nb(III)] is probably equally stable. The intermetallic bond in [Nb(IV)]₂ and [Nb(IV)Nb(II)] permits these to disproportionate rapidly, while the corresponding second-order reactions between monomers are much slower. VIVARELLI's⁶⁻⁸ solutions apparently contained monomeric fluoroniobium complexes^{1,16}, which underwent bimolecular disproportionation and oxidation by protons much more readily than the chloro-complexes studied here.

SUMMARY

The electroreduction of niobium(V) in concentrated solutions of hydrochloric acid was studied by stirred-pool controlled-potential chronoamperometry and coulometry. In dilute solutions, niobium(V) is monomeric and is reduced stepwise to niobium(IV) and niobium(II), which react to form niobium(III). In more concentrated (10 mF) solutions, niobium(V) is dimeric, and is initially reduced to [Nb(V)Nb(IV)], which can exist in three hydrolytic forms. Only one of these forms is further reduced to [Nb(IV)]₂. The latter may dissociate or disproportionate to form [Nb(V)Nb(III)], which can be reduced to [Nb(IV)Nb(III)] and, at more negative potentials, to Nb(III) and Nb(II). At very negative potentials, [Nb(IV)]₂ is reduced to [Nb(IV)Nb(II)], which decomposes rapidly to form two Nb(III) ions. Niobium(II) can be oxidized to a mixture of niobium(III) and (V), while niobium(III) is oxidized entirely to niobium(V). The dimeric species are probably joined by two oxygen bridges and an intermetallic bond. The latter permits the rapid disproportionation of [Nb(IV)]₂ and [Nb(IV)Nb(II)], and may stabilize [Nb(V)Nb(IV)], [Nb(V)Nb(III)] and [Nb(IV)Nb(III)] against dissociation.

APPENDIX I

Disproportionation of the product of controlled-potential electrolysis

If a solution of A is reduced to B, and B disproportionates:



then the differential equations and initial conditions for the concentrations are:

$$d[A]/dt = -\beta[A] + k[B]^2; \quad [A]_{t=0} = [A]^0 \quad (27)$$

$$d[B]/dt = \beta[A] - 2k[B]^2; \quad [B]_{t=0} = 0 \quad (28)$$

At some stage of the reduction, the second-order chemical reaction (26) will become much slower than the first-order electrochemical reaction (25); *i.e.*,

$$k[B] \ll \beta, t \rightarrow \infty \quad (29)$$

$$[B] \gg [A], t \rightarrow \infty \quad (30)$$

and A will be reduced electrochemically almost as fast as it is produced chemically. That is, after a certain time,

$$d[A]/dt \approx 0 \quad (31)$$

Equations (27), (28) and (31) can be combined to yield

$$d[B]/dt = -k[B]^2 \quad (32)$$

whose solution is

$$[B]^{-1} = kt + a \quad (33)$$

where a is a constant. Now the current, i , (in, say, F/sec) is given by⁹

$$i = n\beta V[A] \quad (34)$$

Combining eqns. (27), (31), (33) and (34) yields:

$$i^{-1/2} = (k/nV)^{1/2}t + a(nVk)^{-1/2} \quad (35)$$

which can be differentiated to give

$$d \ln i / dt = -2k/(kt + a) \quad (36)$$

For such a scheme, a plot of $\log i$ vs. t will be concave upward, but a plot of $i^{-1/2}$ vs. t will approach a straight line of slope, $(k/nV)^{1/2}$.

APPENDIX 2

Chemical reaction of reactant and product of the electrochemical process

Consider the scheme:



with the differential equations and initial conditions:

$$d[A]/dt = -\beta[A] - k[A][B]; \quad [A]_{t=0} = [A]^0 \quad (39)$$

$$d[B]/dt = \beta[A] - k[A][B]; \quad [B]_{t=0} = 0 \quad (40)$$

In terms of the dimensionless variables

$$x = [A]k/\beta, \quad x^0 = [A]^0k/\beta, \quad y = [B]k/\beta, \quad y^\infty = [B]^\infty k/\beta \quad (41)$$

where the superscript, ∞ , denotes a final value, GESKE AND BARD¹¹ have shown that

$$x = y + x^0 + 2 \ln(1 - y) \quad (42)$$

$$0 = y^\infty + x^0 + 2 \ln(1 - y^\infty) \quad (43)$$

Define R as the relative yield of B:

$$R \equiv [B]^\infty/[A]^0 = y^\infty/x^0 \quad (44)$$

Figure 5 shows how R and y are affected by variations of x^0 .

In order for eqn. (42) to be real, $(1-y)$ must be positive. This implies, through eqns. (40) and (41), that $[B]$ increases continually throughout the electrolysis:

$$d[B]/dt > 0 \quad (45)$$

Figure 5 shows that as x^0 is increased, the relative yield of B falls to zero, but the absolute yield, $[B]^\infty$, increases to a limit of β/k . Thus high values of $[A]^0$ and β favor a high absolute yield of B, while a low value of $[A]^0$ and a high one of β favor a high relative yield of B.

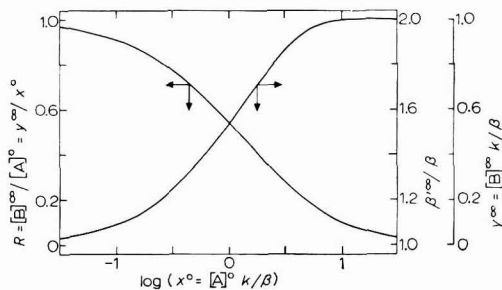


Fig. 5. The effects of x^0 on y^∞ , R , and β'^∞/β , according to eqns. (43), (44) and (47).

The electrolysis current will be given by eqn. (34). The actual slope, β' , of the plot of $\ln i$ vs. t is defined by

$$\beta' = -d \ln i / dt \quad (46)$$

The above equations can be combined to show that

$$\beta = \lim_{t \rightarrow 0} \beta' \leq \beta' = \beta(1+y) \leq \lim_{t \rightarrow \infty} \beta' \equiv \beta'^\infty = \beta(1+y^\infty) \leq 2\beta \quad (47)$$

That is, β' will increase with time from β to $\beta'^\infty \leq 2\beta$; the plot of $\ln i$ vs. t will be concave downward. Figure 5 shows how β'^∞ depends on x^0 . Plots of $\log i$ vs. t calculated numerically by GESKE AND BARD confirm these results and show that β' approaches β'^∞ very rapidly; the curvature is barely noticeable if x^0 is either very small or very large. It would be very difficult to estimate the initial slope β of such a plot in order to calculate k . In one application of these ideas, GESKE¹² estimated β by an independent method, but this is unnecessary. The experimentally measured value of R may be combined with the plot of Fig. 5 to yield values of x^0 ($= [A]^0 k / \beta$) and β'^∞ / β and values of both β and k are easily obtained on combining the latter with experimental values of β'^∞ and $[A]^0$.

If processes (37) and (38) are intermediate in some more extensive sequence of steps, as is true in some of the cases described above, the current integral will be estimated from a plot of $\log i$ vs. t as:

$$Q' = i'0 / \beta'^\infty \quad (48)$$

where $i'0$ is the extrapolated intercept of the final portion of the curve, whose slope is β'^∞ . It is easily shown, however, that the true current integral is

$$Q = nV[A]^0 \left(\frac{1}{2} + \frac{1}{2}R \right) \quad (49)$$

so that

$$Q'/Q = (i'^0/i^0)(\beta/\beta'^\infty) \{2/(1+R)\} \quad (50)$$

Numerical integration of eqns. (39) and (40) for $x^0 = 10, 1,$ and 0.1 , gave $Q'/Q = 1.06, 1.14,$ and 1.08 , respectively. Thus, Q would be appreciably over-estimated by the graphical dissection procedure.

This derivation implicitly assumes that reaction (38) occurs in the bulk of the solution, and hardly at all in the diffusion layer. KARP¹³ has shown that when the characteristic time for such a reaction, t_1 , is much greater than the average time required for an ion or molecule to cross the diffusion layer [cf. eqn. (9)] this assumption is valid; otherwise the treatment must fail. It was shown above that τ was about 3 msec. Taking t_1 as $1/k[A]^0$, the requirement is

$$(k[A]^0)^{-1} = (\beta x^0)^{-1} \gg 3 \cdot 10^{-3} \text{ sec.} \quad (51)$$

Here β was about 10^{-2} sec^{-1} , so

$$x^0 = [A]^0 k / \beta \ll 3 \cdot 10^4 \quad (52)$$

Inserting this value in eqns. (42) and (43) yields:

$$R = [B]^\infty / [A]^0 \gg 10^{-6} \quad (53)$$

The above treatment can therefore be safely relied on whenever the formation of B can be detected coulometrically.

REFERENCES

- 1 J. G. McCULLOUGH AND L. MEITES, *J. Electroanal. Chem.*, 18 (1968) 123.
- 2 Y. ISRAEL AND L. MEITES, *J. Electroanal. Chem.*, 8 (1964) 99.
- 3 Y. ISRAEL, Ph.D. Thesis, Polytechnic Institute of Brooklyn, 1964.
- 4 L. MEITES, *Anal. Chem.*, 27 (1955) 1116.
- 5 H. K. FICKER AND L. MEITES, *Anal. Chim. Acta*, 26 (1962) 172.
- 6 D. COZZI AND S. VIVARELLI, *Ric. Sci.*, 23 (1953) 2244.
- 7 D. COZZI AND S. VIVARELLI, *Z. Elektrochem.*, 58 (1954) 177.
- 8 D. COZZI, S. VIVARELLI AND M. DI STEFANO, *Z. Electrochem.*, 61 (1957) 849.
- 9 L. MEITES, *Record Chem. Progr. Kresge-Hoover Sci. Lib.*, 22 (1961) 81.
- 10 W. J. MOORE, *Physical Chemistry*, Prentice-Hall, Englewood Cliffs, N.J., 2nd ed., 1955, p. 449.
- 11 D. H. GESKE AND A. J. BARD, *J. Phys. Chem.*, 63 (1959) 1057.
- 12 D. H. GESKE, *J. Phys. Chem.*, 63 (1959) 1062.
- 13 S. KARP, Ph.D. Thesis, Polytechnic Institute of Brooklyn, 1967.
- 14 D. C. BRADLEY, *Inorganic Polymers*, edited by F. G. A. STONE AND W. A. G. GRAHAM, Academic Press, New York, 1962, pp. 413-416.
- 15 B. P. BLOCK, *Inorganic Polymers*, edited by F. G. A. STONE AND W. A. G. GRAHAM, Academic Press, New York, 1962, pp. 463, 471.
- 16 K. A. KRAUS AND G. E. MOORE, *J. Am. Chem. Soc.*, 73 (1951) 9.

THE DETERMINATION OF TRACES OF NICKEL IN COBALT BY PULSE POLAROGRAPHY

A. LAGROU AND F. VERBEEK

Laboratory for Analytical Chemistry, University of Ghent (Belgium)

(Received March 4th, 1968)

Purity control of cobalt implies first the determination of its main impurity element, nickel. Traces of nickel are often determined photometrically¹⁻⁷, usually with dimethylglyoxime as colorimetric reagent. The detection limit of about 10 p.p.m. is sometimes too high for the analysis of very pure cobalt compounds. Spectral analysis⁸⁻¹³, which is also frequently used, has a similar sensitivity. On the other hand, several authors¹⁴⁻¹⁸ have described various supporting electrolytes that allow the direct polarographic determination of nickel without separation. LINGANE AND KERLINGER¹⁶ determined down to 0.01% nickel in cobalt and steel samples by classical polarography using a pyridine-pyridinium chloride buffer solution (pH 5.5). DOLEŽAL AND HOFMANN¹⁴ detected as little as 0.005% nickel in a mixture of ethylenediamine tartrate and potassium pyrophosphate. After removal of the bulk of cobalt by precipitating with 1-nitroso-2 naphthol, DYATLOVA AND LAVROVA¹⁵ determined the nickel remaining, down to 10⁻⁴%. Recently, JACKWERTH AND HÖBEL¹⁸ used a differential cathode-ray polarograph to determine approximately 10⁻⁴% nickel in a pyridine-thiocyanate solution. Cathode-ray polarography was also applied by GOTO AND TUKUSHI¹⁹ to the determination of about 0.01% nickel in an ammonia-ammonium chloride buffer.

The present investigation deals with the determination of traces of nickel in cobalt by pulse polarography in pyridine and thiocyanate, respectively. The nickel content of analytical-grade cobalt samples varies from $\pm 1-100$ p.p.m.; without a prior separation procedure, this concentration range is beyond the reach of classical polarography.

EXPERIMENTAL

1. *Apparatus and reagents*

Pulse polarograph, Southern type A 1700 Mark II. The possibilities, measurement of peak heights, and working conditions of this instrument were described in previous papers^{20,21}.

Very pure potassium thiocyanate was prepared by a 24-h electrolysis of a 10 M solution in water at a cathode potential of -1.5 V vs. a saturated calomel electrode (SCE); the electrolysis was carried out in separate electrode compartments under a nitrogen atmosphere.

Analytical-grade pyridine was redistilled.

Water and all other analytical-grade reagents were purified as previously described^{20,21}.

2. Polarographic data

(a) *Pyridine*. The half-wave potentials of the reduction of nickel (II) and cobalt (II) are, respectively, -0.82 and -1.11 V vs. SCE. The first experiments were performed in a 0.25 M pyridine – 0.25 M pyridinium chloride buffer (pH 5.5). In this medium it was possible to determine about 10^{-5} M nickel in a 0.1 M cobalt solution without recording a blank polarogram. However, the reduction peak of a 10^{-6} M nickel solution was situated completely in the slope of the rising base-line. This unfavourable position is probably due to the presence of trace organic compounds in pyridine, which are reduced at the dropping mercury electrode and the reduction wave of which is situated between the nickel and cobalt peaks. On raising the pH, the peak height of this interfering wave gradually decreased, and the wave disappeared completely at pH 8–9. Consequently, low nickel concentrations ($< 5 \cdot 10^{-6}$ M) were determined in pyridine without the addition of hydrochloric acid, the cobalt compound acting as supporting electrolyte. The sensitivity of detection of nickel in 0.25 M pyridine – 0.1 M potassium chloride medium is about $2 \cdot 10^{-8}$ M, corresponding with a peak height of ± 11 mm at maximum sensitivity of the polarograph (drop time 4 sec, 1 V/60 min).

Investigations of the most suitable pyridine concentration showed that a two-fold excess with regard to cobalt was sufficient. Higher concentrations did not interfere, at least not up to a certain limit; high pyridine concentrations (≥ 1 M) decreased the sensitivity, and the nickel peak became asymmetrical. Finally, determinations were usually performed in 0.25 M pyridine – 0.1 M cobalt (as chloride, sulphate, nitrate etc.). In this medium it was possible to determine nickel in the presence of excess cobalt up to a molar concentration ratio, $\text{Co/Ni} = 10^6$ (i.e., 10^{-7} M nickel in 0.1 M cobalt, or about five times the detection limit in the absence of cobalt). This corresponds with a detection limit of 1 p.p.m. nickel in metallic cobalt and approximately 0.2 p.p.m. nickel in cobalt compounds such as $\text{Co}(\text{NO}_3)_2 \cdot 6 \text{H}_2\text{O}$, $\text{CoCl}_2 \cdot 6 \text{H}_2\text{O}$ and others. For unfavourable Co/Ni ratios ($\geq 10^5$, or less than ten times the detection limit) the exact peak height was determined by recording a blank polarogram of a cobalt solution freed from nickel by separation on an anion exchange column^{22,23}. The linearity between peak height and nickel concentration for the analysis of various cobalt compounds (chloride, sulphate, nitrate) was verified by a calibration graph which was linear in the range 10^{-4} – 10^{-7} M nickel. The stability of the solution (pH 8–9) and eventual sorption or precipitation of nickel was checked by regularly recording pulse polarograms of the same solution, which proved that even after 24 h the nickel concentration remained unchanged.

A typical derivative pulse polarogram of traces of nickel present in analytical-grade $\text{Co}(\text{NO}_3)_2 \cdot 6 \text{H}_2\text{O}$, recorded in pyridine medium, is given in Fig. 1. Although the polarogram is recorded using the mercury pool as the reference electrode, the potentials in Fig. 1 are given versus SCE.

(b) *Potassium thiocyanate*. In comparison with pyridine, potassium thiocyanate has some advantages as supporting electrolyte. The half-wave potentials of nickel and cobalt, -0.70 and -1.03 V respectively vs. SCE, differ by 0.33 V when using a tenfold excess of thiocyanate with respect to the cobalt concentration (≥ 0.1 M). A larger

excess gives practically no improvement; neither does the use of thiocyanate-acetate mixtures²⁴. The sensitivity is increased by more than 50%; the peak heights for a $2 \cdot 10^{-8}$ M nickel solution in 0.1 M cobalt-1 M potassium thiocyanate and 0.4 M cobalt-6 M potassium thiocyanate are about 16 and 13 mm respectively at maximum sensitivity of the apparatus, in comparison with 10 and 6 mm in 0.1 M cobalt-0.25 M pyridine and 0.4 M cobalt-1 M pyridine. This means that the sensitivity is increased fourfold *i.e.*, 0.25 p.p.m. in metallic cobalt and nearly 0.06 p.p.m. in cobalt compounds.

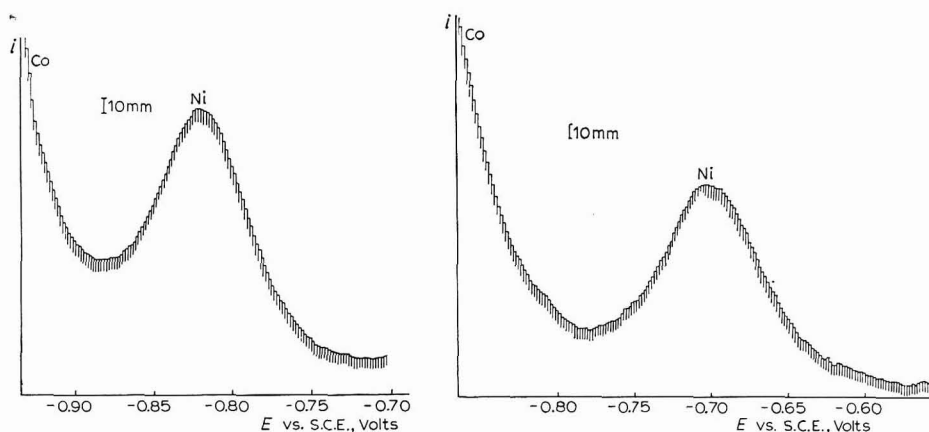


Fig. 1. Pulse polarogram of $1.83 \cdot 10^{-6}$ M Ni and 10^{-1} M Co in 0.25 M pyridine, representing 3.69 p.p.m. Ni in $\text{Co}(\text{NO}_3)_2 \cdot 6 \text{H}_2\text{O}$ (sample 1). Conditions: S 1/5, 35 mV, 3 int., 60 min/V, rec. 1 in./min.

Fig. 2. Pulse polarogram of $3.70 \cdot 10^{-6}$ M Ni and 10^{-1} M Co in 1 M KSCN, representing 7.47 p.p.m. Ni in $\text{Co}(\text{NO}_3)_2 \cdot 6 \text{H}_2\text{O}$ (sample 3). Conditions: S 1/20, 35 mV, 3 int., 60 min/V, rec. 1 in./min.

Nevertheless, some disadvantages have to be considered. In 1 M potassium thiocyanate, cadmium can interfere as its half-wave potential is -0.665 V *vs.* SCE, a difference of only 35 mV from that of nickel. The interference from cadmium is negligible for a molar concentration ratio, $\text{Ni}/\text{Cd} \geq 1$. This is always the case in commercially available cobalt samples. In 1 M potassium thiocyanate there is no interference from copper, as the half-wave potentials of nickel and copper differ by 150 mV. However, in 6 M potassium thiocyanate, both cadmium and copper interfere; for exact nickel determinations the molar concentration ratio, $\text{Ni}/(\text{Cu} + \text{Cd})$, must be higher than 30/1. Although such a concentration ratio is often found in commercially available cobalt samples, it is more convenient to perform the analysis in 1 M potassium thiocyanate. Because of these interferences and as potassium thiocyanate may contain traces of nickel, this electrolyte must be purified before use. No detectable amounts of nickel were found in analytical-grade pyridine and it is therefore preferred for the determination of more than a few p.p.m. of nickel.

A typical derivative pulse polarogram of nickel in the presence of excess cobalt, recorded in thiocyanate medium, is shown in Fig. 2.

3 Procedure

Prepare a 0.1 M (0.4 M) cobalt solution by dissolving the cobalt salt in the minimum quantity of twice-distilled water. Add 0.5 ml (2 ml) pyridine or 2.5 ml (15 ml)

10 *M* potassium thiocyanate and dilute to 25 ml. Record a pulse polarogram and determine nickel by the standard-addition method.

When analysing metallic cobalt, dissolve the sample in concentrated hydrochloric acid with the addition of a few drops of hydrogen peroxide or nitric acid, evaporate to dryness and treat the residue as described above.

The analyses were usually performed in 0.1 *M* cobalt solutions. For very low nickel contents (< 1 p.p.m.) it is preferable to use more concentrated solutions. The limiting concentration ratio, Ni/Co, remains the same (10^6), but more concentrated solutions permit the polarogram to be recorded at a lower sensitivity of the apparatus thus giving increased stability.

TABLE 1
DETERMINATION OF NICKEL IN COBALT (0.1 *M* CO IN 0.25 *M* PYRIDINE)

<i>Ni added</i>		<i>Ni found</i>	
(<i>M</i> · 10 ⁶)	<i>Ni in Co</i> <i>p.p.m.</i>	(<i>M</i> · 10 ⁶)	<i>Ni in Co</i> <i>p.p.m.</i>
0.25	2.49	0.262	2.61
0.50	4.98	0.488	4.86
1.0	9.96	1.03	10.3
2.5	24.9	2.45	24.4
5.0	49.8	4.95	49.3
10	99.6	10.1	100.6

TABLE 2
DETERMINATION OF NICKEL IN COMMERCIALY AVAILABLE COBALT SAMPLES (ANALYTICAL GRADE)

<i>Product</i>	<i>Co concn.</i> (<i>mole/l</i>)	<i>C₅H₅N or KSCN concn.</i>	<i>Ni</i> (<i>p.p.m.</i>)
Co(NO ₃) ₂ · 6 H ₂ O	0.1	0.25 <i>M</i> pyridine	3.69
	c.8	1.2 <i>M</i> pyridine	3.62
Co(NO ₃) ₂ · 6 H ₂ O	0.1	0.25 <i>M</i> pyridine	4.93
	0.1	0.25 <i>M</i> pyridine	7.65
Co(NO ₃) ₂ · 6 H ₂ O	0.4	1 <i>M</i> pyridine	7.51
	0.1	1 <i>M</i> KSCN	7.47
	0.1	6 <i>M</i> KSCN	7.44
	0.4	6 <i>M</i> KSCN	7.78
	0.1	0.25 <i>M</i> pyridine— 0.25 <i>M</i> pyridinium chloride	62.3
CoCl ₂ · 6 H ₂ O	0.1	0.25 <i>M</i> pyridine	13.2
CoCl ₂ · 6 H ₂ O	0.1	0.25 <i>M</i> pyridine— 0.25 <i>M</i> pyridinium chloride	79.6
		1 <i>M</i> pyridine	23.5
CoCl ₂ · 6 H ₂ O	0.4	6 <i>M</i> KSCN	23.0
	0.1	0.25 <i>M</i> pyridine	16.6
CoCl ₂ · 6 H ₂ O	0.1	0.25 <i>M</i> pyridine	16.8
	0.2	0.50 <i>M</i> pyridine	16.3
	0.4	0.8 <i>M</i> pyridine	16.4
	0.1	0.25 <i>M</i> pyridine — 0.25 <i>M</i> pyridinium chloride	48.3
CoAc ₂ · 4 H ₂ O ^a	0.05	0.25 <i>M</i> pyridine — 0.25 <i>M</i> pyridinium chloride	810
Co metal ^a	0.04	0.25 <i>M</i> pyridine — 0.25 <i>M</i> pyridinium chloride	1400

^a pure

RESULTS

A number of analyses was performed on synthetic samples prepared by adding a known quantity of a standardised nickel solution to a cobalt solution freed from nickel on an anionic resin. The results are summarised in Table 1.

In order to check the practical efficiency, the method was also applied to the analysis of various commercially available cobalt samples. Every analysis was duplicated at least, and gave reproducible results within 5%. The results are shown in Table 2. This Table shows that in all the samples analysed, the nickel content is well above the detection limit of the pulse polarographic technique. Also, determinations of nickel carried out in potassium thiocyanate, in pyridine, and at different cobalt concentrations, are in good agreement.

SUMMARY

A pulse polarographic method is described for determining traces of nickel in cobalt, and its compounds, without separation. The detection limit in pyridine is as low as 1 p.p.m. in metallic cobalt, and 0.25 p.p.m. in cobalt compounds, while in potassium thiocyanate these limits are decreased to 0.25 and 0.06 p.p.m., respectively. The method was applied to the analysis of synthetic and commercially available cobalt samples and showed satisfactory sensitivity at various nickel levels.

REFERENCES

- 1 G. DENIGES, *Bull. Soc. Pharm. Bordeaux*, 70 (1932) 106.
- 2 V. M. PESHKOVA, *Zavodsk. Lab.*, 8 (1939) 921; *Chem. Abstr.*, 34 (1940) 1587.
- 3 M. PONTET, *Chim. Anal. Paris*, 37 (1955) 338.
- 4 H. GOTO AND C. OTAKA, *Nippon Kinzoku Gakkai Shi*, 14B No. 4 (1950) 61; *Chem. Abstr.*, 46 (1952) 7468d.
- 5 W. NIELSCH, *Z. Metallk.*, 50 (1959) 234.
- 6 L. D. BRAKI, W. M. MCNABB AND J. F. HAZEL, *Anal. Chim. Acta*, 19 (1958) 39.
- 7 M. STEFFEK, *Chem. Listy*, 57 (1963) 972.
- 8 O. CH. VELICHKO, *Zavodsk. Lab.*, 22 (1956) 1307; *Chem. Abstr.*, 51 (1957) 11170h.
- 9 V. L. GINZBURG, I. N. GRAMENITSKII, S. S. KASHLINSKAYA AND D. M. LIVSHITS, *Izv. Akad. Nauk SSSR, Ser. Fiz.*, 19 (1955) 211; *Chem. Abstr.*, 50 (1956) 3891h.
- 10 C. L. BRIDGER AND G. W. MARKS, *U.S. Bur. Mines, Rep. Invest.*, 4198 (1948) 7.
- 11 S. M. CHERBONOV AND D. M. SHVARTS, *Zavodsk. Lab.*, 16 (1950) 1505; *Chem. Abstr.*, 45 (1951) 10128b.
- 12 J. H. MCCLURE AND R. E. KITSON, *Anal. Chem.*, 25 (1953) 867.
- 13 G. YA. FATEEVA, *Zavodsk. Lab.*, 24 (1958) 461; *Chem. Abstr.*, 54 (1960) 11344i.
- 14 J. DOLEŽAL AND P. HOFMANN, *Chem. Listy*, 48 (1954) 1329, 1610; *Chem. Abstr.*, 49 (1955) 4439.
- 15 N. M. DYATLOVA AND O. YU. LAVROVA, *Vestn. Tekhn. i Ekon. Inform. Vlin. Khim. Prom. SSSR*, 8 (1964) 26; *Anal. Abstr.*, 13 (1966) 3577.
- 16 J. J. LINGANE AND H. KERLINGER, *Ind. Eng. Chem. Anal. Ed.*, 13 (1941) 77.
- 17 P. R. STOUT AND J. LEVY, *Collection Czech. Chem. Commun.*, 10 (1938) 136.
- 18 E. JACKWERTH AND H. HÖBEL, *Z. Anal. Chem.*, 213 (1965) 81.
- 19 H. GOTO AND N. TUKUSHI, *Japan Analyst*, 15 (1966) 114.
- 20 E. TEMMERMAN AND F. VERBEEK, *J. Electroanal. Chem.*, 12 (1966) 158.
- 21 A. LAGROU, J. VANHEES AND F. VERBEEK, *Z. Anal. Chem.*, 224 (1967) 310.
- 22 G. E. MOORE AND K. A. KRAUS, *J. Am. Chem. Soc.*, 72 (1950) 5792; 74 (1952) 843; 75 (1953) 1460.
- 23 K. A. KRAUS AND F. NELSON, *Symposium on Ion-Exchange and Chromatography in Analytical Chemistry*, 1956, *Am. Soc. Testing Mater. Spec. Tech. Publ.*, 195 (1958).
- 24 Y. MIURA, *Japan Analyst*, 8 (1959) 5.

COMPARATIVE OXIDATION OF CHEMISORBED CARBON MONOXIDE, REDUCED CARBON DIOXIDE AND SPECIES FORMED DURING THE METHANOL OXIDATION

M. W. BREITER

General Electric Research and Development Center, Schenectady, N.Y. (U.S.A.)

(Received January 19th, 1968)

INTRODUCTION

The properties of chemisorbed carbonaceous species that are produced during the anodic oxidation of organic fuels or by the interaction at open circuit may be studied¹⁻¹¹ conveniently on electrodes of large real surface. After forming the species, the net composition of which is designated by $C_sH_pO_q$, the bulk concentration of liquid or gaseous fuels is reduced to an acceptable level by appropriate washing or stirring procedures. Then anodic or cathodic charging curves are taken. Anodic charging curves on platinized platinum display arrests due to the oxidation of the chemisorbed species at potentials where the coverage of the surface with OH_{ad} and O_{ad} is small in acidic electrolytes. Similar arrests are obtained during the oxidation of CO_{ad} ^{3,9,11} and the so-called¹² reduced carbon dioxide, $(CO_2)_r$. The latter species result¹¹⁻¹⁷ from the interaction of CO_2 with platinum at open circuit or at constant potential.

The charging curves for the oxidation of equivalent amounts of $C_sH_pO_q$, CO_{ad} , or $(CO_2)_r$, at the same current and electrode, have a similar shape⁹⁻¹¹. The oxidation arrests do not appear at sufficiently different potentials to allow a distinction between the species on this basis at room temperature. The experimental determination of the average number of electrons required for the production of one CO_2 molecule during the oxidation of $C_sH_pO_q$, CO_{ad} , or $(CO_2)_r$ yields⁹⁻¹¹ similar values (≈ 2) in acidic solutions. A value of 2 was reported¹⁵ for the oxidation of $(CO_2)_r$ in alkaline solutions. A differentiation between species with the same oxidation state is not possible in this way either.

New experimental results that allow $C_sH_pO_q$, CO_{ad} , and $(CO_2)_r$ to be classified are described in this communication. The method is based on studies of the temperature-dependence of the oxidation of the chemisorbed species on the same platinized platinum electrode between 1° and 60° in 0.5 M H_2SO_4 .

EXPERIMENTAL

The experiments were carried out in a Pyrex vessel of conventional design on the same platinized cylinder with a geometric surface of 50 cm². The test electrode was aged so that the charge, sQ_H , for the oxidation of a monolayer of H atoms in the absence of organic species did not decrease during the experiments, because of

sintering effects, by more than 5%. The average value of sQ_H was 70 mC/cm². The temperature was maintained within $\pm 1^\circ$ by water from a precision low-temperature bath, flowing through a jacket around the vessel. Measurements were made at 1°, 10°, 20°, 30°, 40°, 50° and 60°. The electrode potential, U , was measured and is subsequently given *versus* a hydrogen electrode in the same electrolyte and at the same temperature as the test electrode. The electrolytic solutions were prepared from reagent-grade chemicals and doubly-distilled water. The electrolyte was stirred with purified helium at 0.5 cm³/sec.

An anodic charging curve was taken with a current, $I = 50$ mA, at the beginning of every series of runs in fresh electrolytic solution to verify the absence of organic fuel in the electrolyte and chemisorbed species on the surface. The electrode was brought back to 0.10 V by a cathodic current of 50 mA. Then the chemisorbed species were formed at the same temperature, T , at which they were oxidized subsequently. The layer of $C_sH_pO_q$ was produced by adding methanol at 0.10 V and maintaining an anodic current of 50 mA for 2000 sec in 0.1 M CH₃OH + 0.5 M H₂SO₄.

The potential-time curve has a shape similar to that of curve 2 in Fig. 6 of ref. 6. There is an arrest between about 0.15 and 0.25 V. After the arrest, the potential increases at first rapidly, and then more slowly, towards the steady-state value. The arrest is longer than the hydrogen branch in 0.5 M H₂SO₄. It results from the removal of H atoms and the oxidation of CH₃OH on a surface partially free of $C_sH_pO_q$. In contrast, the steady-state oxidation of CH₃OH occurs on a surface largely covered with $C_sH_pO_q$.

The electrode potential was adjusted to 0.05 V before replacing the electrolyte five times by fresh sulfuric acid solution freed from molecular oxygen by extensive stirring with purified helium. The washing procedure had proved adequate in previous work^{10,11}. The layer of CO_{ad} was formed by starting the stirring with carbon monoxide (about 1 cm³/sec) at 0.1 V and letting carbon monoxide interact with the test electrode for 2000 sec at open circuit. Stirring with helium for 2000 sec served to remove the carbon monoxide from the electrolyte. The carbon monoxide was research-grade, Matheson. Reduced carbon dioxide was produced by starting the stirring with carbon dioxide (about 1 cm³/sec) at 0.1 V and letting carbon dioxide react with the platinum cylinder for 2000 sec at open circuit. Helium stirring for 3000 sec was used to flush the carbon dioxide (bone dry, Fischer Scientific) from the solution.

EXPERIMENTAL RESULTS

The potential of the electrode on which $C_sH_pO_q$, carbon monoxide, or reduced carbon dioxide were chemisorbed was adjusted to 0.05 V. Charging curves were taken at 50 mA. The $U-t$ curves for the oxidation of $C_sH_pO_q$ and of CO_{ad} at 1°, 20°, 40°, and 60° are compared in Fig. 1.

The curves a', b', c', and d', have a short hydrogen branch between 0.05 and 0.3 V and the characteristic arrest for the oxidation of $C_sH_pO_q$. The electrode potential does not increase much with time t during the initial two-thirds of this arrest. The last third of the arrest consists of a hump which becomes more pronounced with increasing temperature. The total length of the oxidation arrest increases slightly with temperature. The initial potential of the oxidation arrest of $C_sH_pO_q$ decreases by less than 100 mV from 1° to 60°.

The corresponding curves, a, b, c, d, for the oxidation of CO_{ad} consist^{11,18} of two parts. A certain portion ($< 25\%$) of the CO_{ad} , designated as type-II species, is oxidized at less anodic potentials than the rest, called type-I species. The two parts that are marked for curve a are separated by an overshoot of the $U-t$ curves in Fig. 1. The oxidation behavior at room temperature of type-I species is similar⁹⁻¹¹ to that of $\text{C}_8\text{H}_p\text{O}_q$ and $(\text{CO}_2)_r$. Only the temperature-dependence of the oxidation of type-I species is considered in the subsequent discussion. The initial potential of the oxidation arrest of type-I species decreases by about 0.17 V from 1° to 60° . The oxidation arrest of type-I species is longer at a given temperature than that of $\text{C}_8\text{H}_p\text{O}_q$ and also of $(\text{CO}_2)_r$ under the present conditions. The hump in the last portion of the oxidation arrest becomes more pronounced with T , as during the oxidation of $\text{C}_8\text{H}_p\text{O}_q$.

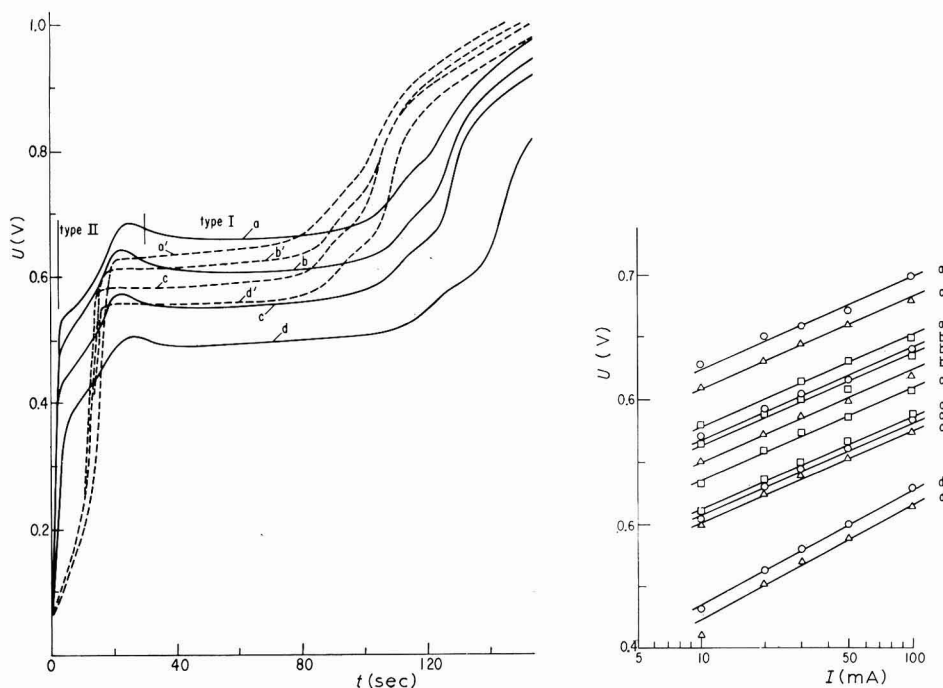


Fig. 1. Anodic charging curves taken at 50 mA in the presence of $\text{C}_8\text{H}_p\text{O}_q$ (---) or CO_{ad} (—) at different temps. (a, a'), 1° ; (b, b'), 20° ; (c, c'), 40° ; (d, d'), 60° .

Fig. 2. Plot of the initial potential of the oxidation arrest vs. $\log I$ at different temps. (a), 1° ; (b), 20° ; (c), 40° ; (d), 60° ; (\square), $\text{C}_8\text{H}_p\text{O}_q$; (Δ), CO_{ad} ; (\circ), $(\text{CO}_2)_r$.

The charging curves for the oxidation of $(\text{CO}_2)_r$ are not shown in Fig. 1, to avoid overcrowding. The $U-t$ curves are similar in shape to the curves, a', b', c', d'. However, the location of the oxidation arrests of $(\text{CO}_2)_r$ depends upon temperature as with the oxidation arrests of type-I species of carbon monoxide. This is demonstrated clearly by the results in Fig. 2.

Plots of the initial potential of the oxidation arrests of $\text{C}_8\text{H}_p\text{O}_q$, type-I species

of CO_{ad} , and $(\text{CO}_2)_r$, versus $\log I$ are shown at 1° , 20° , 40° , and 60° in Fig. 2. Since the increase of potential with time is small in the initial two-thirds of the oxidation arrests, it was possible to determine the values of U for 50 and 100 mA during one run. A current of 50 mA was imposed for this purpose until the desired initial value was reached. Then the current was rapidly increased to 100 mA. The potential was recorded. It levelled off after a short time. The subsequent decrease of I to 50 mA was used as a check that the measurement was still within the first third of the arrest. A similar procedure was employed in a second run to obtain the values of U at 50, 30, 20, 10, and 50 mA. The accuracy in the determination of U during this procedure is about ± 5 mV. This appears satisfactory since the reproducibility of the initial U -value at 50 mA in different runs is not better than ± 5 mV.

DISCUSSION

The experimental points for one type of species scatter around a Tafel line at a given temperature, in Fig. 2. The slope b of the Tafel line

$$U = a + b \log I \quad (1)$$

is practically the same (75 ± 5 mV) between 1° and 60° for $\text{C}_8\text{H}_p\text{O}_q$. A similar temperature-dependence was reported for b in ref. 19. The slope of the Tafel lines for CO_{ad} and $(\text{CO}_2)_r$ is also equal to 75 ± 5 mV between 1° and 40° while it has the larger value of 92 ± 5 mV at 60° . These results illustrate that slope b cannot be used as a diagnostic criterion for a classification of the species between 1° and 40° . The origin of a b -value of 92 ± 5 mV at 60° for CO_{ad} and $(\text{CO}_2)_r$ is not known.

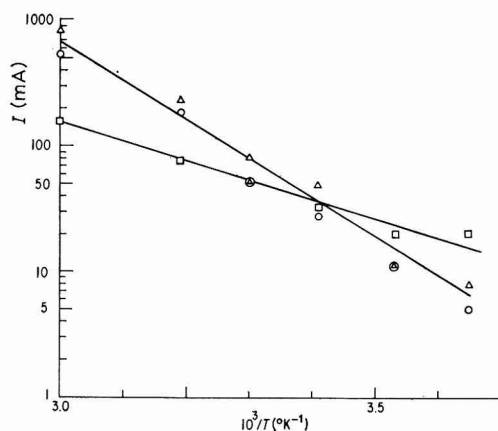


Fig. 3. Plot of $\log I$ vs. $1/T$ at $U = 0.6$, constructed on the basis of the Tafel lines in Fig. 2. (\square), $\text{C}_8\text{H}_p\text{O}_q$; (\triangle), CO_{ad} ; (\circ), $(\text{CO}_2)_r$.

The results in Figs. 1 and 2 demonstrate that the initial U -value of the oxidation arrest of $\text{C}_8\text{H}_p\text{O}_q$ depends much less on temperature at a given current than the corresponding U -value for CO_{ad} or $(\text{CO}_2)_r$. This is shown in a quantitative way by the plot of $\log I$ versus $1/T$ at 0.6 V in Fig. 3. The plot was constructed by interpolation or extrapolation from the experimental Tafel lines. The points obtained

from the oxidation of CO_{ad} and $(\text{CO}_2)_r$ scatter around a common line. A straight line with a different slope has to be drawn through the points for the oxidation of $\text{C}_s\text{H}_p\text{O}_q$. The corresponding grouping of the experimental points is obtained at 0.5 V.

It is concluded that $(\text{CO}_2)_r$ is identical with type-I species of CO_{ad} on platinized platinum in sulfuric acid solution between 1° and 60°, while $\text{C}_s\text{H}_p\text{O}_q$ represents another type of species.

The preceding statement confirms previous conclusions⁹⁻¹¹. These conclusions were of a tentative nature because the arrests for the oxidation of $\text{C}_s\text{H}_p\text{O}_q$, CO_{ad} , and $(\text{CO}_2)_r$ at room temperature appear at potentials that are too close to allow a differentiation between these species. It follows from the results in Fig. 3 that a distinction of the three species is difficult on the basis of oxidation studies in the temperature region where the $\log I-1/T$ curves intersect. This applies to temperatures between 10° and 30° at 0.6 V, and temperatures between 5° and 20° at 0.5 V in the present case.

The formation and oxidation of $(\text{CO}_2)_r$ was studied recently¹⁷ on smooth platinum in 12 M H_3PO_4 at 130°. It was suggested that $(\text{CO}_2)_r$ is the same as the O-type chemisorbed species reported previously as resulting during the oxidation of C_3H_8 ^{20,21} and *n*- C_6H_{14} ²². At room temperature, the O-type species correspond in their properties to $\text{C}_s\text{H}_p\text{O}_q$ formed from methanol, formaldehyde, or formic acid. They are not dehydrogenated and desorbed at potentials of the hydrogen region. The preceding conclusion that $\text{C}_s\text{H}_p\text{O}_q$ and $(\text{CO}_2)_r$ are not identical is valid only at temperatures between 1° and 60° for platinized platinum in 0.5 M H_2SO_4 . There need not be a contradiction to the interpretation¹⁷ of similar measurements on smooth platinum in 12 M H_3PO_4 at 130°.

The experimental heat of activation, ΔH_{an} , of the oxidation of $\text{C}_s\text{H}_p\text{O}_q$ or CO_{ad} and $(\text{CO}_2)_r$ may be determined at $U=0.6$ V and constant coverage, θ , from the slope of the straight lines in Fig. 3:

$$\Delta H_{\text{an}} = -R \left(\frac{\partial \ln I}{\partial 1/T} \right)_{U, \theta} \quad (2)$$

A value of 7 kcal/M was obtained for $\text{C}_s\text{H}_p\text{O}_q$ and of 14 ± 1 kcal/M for type-I species of CO_{ad} and $(\text{CO}_2)_r$. The ΔH_{an} -value is the same for CO_{ad} and $(\text{CO}_2)_r$ and is much larger than for $\text{C}_s\text{H}_p\text{O}_q$.

SUMMARY

The oxidation of chemisorbed carbon monoxide, reduced carbon dioxide, and carbonaceous species produced during the anodic oxidation of methanol was studied on platinized platinum in 0.5 M H_2SO_4 at currents between 10 and 100 mA and temperatures between 1° and 60°. The initial potential of the oxidation arrests in anodic charging curves depends upon temperature in nearly the same way for type-I species of adsorbed carbon monoxide and for reduced carbon dioxide, but in a different way for the chemisorbed carbonaceous species formed from methanol. Reduced carbon dioxide is identical with type-I species of carbon monoxide while the composition of the species originating from methanol differs from that of carbon monoxide.

REFERENCES

- 1 T. O. PAVELA, *Ann. Acad. Sci. Fennicae, Ser. A, II* (1954) 59.
 - 2 A. N. FRUMKIN AND B. I. PODLOVCHENKO, *Dokl. Akad. Nauk SSSR*, 150 (1963) 349.
 - 3 A. B. FASMAN, G. L. PADYUKOVA AND D. V. SOKOLSKII, *Dokl. Akad. Nauk SSSR*, 150 (1963) 856.
 - 4 B. T. PODLOVCHENKO AND E. P. GORGONOVA, *Dokl. Akad. Nauk SSSR*, 156 (1964) 763.
 - 5 L. W. NIEDRACH, *J. Electrochem. Soc.*, 111 (1964) 1309.
 - 6 O. A. PETRY, B. I. PODLOVCHENKO, A. N. FRUMKIN AND H. LAL, *J. Electroanal. Chem.*, 10 (1965) 253.
 - 7 B. I. PODLOVCHENKO, O. A. PETRY, A. N. FRUMKIN AND H. LAL, *J. Electroanal. Chem.*, 11 (1966) 12.
 - 8 H. BINDER, A. KÖHLING AND G. SANDSTEDE, *Adv. Energy Conversion*, 6 (1966) 135.
 - 9 M. W. BREITER, *J. Electroanal. Chem.*, 14 (1967) 407.
 - 10 M. W. BREITER, *J. Electroanal. Chem.*, 15 (1967) 221.
 - 11 M. W. BREITER, *Electrochim. Acta*, 12 (1967) 1213.
 - 12 J. GINER, *Electrochim. Acta*, 8 (1963) 857.
 - 13 J. GINER, *Electrochim. Acta*, 9 (1964) 63.
 - 14 W. VIELSTICH AND U. VOGEL, *Z. Elektrochem.*, 68 (1964) 688.
 - 15 P. R. JOHNSON AND A. T. KUHN, *J. Electrochem. Soc.*, 112 (1965) 599.
 - 16 B. J. PIERSMA, T. B. WARNER AND S. SCHULDINER, *J. Electrochem. Soc.*, 113 (1966) 841.
 - 17 S. B. BRUMMER AND M. J. TURNER, *J. Phys. Chem.*, 71 (1967) 3902.
 - 18 M. W. BREITER, *J. Phys. Chem.*, in print.
 - 19 V. F. STENIN AND B. I. PODLOVCHENKO, *Elektrokhimiya*, 4 (1967) 481.
 - 20 S. B. BRUMMER, J. I. FORD AND M. J. TURNER, *J. Phys. Chem.*, 69 (1965) 3424.
 - 21 S. B. BRUMMER AND M. J. TURNER, *J. Phys. Chem.*, 71 (1967) 2825.
 - 22 S. B. BRUMMER AND M. J. TURNER, *J. Phys. Chem.*, 71 (1967) 3494.
- J. Electroanal. Chem.*, 19 (1968) 131-136

A STUDY OF THE OXIDATION OF ADSORBED FILMS FORMED ON PLATINIZED PLATINUM IN METHANOL, FORMIC ACID AND CARBON DIOXIDE SOLUTIONS

V. N. KAMATH AND HIRA LAL

Department of Chemistry, Indian Institute of Technology, Bombay-76 (India)

(Received October 30th, 1967; in revised form, January 23rd, 1968)

The adsorption of methanol on smooth^{1,2} and platinized³⁻⁵ platinum has been studied recently by a number of investigators. BREITER AND GILMAN¹ were the first to report quantitative data for the potential-dependence of coverage during cyclic voltammetry with a triangular sweep of 30 mV/sec; they showed that maximum adsorption corresponded approximately to a monolayer. These studies were extended by KHAZOVA, VASIL'EV AND BAGOTSKII², and HIRA LAL, PETRY AND PODLOVCHENKO³ to conditions of steady-state polarization at constant potentials.

In the study of methanol adsorption on platinum, it is fortunate that methanol does not undergo any noticeable hydrogenation at room temperature. This led PODLOVCHENKO AND GORGONOVA⁴ to estimate quantitatively the products formed when a clean platinum electrode, initially free from adsorbed hydrogen or oxygen, comes into contact with methanol in acid solutions. They showed that methanol adsorbs dissociatively according to the following scheme:



These results were later confirmed by HIRA LAL, PETRY AND PODLOVCHENKO⁶ for methanol adsorption from acid as well as alkaline solutions. It seems, therefore, that the adsorbed species present on platinum in contact with a methanol solution is a radical of composition, HCO. This is, however, applicable to coverages not exceeding 0.5, since coverages larger than 0.5 are not experimentally observed when a platinum electrode, on open circuit, is brought into contact with a methanol solution⁴. The nature of species adsorbed at higher coverages, normally observed under conditions of polarization^{1-3,5}, is still not known. Indeed, the results of BREITER AND GILMAN¹ suggest that some other species is present at high coverages.

The adsorption of formic acid on platinum has been studied by BREITER⁷ who showed that maximum adsorption corresponded to 260 $\mu\text{C}/\text{true cm}^2$. The fact that the dehydrogenation current is relatively small at a potential of 200 mV has been attributed by BREITER⁸ to the adsorption of the formic acid molecule itself. BRUMMER⁹ has reported that one hydrogen site is freed for every two electrons involved in the oxidation of the adsorbed organic. These results have not been confirmed by MEENAKSHISUNDARAM, VASIL'EV AND BAGOTSKII¹⁰ who showed that one hydrogen site is freed for every electron involved in the oxidation of the adsorbed organic.

They have suggested that the adsorbed species is the COOH radical occupying one site.



The fact that little dehydrogenation current is observed at low potentials (where the platinum surface is already covered with adsorbed hydrogen) has been attributed by them to the following reaction,



The removal of adsorbed hydrogen as molecular hydrogen, according to reaction (3), accounts for the fact that when an initially clean electrode, free of adsorbed hydrogen or oxygen, comes into contact with formic acid, the adsorbed hydrogen and organic are not present in equivalent amounts as is expected from reaction (2).

Therefore formic acid seems to be adsorbed as COOH radicals, each radical occupying one site. This conclusion is, however, not in accord with the results of JOHNSON AND KUHN¹¹, and BREITER¹² who determined the quantity of carbon dioxide formed, together with the anodic charge passed, during the oxidation of the adsorbed film. Their results suggest that the adsorbed species is CO, HCOOH or H₂C₂O₃. In a subsequent paper, BREITER¹³ has postulated H₂C₂O₃ as the likely composition of the adsorbed species*. A similar conclusion has been reached in regard to films formed in methanol and formaldehyde. The results of BIEGLER AND KOCH¹⁵ for methanol are not at variance with the above conclusion.

The reductive adsorption of carbon dioxide on platinum from acid solutions has been studied by GINER¹⁶ who has suggested that the "reduced" carbon dioxide is adsorbed CO or COOH radical. He has further suggested¹⁷ that the adsorbed species formed during the oxidation of methanol and formic acid on platinum is the same as "reduced" carbon dioxide.

The present communication throws some further light on these problems.

EXPERIMENTAL

The platinum electrode (2.0 cm × 0.5 cm) was platinized from 1% H₂PtCl₆ solution at a current density of 2 mA/cm², and allowed to age for several weeks before use. The roughness was evaluated from the hydrogen region of the charging curve, assuming that 0.21 mC/true cm² are required for the ionization of a monolayer of hydrogen adsorbed on platinum¹⁸. The roughness factor ranged from 900 to 1300.

The experimental technique was essentially the same as described earlier^{3,5}. All studies were made at 25 ± 2°. All potentials (φ_r) refer to the reversible hydrogen electrode in the same solution at $p_{\text{H}_2} = 1$ atm.

The adsorbed films were formed as follows. In experiments with methanol and formic acid, the electrode was anodically polarized (usually at 0.5 mA/cm²) in 1 N H₂SO₄ containing the organic (0.5 M) until it attained a steady potential in the Tafel region. The polarization was then stopped and the potential allowed to fall to its steady-state value on open circuit. The cell was then washed with O₂-free acid solution. Eight washings were usually sufficient to remove all organic except that adsorbed on the electrode.

* The possibility that the species adsorbed on platinum in formic acid solutions may have a net composition, H₂C₂O₃, was also suggested by PODLOVCHENKO *et al.*¹⁴.

In the case of experiments with carbon dioxide, the electrode was first brought to the desired potential in the acid solution, and carbon dioxide introduced. The potential was kept constant by cathodic polarization, until the current required became negligibly small (1–2 h). The dissolved carbon dioxide was then removed by bubbling O₂-free nitrogen.

The various parameters required in this study were evaluated from the charging curves taken at an apparent current density of 0.1 mA/cm². Typical charging curves are shown in Fig. 1. Q_{SH} , the charge density required to ionize a monolayer of adsorbed hydrogen, and Q_M , the charge density passed for the complete oxidation of the adsorbed organic, were estimated from the charging curves without and with the presence of adsorbed organic on the electrode, respectively. The charge density,

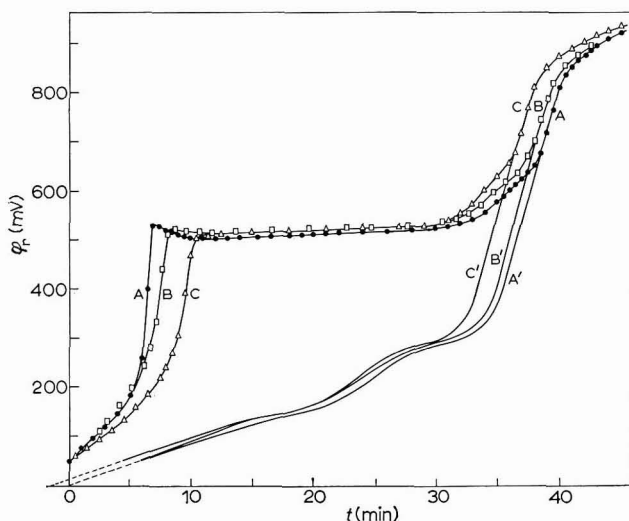


Fig. 1. Charging curves at $1 \cdot 10^{-4}$ A/cm² (apparent) for the oxidation of films formed from 1 N H₂SO₄ solns. containing: (A), 0.5 M CH₃OH; (B), 0.5 M HCOOH; (C), CO₂. A', B', C' are the corresponding charging curves in 1 N H₂SO₄.

Q_H' , required to adsorb hydrogen on the bare sites during the course of the oxidation of the adsorbed organic was estimated as follows. After a certain charge, Q_a , had been passed for the oxidation of the adsorbed organic, the current was reversed and a cathodic charging curve was taken. From the hydrogen region of this cathodic charging curve, Q_H' could be readily evaluated. The technique is similar to that used by BRUMMER⁹ for evaluating the dependence of Q_H' on Q_a during the oxidation of adsorbed formic acid films. In view of the relatively slow charging technique used by us, a certain time will elapse, during cathodic charging, before the electrode potential falls to a value of 400 mV, below which the adsorbed organic does not oxidise. This may tend to make the ratio Q_a/Q_H' somewhat smaller than it should be. It is estimated, however, that this uncertainty should not exceed 5%.

Methanol, formic acid, H₂SO₄ and HCl were analytical-grade reagents, and were used after double distillation. All solutions were made in doubly-distilled water. Cylinder nitrogen and electrolytically prepared hydrogen were purified by the usual

techniques. Carbon dioxide was prepared in a Kipps apparatus and freed of possible traces of H_2S and oxygen by passage through pumice impregnated with copper sulfate, and freshly prepared vanadous sulfate in sulfuric acid, respectively. The carbon dioxide thus prepared caused no significant change in the residual current required to maintain the electrode potential at $\varphi_r = 500$ mV, and was thus considered sufficiently pure for our purpose.

RESULTS AND DISCUSSION

The dependence of coefficient K (Q_M/Q_{SH}) on the potential at which reduced carbon dioxide was formed is illustrated in Fig. 2. In H_2SO_4 solutions (Fig. 2A) the coverage is essentially zero at 0.4 V, and above. As the potential of film formation is reduced below 0.4 V, the coverage increases rapidly and becomes reasonably constant at potentials below 0.25 V. A similar general trend is observed in HCl solutions (Fig. 2B). The coverage is virtually zero at potentials above 0.25 V, and the maximum

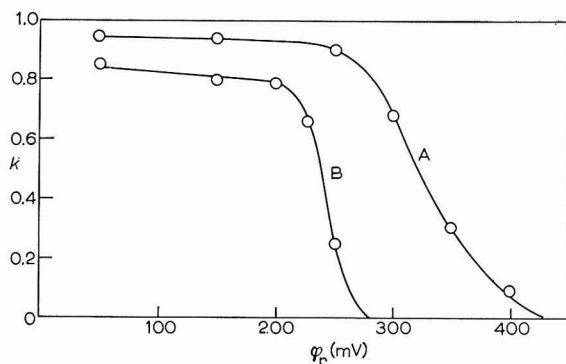


Fig. 2. The dependence of coefficient K on the potential of formation of "reduced" CO_2 in: (A), 0.1 N H_2SO_4 ; (B), 0.1 N HCl.

value in the lower potential region is somewhat smaller than in H_2SO_4 solutions. It may therefore be concluded that the reduction of carbon dioxide by adsorbed hydrogen is only slightly inhibited by chloride ions. The fact that the reduction of carbon dioxide occurs at lower potentials in HCl than in H_2SO_4 solutions is consistent with the fact that the region for the adsorption of hydrogen on platinum extends to approximately 0.25 V in the former, and 0.4 V in the latter solution¹⁹.

The charging curves for the three films studied are shown in Fig. 1. It can be seen that the charging curves with and without the presence of the adsorbed organic, coincide at potentials above 0.65 V, indicating that the oxidation of the adsorbed organic is complete at these potentials. The plateau at $\varphi_r \approx 0.5$ V, corresponding to the oxidation of the adsorbed organic, occurs at almost the same potential for the three films studied. Furthermore, the coverage is also approximately the same; the slightly smaller coverage observed in case of "reduced" carbon dioxide is probably due to the relatively low concentration of dissolved carbon dioxide in the solution.

Figure 1 suggests that the adsorbed films formed from methanol, formic acid and carbon dioxide solutions are similar to each other. The dependence of $Q_{\text{H}'}$ on Q_a

further supports this view. Plots of $\theta_H'*(Q_H'/Q_{SH})$ vs. Q_a are shown in Fig. 3 for the three films studied. The plots are linear and suggest that the films are homogeneous over the entire range of coverage with the organic. This result is in disagreement with the results of BREITER AND GILMAN¹, and BREITER⁷ for methanol and formic acid films, respectively, and supports the general conclusion reached by BRUMMER⁹ in his studies on formic acid films, at least in so far as the homogeneity of the film is concerned.

The various parameters derived from Fig. 3 are tabulated below. The various charge densities referred to in this table correspond to "true" cm² of the platinum surface.

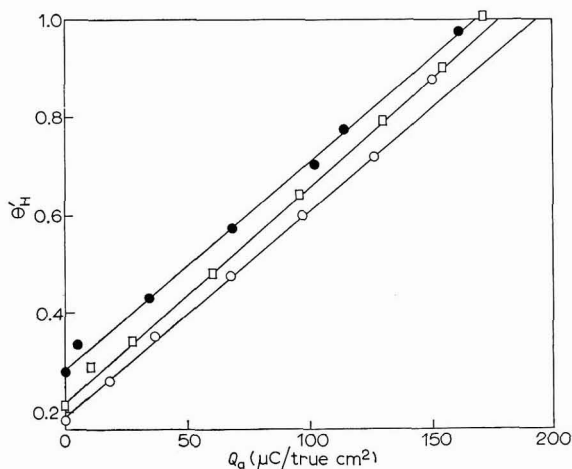


Fig. 3. θ_H' vs. Q_a plots for adsorbed films in H₂SO₄. (○), CH₃OH; (□), HCOOH; (●), CO₂.

TABLE

COULOMETRIC DATA ON THE OXIDATION OF FILMS FORMED IN METHANOL, FORMIC ACID AND CO₂ SOLUTIONS

	dQ_a/dQ_H'	$(\theta_H')_{Q_a=0}$	$(Q_a)_{\theta_H'=1}=Q_M$ ($\mu\text{C}/\text{true cm}^2$)	Q_{SM} ($\mu\text{C}/\text{true cm}^2$)
CH ₃ OH	1.12	0.18	192	234
HCOOH	1.08	0.21	179	227
CO ₂	1.12	0.28	169	235

dQ_a/dQ_H' is close to unity for all the films studied. This result for methanol is consistent with the earlier data according to which the dissociative adsorption of methanol proceeds, in accordance with reaction (1), to the formation of adsorbed HCO radical occupying approximately three platinum atoms. This, together with the linear increase of Q_H' with Q_a , suggests that the same species is adsorbed at the electrode even at high coverages extending to $K = 0.9$.

Our results on formic acid do not support BRUMMER'S observation that

* It is obvious that θ_H' represents the fraction of the surface unoccupied by the adsorbed organic during the course of its oxidation.

dQ_a/dQ_H' equals two, but are in general accord with the data of MEENAKSHISUNDARAM, VASIL'EV AND BAGOTSKII¹⁰. Their value of $Q_M = 175 \mu\text{C}/\text{true cm}^2$ agrees with ours. The data presented in the Table show that the "reduced" carbon dioxide is similar to methanol and formic acid films. The relatively smaller value of Q_M ($169 \mu\text{C}/\text{cm}^2$) corresponds to a surface which was free of the adsorbed organic to the extent of 28%. It is evident that a comparison of Q_M for films formed with various adsorbates, or under different conditions with the same adsorbate, should be based on a constant initial degree of bareness. We define a limiting charge density, Q_{SM} , such that

$$Q_{SM} = Q_M / \{1 - (\theta_H')_{Q_a=0}\}$$

It is evident that Q_{SM} refers to a surface completely covered with the adsorbed organic such that $(\theta_H')_{Q_a=0} = 0$. The values of Q_{SM} are given in the last column of the Table. They are significantly close to each other for the three films studied.

The above results suggest that the species adsorbed on platinum in methanol, formic acid and carbon dioxide solutions is the same. It will be shown in a separate communication that the kinetics of oxidation of these films are also closely similar.

We shall therefore assume that the same species are adsorbed on platinum in contact with methanol, formic acid and CO_2 solutions. A number of possibilities are consistent with the experimentally observed dQ_a/dQ_H' . We shall, however, consider only five such possibilities, *viz.*, CO (2 sites), HCOOH (2 sites), COOH (1 site), HCO (3 sites) and $\text{H}_2\text{C}_2\text{O}_3$ (4 sites). The probability of the existence of such adsorbed intermediates during the oxidation of methanol, formaldehyde, formic acid, and during the reductive adsorption of carbon dioxide, has been variously postulated by earlier workers^{4,6,8-15}.

If the destructive adsorption of methanol were to yield CO, HCOOH, COOH or $\text{H}_2\text{C}_2\text{O}_3$ as the adsorbed intermediate, the ratio $\Delta Q_H/Q_M$ should be 2,2,5 and 2, respectively. Here, ΔQ_H and Q_M are the charge densities required to oxidise the adsorbed hydrogen and the adsorbed intermediate formed when a clean electrode, initially free of adsorbed hydrogen and oxygen (*i.e.*, the initial open-circuit potential of the electrode is in the double-layer region) is brought in contact with methanol. The experimental value of $\Delta Q_H/Q_M$ for the dissociative adsorption of methanol is close to unity⁴. This result is consistent only with HCO as the adsorbed intermediate (reaction 1).

The formation of HCO as the adsorbed intermediate during the oxidation of formaldehyde or the reductive adsorption of carbon dioxide does not, at least in principle, present any difficulty. The question of the formation of HCO during the adsorption or oxidation of formic acid remains to be discussed. In this connection, it is pertinent to examine the mechanism proposed by MEENAKSHISUNDARAM, VASIL'EV AND BAGOTSKII¹⁰ (reactions 2 and 3), and see whether it can explain all the data for the adsorption of formic acid on platinum.

The open-circuit potential decay curves for platinized platinum in 0.5 M formic acid are shown in Fig. 4 for various values of the initial potential, φ_{ri} . In all cases, the steady-state potential finally attained by the electrode has a value of 50–65 mV. Independent of φ_{ri} , the adsorbed films formed on open circuit were almost identical with those formed under conditions of steady-state polarisation. In the case of low φ_{ri} (Fig. 4 C, and D), where the surface is initially covered with substantial amounts of hydrogen, the potential falls to a minimum and then rises

slowly to its steady-state value on open circuit. This minimum occurs at potentials of 15 mV (Fig. 4C) and 10 mV (Fig. 4D). The minimum and the subsequent rise of potential are very susceptible to stirring. These facts can be accounted for by the Rideal reaction (3) followed by the diffusion of molecular hydrogen away from the electrode surface.

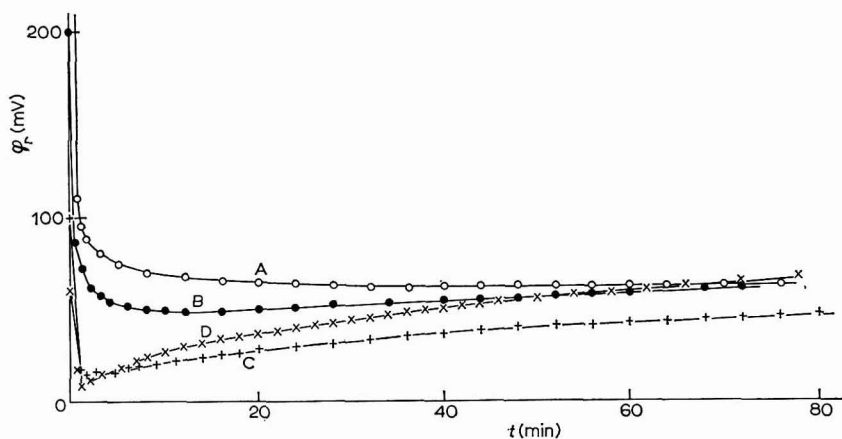


Fig. 4. Open-circuit shift of potential with time, of platinumized platinum electrode in 1 *N* H₂SO₄ solns. containing 0.5 *M* HCOOH at φ_{ri} -values; (○), 500; (●), 200; (+), 100; (×), 60 mV.

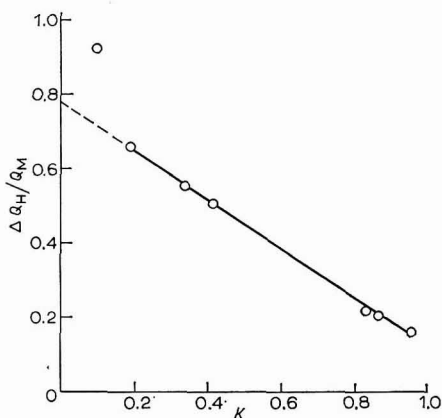


Fig. 5. $\Delta Q_H/Q_M$ vs. K plots for films formed, on open circuit, in 1 *N* H₂SO₄ containing formic acid ($5 \cdot 10^{-5}$ *M* - 0.5 *M*) at $\varphi_{ri} = 450$ mV.

With $\varphi_{ri} = 500$ mV where the electrode surface is initially free of adsorbed hydrogen or oxygen, the potential decays to its steady-state value on open circuit (Fig. 4A). ΔQ_H and Q_M were evaluated from the charging curve after the cell had been washed free of dissolved formic acid. $\Delta Q_H/Q_M$ had a value of 0.2 and tended to increase with decrease in concentration of formic acid during adsorption on open circuit. $\Delta Q_H/Q_M$ -values thus obtained are plotted in Fig. 5 as a function of K . An extrapolation to $K = 0$ gives a value of $\Delta Q_H/Q_M \approx 0.8$. This result suggests that the

dehydrogenation of formic acid according to reaction (2) is probable only at extremely low concentrations of formic acid.

The low values of $\Delta Q_H/Q_M$ at moderately high concentrations of formic acid has been attributed by MEENAKSHISUNDARAM, VASIL'EV AND BAGOTSKII¹⁰ to the fact that the adsorbed hydrogen, formed as a result of reaction (2), is removed from the electrode surface by the Rideal reaction (3). This explanation for the low values of $\Delta Q_H/Q_M$ observed is not plausible. The amount of hydrogen thrown out as molecular hydrogen can be readily evaluated. Thus, for example, the potential decays from an initial value of 500 mV to a final steady-state value of 62 mV in 0.5 M formic acid (Fig. 4A). The electrode had an apparent area of 2 cm² and roughness factor of 1300. The volume of electrolyte was 20 ml. The solubility of hydrogen in 1 N H₂SO₄ at 25° is 1.62 · 10⁻³ ml (S.T.P.)/ml of solution²⁰. From these data, assuming reversible equilibrium between adsorbed and dissolved hydrogen, the amount of hydrogen thrown into solution as the potential is brought from 500 mV to 62 mV was evaluated; it corresponded to 4% of a monolayer of hydrogen. This is obviously too small to account for the low values of $\Delta Q_H/Q_M$ observed in moderately concentrated solutions.

The experimental data may be explained as follows: In very dilute solutions, the dissociative adsorption of formic acid proceeds according to reaction (2), leading to the formation of adsorbed COOH radical. These radicals are stable only under conditions where the surface is sparsely populated by them. At high coverages, radicals adsorbed on adjacent sites interact and thus decompose into carbon dioxide and hydrogen. This means that, in moderately concentrated solutions, formic acid undergoes dehydrogenation leading to the formation of carbon dioxide²¹.



The low values of $\Delta Q_H/Q_M$ during adsorption of formic acid on bare platinum in moderately concentrated solutions are consistent with hydrogenation of formic acid physically adsorbed or weakly chemisorbed on the electrode.



If the above mechanism is correct, noticeable amounts of carbon dioxide should be thrown out into the solution during the open-circuit adsorption of formic acid on bare platinum from moderately concentrated solutions. Considerable carbon dioxide evolution has indeed been reported by BREITER¹³ under these conditions.

On the basis of the mechanism suggested above, the adsorption of formic acid on a hydrogen-covered platinum surface may be expected to proceed according to reaction (5). On a surface partly covered with hydrogen, reaction (4) may also occur to an extent dependent on the initial coverage with hydrogen. Under these conditions, a minimum in the potential decay curves may be expected (Fig. 4, C and D). Since, the minimum in Fig. 4, C and D occurs at potentials close to zero, a part of the adsorbed hydrogen may also be thrown out into solution as molecular hydrogen.

Therefore, it may be concluded that the adsorbed species formed on platinized platinum in methanol, formic acid and carbon dioxide solutions is essentially a radical having the composition, HCO. However, this conclusion is not entirely consistent with the quantitative data on carbon dioxide evolved during the oxidation of films formed in methanol and formic acid solutions. The values of Q_M/Q_{CO_2} obtained by BREITER^{12,13} for methanol (1.7–2.6) and formic acid (2.0–2.2) films are significantly

smaller than the value of 3 expected if the adsorbed species were HCO. More rigorously controlled experiments in this direction should be of great interest. The possibility that COOH radicals are also present to a certain extent cannot, however, be ruled out.

SUMMARY

The oxidation of films formed on platinized platinum in methanol, formic acid and carbon dioxide solutions has been studied. It is shown that approximately one site is bared for every electron involved in the oxidation of these films. It is concluded that the same species is adsorbed in all the cases studied and that it has the composition HCO. It is probable that COOH radicals are also present to a certain extent. A mechanism for the formation of HCO during the adsorption of formic acid on platinum has been proposed.

REFERENCES

- 1 M. W. BREITER AND S. GILMAN, *J. Electrochem. Soc.*, 109 (1962) 622.
- 2 O. A. KHAZOVA, YU. B. VASIL'EV AND V. S. BAGOTSKII, *Elektrokhimiya*, 1 (1965) 84.
- 3 HIRA LAL, O. A. PETRY AND B. I. PODLOVCHENKO, *ibid.*, 1 (1965) 316.
- 4 B. I. PODLOVCHENKO AND E. P. GORGONOVA, *Dokl. Akad. Nauk SSSR*, 156 (1964) 673.
- 5 O. A. PETRY, B. I. PODLOVCHENKO, A. N. FRUMKIN AND HIRA LAL, *J. Electroanal. Chem.*, 10 (1965) 253.
- 6 HIRA LAL, O. A. PETRY AND B. I. PODLOVCHENKO, *Dokl. Akad. Nauk SSSR*, 158 (1964) 1416.
- 7 M. W. BREITER, *Electrochim. Acta*, 8 (1963) 447, 457.
- 8 M. W. BREITER *ibid.*, 10 (1965) 503.
- 9 S. B. BRUMMER, *J. Phys. Chem.*, 69 (1965) 562.
- 10 N. MEENAKSHISUNDARAM, YU. B. VASIL'EV AND V. S. BAGOTSKII, *Elektrokhimiya*, 3 (1967) 193.
- 11 P. R. JOHNSON AND A. T. KUHN, *J. Electrochem. Soc.*, 112 (1965) 599.
- 12 M. W. BREITER *J. Electroanal. Chem.*, 14 (1967) 407.
- 13 M. W. BREITER, *J. Electroanal. Chem.*, 15 (1967) 221.
- 14 B. I. PODLOVCHENKO, O. A. PETRY, A. N. FRUMKIN AND HIRA LAL, *J. Electroanal. Chem.*, 11 (1966) 12.
- 15 T. BIEGLER AND D. F. A. KOCH, *J. Electrochem. Soc.*, 114 (1967) 904.
- 16 J. GINER, *Electrochim. Acta*, 8 (1963) 857.
- 17 J. GINER, *ibid.*, 9 (1964) 63.
- 18 F. G. WILL AND C. A. KNORR, *Z. Elektrochem.*, 64 (1960) 258.
- 19 A. N. FRUMKIN, *Advan. Electrochem. Electrochem. Eng.*, Vol. 3, Interscience Publishers, New York, 1963.
- 20 *International Critical Tables*, Vol. III, 1928, p. 273.
- 21 See also G. C. BOND, *Catalysis by Metals*, Academic Press, London and New York, 1962, p. 431.

FURTHER EXAMPLES OF *para*- AND *ortho*-DISUBSTITUTED BENZENE
DERIVATIVES REDUCED IN A REVERSIBLE TWO-ELECTRON STEP
INTO PRODUCTS OF LIMITED STABILITY

P. ZUMAN*, O. MANOUŠEK AND S. K. VIG**

J. Heyrovský Institute of Polarography, Czechoslovak Academy of Sciences, Prague (Czechoslovakia)

(Received February 24th, 1968)

In the course of the study of benzene derivatives bearing two electronegative groups on the ring, it was possible to demonstrate¹ that the behaviour of *p*-diacetylbenzene is different from that of most of the other substances studied. The change in the wave-height of the more negative wave in the region where reduction of the C₆H₅COCH₂-grouping takes place, and the change of the anodic wave of the electrolysis product obtained by rectangular voltage polarization, indicated formation of an intermediate of biradical character[†] with limited stability. In principle, three schemes were considered, involving hydration, protonation of the parent compound, and acid-base catalysed cleavage of the biradical intermediate. A chronopotentiometric investigation² confirmed that Scheme I gives the best explanation for all the experimental results. pH-Dependence of experimentally found rate constants, k_a , k_b , obtained by chronopotentiometry, is analogous to the dependence of the height of the second reduction step of *p*-diacetylbenzene and of the anodic wave of the primary electrolysis product obtained with the commutator. The reaction limiting the height of the second reduction step and of the anodic wave of the product, is hence the acid-base catalysed cleavage of the biradical. The specific rate constants of this reaction obey a Brønsted relation².

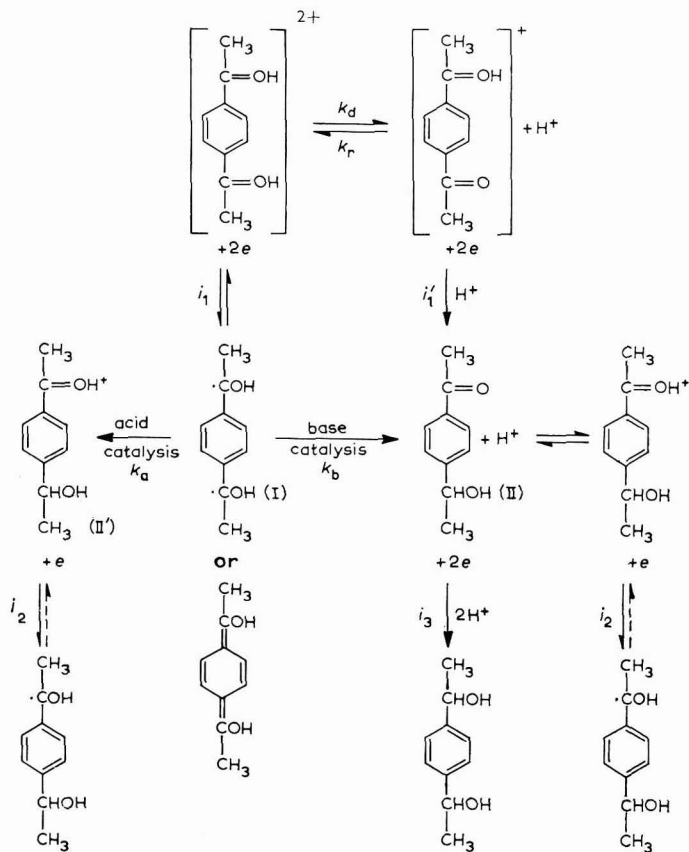
For a more detailed understanding of the mechanism of the chemical reaction responsible for the transformation of the primary electrode product, it was of importance to determine the limits of applicability of the suggested scheme. It was necessary to show how large changes may be realised in the structure of the molecule without changing the course of the electrode process. Furthermore, it was of interest to compare, at least qualitatively, how changes in structure of the parent compound (within the scope of "permitted" changes) affect the stability and reactivity of the primary product.

The result of some investigations along these lines with compounds bearing a carbonyl, nitro- or cyano-group in *para*- or *ortho*-positions are discussed in this paper. The main technique used for the characterization of the stability of the biradical intermediate in this investigation was a rectangular voltage polarization in the commutator method by KALOUSEK³.

* Present address: Department of Chemistry, University of Birmingham, Great Britain.

** Present address: St. Stephen's College, Delhi, India.

† In the text, the term biradical is used for the primary product of the two-electron reduction, even though we have no proof for its existence in the biradical or quinoid structure shown in Scheme I.



Scheme I

EXPERIMENTAL

A pen-recording polarograph LP 60 (Laboratorní přístroje, Praha) was used in most experiments. Polarographic electrolysis was carried out using a Kalousek vessel with a saturated calomel electrode as reference electrode and a dropping mercury electrode with constants, $m=2.1$ mg/sec, $t_1=2.8$ sec at $h=66$ cm in $1 M$ KCl at 0.0 V. *o*-Phthaldialdehyde, terephthaldialdehyde, *o*-phthaldinitrile and *p*-dinitrobenzene were commercial products; terephthalophenone, 4,4'-diacetyldiphenylmethane, terephthaldinitrile and isophthaldinitrile were kindly donated by Dr. O. EXNER.

$0.01 M$ Ethanolic stock solutions were prepared from the electroactive substance. Freshly prepared stock solutions were added to the supporting electrolyte to ensure a $2 \cdot 10^{-4} M$ solution. The final solution usually contained about 5% ethanol; only with terephthalophenone was it necessary to use solutions containing 50% ethanol.

The rectangular voltage polarization was followed using a commutator constructed according to the principle suggested by KALOUSEK^{3,4}. In the scheme used, the auxiliary potential was always kept constant at the potential corresponding to

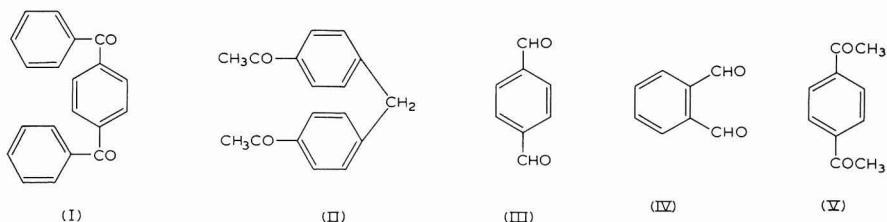
the limiting current, usually of the first wave. Capacity current was recorded in the given supporting electrolyte and subtracted from the current-voltage curve recorded in the presence of the electroactive component.

Cyclic voltametric *i*-*E* curves were recorded using a hanging mercury drop electrode in conjunction with the polarograph OH 102 (Radelkis) using a scan rate of 50 mV/sec.

RESULTS

Carbonyl compounds

Terephthalophenone (I), 4,4'-diacetyldiphenylmethane (II), terephthalaldehyde (III) and *o*-phthalaldehyde (IV) were investigated:



The polarographic behaviour of terephthalophenone (I) is analogous to that of *p*-diacetylbenzene (V)¹. In acidic media, the first two-electron wave corresponds to a reversible process; this was shown with the commutator by the formation of an anodic wave on the curve obtained (Fig. 1) at the same potential as that of the original cathodic wave. In comparison with *p*-diacetylbenzene, the decrease of height of the anodic wave with increase in pH is shifted with (I) towards higher pH-values. With increasing acidity, no decrease in the height of the anodic wave obtained with

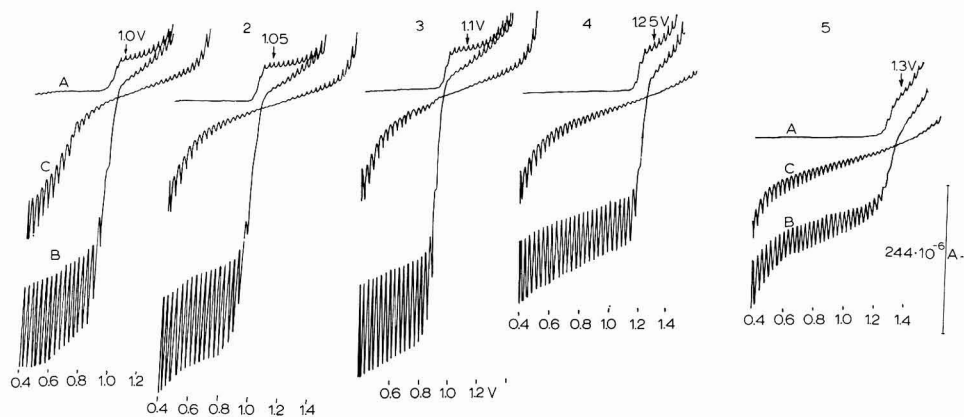


Fig. 1. Polarographic curves of terephthalophenone using Kalousek commutator method. $2 \cdot 10^{-4}$ M depolarizer, 50% ethanol. (A), original *i*-*E* curve; (B), curve obtained with commutator; (C), curve obtained with commutator for the supporting electrolyte: (1), 2.5 M; (2), 0.5 M; (3), 0.05 M H₂SO₄; (4), acetate buffer pH 4.9; (5), phosphate buffer pH 6.9. Mercurous sulphate reference electrode; arrows on original *i*-*E* curves indicate value of the auxiliary potential; frequency of commutation 6 cycles/sec.

the commutator was observed and the wave shows practically the same wave-height in 0.1 *N* and 5 *N* H₂SO₄ (Fig. 1). Both the increase in size of the pH-region in which the anodic wave is observed, and the extension of the range in which the height of the wave reaches its limiting value, indicates greater stability of the biradical formed from terephthalophenone (I) than that from *p*-diacetylbenzene. This was also confirmed by polarization with triangular sweeps. Whereas for *p*-diacetylbenzene (V) it was possible to obtain anodic peaks only when using oscilloscopic techniques and scanning rates of the order 1 V/sec, for terephthalophenone (I) it was possible to obtain a reversible anodic peak with a hanging mercury drop electrode with a scanning rate of 0.05 V/sec (Fig. 2).

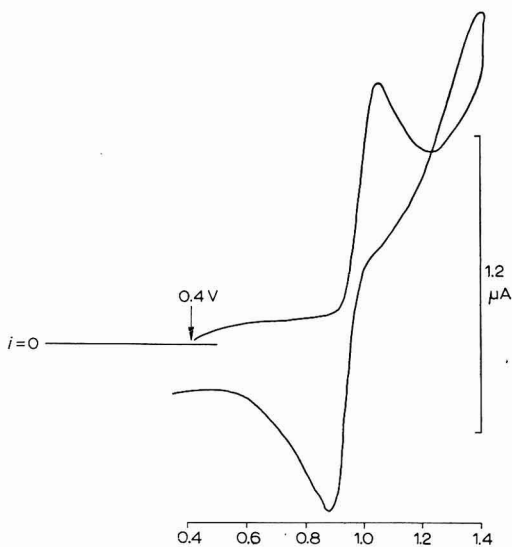


Fig. 2. Current-voltage curve of terephthalophenone using hanging mercury drop electrode. $2 \cdot 10^{-4}$ *M* depolarizer, 0.25 *M* H₂SO₄, 50% ethanol, triangular voltage sweep, 50 mV/sec, hanging mercury drop "Metrohm", polarograph OH 102.

As expected, 4,4'-diacetyldiphenylmethane (II) does not give a reduction product of limited stability in acidic media, which would give an anodic wave using the commutator method.

Terephthalaldehyde (III) at pH < 3 behaves similarly to *p*-diacetylbenzene. A two-electron reversible cathodic wave was followed by a more negative wave, the height of which approached that of a one-electron process. Simultaneously, an anodic wave was observed on the curve obtained with the commutator, the height of which changed with pH in a bell-shaped curve (Fig. 3). The discontinuity at that part of the curve corresponding to a change from solutions of a strong acid to buffered solutions, indicates that the reaction causing the cleavage of the biradical is generally acid-base catalysed. The range in which the biradical of (III) gives an anodic wave, is more narrow than that observed for (V) and does not show a pH-independent section. This indicates that the biradical formed in the reduction of terephthalaldehyde (III) has a shorter life-time than that formed from *p*-diacetylbenzene (V).

The waves of *o*-phthalaldehyde (IV) are strongly affected by hydration and do not show any measurable anodic wave with the commutator.

Nitro compounds

p-Dinitrobenzene is known⁵ to give a reversible wave in water-containing dimethylformamide media. We were able to show that in aqueous acidic media a product of limited stability is also formed, which gives an anodic wave when the commutator is used. The anodic wave is small and observed over a narrow pH-range, but the shape of the pH-dependence shows the general pattern, and the abrupt change accompanying transition from strong acid solution to buffer solutions indicates acid-base catalysis of the cleavage reaction. The product formed in this process is hence considerably less stable than that obtained with terephthalaldehyde (III).

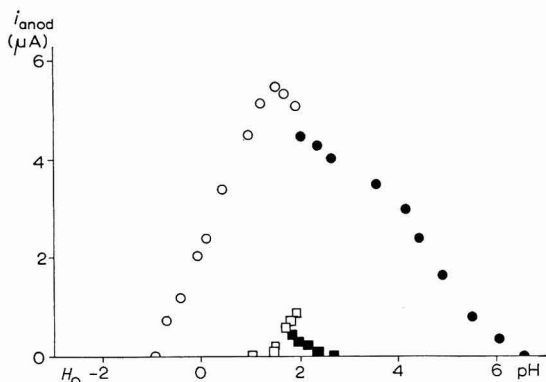
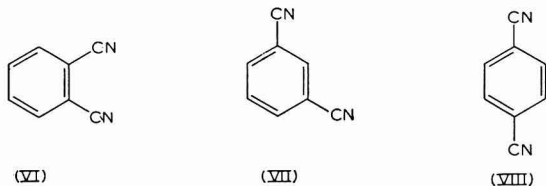


Fig. 3. pH-Dependence of heights of anodic waves obtained with Kalousek commutator method for terephthalaldehyde and *p*-dinitrobenzene. $2 \cdot 10^{-4} M$ depolarizer, 5% ethanol, auxiliary potential at limiting current of original reduction wave. (Circles), terephthalaldehyde; (squares), *p*-dinitrobenzene; (white points), sulphuric acid solns.; (black points), Britton-Robinson buffers.

Dinitriles

o-Phthaldinitrile (VI), isophthaldinitrile (VII) and terephthaldinitrile (VIII) were shown to behave differently from *p*-diacetylbenzene (V). At lower pH-values, no anodic wave is observed for these substances using the commutator method.



At high pH-values, for compounds (VI) and (VIII) the formation of the anodic cyanide wave was observed, and is discussed elsewhere⁶. At $\text{pH} > 5$, in addition to this cyanide wave, a small anodic wave was observed on the curves obtained with the commutator for *o*- (VI) and terephthaldinitrile (VIII). The height of this anodic wave, indicating a reversible process, was higher for the *ortho*-derivative (VI) than

for the *para*-derivative (VIII). No such effect was observed for isophthaldinitrile (VII) (Fig. 4).

The height of the anodic waves obtained with the commutator for dinitriles (VI) and (VIII) increases with increasing pH (Fig. 5) and reaches its limiting value at about pH 8. At higher pH-values, up to pH 12, the height of this wave remains unchanged, provided hydrolysis does not take place.

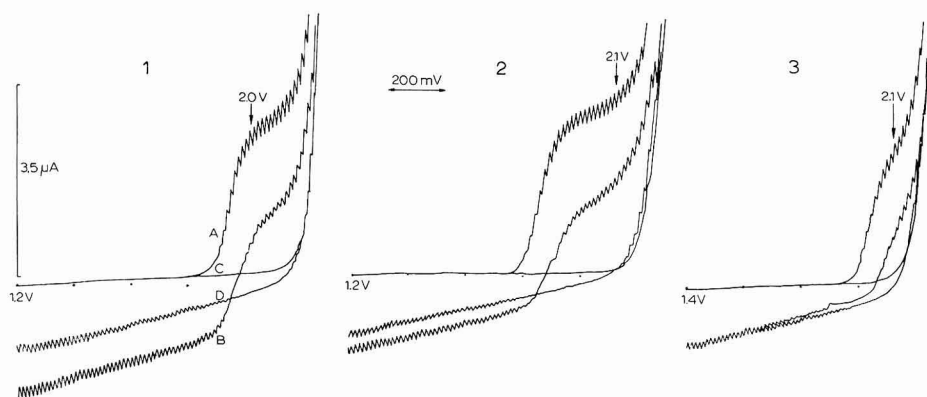


Fig. 4. Comparison of anodic waves of benzodinitriles obtained with Kalousek commutator method. Britton–Robinson buffer pH 9.9. (A) and (C), original i - E curves; (B) and (D), curves obtained with commutator; (A) and (B), $5 \cdot 10^{-4} M$ depolarizer; (C) and (D), supporting electrolyte. (1), *o*-phthaldinitrile; (2), terephthaldinitrile; (3), isophthaldinitrile. Mercurous sulphate electrode; arrows on original i - E curves indicate value of auxiliary potential; frequency of commutation 6 cycles/sec.

The potential of the anodic wave on the curve obtained with the commutator is identical with the half-wave potential of the original reduction wave. Therefore, only one anodic–cathodic wave is observed on the curve obtained with rectangular voltage polarization (Fig. 5). The ratio of the height of the anodic wave obtained with the commutator and the original cathodic wave shows no dependence on dinitrile concentration below $1 \cdot 10^{-3} M$.

The height of the anodic wave corresponding to an oxidation of the product of electrolysis formed at the potential chosen on the auxiliary potentiometer, increased with increasing negative auxiliary potential. The height reaches a limiting value when the auxiliary potential reaches the value corresponding to the limiting current of the original d.c. curve. The ratio of the height of the anodic wave obtained with the commutator, $(i_a)_{\text{com}}$, and the original cathodic wave, $(i_d)_{\text{orig}}$, increases with decreasing temperature. This indicates that the oxidizable species is more stable at lower temperatures.

T ($^{\circ}C$)	6°	10°	15°	20°	25°
$\frac{(i_a)_{\text{com}}}{(i_d)_{\text{orig}}}$	0.28	0.275	0.24	0.23	0.21

The ratio of the two wave-heights also increases with increasing ethanol concentration:

$[C_2H_5OH]$ (%)	5	10	15	20
$(i_a)_{com}$ (μA)	0.55	0.82	1.00	0.98
$(i_a)_{orig}$ (μA)	3.37	3.12	2.92	2.42
$(i_a)_{com}/(i_a)_{orig}$	0.16	0.26	0.34	0.40

With increasing ethanol concentration, not only does the ratio of wave-heights increase (indicating that the intermediate is more stable at higher ethanol concentrations), but the absolute value of the height of the original cathodic wave, $(i_a)_{orig}$, decreases, whereas that of the anodic wave increases.

Controlled-potential electrolysis at the potential of the limiting current of nitriles (VI)–(VIII) gave only cyanide ions. No reversible anodic wave was observed after prolonged electrolysis.

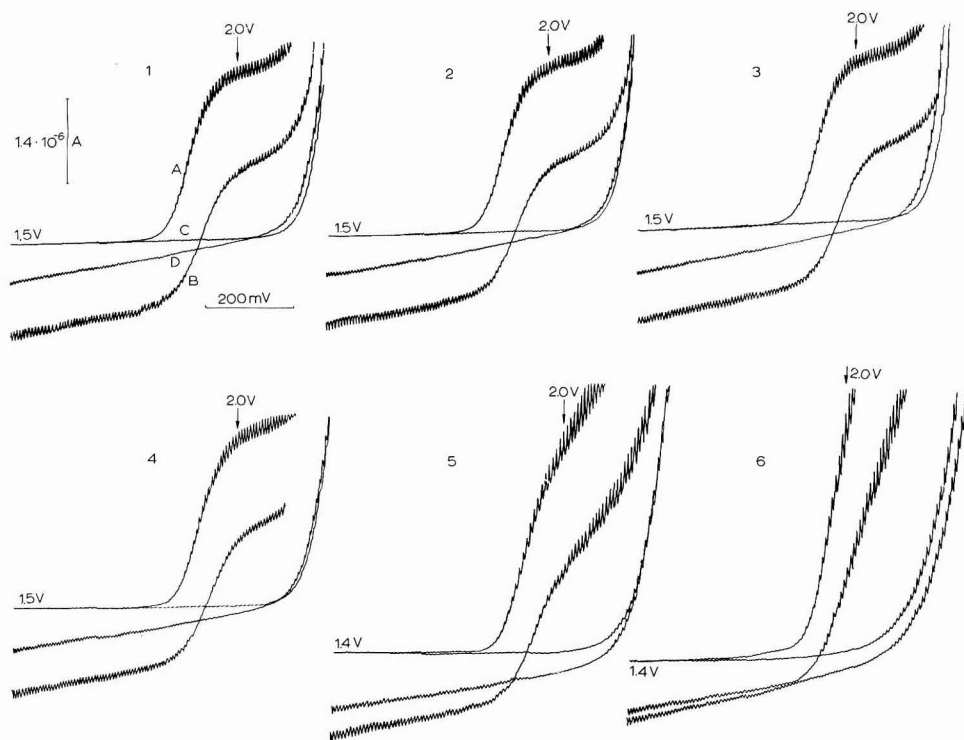


Fig. 5. pH-Dependence of anodic waves obtained with Kalousek commutator method for *o*-phthaldinitrile. $5 \cdot 10^{-4} M$ depolarizer, Britton–Robinson buffers, pH: (1), 12.7; (2), 11.2; (3), 10.0; (4), 8.9; (5), 7.9; (6), 7.1. (A) and (C), original *i*-*E* curves; (B) and (D), curves obtained with commutator; (A) and (B), solns. *o*-phthaldinitrile; (C) and (D), supporting electrolyte. (1)–(4), starting at $-1.5 V$; (5) and (6), at $-1.4 V$; mercurous sulphate electrode, arrows on original *i*-*E* curves indicate value of auxiliary potential; frequency of commutation 6 cycles/sec; regulated drop-time, $t_1 = 2.2$ sec; $m = 2.8$ mg/sec.

DISCUSSION

The type of behaviour corresponding to Scheme I, in which the biprotonated form is reversibly reduced in a two-electron step to a biradical, has so far been found only for *p*-dicarbonyl compounds, (I), (III) and (V). Neither is the scheme followed when one or both of the carbonyl groups are transformed into ketimino groups in semicarbazones, nor for systems in which one or both of the carbonyl groups are exchanged for cyano groups. Both carbonyl groups need to be ketonic or aldehydic groups, since it was found¹ that the reduction according to Scheme I does not take place when one or both of the carbonyl groups are a part of a carboxyl grouping*.

The stabilization of the biradical is attributed to the contribution of the canonical form with quinoid structure. This is supported by the fact that in 4,4'-diacetyl-diphenylmethane, where the conjugation interaction of the two acetyl groups in the aromatic system is blocked and where a formation of a two-electron reduction product with a quinoid structure is impossible, the formation of the product giving a reversible anodic wave was not observed. The life-time and the pH-range in which the biradical is stable increases in compounds of the type, RCO-C₆H₄-COR in the sequence, R=H < CH₃ < C₆H₅. This is in accordance with the expected polar and conjugation effects of these groups. For aldehydes, hydration can be a complicating factor.

Reduction of *o*-phthaldinitrile (VI) and terephthaldinitrile (VIII) differ from that of isophthaldinitrile (VII). This is in accordance with the observation⁷ of the reduction of these compounds in aprotic media, where compounds (VI) and (VIII) give stable radical anions and two one-electron reduction steps, whereas (VII) gives only one one-electron step and a low yield of a radical anion, which is attributed to its cleavage in side reactions.

As the half-wave potentials of dinitriles (VI) and (VIII) are pH-independent, it can be deduced that no proton transfer occurs, prior to the first electron uptake. It can thus be assumed that a radical anion is formed in the first electron uptake and that this is oxidised in the anodic wave. Even when the formation of the radical dianion cannot be excluded, the sufficient stability of the observed species to give the anodic wave with the commutator suggests that the dianion formation is less probable in view of the findings on reactivity of dianions reported by REINMUTH⁷. The reaction causing the cleavage of the oxidizable species is independent of pH and dinitrile concentration, but its rate decreases with decreasing temperature and increasing ethanol content. It seems that the radical anion, which is reported for compound (VI) to be stable in dimethylformamide media for several hours, has a life-time of the order of seconds in aqueous media. The stability of this radical anion is greater for compound (VI) than for the *para*-derivative (VIII), but undergoes consecutive chemical and electrochemical reactions to produce benzonitrile and cyanide ions. The process seems to be analogous to that observed⁷ at very negative potentials (−2.8 V) in dimethylformamide solutions. Whereas in aqueous solutions benzonitrile is the final product (at −1.8 V), in dimethylformamide benzonitrile is further reduced.

The products of reductions of *o*- and *p*-dinitriles in aqueous media, therefore

* Experimental evidence for the *p*-dinitro compound is insufficient to enable us to draw any conclusions as to the course of the electrode process concerned.

show limited stability, but the process is different from that observed¹ for *para*-dicarbonyl compounds.

SUMMARY

Only those benzene derivatives (bearing two electronegative groups) with two carbonyl groups in the *para*-position were found to be reduced in acid media in one two-electron reversible step to form a biradical or a quinoid product of limited stability. The life-time of the primary product of $\text{RCOC}_6\text{H}_4\text{COR}$ increased in the sequence: $\text{R}=\text{H} < \text{CH}_3 < \text{C}_6\text{H}_5$. Exchange of one of the carbonyl groups for an oxime- or carboxy-group prevents this type of process. *p*-Dinitrobenzene was shown by rectangular voltage polarization to give a rather unstable reduction product in acid media. *Ortho*- and *para*-benzenedinitriles give radical anions of limited stability in aqueous alkaline media.

REFERENCES

- 1 YU. KARGIN, O. MANOUŠEK AND P. ZUMAN, *J. Electroanal. Chem.*, 12 (1966) 443.
- 2 O. FISCHER, L. KIŠOVÁ AND J. ŠTĚPÁNEK, *J. Electroanal. Chem.*, 17 (1968) 233.
- 3 M. KALOUSEK, *Collection Czech. Chem. Commun.*, 13 (1948) 105.
- 4 M. RÁLEK AND L. NOVÁK, *Collection Czech. Chem. Commun.*, 21 (1956) 248.
- 5 J. Q. CHAMBERS III AND R. N. ADAMS, *J. Electroanal. Chem.*, 9 (1965) 400.
- 6 O. MANOUŠEK, P. ZUMAN AND O. EXNER, *Collection Czech. Chem. Commun.*, in the press.
- 7 P. H. RIEGER, I. BERNAL, W. H. REINMUTH AND G. K. FRAENKEL, *J. Am. Chem. Soc.*, 85 (1963) 683.

J. Electroanal. Chem., 19 (1968) 147-155

POLAROGRAPHY IN THE STUDY OF CLASSICAL ORGANIC FUNCTIONAL GROUP REACTIONS

II. POLAROGRAPHIC BEHAVIOUR OF 4-CYANOCINNAMIC ACID AND ITS ETHYL ESTER

M. J. D. BRAND AND B. FLEET

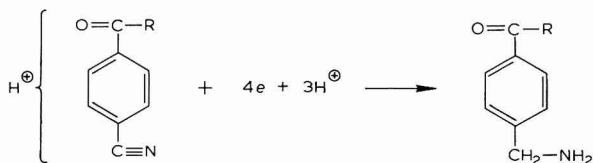
Chemistry Department, Imperial College of Science and Technology, London (England)

(Received March 18th, 1968)

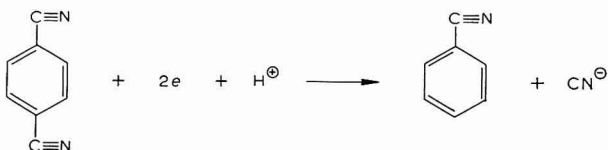
In a recent study¹ of the polarographic behaviour of a series of substituted cinnamic acids, it was shown that the half-wave potential of the reduction of the C=C bond obeyed the modified Hammett equation²

$$\Delta E_{\frac{1}{2}} = \sigma \rho'$$

Among the compounds studied, the only one to deviate from this equation was 4-cyanocinnamic acid. The anomalous behaviour of 4-cyano derivatives in linear free-energy relationships has previously been observed². MANOUSEK AND ZUMAN³ have studied the polarographic reduction of the 4-cyano substituent in benzaldehyde, acetophenone, benzoic acid and benzonitrile. In acid solution, the cyano-group in substituted carbonyl compounds was reduced in the protonated complex to a primary amine in a single 4-electron wave,



followed by a wave for reduction of the carbonyl group. At pH-values above 7, a 2-electron fission of the cyano-group was observed for compounds of the type, $\text{XC}_6\text{H}_4\text{CN}$ where $\text{X} = p\text{-COO}^-$ and $p\text{-CN}$. Thus, in the case of terephthalic acid dinitrile in 0.02 M NaOH, the reaction is as follows:



The liberation of cyanide ions is confirmed by the appearance of an anodic wave.

The behaviour of 4-cyanocinnamic acid was so markedly different from that of the other derivatives that a more detailed study was undertaken.

EXPERIMENTAL

Reagents

4-Cyanocinnamic acid and 3,4-dichlorocinnamic acid were synthesised from the corresponding aldehydes by a modified Doebner reaction⁴.

Ethyl 4-cyanocinnamate was synthesised from the parent acid. Treatment of the acid with thionyl chloride yielded the acid chloride which was then reacted with ethanol. The ester was distilled under reduced pressure and recrystallised from small volumes of ethanol. This compound does not appear to have been reported before; it was obtained as a white crystalline solid, m.p. 67.5°–68.5°, and its composition was established by elemental analysis (calc.: C, 71.62; H, 5.51; N, 6.96%. Found: C, 71.47; H, 5.76; N, 6.67%). The structure of the compound was confirmed by i.r. and N.M.R. spectroscopy.

$5 \cdot 10^{-3}$ M stock solutions of each compound were prepared in absolute ethanol. Buffer solutions were prepared from AnalaR reagents using glass-distilled water. Solutions for polarography were prepared in 50% ethanol by mixing measured volumes of ethanol, stock solution of depolariser, water and aqueous buffer solution.

Apparatus

Apparatus for d.c. polarography, half-wave potential measurements and microcoulometry has been described previously¹. The DME capillary constants measured at the potential of the SCE in 0.1 M potassium chloride solution were $t=4.7$ sec, $m=1.45$ mg sec⁻¹, at $h=60$ cm.

A.c. polarograms were obtained with a General Purpose Polarograph and Univector (Cambridge Limited, London). A Kalousek cell was used in which a platinum wire counter electrode was placed near to the DME. The counter electrode was connected to the SCE reference electrode through a 5000 μ F capacitor.

Oscillopolarograms were measured with a Polaroscope P 576 (Krizik, Prague) at a hanging mercury drop electrode (HMDE).

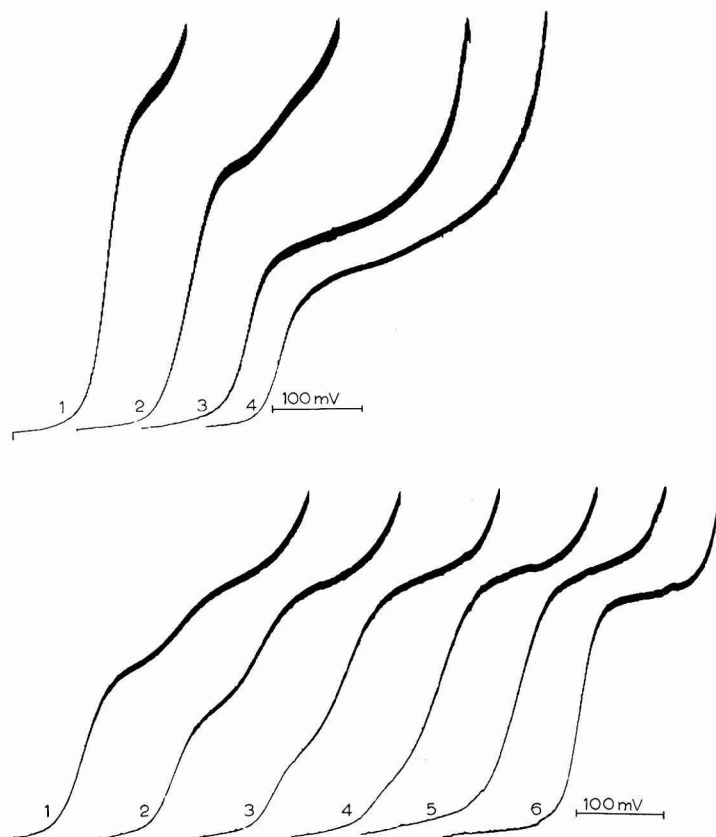
Cyclic voltammograms were also measured at a HMDE using the d.c. polarograph for slow sweep rates and an instrument specially designed for fast sweep rates⁵.

Absorbance measurements in the u.v. were made with a DB spectrophotometer (Beckmann Instruments Limited, Fife) using 1-cm quartz cells.

RESULTS AND DISCUSSION

In contrast to cinnamic acids containing electroinactive substituents, where a single pH-dependent polarographic wave was observed over the pH range 4–8, the behaviour of 4-cyanocinnamic acid was more complex. The appearance of a wave at low pH-values was the first significant deviation from the behaviour of simple substituted cinnamic acids. The height of this wave decreased with increasing pH-values until at pH 5.5 it had reached approximately half its limiting value (Fig. 1). A slight increase in wave height was observed between pH 6 and 7 and at higher pH-values the single wave split into two waves. The wave at more positive potentials decreased in height with increasing pH, while the total height of the two waves remained constant (Fig. 2). The complete polarographic dissociation curve (Fig. 3) showed the presence of three separate electrode processes; that in acid solution (I), and two processes

above pH 7, (II, the more positive wave) and (III). The increase in wave height between pH 6 and 7 was attributed to a mixed electrode process consisting of reactions I and II. The onset of this mixed process was further characterised by a slight increase followed by a sudden decrease in the slope of the polarographic wave between



Figs. 1-2. pH-dependence of waves of $5 \cdot 10^{-4} M$ 4-cyanocinnamic acid in 50% ethanol. Fig. 1 pH: (1), 1.68; (2), 3.52; (3), 4.77; (4) 5.81. Starting potentials: (1), -0.9 ; (2), -1.0 ; (3), -1.1 ; (4), -1.2 V vs. SCE. Sensitivity, $6 \mu A$ f.s.d. Fig. 2 pH: (1), 7.9; (2), 8.3; (3), 8.7; (4), 9.2; (5), 11.0; (6), 13.0. Starting potential, -1.4 V vs. SCE. Sensitivity, $4 \mu A$ f.s.d.

pH 5.9 and 6.1, the $n\alpha$ -values obtained from logarithmic analysis of the wave shape were significantly different from those corresponding to processes I and II in the region of the mixed process (Table 1). One further observation was made from the general morphology of the waves; the slope of the wave at high pH-values increased until at pH 13 the wave shape indicated apparent Nernstian reversibility.

Determination of n and product analysis

A preliminary comparison of wave heights for processes I, II and III with the 2-electron wave for the unsubstituted acid indicated that processes II and III involved 2 electrons. As process I gave waves twice as high as II, I would correspond

to a 4-electron reaction. A more accurate value of the number of electrons transferred in each reaction was obtained from microcoulometric measurements at the DME at pH-values corresponding to single waves for processes I, II and III. The results

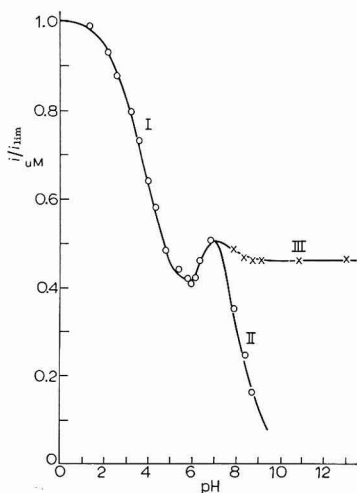


Fig. 3. Polarographic dissociation curve of 4-cyanocinnamic acid. (○), First wave; (×), total wave height.

TABLE I

DEPENDENCE OF CURRENT AND $n\alpha$ -VALUES FOR THE REDUCTION OF 4-CYANOCINNAMIC ACID AND ITS ETHYL ESTER

pH	Acid				Ester	
	Currents (μA) ^a		$n\alpha$		Currents (μA) ^a	$n\alpha$
	1st wave	2nd wave	1st wave	2nd wave		
1.32	3.15		1.65		2.94	1.24
1.68	3.20		1.65		3.04	1.24
2.13	2.98		1.48		2.84	1.24
2.58	2.80		1.36		2.64	1.24
3.27	2.54		1.39		2.16	1.24
3.52	2.34		1.39		1.98	1.24
4.02	2.04		1.39		1.81	1.49
4.32	1.85		1.39		1.81	1.69
4.77	1.54		1.39		1.69	1.76
5.35	1.46		1.39		1.61	1.77
5.81	1.33		1.50		1.55	1.47
5.89	1.31		1.48		1.53	1.47
6.09	1.34		1.08		1.50	1.47
6.35	1.47		1.08		1.46	1.47
6.83	1.62		1.08		1.38	1.47
7.87	1.12	0.45	1.58		1.17	1.47
8.31	0.78	0.70	1.58		1.09	1.47
8.73	0.51	0.96			1.10	1.47
9.19	0.24	1.23			1.10	1.47
10.84		1.47		1.29	1.06	1.47
13.0		1.47		2.0		

^aDepolariser conc., 5.10^{-4} M.

obtained (Table 2) confirmed the n -values suggested by wave height comparison.

Unequivocal interpretation of the course of the electrode process can only be obtained from identification of the electrolysis products. The products of each reaction were identified in the residual solution from microcoulometry at the DME, as it was previously pointed out¹ that controlled-potential electrolysis at a mercury pool electrode can result in appreciable dimerisation of the free radical intermediate formed in the electroreduction.

TABLE 2

MICROCOULOMETRICALLY-DETERMINED n -VALUES FOR 4-CYANOCINNAMIC ACID

pH	Medium	n
1.32	6 N Sulphuric acid in 50% ethanol	4.08
6.83	Acetate buffer in 50% ethanol	2.44
		1.95
		2.16
13	0.1 N Sodium hydroxide in 50% ethanol	1.80
		2.65

In acid solution ($n=4$, electrode reaction I) the presence of a primary amine in the electrolysis products was proved by formation of a coloured Schiff's base with *p*-dimethylaminobenzaldehyde⁶, and by formation of a fluorescent Schiff's base with salicylaldehyde.

Possible 2-electron reductions for 4-cyanocinnamic acid are:

- (i) Fission of the C-CN bond to form free cyanide ion and cinnamic acid.
- (ii) Reduction of the $-C\equiv N$ group to form a substituted benzaldimine.
- (iii) Reduction of the C=C bond to give the saturated acid.

These possibilities were distinguished by testing for the presence of free cyanide ion and simultaneous monitoring of the C=C concentration. The anodic polarographic wave of the cyanide ion provided a convenient method for determining this species, while the C=C bond concentration was followed by u.v. spectrometry. The absence of cyanide ion in the solution after controlled-potential electrolysis was proved at pH 6.8 and 13. The possibility of interference with the anodic wave was excluded by subsequently adding cyanide to the solution, when a well defined anodic wave was obtained.

The u.v. absorbance of the C=C bond at $283\text{ m}\mu$ was followed during the controlled-potential electrolysis at pH 6.8 and 13. After various periods of electrolysis, the decrease in wave height was measured, and a sample of the solution taken for analysis. The sample was diluted to a known volume and the absorbance measured; the C=C bond concentration was obtained from a prepared linear calibration curve. Graphs of % decrease in wave height against % decrease in C=C bond concentration showed a 1:1 rectilinear relationship at both pH-values. It was apparent from these results that the 2-electron electrode processes II and III both resulted in formation of the saturated acid $NCC_6H_4CH_2CH_2COOH$.

Electrode reaction mechanisms

The dependence of half-wave potential on pH (Fig. 4) showed four linear regions corresponding to processes I, II, III, and the mixed process. Reaction I

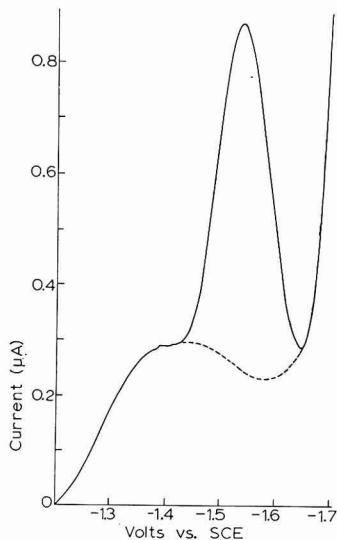
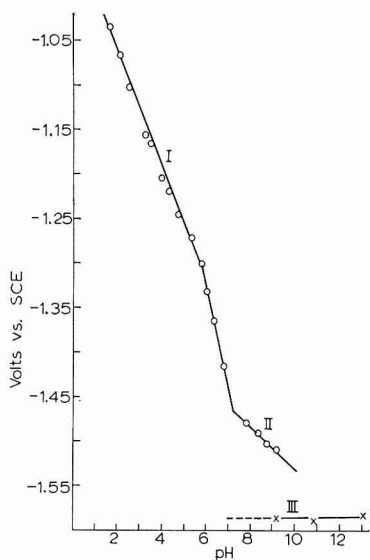
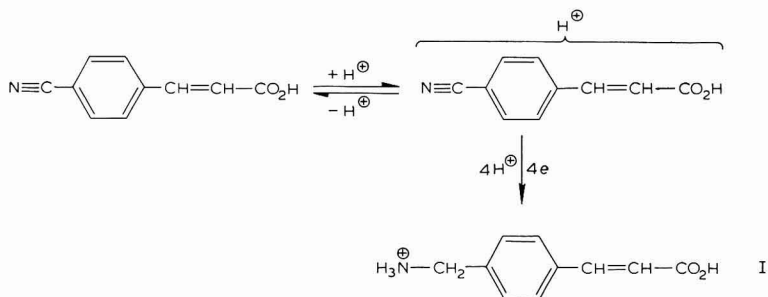


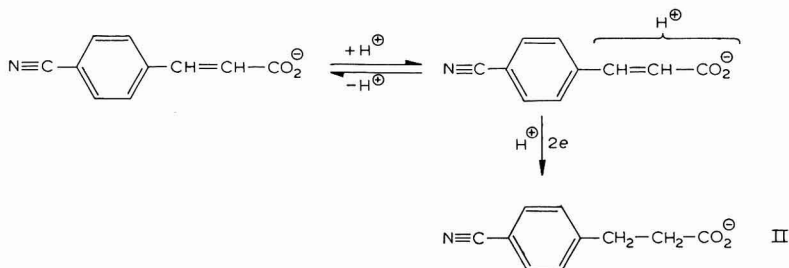
Fig. 4. Dependence of half-wave potentials of 4-cyanocinnamic acid on pH.

Fig. 5. A.c. polarogram of $5 \cdot 10^{-4} M$ 4-cyanocinnamic acid in 50% ethanol at pH 13. (....), baseline obtained with supporting electrolyte.

occurred at low pH-values where the acid was largely undissociated in solution. The dependence of $E_{1/2}$ on pH suggested that protonation was the rate-determining step in the reaction,

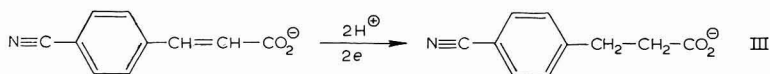


Reaction II occurred above pH 7 where the acid existed as an anion in solution; again, a protonated complex was the electroactive species,



The mechanism of this reaction was identical with that previously found for cinnamic acids containing electroinactive substituents¹. However, the latter group of compounds were reduced over a different pH-range; accurate values of $E_{1/2}$ were measured from pH 5–7. Half-wave potentials of 4-cyanocinnamic acid measured over this pH-range corresponded to a different electrode mechanism (I and the mixed process) and so structural correlation with the other acids was not possible. Extrapolation of the $E_{1/2}$ -pH plot for process II to the pH region 5–7 gave $E_{1/2}$ -values approximately 100 mV more positive than those predicted by the Hammett equation. In so far as this procedure was justified, it suggested that the presence of the conjugated electroactive CN-group influenced the reactivity of the C=C bond.

Process III was also observed in alkaline solution where the anion was the predominant species present. The half-wave potential was independent of pH; in this case protonation was not the first step in the reaction. The overall reaction was formulated,



Logarithmic analysis of the wave shape at pH 13 indicated an apparently reversible 2-electron wave, whereas reaction III clearly indicated that the process was chemically irreversible.

A.c. polarography also indicated the reversibility of the first step in the reaction at pH 13 (Fig. 5). The height of the a.c. peak was found to decrease with decreasing pH-value, so that no peak was observed at pH 11. Limitations of the instrument prevented further mechanistic information being obtained from these measurements. Oscillopolarography proved the irreversibility of the overall reaction (Fig. 6), and cyclic voltammetry, using sweep rates from 0.025 to 1000 V sec⁻¹ (Fig. 7) indicated that the intermediate radical was extremely short-lived. It was not, of course, possible to distinguish between the EEC and the ECE mechanisms from this evidence;

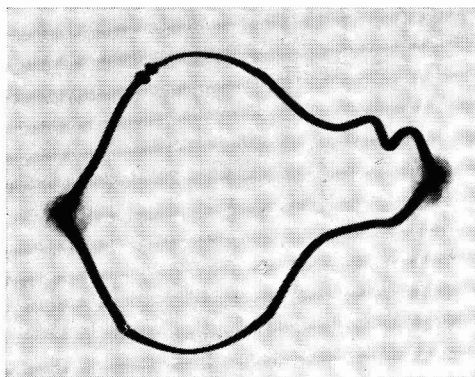


Fig. 6. Oscillopolarographic $dE/dt = f(E)$ curve for $5 \cdot 10^{-4} M$ 4-cyanocinnamic acid in 50% ethanol at pH 13.

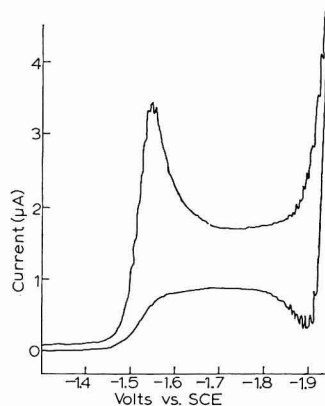
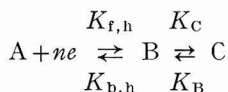


Fig. 7. Cyclic voltammogram of $5 \cdot 10^{-4} M$ 4-cyanocinnamic acid in 50% ethanol at pH 13. Voltage sweep rate, 25 mV sec⁻¹.

the reaction rates were obviously outside the accessible range of the available instruments.

KIVALO⁷ has surveyed electrode processes involving chemical reaction of the product of the electron transfer. This type of process can be represented by the scheme

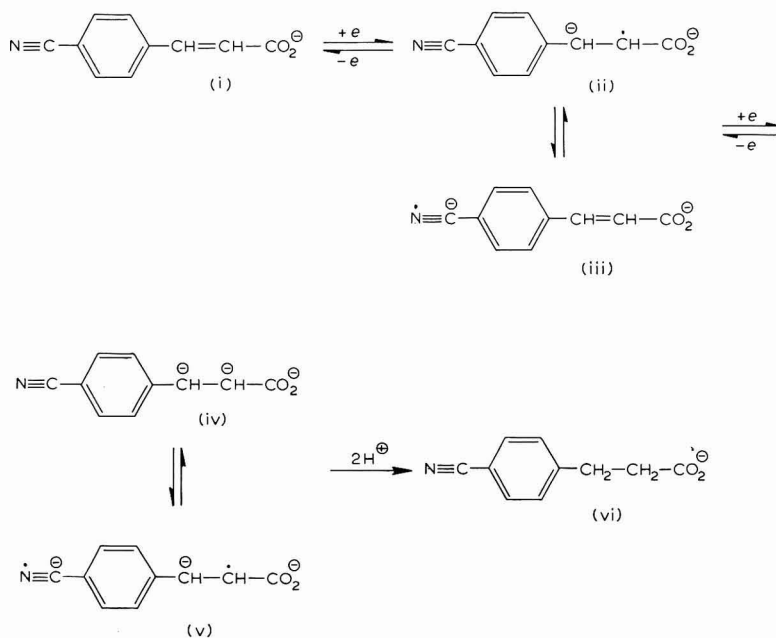


where $K_{f,h}$ and $K_{b,h}$ refer to the rates of the electron transfer reaction, and K_C and K_B to the chemical reaction, which in most cases is protonation.

The conditions under which an apparently reversible polarographic wave is observed for an overall irreversible process are that the rate of the electron transfer occurs very much faster than the irreversible chemical reactions. Alternatively, if the subsequent chemical reaction is reversible, then even if the electron transfer is slow, a reversible wave will be observed.

In the case of 4-cyanocinnamic acid two possible schemes could account for the "pseudo" reversible polarographic wave.

(a) The reduction could occur by an EEC process.



The addition of the first electron would result in the formation of the free radical (ii), which could rearrange to (iii) in order to achieve the maximum separation between the charged centres. Species (v) is a more probable product of the addition of the second electron than is (iv). The possibility that the addition of a proton might occur simultaneously with the addition of the second electron cannot be discounted.

(b) Alternatively, an ECE mechanism could occur. This would involve a reversible protonation of (ii) or (iii) as the second step. This mechanism would result

in the appearance of two 1-electron waves provided that the rate of protonation was slow, relative to the rate of the electron transfer. As a single 2-electron wave was observed, then this could only be accounted for if the rate of protonation was comparable to the rate of electron addition. In this latter case, a dependence of $E_{1/2}$ on pH would be expected, but was not in fact observed.

Hence, it is probable that the reduction occurs by the EEC mechanism (process (III)). The observed increase in the slope of the wave on increasing the pH over the range 7–13 can be attributed to a decreasing rate of protonation; thus at very high pH-values the rate of protonation is very slow compared with the rate of electron transfer, and a "pseudo" reversible wave is observed.

The rather unusual behaviour of 4-cyanocinnamic acid at high pH-values was correlated with the structure of the compound. Two possibilities existed; (a) that the effect was characteristic of the CN-group, *i.e.*, it was able to stabilise the intermediate free radical, or (b) that the effect was solely dependent on the total inductive effect operating on the C=C bond. In this latter case, a substituted cinnamic acid with a similar total σ -value should exhibit the same behaviour. The compound, 3,4-dichlorocinnamic acid ($\sigma=0.600$, for the 4-CN group $\sigma=0.628$) showed no such anomalous behaviour; its properties were completely analogous to those of the simple cinnamic acids described previously. Therefore, it was concluded that the presence of the conjugated CN-group stabilised the free radical intermediate by delocalisation of the negative charge.

Polarographic behaviour of ethyl 4-cyanocinnamate

Dissociation of the carboxyl group in ethyl 4-cyanocinnamate was not possible, and the compound represented a mechanistically simpler system than did the parent acid. A single polarographic wave was observed, the height of which varied with pH (Fig. 8). At pH-values above 7, hydrolysis of the ester occurred, and a second wave was observed at a more negative potential; at very high pH-values the rate of hydrolysis became too rapid for accurate measurements of the ester wave. The hydrolysis wave was due to reduction of the anion by processes II and III described previously.

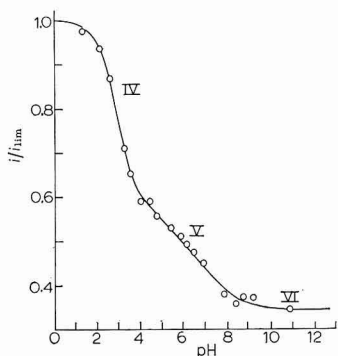


Fig. 8. Polarographic dissociation curve of ethyl 4-cyanocinnamate.

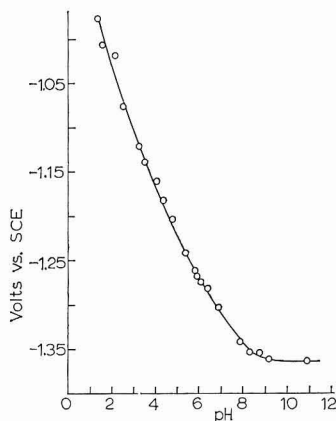
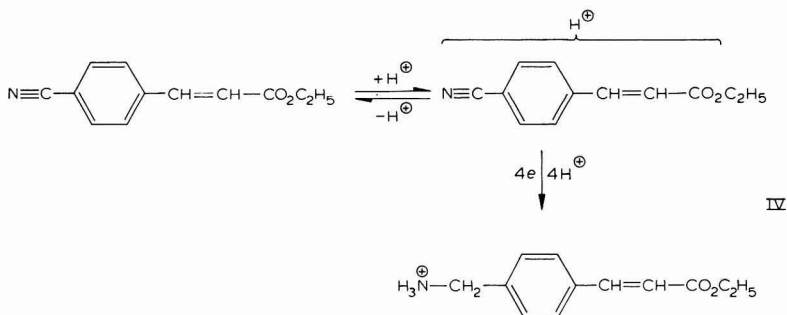


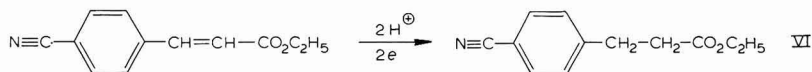
Fig. 9. Dependence of half-wave potentials of ethyl 4-cyanocinnamate on pH.

Over the pH-range 7-9, where two waves were observed for the anion, the hydrolysis wave was too poorly defined for resolution into two waves. The polarographic dissociation curve for the ester indicated three electrode processes: that in acid solution (IV), a mixed process (V) between pH 4 and 8, and a process in alkaline solution (VI).

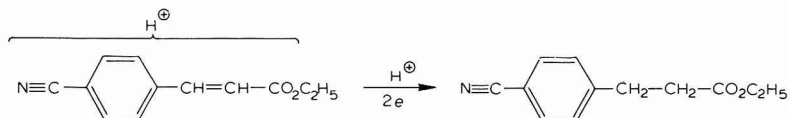
Comparison of wave heights of the ester with those of the acid suggested that process IV involved a 4-electron transfer, and process VI, 2 electrons. The pH-dependence of half-wave potentials (Fig. 9) indicated that a protonated complex of the ester was the electroactive species up to pH 8, when the ester was reduced in unprotonated form. The structural analogy to the acid suggested reaction IV for the ester to be identical with reaction I for the acid,



Similarly, reaction VI for the ester was analogous to reaction III for the acid, where proton addition was not the first step,



The mixed process for the ester, V, involved reduction of the CN-group and the C=C bond. As the $E_{1/2}$ -pH plot did not show a significant change in slope in the region of the mixed process, it was likely that the C=C bond was reduced in the protonated complex.



Simultaneous occurrence of this reaction and reaction IV were observed as the mixed process, V. As with the acid, the beginning of the mixed process was characterised by an increase in $n\alpha$ -value, followed by a sudden decrease between pH 5.4 and 5.6 (Table 2).

ACKNOWLEDGEMENTS

The authors wish to express their thanks to Dr. P. ZUMAN for discussing the results presented in this paper. Dr. M. E. PEOVER of the National Physical Laboratory, Teddington, kindly performed the fast sweep cyclic voltammetry. M. J. D. B. wishes to thank Murex Limited for financial support.

SUMMARY

The polarographic behaviour of 4-cyanocinnamic acid in 50% ethanolic solution shows a marked dependence on pH. At low pH-values a single 4-electron wave is observed, the height of which decreases with increasing pH; the protonated undissociated acid is reduced to a primary amine. A mixed process is observed between pH 6 and 7, and at higher pH-values two waves appear, the total height of which remains constant. The height of the more positive wave decreases with increasing pH, and corresponds to reduction of the C=C bond in a protonated complex of the anion. The more negative wave also corresponds to reduction of the C=C bond in the anion, but in this case electron transfer is the first step in the reaction. At high pH-values the slope of this wave increased, and indicated apparent reversibility, although the overall reaction was irreversible.

The behaviour of the ester is simpler. At low pH-values the ester is reduced, as a protonated complex, to a primary amine. At pH-values above 7, hydrolysis occurs, but the C=C bond is reduced in the unprotonated ester itself. A mixed process was observed between pH 4 and 8.

REFERENCES

- 1 M. J. D. BRAND AND B. FLEET, *J. Electroanal. Chem.*, 16 (1968) 341.
- 2 P. ZUMAN, *Collection Czech. Chem. Commun.*, 25 (1960) 3225.
- 3 O. MANOUSEK AND P. ZUMAN, *Chem. Commun., (London)*, 8 (1965) 158.
- 4 *Organic Synthesis*, edited by N. RABJOHN, Wiley, New York. Collected Volume, 4 (1963) 732.
- 5 M. E. PEOVER AND B. S. WHITE, *J. Electroanal. Chem.*, 13 (1967) 93.
- 6 F. FEIGL, *Spot Tests in Organic Analysis*, Elsevier, Amsterdam, 6th edn, 1960, p. 278.
- 7 P. KIVALO, *Acta Chem. Scand.*, 9 (1955) 221.

J. Electroanal. Chem., 19 (1968) 157-167

ALTERNATING CURRENT POLAROGRAPHY OF NUCLEOSIDES

VLADIMÍR VETTERL*

Institute of Biophysics, Czechoslovak Academy of Sciences, Brno (Czechoslovakia)

(Received March 12th, 1968)

INTRODUCTION

Most physical and physico-chemical methods used currently in the study of the properties of nucleic acids (ultracentrifugation, optical methods, viscosimetry) are concerned with the properties of nucleic acids in solution. In the living cell, nucleic acids come into contact with various types of boundaries (surface of ribosomes, nuclear membrane, etc.). New findings on the structure and the function of nucleic acids might thus be furnished by the study of interaction of nucleic acids with surfaces. Recently, electrochemical methods permitting the study of the reducibility¹⁻⁴ and adsorbability⁴⁻⁶ of nucleic acids and their components have been used for this purpose.

To elucidate the mechanism of adsorption of nucleic acids on the electrode surface, we studied the adsorption of bases currently occurring in nucleic acids, and derivatives of analogous structure. We used the method of measurement of differential capacity of the electrode double-layer⁷, and BREYER'S⁸ alternating current polarography (a.c. polarography)⁹. The curves of the dependence of the differential capacity on the potential (capacity curves), and the a.c. polarograms of certain purine and pyrimidine derivatives, show relatively sharp limited minima—"pits"—at higher solution concentrations; these are characteristic of the association of adsorbed molecules¹⁰. In the range of potentials at which a "pit" appears on the capacity curve, the associated molecules form a surface film on the electrode surface. The greatest tendency for intermolecular associations in the electrode surface is shown by bases currently occurring in nucleic acids¹¹.

The a.c. polarograms of nucleosides have, as a rule, a more complicated course than a.c. polarograms and/or capacity curves of the corresponding bases¹².

In the present paper we report on the dependence of the shape of the a.c. polarograms of nucleosides currently occurring in nucleic acids, on the concentration.

EXPERIMENTAL

The a.c. polarograms were obtained at a temperature of 25° on a GWP 563 polarograph (Akademie-Werkstätten für Forschungsbedarf, Berlin-Adlershof, Germany)¹³ at a frequency of 78 c/sec, amplitude 18 mV, sensitivity 15 μ A/full-scale deflection and damping 6. The height of the mercury column was $h=40$ cm, the capillary flow rate measured at open circuit, $m=5.65$ mg/sec, and the drop time, $t=2.5$ sec. The potential was measured relative to the saturated calomel electrode.

* Present address: Département de Biologie, Commissariat à l'Énergie Atomique, C.E.N. de Saclay, Gif-sur-Yvette (France).

All chemicals were analytical-grade from Calbiochem (except guanosine, from Lachema, Czechoslovakia). The background electrolyte was 0.5 M NaF with 0.1 M phosphate buffer, pH 7.0.

RESULTS AND DISCUSSION

The a.c. polarograms of uridine, thymidine, and cytidine (Fig. 1) take a simple

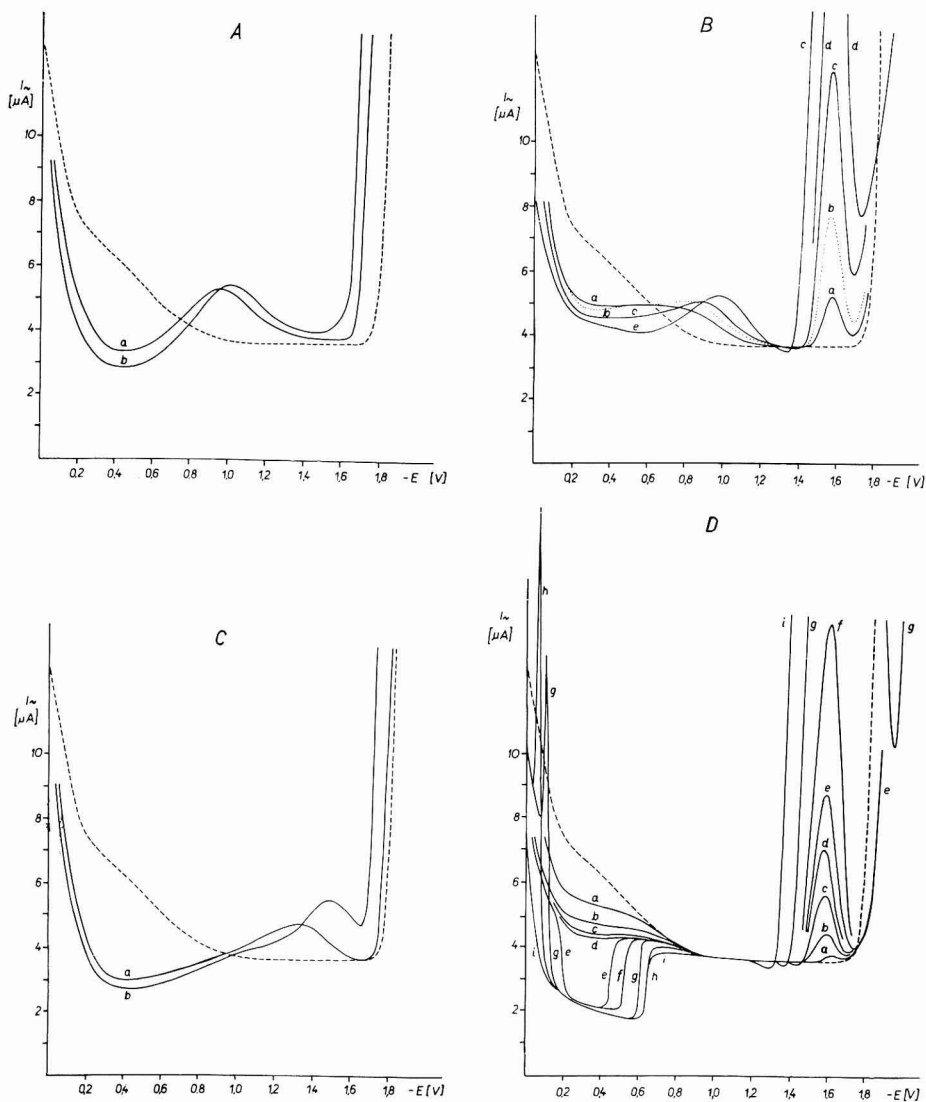


Fig. 1. A.c. polarograms of nucleoside solns. in 0.5 M NaF+0.1 M phosphate buffer, pH 7.0, at 25°. (A) uridine: (a), 1.0; (b), 5.5 mM. (B) cytidine: (a), 0.12; (b), 0.23; (c), 0.46; (d), 0.92; (e), 17 mM. (C) thymidine: (a), 8.0; (b), 42 mM. (D) deoxycytidine: (a), 0.044; (b), 0.24; (c), 0.46; (d), 0.68; (e), 0.90; (f), 1.8; (g), 7.3; (h), 10; (i), 50 mM.

course with the minimum in the neighbourhood of -0.4 to -0.6 V and cathodic desorption maxima at potentials of -0.9 to -1.5 V. The anodic desorption maxima are not recorded on the polarograms. The „pits” characteristic of the association of the adsorbed molecules are not formed on the alternating current polarograms of these nucleosides even at concentrations approaching saturation value. The high peak of cytidine at a potential of -1.6 V is apparently caused by the reduction of cytosine¹⁻³, the dependence of the height of the peak on the concentration being linear. A maximum of the same character can also be observed on the alternating current polarogram of deoxycytidine. With the exception of cytidine and deoxycytidine, all the other nucleosides tested are, under the given experimental conditions,

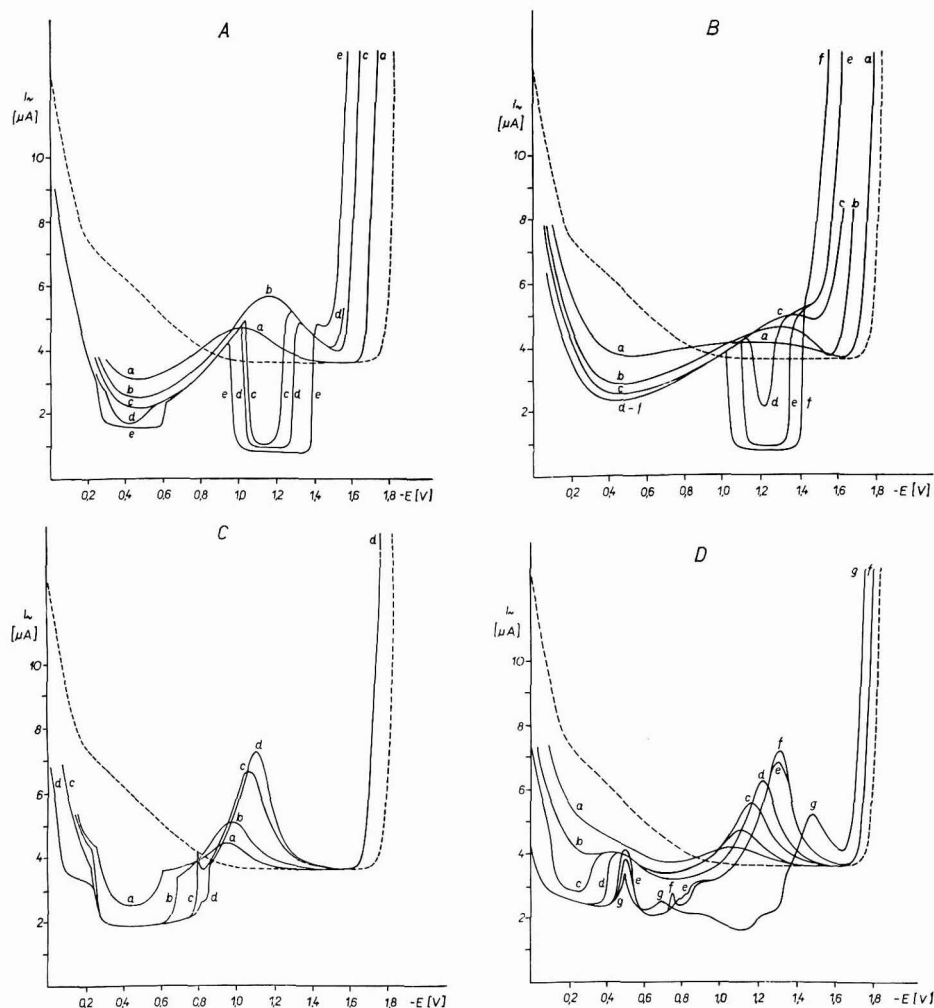


Fig. 2. (A) adenosine: (a), 0.55; (b), 1.1; (c), 3.3; (d), 4.4; (e), 11 mM. (B), deoxyadenosine: (a), 0.084; (b), 0.66; (c), 4.6; (d), 4.7; (e), 6.2; (f), 11 mM. (C) guanosine: (a) 0.10; (b), 0.19; (c), 0.52; (d), 0.78 mM. (D) deoxyguanosine: (a), 0.056; (b), 0.11; (c), 0.26; (d), 0.56; (e), 1.1; (f), 1.8; (g), 9.5 mM.

non-reducible¹⁴ and the maxima observed on the a.c. polarograms are altogether of a capacitive character.

At higher concentrations of deoxycytidine there is association of the adsorbed molecules, indicated by the formation of a "pit" on the a.c. polarograms. With increasing concentration of the solution, the association is strengthened; a higher intensity of the electrode's electrostatic field is necessary for the destruction of the surface film and the "pit" widens. A cathodic desorption maximum does not appear (if association of the molecules takes place, the desorption maxima become latent¹⁰). On the anodic edge of the association "pit", a very sharp maximum arises as a result of the destruction of the surface film. The change in state of the adsorbed molecules occurs at a very close concentration interval (compare the a.c. polarograms of deoxycytidine marked, d, e, which correspond to concentrations of 0.68 mM and 0.9 mM) as in the case of the association of the adsorbed molecules of the bases⁷.

The a.c. polarograms of adenosine (Fig. 2) display (up to a concentration of approximately 1.1 mM) a simple course with a minimum around -0.4 V caused by noncharged-site controlled adsorption¹⁵. At concentrations above 1.1 mM, association takes place in the neighbourhood of a potential of -1.1 V, and at concentrations exceeding 3.3 mM, association occurs also at about -0.4 V. On the other hand, with deoxyadenosine this second association area does not appear even at the highest concentrations. The existence of two separate areas in which association of adenosine molecules takes place, might indicate that when the potential of the electrode changes, the association capacity of the adsorbed molecules alters through a change of their orientation in the electrode surface. When the temperature is increased, the tendency to association and desorption decreases, as with diminution in the concentration (Fig. 3).

The a.c. polarograms of guanosine solutions (Fig. 2) show that guanosine molecules begin to associate at potentials about -0.5 V. As the concentration increases, the association "pit" widens, and at the highest concentrations (curve d, concentration 0.78 mM) it displays a step-like course which is usually observed on capacity curves⁷.

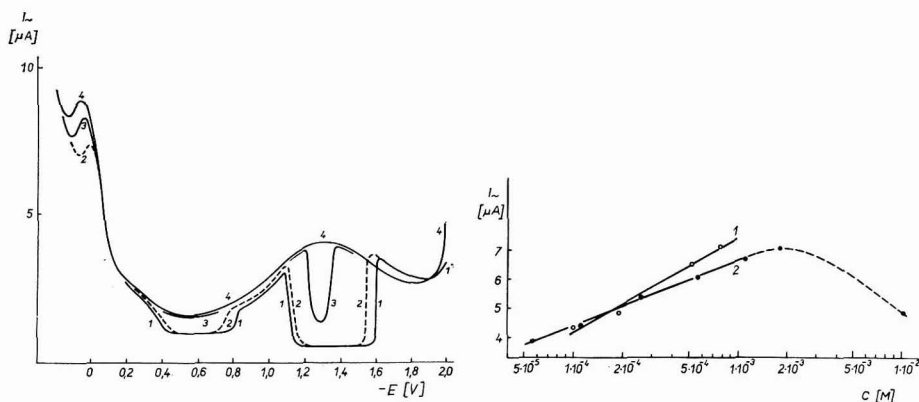


Fig. 3. Dependence of a.c. polarogram of 1.9 mM adenosine soln. in 0.25 M NaF, on temp. (1) 13°, (2) 18°, (3) 30°, (4) 35°.

Fig. 4. Dependence of height of desorption maximum of a.c. polarograms of (1) guanosine and (2) deoxyguanosine, on concn.

when poly-molecular layers¹⁶ form. On curve c there is a sharp maximum at a potential of -0.8 V; this arises through the destruction of the surface film (as with the maximum of deoxycytidine at potentials about -0.1 V). Desorption maxima can be seen on the a.c. polarograms of guanosine; the height of these maxima increases proportionally to the logarithm of the concentration of the solution (Fig. 4); this is in agreement with theoretical predictions¹⁷.

With deoxyguanosine, association of the adsorbed molecules occurs about -0.2 V. The a.c. polarograms of solutions of concentration above 1.1 mM (curves e, f, g) are more complicated apparently as a result of reorientation of the molecules in the electrode surface when the potential changes and also by aggregation of deoxyguanosine in the solution¹⁸⁻²⁰. A more detailed analysis of the a.c. polarograms of deoxyguanosine necessitates further studies.

SUMMARY

A.c. polarograms of nucleosides currently occurring in nucleic acids exhibit a minimum at a potential of about -0.4 V, caused by the adsorption of nucleosides on the electrode surface. At higher concentrations of deoxycytidine, adenosine, guanosine, and deoxyguanosine, association of the adsorbed molecules takes place in the neighbourhood of this potential. With deoxyadenosine, association of the molecules occurs at about a potential of -1.2 V. With adenosine, association occurs at both -0.4 V and -1.2 V, approximately. As with bases, the transition from the non-associated to the associated state occurs over a close concentration interval in which the adsorption isotherm has an inflection point. With uridine, thymidine, and cytidine, no association of the adsorbed molecules takes place under the given experimental conditions, even at concentrations approaching saturation value. At pH = 7.0, most of the nucleosides tested are polarographically non-reducible and the maxima observed on the a.c. polarograms are of a capacitive character. Only the peak for cytidine and deoxycytidine at a potential of -1.6 V is caused by reduction of cytosine.

REFERENCES

- 1 B. JANÍK AND P. J. ELVING, *Chem. Rev.*, in press.
- 2 B. JANÍK AND E. PALEČEK, *Arch. Biochem. Biophys.*, 105 (1964) 225.
- 3 D. L. SMITH AND P. J. ELVING, *J. Am. Chem. Soc.*, 84 (1962) 1412.
- 4 E. PALEČEK AND V. VETTERL, *Biopolymers*, in press.
- 5 I. R. MILLER, *J. Mol. Biol.*, 3 (1961) 229, 357.
- 6 H. BERG, H. BÄR AND F. A. GOLLMICK, *Biopolymers*, 5 (1967) 61.
- 7 V. VETTERL, *Collection Czech. Chem. Commun.*, 31 (1966) 2105.
- 8 B. BREYER AND H. H. BAUER, *Alternating Current Polarography and Tensammetry*, Interscience Publishers, John Wiley, New York, 1963.
- 9 V. VETTERL, *Abhandl. Deut. Akad. Wiss. (Berlin) Kl. Med.*, (1966) 493.
- 10 W. LORENZ, *Z. Elektrochem.*, 62 (1958) 192.
- 11 V. VETTERL, *Experientia*, 21 (1965) 9.
- 12 V. VETTERL, *Biophysik*, submitted for publication.
- 13 W. SKALWEIT AND H. JEHRING, *Chem. Tech. (Berlin)*, 16 (1964) 290.
- 14 E. PALEČEK AND B. JANÍK, *Arch. Biochim. Biophys.*, 98 (1962) 527.
- 15 B. JANÍK AND P. J. ELVING, *J. Am. Chem. Soc.*, in press.
- 16 V. J. MELIK-GAYKAZYAN, *Zh. Fiz. Khim.*, 26 (1952) 1184.
- 17 B. B. DAMASKIN AND N. B. GRIGORIEV, *Dokl. Akad. Nauk SSSR*, 147 (1962) 135.
- 18 O. JARDETSKY, *Biopolymers Symposia*, 1 (1964) 501.
- 19 R. V. RAVIDRANATHAN AND H. T. MILES, *Biochim. Biophys. Acta*, 94 (1965) 603.
- 20 M. P. SCHWEIZER, S. I. CHAN AND P. O. P. TS'0, *J. Am. Chem. Soc.* 87 (1965) 5241.

SHORT COMMUNICATION

Studies on hydroxycyanogen compounds. II. Composition of Co(II)-, Ni(II)-, Cu(II)- and Zn(II)-hydroxycyanomolybdates(IV) by amperometry and conductometry

This report deals with the amperometric and conductometric studies on the composition of the insoluble cobalt, nickel, copper, and zinc complexes of tripotassium aquotrihydroxotetracyanomolybdate(IV).

Experimental

Tripotassium aquotrihydroxotetracyanomolybdate(IV) dihydrate, $K_3[Mo(CN)_4(OH)_3(H_2O)]$, was prepared as described earlier² and its solution strength determined potentiometrically against $K_3Fe(CN)_6$ ².

Solutions of cobalt chloride, nickel chloride, copper sulphate and zinc sulphate were obtained by dissolving A.R. crystals in doubly-distilled water; the concentration was determined by standard analytical methods³.

Amperometric titrations were carried out using the Fischer Electropode. The electrodes used were the DME and SCE; KCl (0.1 M) and gelatin (0.01%) were used as base electrolyte and maximum suppressor, respectively. The solutions were deoxygenated by passing purified nitrogen gas. The potentials applied during the titrations were as follows: Co(II), -1.35 V; Ni(II), -1.2 V; Cu(II), -0.5 V; Zn(II), -1.2 V.

A Cambridge conductivity bridge (No. L-350140) with a dip cell (No. PR 9510, cell constant = 1.46) was used for conductance measurements.

All measurements were made at $30 \pm 0.1^\circ$ except for Zn(II) for which measurements were carried out at $60 \pm 0.1^\circ$.

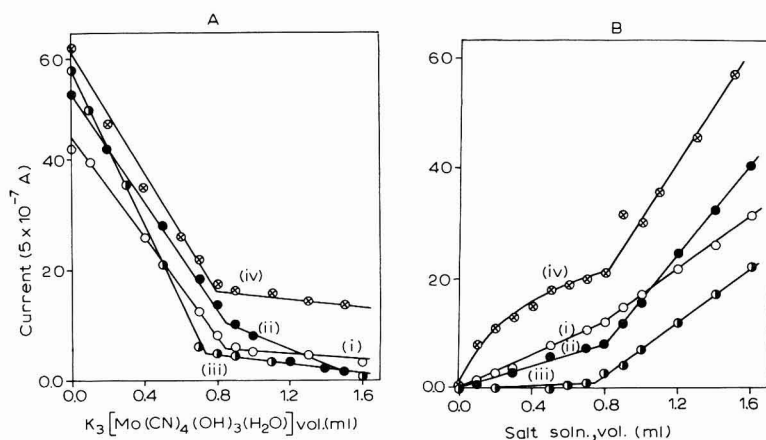


Fig. 1A. Direct amperometric titrations. 20 ml 0.004 M (i), $CoCl_2$; (ii), $NiCl_2$; (iii), $CuSO_4$; (iv), $ZnSO_4$ vs. 0.1 M $K_3[Mo(CN)_4(OH)_3(H_2O)]$. B. Reverse amperometric titrations. 20 ml 0.004 M $K_3[Mo(CN)_4(OH)_3(H_2O)]$ vs. 0.1 M (i), $CoCl_2$; (ii), $NiCl_2$; (iii), $CuSO_4$; (iv), $ZnSO_4$.

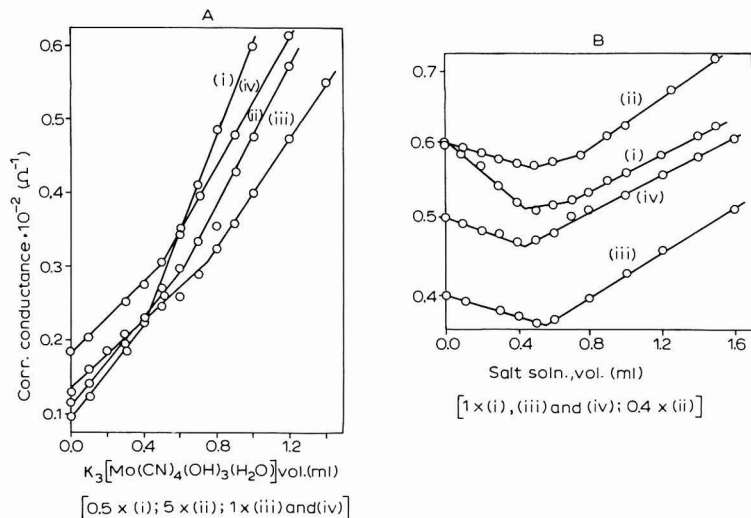
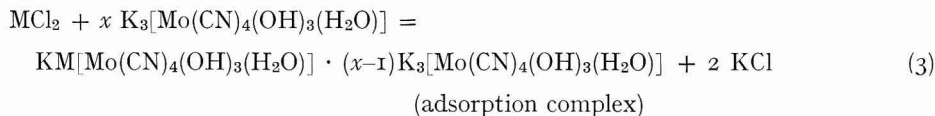
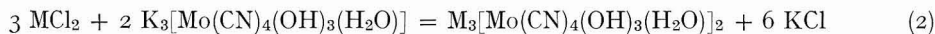


Fig. 2A. Direct conductometric titrations. (i), 20 ml 0.005 *M* CoCl₂ vs. 0.5 *M* K₃[Mo(CN)₄(OH)₃(H₂O)]; (ii), 15 ml 0.005 *M* NiCl₂ vs. 0.025 *M* K₃[Mo(CN)₄(OH)₃(H₂O)]; (iii), 15 ml 0.005 *M* CuSO₄ vs. 0.1 *M* K₃[Mo(CN)₄(OH)₃(H₂O)]; (iv), 10 ml 0.005 *M* ZnSO₄ vs. 0.1 *M* K₃[Mo(CN)₄(OH)₃(H₂O)]. B. Reverse conductometric titrations. (i), 25 ml 0.01 *M* K₃[Mo(CN)₄(OH)₃(H₂O)] vs. 0.5 *M* CoCl₂; (ii), 20 ml 0.01 *M* K₃[Mo(CN)₄(OH)₃(H₂O)] vs. 1.0 *M* NiCl₂; (iii), 15 ml 0.01 *M* K₃[Mo(CN)₄(OH)₃(H₂O)] vs. 0.25 *M* CuSO₄ (in 20% ethanol); (iv), 15 ml 0.0033 *M* K₃[Mo(CN)₄(OH)₃(H₂O)] vs. 0.1 *M* ZnSO₄.

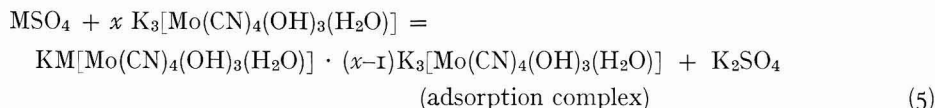
Result and discussion

Typical curves are shown in Figs. 1A, 1B, 2A and 2B.

The reactions between potassium aquohydroxomolybdocyanide and cobalt/nickel chloride may be represented by the following stoichiometric equations:



and between copper/zinc sulphate by:



Both the amperometric and conductometric methods (Figs. 1A, 1B, 2A, and 2B) give a combining ratio of 1:1 for the reactants, indicating the formation of $\text{KM}^{\text{II}}[\text{Mo}^{\text{IV}}(\text{CN})_4(\text{OH})_3(\text{H}_2\text{O})]$ (M = metal ion) in accordance with eqns. (1) and (4). In the case of Ni/Co, the results of reverse conductometric titrations (Fig. 2B, curves (i) and (ii) give one more ratio of 3:2 (metal: hydroxomolybdocyanide). For this ratio, the complex formed would have the composition $\text{M}_3^{\text{II}}[\text{Mo}^{\text{IV}}(\text{CN})_4(\text{OH})_3(\text{H}_2\text{O})]_2$.

However, nearly all the titrations give a little more hydroxomolybdocyanide than required by the stoichiometric eqns. This may be due to adsorption of the $[\text{Mo}(\text{CN})_4(\text{OH})_3(\text{H}_2\text{O})]^{3-}$ ion on the freshly precipitated complex.

Acknowledgement

We thank Professor A. R. Kidwai for the provision of facilities and the C.S.I.R. (New Delhi) for the award of a fellowship to one of us (K.U.)

*Department of Chemistry,
Aligarh Muslim University,
Aligarh (India)*

KABIR-UD-DIN
A. A. KHAN
M. A. BEG

1 W. R. BUCKNALL AND W. WARDLAW, *J. Chem. Soc.*, (1927) 2981; N. V. SIDGWICK, *Chemical Elements and Their Compounds*, Vol. II, Oxford University Press, 1950, p. 1056; A. W. ADAMSON AND J. R. PERUMAREDDI, *Inorg. Chem.*, 4 (1965) 247.

2 KABIR-UD-DIN, A. A. KHAN AND M. A. BEG, *J. Electroanal. Chem.*, in press.

3 *Standard Methods of Chemical Analysis*, Vol. 1, edited by N. H. FURMAN, 6th ed., 1962, pp. 382, 700, 404, 1231, Van Nostrand, Princeton, N.J.

Received January 1st, 1968; in revised form, February 11th, 1968

J. Electroanal. Chem., 19 (1968) 175-177

BOOK REVIEWS

Electrical Properties of Semiconductor Surfaces by DANIEL R. FRANKL, International Series of Monographs on Semiconductors, Volume 7, Pergamon Press, Oxford, 1967, $16 \times 23\frac{1}{2}$ cm², 310 pages. Price 84 s.

This is on the whole a good book, written in a clear style. Each chapter begins with a brief survey of the status of the topic dealt with in the chapter and the reader has therefore, a useful idea of what the chapter is about before starting on the main text. A summary concludes each section. There are seven chapters: (1) Equilibrium properties (20 pages); (2) Surface Space-Charge Layer in Equilibrium (27 pages); (3) Non-equilibrium Conditions (45 pages); (4) Field Effects and Related Topics (64 pages); (5) Preparation of Surfaces (29 pages); (6) Theory of Surface States (9 pages) and (7) Surface States on Common Semiconductors (93 pages).

The basic ideas pertinent to semiconductor surface research are outlined in the first four chapters and are illustrated by an appropriate presentation of the experimental results. It is the opinion of the reviewer, however, that it is dangerous to give the reader the impression that a topic like Semiconductor Surface Research stands as an isolated discipline in physical chemistry. The author has not always avoided this danger. In particular, Chapter 2 on Space-Charge Theory should have contained some references to systems, other than semiconductor surfaces, where space charges are present. Thus, the name of GOUY, who was the first to solve the Poisson-Boltzmann equation (for electrolyte solutions in contact with a charged surface) should have been mentioned. This would have been more than a matter of

J. Electroanal. Chem., 19 (1968) 177-178

mere historical interest. Section 2.4 (on basic assumptions) would have gained in interest had something of the work of ONSAGER, KIRKWOOD and later theoreticians been mentioned. Section 2.3 (Thin Slabs) would have gained by the inclusion of results from colloid chemistry. As Chapter 2 stands, some readers will be puzzled as to *why* L_D is called Debye length. Chapters 5, 6 and 7 contain results of experimental work. The author has succeeded in arranging the multitude of papers to be considered here, in an easily surveyable way. Such a survey can only be made on the basis of an extremely simplified interpretation of the experimental data. One may argue that it is still too early for such a philosophy. Thus, the author writes (p. 212) "The paper by LUASHENKO *et al.* is most difficult to reconcile, since standard techniques were employed and the work appears to have been carried out with great care". One is inclined to ask: why not take this paper at face-value? A similar comment can be made on the discussion of the work of ALLEN AND GOBELI (AG) which is compared with the work of VAN LAAR AND SCHEER (vLS) (pp. 195-207). One question here is: does tail emission (*i.e.*, the electron emission from a semiconductor as a result of the incidence of light at frequencies close to the threshold value) emerge from surface states? The answer implied by AG is: "occasionally", and the answer by vLS is: "always". The arguments in favour or against these answers are scattered over the pages in about a one to one ratio, but the author gives AG the benefit of the doubt.

Another point is the continued discussion on the cleanliness of a surface. To arrive at a conclusion in this matter, a careful consideration of the equipment (geometry of apparatus, etc.) used by each worker should have priority rather than the more indirect way followed by the author. The author sometimes judges the value of experiments on a preconceived opinion which he has based on his knowledge of other, more or less related, experiments (section 7.3).

In sections 7.4 and 7.6, the effect of copper traces on the electrical properties of technical Ge surfaces (7.4) and the Ge/electrolyte interface (7.6) are considered in detail (although the effect of pH on copper deposition from an electrolyte solution is not mentioned). Deposited copper forms surface states (BRATTAIN AND BODDY) and the work done in this field must be of interest to every electrochemist. The view that this work is of prime importance is therefore justified but the study of the anodic dissolution of germanium (BRATTAIN AND GARRETT) and the study of the interface between germanium and aqueous redox systems (GERISCHER) which are of equal interest, are not included. Also, consideration of the work of the Russians is lacking in section 7.6, and the reviewer therefore considers this section to be the only really weak point in the book. This does not affect the final conclusion that all those interested in the study of semiconductor surfaces will read this book with pleasure and will find, with relatively little effort, much information. Taken with the now well-known book of MANY, GOLDSTEIN AND GROVER it constitutes a fund of information which will be invaluable to university teachers, industrial physical chemists and advanced students.

The book is well-produced and contains few printing errors. The price is moderate in view of the over-all high quality achieved by the author.

M. J. SPARNAAY,
Philips Research Laboratories, Eindhoven

Electrosorption, edited by E. GILEADI, Plenum Press, New York, 1967, 221 pages, \$ 12.50.

This volume contains 7 chapters dealing with adsorption and double-layer structure: (1) Isotherms (18 pages, GILEADI); (2) Adsorption of organic substances at solid electrodes (33 pages, PIERSMA); (3) Mass transfer controlled adsorption (18 pages, REDDY); (4) Oxide film growth (13 pages, GENSHAW); (5) Potential of zero charge (28 pages, ARGADE AND GILEADI); (6) Solvent (water) and double-layer structure (29 pages, MULLER); (7) Statistical-mechanical and local thermodynamic balance theories of double layer (71 pages, HURWITZ).

Chapters 2 and 4 deal solely with solid electrodes while chapter 5 is mostly concerned with this type of electrode. The material of the other chapters originated largely in the study of the mercury electrode but finds application to solid electrodes, generally with added complications. Thus, about one-third of the book pertains solely to solid electrodes.

The material is not intended to be a complete review or to deal mostly with original work. Actually, the level varies, as noted by the editor, from a simple analysis of the most useful isotherms in electrode adsorption studies to HURWITZ's rather arduous chapter. Many readers will probably find PIERSMA's chapter 2 the most informative and useful one in relation to current work. His realistic evaluation shows the serious experimental limitations in electrode-electrolyte adsorption as compared with metal-gas adsorption, but the author is not without hope. Information, sometimes conflicting and often tentative, is accumulating rapidly (129 references, mostly since 1960) but no synthesis of ideas has yet emerged.

The two other chapters (4 and 5) dealing specifically with solid electrodes are of a more tutorial nature. GENSHAW's chapter 4 of oxide growth is largely outside the realm of adsorption and is primarily concerned with films more than one layer thick (insulator, semiconducting and conducting films). Classical treatments of oxide growth are clearly reviewed, but the oxygen electrode is not discussed, and the question of why oxides are important in electrode kinetics is dealt with in one page (p. 85). Chapter 5 on the point of zero charge discusses with competence the effect of the nature of the electrode and glosses over in a highly superficial way (less than 1 page per topic) the effects of adsorption of ions, organic substances, and hydrogen or oxygen. The authors should have refrained from giving electrocapillary curves for CNS^- , Cs^+ (concentrations omitted in these two sets of curves) and phenol (pp. 100 and 101) obtained recently in their laboratory since the reader surely is familiar with this type of very old information. PARSONS' basic treatment of the Esin and Markov effect, which related the shift of the point of zero charge to the isotherm, would have been far more valuable than these electrocapillary curves and would have taken no more space. In addition to the foregoing topics, ARGADE AND GILEADI also consider briefly the Frumkin double-layer correction in kinetics and give a survey of techniques for the determination of the point of zero charge.

Chapter 1 on isotherms (linear, LANGMUIR, TEMKIN, FRUMKIN) reads well and deals mostly with material that has become classical by now. The experimental test of isotherms is only given scant notice. GILEADI blatantly overquotes the work of the BOCKRIS and CONWAY groups (14 references out of a total of 23) with which he was associated, while FRUMKIN and PARSONS, who are in the forefront of isotherm analysis,

are quoted only once each (self-quoting is not bad *per se* but it must be justified!). PARSONS' first detailed discussion of isotherms and equations of state, as applied to double-layer phenomena (1955–57) is not quoted, and his 1955 suggestion of using the charge density on the electrode is mentioned with reference to a 1964 paper. The early extensive work of FRUMKIN on the use of LANGMUIR and TEMKIN isotherms is not quoted either.

We now come to chapters (3, 6 and 7) dealing with material essentially developed for the mercury electrode and with only very limited application to solid electrodes thus far. REDDY's chapter on mass-transfer controlled adsorption is clear. This reviewer wonders why the author went over the mathematical details on the Laplace transformation. It would have sufficed to state clearly the problems and assumptions being made, and then give the solutions in the time-domain and their interpretation. Present-day first-year graduate students in chemistry easily know how to handle this type of mathematics.

MULLER's chapter 6 on the role of the solvent on the double-layer structure strongly argues in favor of the BOCKRIS' group views. The frequency dispersion of the resistive part of the double-layer impedance is accounted for by water relaxation by transposition of dielectric relaxation theory. It is firmly stated that the various experimental artifacts were eliminated. This may be so, but more experimental work seems clearly in order. In the second part of his chapter, MULLER covers the solvent displacement analysis of adsorption which was rather recently revived and developed by the BOCKRIS group. Altogether, this is a well-written chapter, even if some of its material does not rest on a very solid experimental foundation.

HURWITZ's scholarly chapter, which takes up one-third of the book, is intended for a more restricted group of electrochemists than the other chapters. His statement (p. 177) that the seemingly good agreement between the Gouy–Chapman theory and experiment cannot be explained by more rigorous statistical–mechanical theories and may seem fortuitous, will puzzle experimentalists despite their awareness of the approximate nature of their favored approach. Actually the statistical–mechanical approach has also serious limitations (p. 190) and the author sees a way of escaping this quandary by recourse to local thermodynamic theory.

Summing up, chapters are of markedly uneven quality but cover material electrochemists ought to be familiar with. Coverage is highly topical, and some important problems are not treated, *e.g.*, the correlation between exchange current and standard free energy of adsorption. The extensive work of the FRUMKIN school, to name one, certainly does not stand out in this book, and the optics are often focussed on the work of the BOCKRIS group. A broader outlook would have resulted in a better and more useful book.

PAUL DELAHAY, New York University

CONTENTS

Application of the method of time-domain reflectometry to the study of electrode processes R. PAYNE (Bedford, Mass., U.S.A.)	1
A.c. polarographic base-current depressions not due to adsorption D. BRITZ AND H. H. BAUER (Buffalo, N.Y. and Lexington, Ky., U.S.A.)	15
Stofftransport an einer Doppelelektrode in der Wand einer Strömungskanal B. BRAUN (München, Deutschland)	23
Moving boundary analysis O. HELLO (Hobart, Tasm., Australia).	37
Double-layer charging in constant-current chronopotentiometry at a mercury-film electrode W. T. DE VRIES (Haifa, Israel)	41
Effect of double-layer charging in programmed-current chronopotentiometry W. T. DE VRIES (Haifa, Israel)	55
The admittance of the ideal reversible electrode with adsorption of reactants. Analysis of theoretical aspects P. DELAHAY (New York, N.Y., U.S.A.).	61
On the impedance of galvanic cells. XXIV. The impedance of the $\text{In}^{3+}/\text{In}(\text{Hg})$ electrode reaction in KSCN and KCl solution B. TIMMER, M. SLUYTERS-REHBACH AND J. H. SLUYTERS (Utrecht, Netherlands).	73
Electrode kinetics and double-layer structure. II. The potential-dependence of the kinetic parameters of the $\text{Zn}^{2+}/\text{Zn}(\text{Hg})$ electrode reaction M. SLUYTERS-REHBACH, J. S. M. C. BREUKEL AND J. H. SLUYTERS (Utrecht, Netherlands)	85
Chronopotentiometry of the Ag-AgCl system and analysis for the chloride ion R. E. MEYER, F. A. POSEY AND P. M. LANTZ (Oak Ridge, Tenn., U.S.A.)	99
The electroreduction of niobium(V) in hydrochloric acid solutions at mercury electrodes. II. Controlled-potential coulometry and stirred-pool chronoamperometry J. G. McCULLOUGH AND L. MEITES (Brooklyn, N.Y., U.S.A.)	111
The determination of traces of nickel in cobalt by pulse polarography A. LAGROU AND F. VERBEEK (Ghent, Belgium)	125
Comparative oxidation of chemisorbed carbon monoxide, reduced carbon dioxide and species formed during the methanol oxidation M. W. BREITER (Schenectady, N.Y., U.S.A.)	131

(Continued from previous page)

A study of the oxidation of adsorbed films formed on platinized platinum in methanol, formic acid and carbon dioxide solutions V. N. KAMATH AND HIRA LAL (Bombay, India)	137
Further examples of <i>para</i> - and <i>ortho</i> -disubstituted benzene derivatives reduced in a reversible two-electron step into products of limited stability P. ZUMAN, O. MANOUŠEK AND S. K. VIG (Prague, Czechoslovakia)	147
Polarography in the study of classical functional group reactions. II. Polarographic behaviour of 4-cyanocinnamic acid and its ethyl ester M. J. D. BRAND AND B. FLEET (London, Great Britain)	157
Alternating current polarography of nucleosides V. VETTERL (Brno, Czechoslovakia)	169
<i>Short communication</i>	
Studies on hydroxocyanogen compounds. II. Composition of Co(II)-, Ni(II)-, Cu(II)- and Zn(II)-hydroxocyanomolybdates(IV) by amperometry and conductometry KABIR-UD-DIN, A. A. KHAN AND M. A. BEG (Aligarh, U.P., India)	175
<i>Book reviews</i>	177

COPYRIGHT © 1968 BY ELSEVIER SEQUOIA S.A., LAUSANNE
PRINTED IN THE NETHERLANDS

RADIATION RESEARCH REVIEWS

Editors: G. O. PHILLIPS (Salford) and R. B. CUNDALL (Nottingham)
Consultant Editor: F. S. DAINTON, F. R. S. (Nottingham)

The objective of RADIATION RESEARCH REVIEWS is to secure from leading research workers throughout the world review papers giving broad coverage of important topics on the physical and chemical aspects of radiation research. The main emphasis will be on experimental studies, but relevant theoretical subjects will be published as well.

Tabulated data helpful to workers in the field will also be included.

RADIATION RESEARCH REVIEWS appears in four issues per approx. yearly volume. Subscription price per volume Dfl. 90.00 plus Dfl. 3.00 postage or equivalent (£10.9.6 plus 7s. or US\$25.00 plus US\$0.85).

For further information and specimen copy write to:



**Elsevier
Publishing
Company**

P.O. Box 211, AMSTERDAM The Netherlands